Sedimentology and Stratigraphy of the Tauranga Group in Hamilton City for Geological and Earthquake Modelling

A thesis

submitted in partial fulfilment

of the requirements for the degree

of

Master of Science (Research) in Earth Sciences

At

The University of Waikato

By

Joshua W. Smith

THE UNIVERSITY OF
WAIKATO
Te Whare Wānanga o Waikato

2025

Abstract.

This study was conducted to investigate the shallow stratigraphy of the Hamilton Central Business District, a city that overlies Hamilton Basin. The study focused on analysing three geotechnical cores and an exposed outcrop in Hamilton City near the Waikato River. Analysis included core logging, facies classification and paleoenvironmental interpretation, 3D structure-from-motion outcrop modelling, radiocarbon dating, as well as mineralogical assessment using X-ray diffraction. Seven unique lithofacies were identified in the cores, six of which were deposited in a braided river system; the seventh was volcanic in origin. The facies include a structureless muddy sandy gravel (F1), structureless sandy mud to muddy sand (F2), current-ripple laminated to cross-bedded muddy sand (F3), planar-bedded sandy mud to muddy sand (F4), current-ripple laminated to cross-bedded sandy mud (F5), structureless to planar bedded peat (F6A) and coal (F6B). These facies are typical of the Piako and Walton Subgroups of the Tauranga Group. The outcrop studied was a free face spanning approximately 20 metres in height and consisted of strata typical of the Hinuera Formation. One section of the outcrop showed potential evidence of liquefaction.

Overall, the strata were structured or structureless, consisting of mud, sand, gravel, and organic layers. Sediments were highly pumiceous, and partially rhyolitic at times, with bed thickness ranging from sub-decimetre to metre-scale. These units, when packaged, showed several whole and partial cycles of active and abandoned river channels, indicating significant channel migration and flooding events typical of a braided-river system. The constantly migrating channels have resulted in the units encountered having laterally discontinuous physical characteristics; notably, the mineralogical composition was highly similar across samples and cores. Liquefaction susceptibility was compared with previous seismic studies, with a focus on the physical characteristics of the sediments encountered during this investigation and those of comparable sedimentary basins.

The complexities of a braided river system's horizontal and vertical geometry in a geological modelling context were discussed, along with potential solutions to minimise scaling issues encountered when creating a coarse-scale 3D geological model. The vertical extent of some of the facies encountered during the investigation (F3 to F6B) was identified as the most at risk of over- or under-estimation during data upscaling. Near-well upscaling, confined by border cells, in combination with stochastic modelling, was suggested to resolve some of the scaling issues that will be encountered during model development.

Acknowledgements.

I would like to thank the University of Waikato for providing my project, as well as the education, resources, facilities, and space, to undertake my research. Were it not for the support and use of the technical equipment, laboratories, and office facilities available, I would not have completed.

Thank you to my supervisor Dr Andrew la Croix. The information, time, expertise, and resources that you have provided were key to the success of my project. I have always appreciated the ability to have an impromptu catch up or chat, whether short or long, despite you being busy yourself.

To the University of Waikato technical team, specifically Annette Rogers, Kirsty Vincent, Greg Barkle, and formerly Dr Deonie Castle, thank you for the instruction, guidance, and patience with me as I imposed in the various laboratory spaces and hogged your equipment, especially with the particle sizer. I would not have finished without the support of you all and the flexibility in your schedules to accommodate my research.

Dr Marlena Prentice, future doctor David Gardiner, and the Earth Science team, thank you for supporting me with various conversations and answers to questions, especially when defining the geological units within my cores and differentiating volcanic features and minerals. Thank you also to future doctor Vinay Nelli for the friendly support and feedback.

Thank you to my friends, who are closer to family, Bailey and Kyra. The rants, debriefs, chats, feedback, and general company have meant a lot to me and have kept me sane over the last two years, couldn't have done it without you Bails. Kyra, the love and support that you have shown to me over the past five years have meant the world to me, I owe you thanks for more than just my studies, to which you have always been my biggest supporter. I know we will both go far in life.

An enormous thank you to my Mum and Dad for their constant support, both financial and motivational, and for listening to my many complaints and stresses as I undertook this challenge. You both have made my studies more bearable and manageable.

Contents

Table of Figures.

Table of Tables.

1. Chapter One – Background and Introduction.

1.1. Introduction.

Seismic hazards are a complex worldwide issue that encompasses many elements, including ground motion, liquefaction, lateral displacement, ground deformation, and landslides, all of which can be exaggerated within a sedimentary basin due to seismic wave amplification and the basin effect. The basin effect refers to the refraction of seismic waves, following Snell's Law, at an impedance contrast between media with differing physical characteristics that become trapped, leading to seismic amplification. Amplification of seismic waves within a sedimentary basin occurs when seismic waves reverberate between the soft sedimentary layers that have infilled the basin, which in turn manifests an increase, or amplification, in ground motion (Rial *et al.*, 1992; Luzón *et al.*, 2002). Currently, researchers have a variety of methods available to categorise the geology of a site, including the collection of geological, geotechnical, and seismic wave data, which can be utilised in the creation of one-dimensional (1D), two-dimensional (2D), and three-dimensional (3D) geological models. The further development of these models is important when considering options to reduce the consequences associated with the seismic hazards listed previously.

New Zealand is a seismically active country; thus, earthquakes are relatively common, with consequences to both infrastructure and population centres. Situated at the boundary of the Indo-Australian and Pacific plates, and part of the Pacific Ring of Fire, New Zealand has experienced multiple significant earthquakes in recent history. The 2010/2011 Canterbury Earthquake Sequence (Webb *et al.*, 2011), the 2013 Cook Strait Earthquake Sequence (Holden *et al.*, 2013), and the 2016 Kaikōura earthquake (Bradley *et al.*, 2018) have all shown varying degrees of seismic amplification.

Located atop the Hamilton Basin (Figure 1.1), this investigation focuses on Hamilton City (110 km^2), located in central Waikato, New Zealand, the most populous city in the region and fourth most populous in the nation. Shallow marine, and some near-shore/continental, sedimentation began in the Hamilton Basin, a sedimentary basin, from the late Eocene, ~35 Ma, to the Pliocene; after which, several volcanic events drove sedimentation from ~5.6 Ma (Selby & Lowe, 1992). Though few faults are evident within the Hamilton Basin, the most notable being the Waipa Fault that runs NS along the western side of the basin (Kamp & Lowe, 1981), recent research has uncovered several new fault zones proximal to Hamilton City (Moon & de Lange, 2017; Spinardi *et al.,* 2017). Current basin geomorphology consists of low rolling hills, alluvial plains, and low

terraces (Lowe, 2010). The most common units encountered within the Hamilton Basin belong to the Tauranga Group, including the most widespread Hinuera Formation (Sherwood, 1972; Hume *et al.*, 1975) and the Walton Subgroup, first defined by Kear & Schofield (1978). While certain units within the Hamilton Basin have been analysed thoroughly, the basin formation and geological history remain poorly constrained.

Figure 1.1. Map of Hamilton City and location within New Zealand. O) Outcrop. 1) 20-1006. 2) 21-0437. 3) Ferrybank.

1.1.1. Aims.

This study aims to investigate the shallow stratigraphy (<30 m) of the Hamilton Central Business District (CBD), including the adjacent Waikato River, to gain more information on the geological units present and to assess relative seismic hazards.

This investigation focused on the following objectives:

1. Determine the physical and chemical characteristics of strata in cores and outcrops.
2. Build structure-from-motion 3D models of outcrops exposed along the Waikato River within Hamilton CBD to facilitate stratigraphic correlation between sites.
3. Interpret the paleoenvironments and physical processes that were operating at the time of deposition of the stratigraphic units.
4. Qualitatively link the characteristics of the Tauranga Group stratigraphy to seismic hazards in Hamilton Basin.

This thesis will follow a manuscript-style format with three self-contained chapters. The present chapter, Chapter One, introduces the study and reviews previous research. Chapter Two constitutes the bulk of the new research, presenting the methods and results and discussing their implications. Chapter Three summarises the study, links the main research questions to its outcomes, and highlights limitations and potential future research directions.

1.2. Sedimentary Basins & Seismic Wave Amplification.

1.2.1. Earthquakes and the Basin Effect.

From a seismic hazard point of view, sedimentary basins are some of the least desirable areas to build upon, yet many of the world's largest cities reside atop these basins (Wirth *et al.*, 2019). Two major factors restricting the accurate 3D modelling of a sedimentary basin are the unique basin floor topography and how the sedimentary layers within will respond differently to seismic events (Rial *et al.*, 1992; Qin *et al.*, 2012).

The basin effect refers to the trapping of seismic waves and the seismic amplification caused within a sedimentary basin as the waves refract at the impedance contrast between different media, following Snell's/Descartes' Law (1637/1912) of refraction. Generally, larger basins will be subject to more significant amplification than smaller basins (Feng & Ritzwoller, 2017). While refraction is most notable between highly contrasting media, such as the bedrock to infill contact, seismic waves will continue to refract between the impedance contrasts of the soft sedimentary infill. Seismic waves cannot re-enter the surrounding bedrock as the energy required

to re-enter a harder medium exceeds that of a softer medium (Qin *et al.*, 2012). Vertical seismic waves become trapped within the basin floors concave topography (Figure 1.2), while horizontal seismic waves rebound upon invisible boundaries known as caustics, lens-like areas that focus seismic wave energy, leading to significant damage where a caustic intersects with the surface as the amplification increases peak ground acceleration (Rial *et al.*, 1992).

The final factor within a sedimentary basin that results in abnormally large destruction during seismic events is double resonance. Double resonance occurs where a building's natural frequency coincides with that of the underlying geology, resulting in both vibrating, or resonating, together (Rial *et al.*, 1992), and can lead to significant damage to multi-storey buildings.

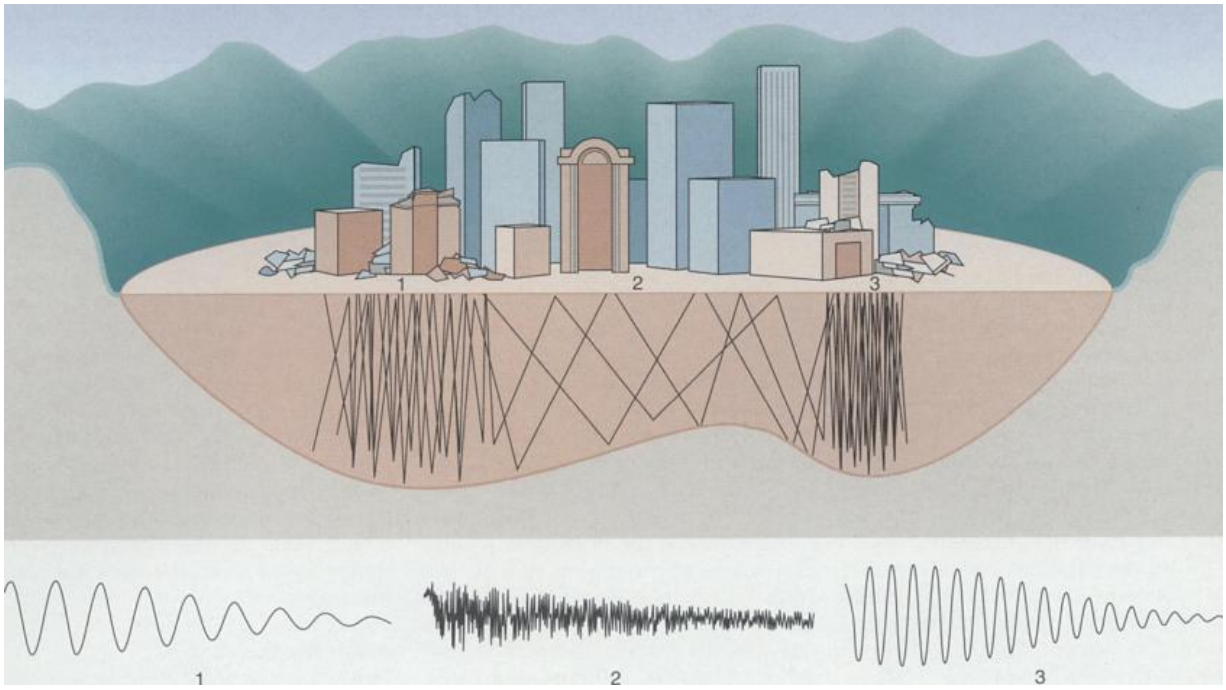

Figure 1.2. Example of seismic amplification within a sedimentary basin relating to basin floor topography (from Rial *et al.*, 1992).

1.2.2. Shallow Stratigraphy (<30 m Depth).

A site's ground motion depends on three key factors: the rupture characteristics (magnitude, depth, proximity), wave trajectory, and the local site conditions (Luzón *et al.*, 2002). Upon rupture, seismic waves travel outward at different trajectories; the geology, geomorphology, and topography will influence the intensity and duration of ground shaking, as well as the potential for amplification (Rial *et al.*, 1992; Luzón *et al.*, 2002). The shallow stratigraphy of a sedimentary basin is of greatest concern when considering seismic amplification, as this is the contact on which we typically develop. Soil layers 0 to 15 m deep have high levels of ground motion focusing at both the surface and near surface (Liu *et al.*, 2022), resulting in a significant hazard to both

surface and subsurface infrastructure. Each type of seismic wave can behave differently within a sedimentary basin. Studies have suggested that the degree of seismic amplification can be higher or lower depending on the wave type and the position within the basin (Wirth *et al.*, 2019).

1.2.3. Seismic Amplification within Sedimentary Layers.

Stratigraphy will vary between sedimentary basins due to differing processes and materials. Current methods used to differentiate strata within a sedimentary basin include horizontal to vertical spectral ratio (HVSR), surface wave methods (SWMs), geological boreholes, 2D and 3D seismic reflection data, and well logs. Data obtained from these methods can be used to create 1D, 2D, and 3D geological models.

1.2.3.1. Horizontal to Vertical Spectral Ratio (HVSR).

The HVSR is a passive-seismic method that makes use of 3-component broadband seismometers, often deployed in an array to increase accuracy and modelling confidence, recording the microtremors of the sedimentary infill that overlies a sedimentary basin's bedrock (Nakamura, 1989). The 3-component seismometers are oriented to magnetic North and typically record for 30 to 120 minutes, depending on the proximity to the basin edge, with the recording time increasing as depth increases. The HVSR method uses a well-defined peak to infer the location's fundamental site period down to a significant impedance contrast, typically the site's bedrock (Field *et al.*, 1990). A lower HVSR frequency, or longer wave period, indicates a greater depth to bedrock, whereas the reverse is valid for a higher frequency (Jeong & Wotherspoon, 2019). This method does not account for the differences in soil velocities and relies on a depth-velocity model for depth of basin calculation, which can have errors as great as 50% (Jeong & Wotherspoon, 2019).

1.2.3.2. Surface Wave Methods (SWMs).

SWMs can be broken into three sub-methods: active source, passive source, and inversion. SWMs record the shear wave velocity (V_S) profiles with respect to depth, where changes in V_S can imply a change in strata (Foti *et al.*, 2011). The active source method involves the recording of a source by an array of geophones at preset offsets, before being processed and cleaned (Socco & Strobbia, 2004). The passive source method records microtremor vertical motion through an array of geophones (Socco & Strobbia, 2004). The inversion methodology refers to the forward modelling of the collected data. Hundreds of thousands of models are rendered to create a line of best fit within the dispersion curves to show both the median V_S profile and potential errors and uncertainties.

1.2.3.3. Boreholes/Well-logs.

Boreholes combined with well-logs provide an incredibly detailed snapshot of the strata below the Earth's surface and, where multiple boreholes are used, can be linked to create extensively detailed geological models. Samples derived from a borehole can be subjected to a range of additional analyses, including X-radiographic imaging, X-ray-diffraction (XRD), X-ray-fluorescence (XRF), radiometric dating, grain size analysis, and biostratigraphy. Upon completion of the drilling, wireline loggers are descended to record information regarding the lithology and fluids present. Conventional well-log measurements include an acoustic, bulk density, natural gamma-ray, calliper, spontaneous potential, and neutron log (Lai *et al.*, 2022). The combination of these different methods and data increases the confidence of geological interpretations.

1.2.3.4. 2D and 3D Seismic Reflection Data.

Seismic profiles based on reflection data can accurately map depths kilometres thick and show differences in strata at resolutions as fine as 50 to 100 m thick (Mooney, 2021). These profiles are obtained by observing the behaviour of seismic waves travelling away from a source, through the subsurface strata, and how these waves change in velocity and amplitude at impedance contrasts (Mooney, 1989). The reflection data is then processed and interpreted by both the worker and the computer, and can be forward-modelled.

1.2.3.5. Seismic Models.

The creation and utilisation of accurate seismic models are regarded as among the most important issues in seismology and earthquake engineering fields (Qin *et al.*, 2012). Seismic models can be derived from either 1D, 2D, or 3D measurement techniques, where 1D employs data from a single source, 2D models utilise a series of measurements across a profile, and 3D data sets that include data obtained from a planar grid layout. The combination of 3D models and numerical modelling to solve complex wave equations has been suggested by Qin *et al.* (2012) to create accurate models that factor in a sedimentary basin's unique strata and physical characteristics.

1.2.4. Global Examples of Basin Amplification.

1.2.4.1. Mexico City – 1985.

In September 1985, two large (M_W7.5 to M_W8.1) shallow subduction fault earthquakes occurred along the subducting Cocos plate (beneath the North American plate). The epicentre was ~400 km from Mexico City and ~16 km deep (Chiang & Chang, 1991; Arciniega-Ceballos *et al.*, 2018; Mayoral *et al.*, 2019), and resulted in the loss of thousands of lives and buildings. Mexico City is

an interesting example of seismic amplification hazards, as the city is built on both hard rock and soft soil deposits, the latter originating from reclaimed land atop soft lake sediments known as the Lake Zones (Chiang & Chang, 1991; Mayoral *et al.*, 2019). The most significant damage to the city occurred within ~3 km of the Lake Zones (Chiang & Chang, 1991), where many buildings >5 storeys collapsed and peak ground acceleration was up to five times that of the Hill Zone (Chiang & Chang, 1991; Arciniega-Ceballos *et al.*, 2018; Mayoral *et al.*, 2019). The Lake Zone stratigraphy consists of a soft clay layer, interbedded with sandy silts and silty sands, up to 30 m thick that overlies a 4 m thick very dense sandy silt, which in turn rests upon a stiff clay layer up to a depth of 60 m (Chiang & Chang, 1991; Arciniega-Ceballos *et al.*, 2018; Mayoral *et al.*, 2019). The Hill Zone, areas within Mexico City overlying hard rock, consists of hard soils derived from volcanic tuffs and lava flows (Arciniega-Ceballos *et al.*, 2018).

1.2.4.2. Gorkha – 2015.

In April 2015, a M_W7.6 earthquake occurred ~15 km deep and ~80 km Northwest of Kathmandu, Nepal, resulting in more than 8,500 deaths (Tallett-Williams *et al.*, 2016). The Kathmandu Valley, an intermontane basin ~20 km wide (Pagliaroli, 2018), consists of irregular layers of uncemented fluvio-lacustrine sediments, up to 400 m deep in parts, including clays, silts, sands, gravels, and lignites (Tallett-Williams *et al.*, 2016; Pagliaroli, 2018). Particle grain sizes observed here are similar to the Hamilton Basin upper stratigraphy and could thus behave similarly during a seismic event. Particle grain sizes observed here are similar to the Hamilton Basin upper stratigraphy and could thus behave similarly during a seismic event. Seismic amplification within the Kathmandu Valley was observed during the 2015 earthquake at soft soil sites and showed an increase in long-period spectral acceleration (Pagliaroli, 2018). Despite the known seismic risk within the Kathmandu Valley, there had been few studies prior to this seismic event relating to the movement of the soft soils within, though it is now known that the subsoil conditions within the Kathmandu Valley were highly influential in how the ground responded to the seismic event

1.2.5. New Zealand Examples of Basin Amplification.

1.2.5.1. Canterbury, 2010/2011.

Two major earthquakes occurred in Canterbury in September 2010 (M7.1) and February 2011 (M6.3), which resulted in 185 deaths and billions in damage to the city of Christchurch (Bannister & Gledhill, 2012). Similar to the Hamilton Basin, the shallow stratigraphy of the Canterbury Basin is derived from low-strength sediments with depth to basement within Christchurch City ranging from 600 to 1200 m (Webb *et al.*, 2011). The seismic peaks and amplification within Christchurch

City, many of which exceeded the design spectra, have been linked to the Canterbury Basin's floor topography and sedimentary infill (Webb *et al*., 2011).

1.2.5.2. Cook Strait, 2013.

In July 2013, a series of earthquakes ranging from M_W5.5 to M_W6.6 occurred across the Cook Strait. Seismicity within the Cook Strait has typically occurred between depths of 6 to 18 km (Holden *et al*., 2013). Despite ground shaking being defined as moderately intense for a short period, several seismic monitoring sites within the Wellington region registered very high spiked responses, amplifications of ~1 second, likely due to basin resonance effects (Holden *et al*., 2013). Compared to other sites, sites overlying the reclaimed land beneath the Wellington Port received up to twice as intense ground shaking; high-rise buildings 6 to 12 storeys were the most impacted (Holden *et al*., 2013).

1.2.5.3. Kaikōura, 2016.

Located ~150 km from the earthquake source, the 2016 M_W7.8 Kaikōura earthquake significantly damaged mid-rise structures within Wellington City (NZSEE, 2021). Mid-rise buildings were damaged at a disproportionately high rate as 3D basin amplification effects were observed within the 1 to 2 second spectral interval periods; these spectral interval periods are of the most significant importance to mid-high rise buildings (Bradley *et al*., 2018). This seismic event caused notable damage and shows that fault movement does not need to be proximal to cause damage.

1.3. Earthquake Hazard in New Zealand.

1.3.1. New Zealand’s Major Fault Zones.

New Zealand, a seismically active country residing over the Australian and Pacific plates, experiences regular seismic events. The boundaries between the Australian and Pacific plates are not linear throughout New Zealand. South of the South Island and west of Stewart Island, the Australian plate subducts beneath the Pacific plate to form the Puysegur Subduction Front (Puysegur Trench), a convergent boundary (Lamarche & Lebrun, 2000). The West Coast of the South Island is marked by the Alpine Fault, a transform boundary responsible for the mountainous terrain of the Southern Alps. East of the North Island is a zone of convergence as the Pacific plate subducts beneath the Australian plate, forming the Hikurangi Subduction Front (Hikurangi Trough); this boundary is the key driver for the Taupo Volcanic Zone (Taupo Rift) (Cole & Lewis, 1981). These plate boundaries give rise to numerous faults and fault systems within New Zealand (Figure 1.3), though not all remain active, which pose significant seismic hazards. Active

faults within New Zealand must show evidence of displacement and/or deformation at the ground-to-surface interface within the last 125 ka (Seebeck *et al.*, 2022); the one exception is the Taupo Rift. Due to the rapid evolution of the Taupo Rift, present faults are defined as active regardless of whether there is evidence of movement within the past 25 ka (Seebeck *et al.*, 2022).

1.4. Hamilton Basin Seismic History.

There is little evidence of major faulting events in the Hamilton Basin, though recent studies have unearthed near-surface evidence of faulting within and near Hamilton City (Moon & de Lange, 2017; Spinardi *et al.*, 2017). One of the recently identified fault zones, the Horotiu Fault Zone, shows displacement of the Hinuera Formation, indicating that seismic activity occurred within the late Pleistocene (Moon & de Lange, 2017). The proximity to the Kerepehi Fault and these newly identified fault zones shows that the current seismic hazard to Hamilton City may need updating. The presence of new faults is important for seismological modelling as they may provide insights into the recurrence intervals of paleo seismic events and the intensity of said events; factors that previously would not have been considered and could change an areas known seismic hazard.

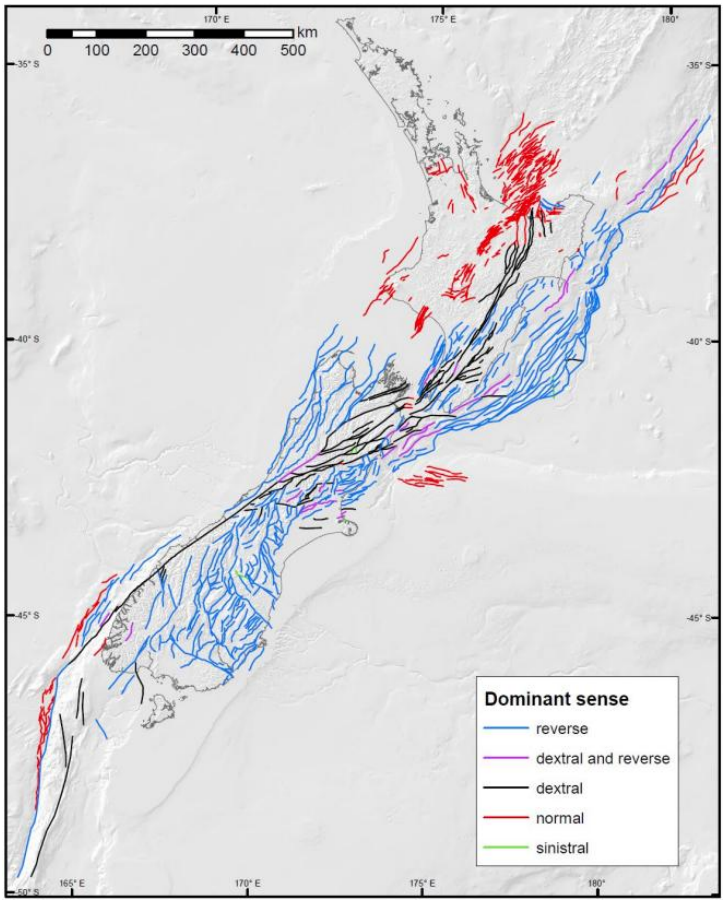

Figure 1.3. Fault zones identified within the NZCFM v1.0 are grouped by the fault zones' dominant sense of movement (from Seeback *et al.*, 2022).

1.4.1. Kerepehi Fault.

Extending NNW from the Taupo Rift and SSE across the Hauraki Plains, Hauraki Basin, the Kerepehi Fault has an onshore length of ~80 km and features six ruptures onshore and four offshore (Persaud *et al.*, 2016). Despite a recurrence interval of ~1000 years (~0.1% per year), the Kerepehi Fault has shown activity within the Holocene (Persaud *et al.*, 2016) and represents a significant seismic hazard for the surrounding regions. Previous fault scarps within the Kerepehi Fault range from 1 to 8 m in height; the fault is thought capable of triggering earthquakes ranging from M_W5.5 to M_W7.0, and up to M_W7.2 to M_W7.4 where all onshore fault segments rupture are once (Persaud *et al.*, 2016). Tauranga City could be subject to a maximum shaking of 6 to 7 on the Modified Mercalli Intensity Scale (MMI), while areas on the Hauraki Plains range from MMI 8 to MMI 9 (Persaud *et al.*, 2016). Were the Kerepehi Fault to rupture, Hamilton City is likely to experience a higher, degree of seismic activity, or lower in certain areas, up to two to three times more intense than other proximal cities due to overlying the Hamilton Basin (Dempsey *et al.*, 2021). The increased seismic motion in Hamilton City could exacerbate liquefaction potential and result in intense damage to multi-storey buildings, similar to the 2010/2011 Christchurch and 2016 Kaikōura Earthquake Sequences (Dempsey *et al.*, 2021).

1.4.2. Recently Identified Faults.

The two largest inferred faults within the Hamilton Basin that have high confidence are the Waipa Fault, a fault that runs NS along the western side of the basin (Kamp & Lowe, 1981), and the Taupiri Fault, a fault found shadowing the margin along the Hakarimata Ranges between Taupiri and Ngāruawāhia (Moon & de Lange, 2017). Until recently, the seismic hazard within the Hamilton Basin was considered low risk due to the lack of identified surface fault traces (Spinardi *et al.*, 2017). Recent developments in the north of Hamilton City have unearthed strong evidence, recently faulted tephra, of new fault zones within Hamilton City and the surrounding areas (Moon & de Lange, 2017; Spinardi *et al.*, 2017). These new fault zones are the Horotiu, Kukutaruhe, and Te Tatua o Wairere Fault Zones (Figure 1.4). The fault zone is characterised by steep, 51 to 84°, normal faulting, and does not show definitive evidence of movement within the last 350 ka (Spinardi *et al.*, 2017), except in one instance. Moon & de Lange (2017) found a section of the Horotiu Fault Zone that has displaced part of the Hinuera Formation, a significant find as the Hinuera Formation was deposited in the late Pleistocene. New rupture modelling for the Kerepehi Fault suggests that there will be a significantly stronger shaking intensity within Hamilton City during a seismic event (Moon & de Lange, 2017). The depths of these new faults and fault zones remain uncertain, despite the interpretation of seismic reflection data (Moon & de Lange, 2017).

It is important to note that the absence of depth data could impact current seismological models; therefore, such models may need to be updated once fault depths are obtained.

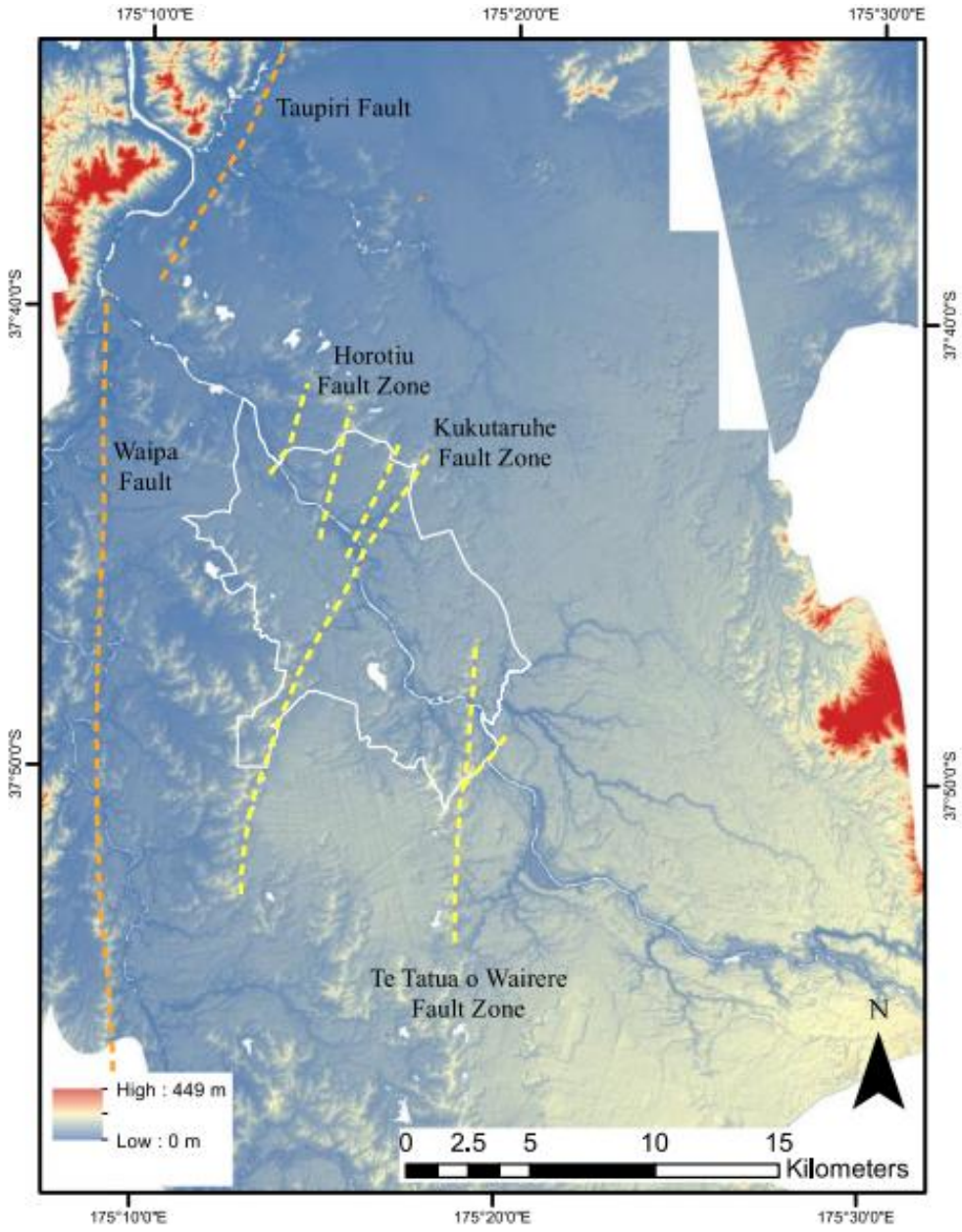

Figure 1.4. Inferred fault zones within the Hamilton Basin; the newly identified Horotiu, Kukutaruhe, and Te Tatua of Wairere fault zones within or proximal to Hamilton City (from Spinardi *et al.*, 2017).

1.4.3. Liquefaction.

Sediments deposited during the Holocene, especially recent sediments (<0.5 ka), have the highest liquefaction potential (Kleyburg *et al.*, 2015). Despite the Hinuera Formation being deposited during the late Pleistocene, CPT investigations have determined that there is a low to

high risk of liquefaction occurring during a seismic event (Kleyburg *et al.*, 2015; McKay, 2017). Unsurprisingly, the Hinuera Formation, with abundant peat, sand and silt, and combinations of the three, poses a liquefaction risk (McKay, 2017). Paleoliquefaction induced by seismic events has been identified as injection structures penetrating surrounding units (Kleyburg *et al.*, 2015). The greatest liquefaction risk within the Hamilton Basin is linked localised to areas with high water tables (Kleyburg *et al.*, 2015), such as in interfluves and floodplains (McKay, 2017).

1.5. Hamilton Basin Geological History.

1.5.1. Basin Formation.

Hamilton Basin, in the Waikato region, is a roughly oval-shaped depression that extends ~80 km north to south and ~40 km wide (Figure 1.5) and is almost entirely surrounded by mountain ranges up to 300 m high (Selby & Lowe, 1992). Several rivers and tributaries flow through the basin, the most notable being the Waikato River. Initial terrestrial and marine sedimentation began in the late Eocene (35 Ma) and resulted in the formation of the Te Kuiti Group (Selby & Lowe, 1992). During the Pliocene (~5.6 Ma), rhyolitic and andesitic volcanism occurred to the North in the Coromandel Peninsula, while andesitic and dacitic volcanism began along the Eastern ranges (Pirongia & Karioi); uplift in the lowlands also occurred during this period (Selby & Lowe, 1992). Volcanism continued into the mid-Quaternary (1.0 to 0.5 Ma) and resulted in the formation of ignimbrite sheets and the deposition of volcaniclastic alluvium (Selby & Lowe, 1992). The ancestral Waikato River flowed through the Hauraki Plains in the late Pleistocene before changing direction and flowing into the Hamilton Basin ~24 to 19 ka (Selby & Lowe, 1992). The Waikato River's change in direction allowed the fluvial deposition of volcaniclastic material that would later be defined as the Hinuera Formation. The basin has few known faults, with several suspected or inferred, including the Waipa Fault. The Waipa Fault runs North to South on the Western side of the Hamilton Basin; however, the exact location is unclear due to the overlying Pleistocene deposits (Kamp & Lowe, 1981). Recent research by Moon & de Lange (2017) has identified several new fault zones within the Hamilton Basin (Figure 1.4).

1.5.2. Basin Landforms and Geomorphology.

The surface geomorphology has undergone significant change over the last 100 ka. Present-day geomorphology can be divided into three distinct landforms: low rolling hills, alluvial plains, low terraces, and indistinct recent gullies (Lowe, 2010). The younger Hinuera Formation overlies and partially buries the significantly older low hills of the Walton Subgroup (Figure 1.6); these two units form the majority of the current landscape within the Hamilton Basin.

1.5.2.1. Low Rolling Hills (Hamilton Hills).

The Hamilton Hills are composed of a combination of ignimbrite, weathered clayey tephra, and alluvially derived gravelly clay, topped by a thin layer of silty tephra (Lowe, 2010). The deepest ignimbrites range from 10 to 20 m thick, with three distinct ignimbrites present. Originating from the Mangakino Volcanic Centre, the Ongatiti Ignimbrite erupted ~1.21±0.04 Ma (Houghton *et al.*, 1995) through a series of pyroclastic flows and is the oldest ignimbrite present within the Hamilton Hills. Kidnappers Ignimbrite erupted ~1.0 Ma from the Mangakino Volcanic Centre through a phreatomagmatic eruption that generated a fine-grained fall deposit, ~1200 km^3, as well as a widespread, non-welded ignimbrite (Cooper *et al.*, 2017). The Rocky Hill Ignimbrite also erupted ~1.0 Ma (Lowe, 2010), following shortly after a period of erosion, generating ~200 km^3 of partly-welded ignimbrite (Cooper *et al.*, 2017). Overlying these ignimbrites is a layer of weathered clayey tephra originating from the Kauroa Ash Formation (Lowe, 2010) and the Hamilton Ash. The Hamilton Ash was deposited 0.38±0.04 Ma (Lowe *et al.*, 2001), after a period of significant erosion in which the majority of the Kauroa Ash was lost, and comprises eight or nine separate ash beds (McCraw, 1967) ~1 to 3 m thick (McCraw, 1967; Lowe, 2010). The Karapiro Formation was deposited within the Hamilton Hills ~0.5 Ma and is derived from the erosion of older ignimbrites, resulting in a gravelly alluvial clay of variable thickness (Kamp & Lowe, 1981; Lowe, 2010).

1.5.2.2. Alluvial Plains.

The Alluvial Plains located within the Hamilton Basin are derived mostly from volcanogenic alluvium deposited in two distinct depositional periods by the ancient Waipa and Waikato Rivers, the latest of which concluded 16 to 12 ka (Schofield, 1965). The alluvial plain surface, or the Hinuera surface, shows a gentle vertical slope of ~1 m per 1 km of horizontal distance, with a series of paleochannels, low ridges/bars, and swales (Lowe, 2010). The very gentle slope is derived from an alluvial fan form originating from the Maungatautari Gorge (Sherwood, 1972; Lowe, 2010). The paths of both the Waikato and Waipa Rivers have changed within the last 100 ka, with the Waikato River showing a significant shift as its flow path transitioned from a high-energy braided river system to the current entrenched river, abandoning paleochannels and forming low terraces (Lowe, 2010).

1.5.2.3. Low Terraces.

The lowermost terraces bordering the Waikato River, up to 30 m high, are highly pumiceous and were deposited ~1.8 ka during a break-out flood event from a large-scale eruption originating in the Taupo Volcanic Zone (Lowe, 2010). As flood waters receded, large quantities of pumiceous

gravels were abandoned in the areas surrounding the Waikato River, ultimately forming the Taupo Pumice Alluvium.

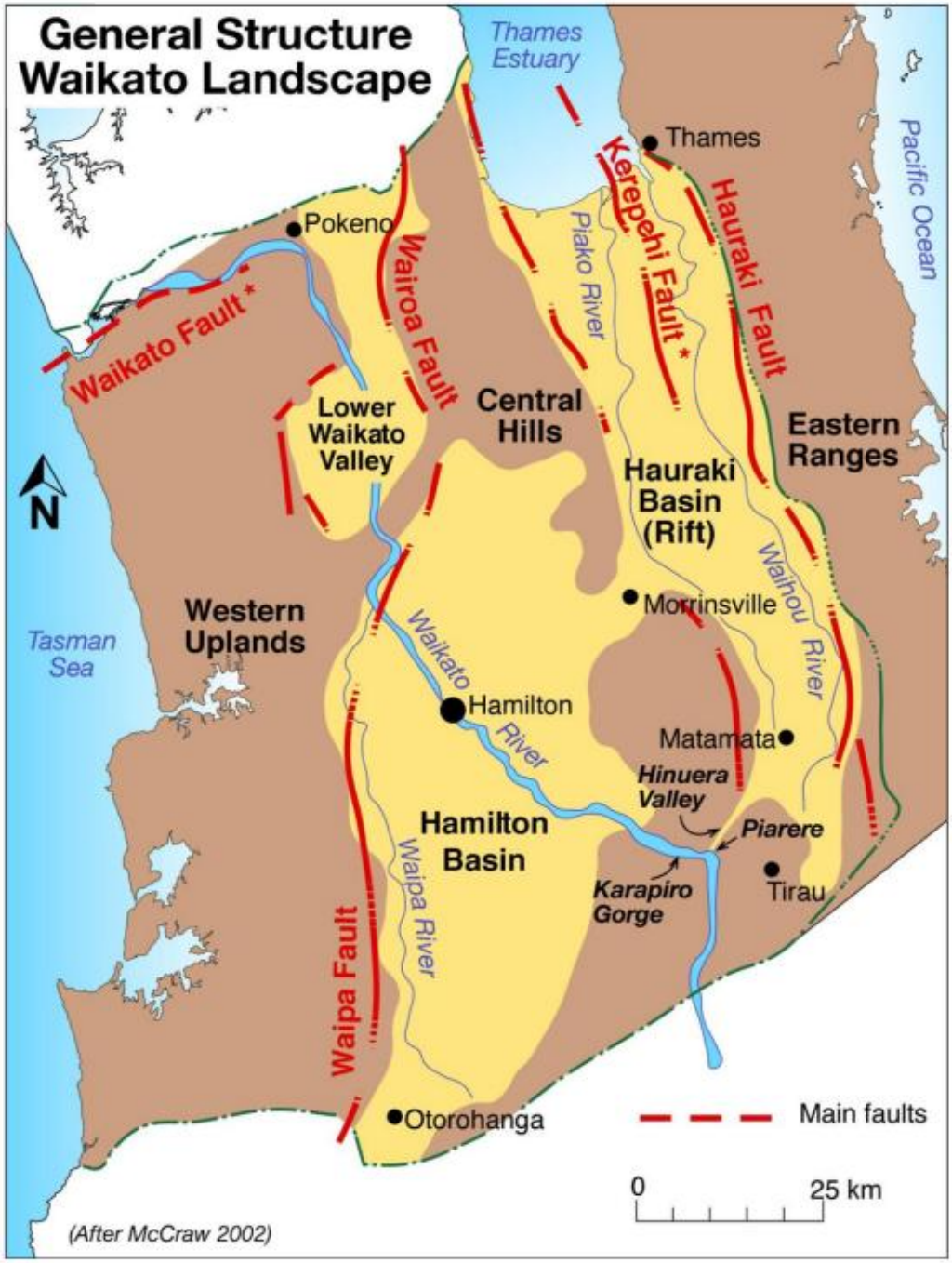

Figure 1.5. General structure and faulting of the Waikato landscape (from Lowe, 2010).

1.5.3. Tauranga Group.

Hamilton Basin has been infilled with Pleistocene to late Pleistocene alluvial sediments up to 300 m thick; these sediments are defined as the Tauranga Group (Sherwood, 1972; Petch & Marshall, 1988). The Tauranga Group, overlying the Waitemata Group, marks the beginning of terrestrial

deposition within the Quaternary period (Petch & Marshall, 1988), and comprises three Subgroups: the Frankton Subgroup, Walton Subgroup, and Piako Subgroup (Figure 1.7). The Frankton Subgroup will not be discussed further, as it lies sufficiently deep in the subsurface to have not been encountered in this study (>250 m deep) (Petch & Marshall, 1988). Overlying the Frankton Subgroup is the Walton Subgroup, which consists of three members: the Puketoka Formation, 2.40 to 1.63 Ma (Kear & Schofield, 1978), Waerenga Gravels, and the Karapiro Formation, ~0.50 Ma (Lowe, 2010). Sediments within the Walton Subgroup were predominantly deposited in either lacustrine or river environments (Selby & Lowe, 1992) and typically consist of gravel, clay, sand, and lignite (Henderson & Bartrum, 1913; Kear & Schofield, 1978).

Sediments from the most recent depositional period in the Hamilton Basin belong to the Piako Subgroup, which consists of the Hinuera Formation, Taupo Pumice Alluvium (TPA), and Undifferentiated Holocene Sediments (Petch & Marshall, 1988). Of the units within the Piako Subgroup, the Hinuera Formation is the most widespread, covering an area of approximately 2000 km^2 (Sherwood, 1972; Hume *et al.*, 1975), whereas the TPA is more localised and proximal to the Waikato River (Schofield, 1965).

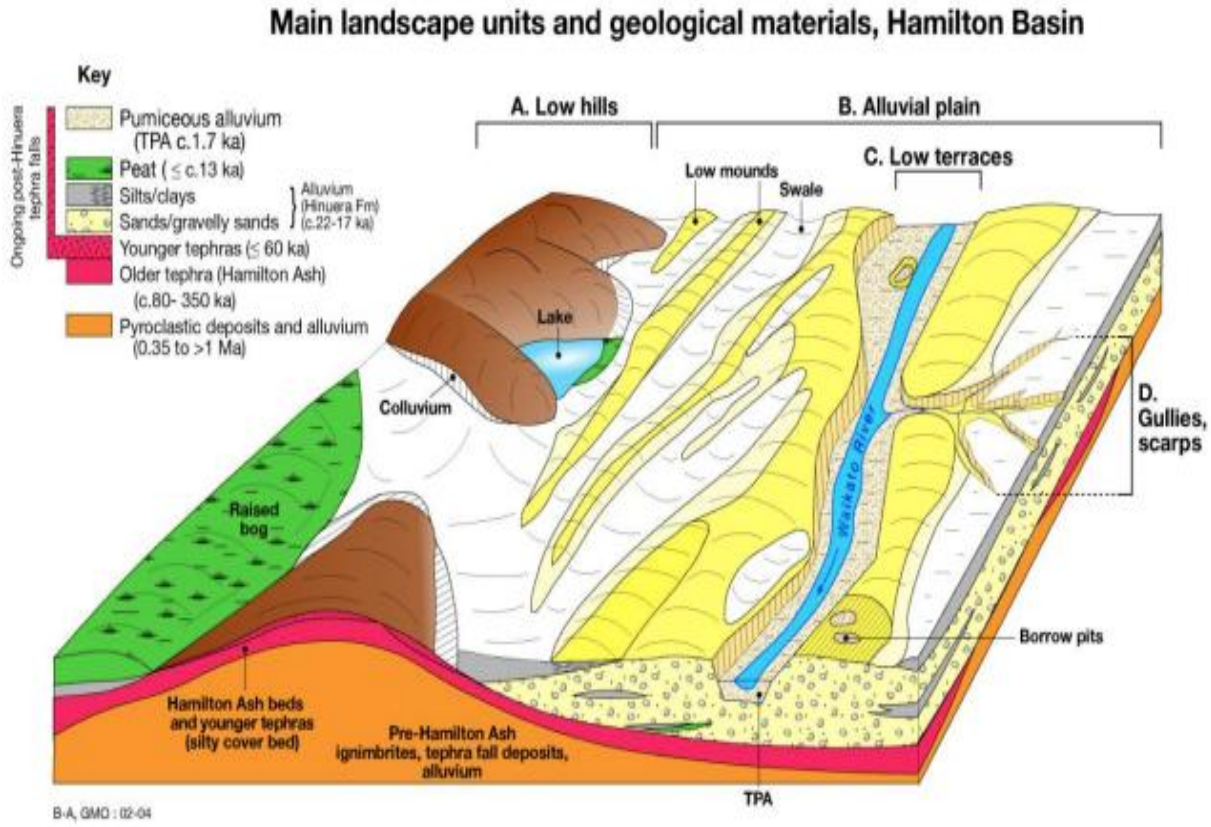

Figure 1.6. Idealised main landscape units and composition of geological units of the Hamilton Basin (from Lowe, 2010).

1.5.3.1. Walton Subgroup.

The Walton Subgroup, as defined by Kear & Schofield (1978), includes three units: the Puketoka Formation, Waerenga Gravels, and Karapiro Formation. Except for the Waerenga Gravels, these units differ significantly from the underlying Frankton Subgroup (Henderson & Bartrum, 1913). Henderson & Bartrum (1913) note that these differences are due to their highly pumiceous and rhyolitic composition. The majority of the Walton Subgroup was deposited during the Pleistocene as either lacustrine deposits or as meandering and braided river deposits, originating from the South Waikato and the surrounding mountain ranges on a low-relief, low-angled fan (Selby & Lowe, 1992). The sediments comprising the Walton Subgroup are terrestrial in origin, including gravel, sand, silt, clay, lignite, and portions of unconsolidated ignimbrite in the distal deposits, all of which are highly pumiceous (Henderson & Bartrum, 1913; Kear & Schofield, 1978). Upon cessation of deposition, fluvial erosion began to incise the surrounding landscape, forming hills and terraces tens of metres high (Selby & Lowe, 1992). The youngest member of the Walton Subgroup, the Karapiro Formation, is highly weathered in exposed sections, suggesting that the landscape remained relatively stable for thousands of years before deposition of the Hinuera Formation began (Selby & Lowe, 1992). These units are largely observed as low hills to the west and south-west of the Hamilton Basin, with one notable deposit in the eastern margin near the Hauraki Basin.

1.5.3.1.1. Puketoka Formation.

The Puketoka Formation was deposited during the late Tertiary to early Quaternary period (2.40 to 1.63 Ma) during a period of extreme acid volcanism and overlies the mudstones and lignites of the Whangamarino Formation (Battey, 1949; Kear & Schofield, 1978). First defined by Battey (1949), the Puketoka Formation consists of two distinct sediment types: a well-sorted pumice deposit originating from both lacustrine and fluviatile processes, bound by common beds, and a massive, unsorted deposit dominated by pumiceous material, with distal deposits including material derived from ignimbrite flows. Common deposits include highly pumiceous sand, silt, siltstone, and sandstone, and can be current-bedded, micro-bedded, or massive (Battey, 1949; Kear & Schofield, 1978).

1.5.3.1.2. Waerenga Gravels.

The Waerenga Gravels were not encountered during this investigation as the unit's deposition location was restricted to old valleys cut within the Pateroa Ranges and near the Waipuna Valley (Kear & Schofield, 1964). The Waerenga Gravels were formed during the Mesozoic Era and consist of highly weathered pebbles, typically derived from the Hokonui rocks, surrounded in a sandy to

sandy-clayey matrix (Kear & Schofield, 1964). The formation method of these gravels is unconfirmed; however, Selby & Lowe (1992) speculate that depositional fans extending from the surrounding Pateroa Range and Hokonui Rocks are the most likely method of deposition.

1.5.3.1.3. Karapiro Formation.

The Karapiro Formation was deposited during a period of extreme acid volcanism, spanning several deposition periods from the mid to late Pleistocene, and includes all sediments within the Walton Subgroup younger than the Puketoka Formation (Healy, 1946; Kear & Schofield, 1978). Presenting no thicker than a few metres (Lowe, 2010), the Karapiro Formation is most commonly found in the Hamilton Lowland and includes sand, silt, clay, gravel, grit, and sandstone, the colours of which are distinct from the similar Puketoka formation and range from pale white to pink, red, or brown, likely due to the deep weathering of ferromagnesian minerals (Healy, 1946; Kear & Schofield, 1978). Lithological structures observed within these terraces most commonly include current-bedded volcanic grits or massive, poorly sorted pumiceous and rhyolitic gravelly sands, the latter of which would be identical to the Hinuera Formation were it not for the degree of weathering within the Karapiro Formation. Less common deposits include boulder conglomerates, consisting of unweathered, subrounded greywacke and ignimbrite boulders within a quartz, pumice and sand matrix, and horizontally bedded subaqueous clay/pumiceous sand ash deposits with sparse greywacke pebble inclusions (Healy, 1946; Kear & Schofield, 1978).

1.5.3.2. Piako Subgroup.

Two main units are defined within the Piako Subgroup: the Hinuera Formation and the Taupo Pumice Alluvium. The Piako Subgroup also includes numerous recent, undifferentiated units, such as peat bogs and lacustrine sediments, and rarely aeolian-derived sediments (Kear & Schofield, 1978). The most recent deposition of the Hinuera Formation between 24 to 19 ka (Selby & Lowe 1992) and 16 to 12 ka (Schofield, 1965); the TPA was deposited ~1.8 ka (Kear & Schofield, 1978; Grant, 1985).

1.5.3.2.1. Hinuera Formation.

Deposited during the late Pleistocene, the Hinuera Formation extends from 60 m (Lowe, 2010) to 90 m (Kear & Schofield, 1964) in thickness and is most likely found within the Hamilton Basin and the Southern regions of the Hauraki Lowlands (Figure 1.8). The Hinuera Formation was deposited in the many sub-environments found within a braided river system atop an alluvial fan during two significant depositional phases (Sherwood, 1972; Hume *et al.*, 1975). Deposition of the Hinuera Formation prior to the Waikato River's change in flow direction, known as the Hinuera disjunction,

is classified as Hinuera-1 Surface, while the deposition that occurred after the disjunction is defined as the Hinuera-2 Surface (Schofield, 1965). The deposition of the younger Hinuera-2 Surface occurred between ~24 to 19 (Selby & Lowe, 1992) ka and ~16 to 12 ka (Schofield, 1965). The Hinuera Formation's sediments typically consist of volcanically derived quartz, plagioclase, pumiceous gravels, glass, and heavy minerals including hypersthene, magnetite, augite, biotite, epidote, and hornblende (Kamp & Lowe, 1981). The Hinuera Formation dominates the Hauraki Plains and is frequently observed in the Hamilton Lowlands between the Hamilton Hills (Hume *et al*., 1975).

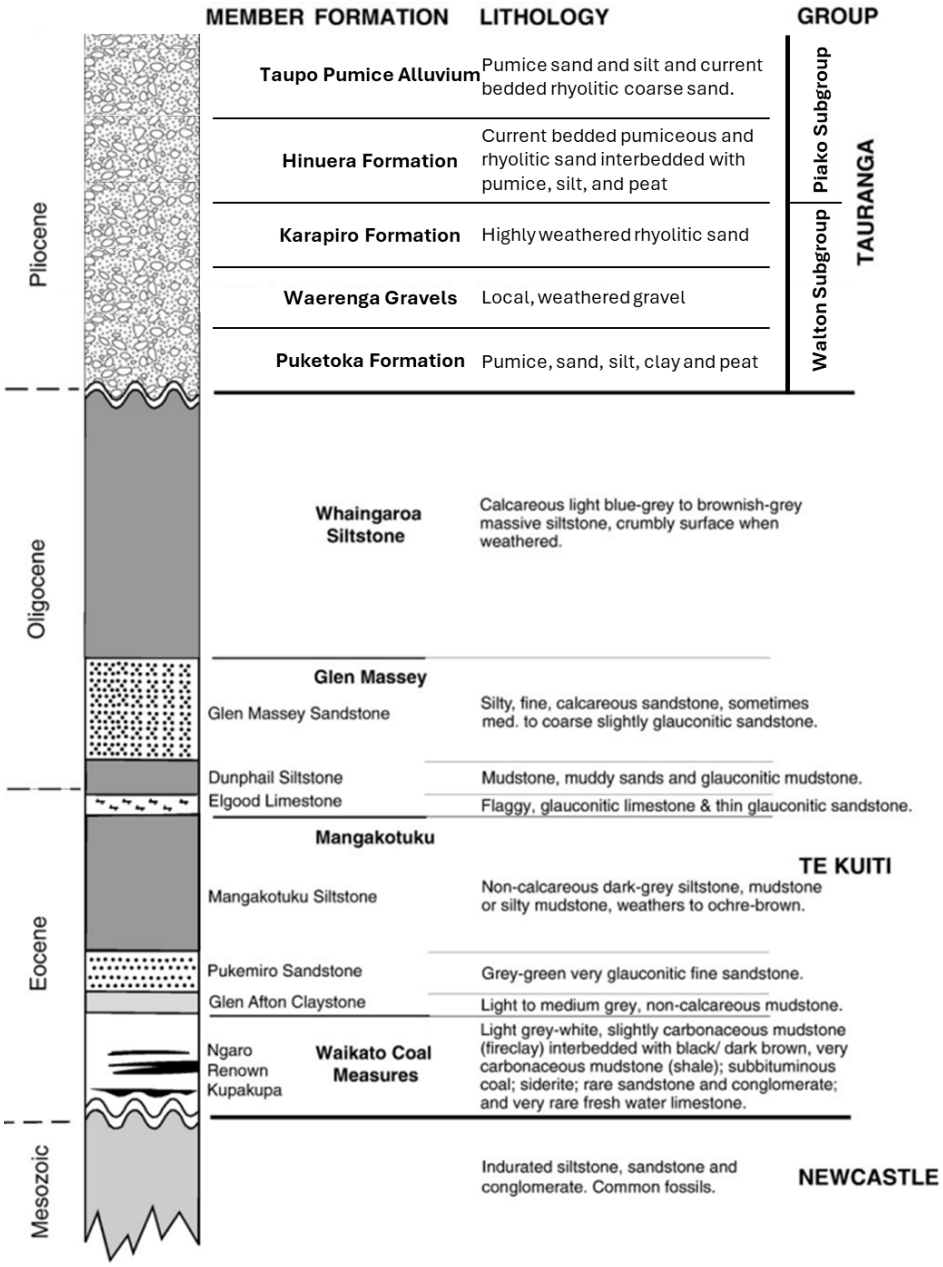

Figure 1.7. Stratigraphic Column of the Hamilton Basin (modified from Sherwood, 1972; Mares *et al*., 2009).

Despite the extensive variability in physical accessories across the Hinuera Formation (Schofield, 1965; Hume *et al.*, 1975), similar key physical characteristics are observed over a macro scale (Sherwood, 1972; Hume *et al.*, 1975) and present in five primary lithologies (layers one through five). Layer one dominates the Hinuera Formation and consists of a moderately to poorly sorted, cross-stratified, slightly gravelly quartzofeldspathic sand with rhyolitic and pumiceous gravels (Schofield, 1965; Hume *et al.*, 1975). Layer two shows a very poorly sorted, rhyolitic sandy gravel or gravelly sand, and is either horizontally stratified or structureless (Hume *et al.*, 1975); whereas layer three presents a cross-stratified, moderately well to well-sorted quartzofeldspathic sand (Schofield, 1965; Hume *et al.*, 1975). Layer four consists of a pumiceous silt, while layer five shows peat-rich beds (Hume *et al.*, 1975).

1.5.3.2.2. Taupo Pumice Alluvium (TPA).

The TPA deposits within the Hamilton Basin were deposited via the Waikato River during a breakout flood event from temporary lake formation (Kear & Schofield, 1978) and often directly overlie the earlier airfall deposits (Grant, 1985). With deposits up to ~30 m thick (Lowe, 2010), the TPA consists of two main units located proximal to the Waikato River terraces: the Melville Pumice and the Hopuhopu Sand. The Melville Pumice deposits consist of a well-bedded, rarely cross-bedded, creamy white pumice, ranging from a sand to sandy conglomerate, with inclusions of charcoal and pumice pebbles up to 5 cm in size (Kear & Schofield, 1978). The Hopuhopu sand is a current-bedded, coarse, gritty sand composed of quartz, ferromagnesian crystals, pumice clasts, and rhyolitic material (Kear & Schofield, 1978).

1.5.4. Kauroa & Hamilton Ash

Two strongly weathered, silicic-dominated, and clay-rich ash deposits are observed within the Hamilton Basin: the Kauroa Ash and Hamilton Ash. Deposited ~2.24 Ma through numerous depositional events, the Kauroa Ash is up to 12 m thick (Lowe *et al.*, 2001). The Hamilton Ash, 3 to 6 m thick (Tonkin, 1970), lies unconformably over the Kauroa Ash and was deposited 350 to 100 ka (Selby & Lowe, 1992; Lowe *et al.*, 2001) and consists of eight unique beds. Multiple recent (<50 ka) tephra units overlie the youngest of the Hamilton Ash beds (Selby & Lowe, 1992).

1.6. Physical Geological Unit Properties - Earthquake Modelling.

The physical properties, namely structure and clast size, are especially important for seismic modelling because of the responses these layers exhibit during seismic events. The Hinuera Formation would be particularly responsive to seismic stress due to the nature of the soft sediments found within. Soft sediment deformation occurs in fine-grained sand to mud,

unconsolidated to semi-unconsolidated, water-logged sediments (Lowe, 1975) are subjected to sufficient stress, such as an earthquake (Allen, 1986). These conditions are typically observed in shallow stratigraphy and are exacerbated where sediments were deposited rapidly and recently (Allen, 1986). As the formations introduced above are observed in the near-surface, the accurate description and interpretation of their physical characteristics are very important when developing a seismological model.

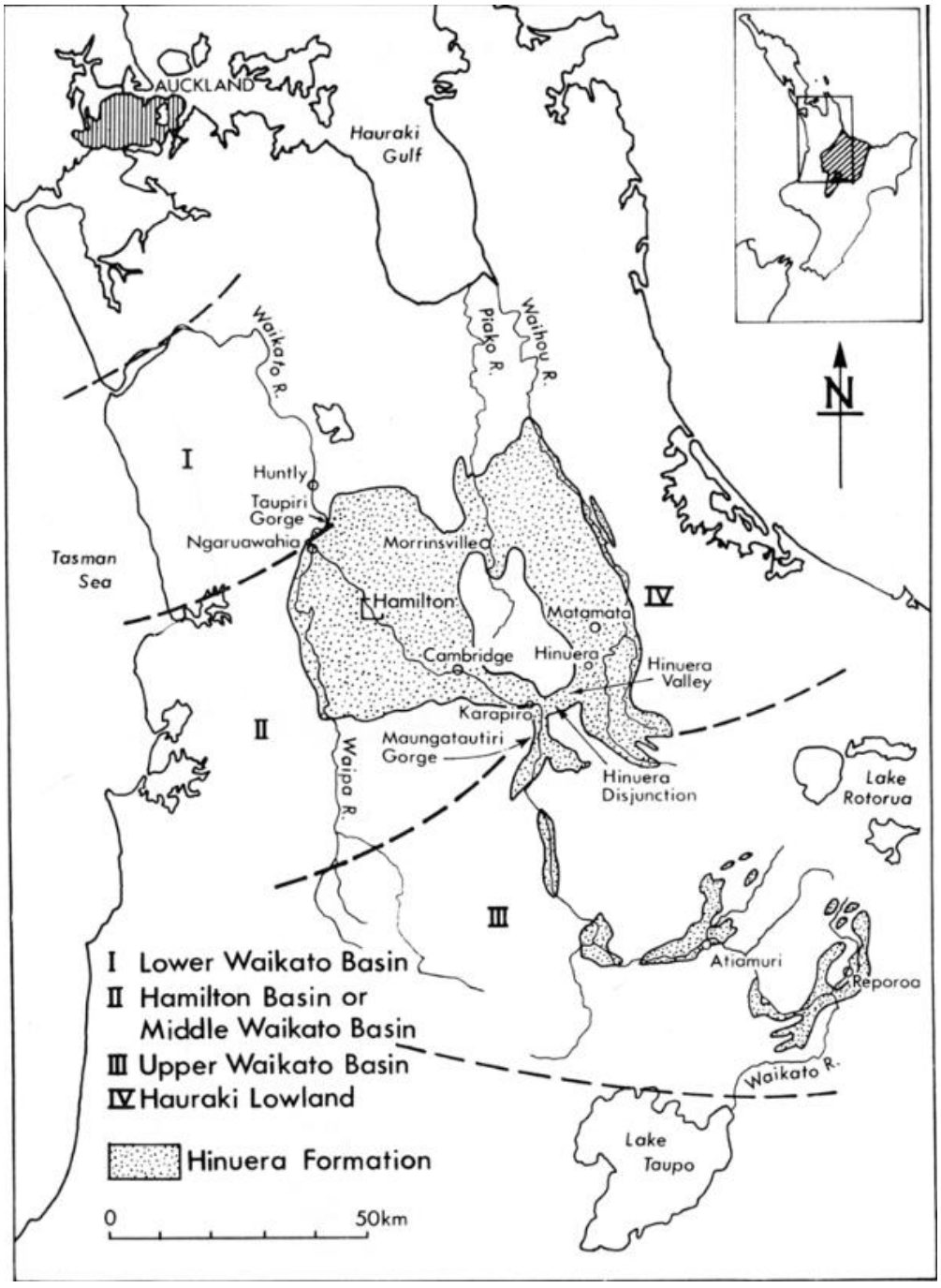

Figure 1.8. Hinuera Formation extent within the Hamilton and Hinuera basins (from Hume *et al.*, 1975).

1.7. Purpose of Study.

This investigation aims to examine a series of outcrops and cores in Hamilton City using a range of methods, including XRD, particle size analysis, photogrammetry, X-ray analysis of sedimentary structures, radiocarbon dating, and facies analysis. These methods will help determine the relevant paleoenvironments and physical processes at the time of deposition of the stratal infill in the Hamilton Basin, with an emphasis on the shallow stratigraphy (<30 m). The shallow stratigraphy is particularly important for earthquake engineering and infrastructure development. The results of this investigation are expected to be useful for informing earthquake modelling of the Hamilton Basin. The physical properties and structures of the geological units investigated are required to better inform future analysis and forward geological modelling, as these models will be unique to the Hamilton Basin; thus, the unique units found within will need to be accurately defined.

1.8. References.

Allen, J. R. L. (1986). Earthquake Magnitude-Frequency, Epicentral Distance, and Soft-Sediment Deformation in Sedimentary Basins. *Sedimentary Geology, 46*(1-2), 67-75. doi.org/10.1016/0037-0738(86)90006-0

Arciniega-Ceballos, A., Baena-Rivera, M., Sánchez-Sesma, F. J. (2018). The 1985 (M8.1) Michoacán Earthquake and Its Effects in Mexico City. In: Kruhl, J., Adhikari, R., Dorka, U. (eds) *Living Under the Threat of Earthquakes*. *Springer Natural Hazards*. Springer, Cham. doi.org/10.1007/978-3-319-68044-6_4

Bannister, S., Gledhill, K. (2012). Evolution of the 2010-2012 Canterbury Earthquake Sequence. *New Zealand Journal of Geology and Geophysics, 55*(3), 295-304. doi.org/10.1080/00288306.2012.680475

Battey, M. H. (1949). The Geology of the Tuakau-Mercer Area, Auckland. *Transactions and Proceedings of the Royal Society of New Zealand, 77*(3), 429-455.

Bradley B.A., Wotherspoon L.M., Kaiser A.E., Cox B.R., Jeong S. (2018). Influence of Site Effects on Observed Ground Motions in the Wellington Region from the M_w 7.8 Kaikōura, New Zealand, Earthquake. *Bulletin of the Seismological Society of America*, *108*(3B): 1722–1735. doi.org/10.1785/0120170286

Chiang, H. H., Chang, N. Y. (1991). Earthquake Ground Motion Amplification in Mexico City. *International Conferences on Recent Advances in Geotechnical Earthquake Engineering and Soil Dynamics, 9*.

Cole, J. W., Lewis, K. B. (1981). Evolution of the Taupo-Hikurangi Subduction System. *Tectonophysics, 72*(1-2), 1-21. doi.org/10.1016/0040-1951(81)90084-6

Cooper, G. F., Morgan, D. J., Wilson, C. J. N. (2017). Rapid Assembly and Rejuvenation of a Large Silicic Magmatic System: Insights from Mineral Diffusive Profiles in the Kidnappers and Rocky Hill Deposits, New Zealand. *Earth and Planetary Science Letters, 471*(1), 1-13. doi.org/10.1016/j.epsl.2017.05.036

Dempsey, D., Eccles, J. D., Huang, J., Jeong, S., Nicolin, E., Stolte, A., Wotherspoon, L., Bradley, B. A. (2021). Ground Motion Simulation of Hypothetical Earthquakes in the Upper North Island of New Zealand. *New Zealand Journal of Geology and Geophysics, 64*(4), 570-588. doi.org/10.1080/00288306.2020.1842469

Descartes, R. (1637/1912). *Discourse on Method, Optics, Geometry, and Meteorology* (P. J. Olscamp, Trans.). Indianapolis, IN: Bobbs-Merrill. *(Original work published 1637)*.

Feng, L., Ritzwoller, M. H. (2017). The Effect of Sedimentary Basins on Surface Waves That Pass Through Them. *Geophysics Journal International, 211*, 572-592. doi.org/10.1093/gji/ggx313

Field, E. H., Hough, S. E., Jacob, K. H. (1990). Using Microtremors to Assess Potential Earthquake Site Response: A Case Study in Flushing Meadows, New York City. *Bulletin of the Seismological Society of America, 80*(6), 1456-1480. doi.org/10.1785/BSSA08006A1456

Foti, S., Parolai, S., Albarello, D., Picozzi, M. (2011). Application of Surface-Wave Methods for Seismic Site Characterization. *Surveys in Geophysics, 32*, 777-825. doi.org/10.1007/s10712-011-9134-2

Grant, P. J. (1985). Major Periods of Erosion and Alluvial Sedimentation in New Zealand During the Late Holocene. *Journal of the Royal Society of New Zealand, 15*(1), 67-121.

Healy, J. (1946). Geology of the Karapiro District, Cambridge. *New Zealand Journal of Science and Technology, B27*(3), 199-217.

Henderson, J., Bartrum, J. A. (1913). The Geology of the Aroha Subdivision Hauraki, Auckland. *Bulletin (New Zealand Geological Survey), 16*.

Holden, C., Kaiser, A., Van Dissen, R., Jury, R. (2013). Sources, Ground Motion and Structural Response Characteristics in Wellington of the 2013 Cook Strait Earthquakes. *Bulletin of the New Zealand Society for Earthquake Engineering, 46*(4), 188-195. doi.org/10.5459/bnzsee.46.4.188-195

Houghton, B. F., Wilson, C. J. N., McWilliams, M. O., Lanphere, M. A., Weaver, S. D., Briggs, R. M., Pringle, M. S. (1995). Chronology and Dynamics of a Large Silicic Magmatic System: Central Taupo Volcanic Zone, New Zealand. *Geology, 23*(1), 13-16. doi.org/10.1130/0091-7613(1995)023<0013:CADOAL>2.3.CO;2

Hume, T. M., Sherwood, A. M., Nelson, C. S. (1975). Alluvial Sedimentology of the Upper Pleistocene Hinuera Formation, Hamilton Basin, New Zealand. *Journal of the Royal Society of New Zealand, 5*(4), 461-462.

Jeong, S., Wotherspoon, L. M. (2019). *Development of a Waikato Basin T_0 and Depth Model by the H/V Spectral Ratio Method*. Paper presented at the 2019 Pacific Conference on Earthquake Engineering and Annual NZSEE Conference, Christchurch, New Zealand.

Kamp, P. J., Lowe, D. J. (1981). Quaternary Stratigraphic, Landscape, and Soils of the Hamilton Basin. *Geological Society of New Zealand Miscellaneous Publication 29B*, pp. 14-28.

Kear, D., Schofield, J. C. (1964). Stratigraphic Summary, Ngāruawāhia Subdivision. *New Zealand Journal of Geology and Geophysics, 7*, 892-893.

Kear, D., Schofield, J. C. (1978). Geology of the Ngāruawāhia Subdivision. *New Zealand Geological Survey Bulletin, 88*, 1-168.

Kirkman, J. H. (1980). Mineralogy of the Kauroa Ash Formation of South-West and West Waikato, North Island, New Zealand. *New Zealand Journal of Geology and Geophysics, 23*(1), 113-120. doi.org/10.1080/00288306.1980.10424196

Kleyburg, M. A., Moon, V. G., Lowe, D. J., Nelson, C. S. (2015). Paleoliquefaction in Late Pleistocene Alluvial Sediments in Hauraki and Hamilton Basins, and Implications for Paleoseismicity. *Proceedings, 12th Australia New Zealand Conference on Geomechanics (ANZ 2015), 22-25 February, 2015, Wellington, pp. 524-531*.

Lai, J., Wang, G., Fan, Q., Pang, X., Li, H., Zhao, F., Li, Y., Zhao, X., Zhao, Y., Huang, Y., Bao, M., Qin, Z., Wang, Q. (2022). Geophysical Well-Log Evaluation in the Era of Unconventional Hydrocarbon Resources: A Review on Current Status and Prospects. *Surveys in Geophysics, 43*, 913-957. doi.org/10.1007/s10712-022-09705-4

Lamarche, G., Lebrun, J-F. (2000). Transition from Strike-Slip Faulting to Oblique Subduction: Active Tectonics at the Puysegur Margin, South New Zealand. *Tectonophysics, 316*(1-2), 67-89. doi.org/10.1016/S0040-1951(99)00232-2

Liu, Z., Qiao, Y., Cheng, X., Naggar, M. H. (2022). Nonlinear Seismic Response and Amplification Effect of 3D Sedimentary Basin Based on Bounding Surface Constitutive Model. *Soil Dynamics and Earthquake Engineering, 158*, 1-15. doi.org/10.1016/j.soildyn.2022.107292

Lowe, D.J. (2010). Introduction to the Landscapes and Soils of the Hamilton Basin. *In*: Lowe, D. J., Neall, V. E., Hedley, M., Clothier, B., Mackay, A. 2010. Guidebook for Pre-conference North Island, New Zealand 'Volcanoes to Oceans' field tour (27- 30 July). 19th World Soils Congress, International Union of Soil Sciences, Brisbane. *Soil and Earth Sciences Occasional Publication No. 3*, Massey University, Palmerston North, pp. 1.24-1.61.

Lowe, D. J., Tippett, J. M., Kamp, P. J. J., Liddell, I. J., Briggs, R. M., Horrocks, J. L. (2001). Ages on Weathered Plio-Pleistocene Tephra Sequences, Western North Island, New Zealand. *In*: Juvigné, E. T., Raynal, J-P. (Eds), "Tephras: Chronology, Archaeology", CDERAD éditeur, Goudet. *Les Dossiers de l'Archéo-Logis 1*, 45-60.

Lowe, D. R. (1975). Water Escape Structures in Coarse-Grained Sediments. *Sedimentology, 22*, 157-204. doi.org/10.1111/j.1365-3091.1975.tb00290.x

Luzón, F., Palencia, V. J., Morales, J., Sánchez-Sesma, F. J., García, J. M. (2002). Evaluation of Site Effects in Sedimentary Basins. *Física de la Tierra, 14*, 183-214.

Mares, T. E., Radliński, A. P., Moore, T. A., Cookson, D., Thiyagarajan, T., Ilavsky, J. Klepp, J. (2009). Assessing the Potential for CO_2 Adsorption in a Subbituminous Coal, Huntly Coalfield, New Zealand, Using Small Angle Scattering Techniques. *International Journal of Coal Geology, 77*, 54-68. doi/10.1016/j.coal.2008.07.007

Mayoral, J. M., Asimaki, D., Tepalcapa, S., Wood, C., Roman-de la Sancha, A., Hutchinson, T., Franke, K. Montalva, G. (2019). Site Effects in Mexico City Basin: Past and Present. *Soil Dynamics and Earthquake Engineering, 121*, 369-382. doi.org/10.1016/j.soildyn.2019.02.028

McCraw, J. D. (1967). The Surface Features and Soil Pattern of the Hamilton Basin. *Earth Science Journal, 1*(1), 59-74.

McKay, A. M. (2017). Evaluating Soil Landscape Models to Predict Liquefaction Susceptibility in the Hinuera Formation, Hamilton Basin (Thesis, Master of Science (MSc)). The University of Waikato, Hamilton, New Zealand. hdl.handle.net/10289/11635

Moon, V., De Lange, W. EQC. (2017). *Potential Shallow Seismic Sources in the Hamilton Basin*. (EQC 16/717).

Mooney, W. D., 1989, Seismic Methods for Determining Earthquake Source Parameters and Lithospheric Structure, *in* Pakiser, L. C., and Mooney, W. D., Geophysical framework of the continental United States: Boulder, Colorado, Geological Society of America Memoir 172.

Mooney, W. D. (2021). The Moho Discontinuity. *Encyclopedia of Geology, 2*, 732-743. doi.org/10.1016/B978-0-08-102908-4.00049-7

Nakamura, Y. (1989). A Method for Dynamic Characteristics Estimation of Subsurface Using Microtremor on the Ground Surface. *Quarterly Report of RTRI, 30*(1), 25-33.

Pagliaroli, A., Aprile, V., Chamlagain, D., Lanzo, G., Poovarodom, N. (2018). Assessment of Site Effects in the Kathmandu Valley, Nepal, During the 2015 M_W 7.8 Gorkha Earthquake Sequence Using 1D and 2D Numerical Modelling. *Engineering Geology, 239*, 50-62. doi.org/10.1016/j.enggeo.2018.03.011

Petch, R. A., Marshall, T. W. (1988). Ground Water Resources of the Tauranga Group Sediments in the Hamilton Basin, North Island, New Zealand. *Journal of Hydrology, 27*(2), 81-98. jstor.org/stable/43944613

Persaud, M., Villamor, P., Berryman, K. R., Ries, W., Litchfield, N., Alloway, B. V. (2016). The Kerepehi Fault, Hauraki Rift, North Island, New Zealand: Active Fault Characterisation and Hazard. *New Zealand Journal of Geology and Geophysics, 59*(1), 117-135. doi.org/10.1080/00288306.2015.1127826

Qin, Y., Wang, Y., Takenaka, H., Zhang, X. (2012). Seismic Ground Motion Amplification in a 3D Sedimentary Basin: The Effect of the Vertical Velocity Gradient. *Journal of Geophysics and Engineering, 9*, 761-772. doi.org/10.1088/1742-2132/9/6/761

Rial, J. A., Saltzman, N. G., Ling, H. (1992). Earthquake-Induced Resonance in Sedimentary Basins. *American Scientist, 80*(6), 566-578. jstor.org/stable/29774781

Schofield, J. C. (1965). The Hinuera Formation and Associated Quaternary Events. *New Zealand Journal of Geology and Geophysics, 8*(5), 772-791. doi.org/10.1080/00288306.1965.10422116

Seebeck H., Van Dissen R. J., Litchfield N. J., Barnes P. M., Nicol A., Langridge R. M., Barrell D. J. A., Villamor P., Ellis S. M., Rattenbury M. S., Bannister S., Gerstenberger M. C., Ghisetti F., Sutherland R., Fraser J., Nodder S. D., Stirling M. W., Humphrey J., Bland K. J., Howell A., Mountjoy J. J., Moon V., Stahl T., Spinardi F., Townsend D. B., Clark K. J., Hamling I. J., Cox S. C., de Lange W., Wopereis P., Johnston M., Morgenstern R., Coffey G. L., Eccles J. D., Little T. A., Fry B., Griffin J., Townend J., Mortimer N., Alcaraz S. A., Massiot C., Rowland J., Muirhead J., Upton P., Hirschberg H., Lee J. M. (2022). New Zealand Community Fault Model – Version 1.0. Lower Hutt (NZ): *GNS Science*, 96 p. (GNS Science report; 2021/57).

Selby, M. J., Lowe, D. J. (1992). The Middle Waikato Basin and Hills. *Landforms Of New Zealand, 2*, 233-255.

Sherwood, A. M. (1972). Sedimentary Structures, Features, and Paleoenvironments of the Hinuera Formation. [Thesis, University of Waikato]. Research Commons.

Socco, L. V., Strobbia, C. (2004). Surface-Wave Method for Near-Surface Characterization: A Tutorial. *Near Surface Geophysics, 2*(4), 165-185. doi.org/10.3997/1873-0604.2004015

Spinardi, F., Campbell, B. R., Moon, V., Pittari, A., Fox, B. R. S., de Lange, W. (2017). Unravelling Fault Structures of the Hamilton Basin. *Proc. 20th NZGS Geotechnical Symposium*. Eds. GJ Alexander & CY Chin, Napier.

Tallett-Williams, S., Ghosh, B., Wilkinson, S., Fenton, C., Burton, P., Whitworth, P., Datla, S., Franco, G., Trieu, A., Dejong, M., Novellis, V., White, T., Lloyd, T. (2016). Site Amplification in the Kathmandu Valley During the 2015 M7.6 Gorkha, Nepal Earthquake. *Bulletin of Earthquake Engineering, 14*, 3301-3315. doi.org/10.1007/s10518-016-0003-8

Tonkin, P. J. (1970). Contorted Stratification with Clay Lobes in Volcanic Ash Beds, Raglan – Hamilton Region, New Zealand. *Earth Science Journal, 4*(2), *129-140*.

Webb, T. H., Bannister, S., Beaven, J., Berryman, K., Brackley, H., Cousins, J., Fry, B., Gerstenberger, M., Holden, C., Kaiser, A., McSaveney, E., McVerry, G., Pettinga, J., Reyners, M., Rhoades, D., Somerville, P., Stirling, M., Van Dissen, R., Villamor, P., Wallace, L., Zhao, J. (2011). The Canterbury Earthquake Sequence and Implications for Seismic Design Levels. *GNS Science*, 88 p. (GNS Science Consultancy Report; 2011/183).

Wotherspoon, L., Hayden, C., Stolte, A., Bradley, B., Lee, R., Jeong, S., & Kaiser, A. (2020). *'Rapid' Geophysical Characterisation of New Zealand Sedimentary Basins Using the Horizontal-to-Vertical Spectral Ratio Method* (Version 1.0; EQC Report No. 18/761). Earthquake Commission.

Wirth, E. A., Vidale, J. E., Frankel, A. D., Pratt, T. L., Marafi, N. A., Thompson, M., Stephenson, W. J. (2019). Source-Dependent Amplification of Earthquake Ground Motions in Deep Sedimentary Basins. *Geophysical Research Letters, 46*, 6443-6450. doi.org/10.1029/2019GL082474

2. Chapter Two – Facies Analysis and Stratigraphy of Shallow Strata in Hamilton Basin.

2.1. Introduction.

2.1.1. Hamilton Basin – Paleobasin to Present Day.

Located within the Waikato region, the Hamilton Basin is a roughly oval-shaped depression that extends ~80 km north to south and ~40 km wide east to west (Selby & Lowe, 1992). Terrestrial and marine sedimentation in the Hamilton Basin began ~35 Ma, and rhyolitic, andesitic, and dacitic volcanism has been occurring since ~5.6 Ma; uplift in the lowlands also occurred during this period (Selby & Lowe, 1992). Volcanism continued until ~1.0 to 0.5 Ma, resulting in ignimbrite sheets and volcaniclastic alluvium, the latter being deposited via the Waipa and Waikato rivers (Selby & Lowe, 1992). The Waipa Fault runs NS along the western side of the basin (Kamp & Lowe, 1981), and the Taupiri Fault traces the margin of the Hakarimata Ranges (Moon & de Lange, 2017). Recently discovered faults include the Horotiu, Kukutaruhe, and Te Tatua o Wairere Fault Zones; their last movement and depth remain undetermined (Moon & de Lange, 2017; Spinardi *et al.*, 2017).

Current basin geomorphology (Figure 2.1) includes low hills (Walton Subgroup), alluvial plains (Hinuera Formation), low terraces (Taupo Pumice Alluvium), and recent gullies, with the formerly braided, now entrenched, Waipa and Waikato rivers flowing south to north. The Walton Subgroup's units typically consist of terrestrially derived, highly pumiceous, gravel, sand, clay, lignite, and unconsolidated ignimbrite (Henderson & Bartrum, 1913; Kear & Schofield, 1978); the Hinuera Formation (<90 m thick) consists of gravel, sand, silt, peat, and pumice (Schofield, 1965; Hume *et al.*, 1975); the Taupo Pumice Alluvium (TPA) (<30 m thick) (Lowe, 2010), presents as two main units, the Melville Pumice and Hopuhopu Sand, and comprises of pumice, sand, and sandy conglomerates (Kear & Schofield,1978).

2.1.2. Study Area.

The area investigated in this study is the Hamilton City Central Business District (CBD) and the proximal section(s) of the Waikato River (Figure 2.2). Hamilton City, the fourth-most populous city in New Zealand, covers 110 km^2 and lies atop the Hamilton Basin. The outcrop investigated is located at 37°45'45.26" S 175°15'54.51" E, core 20-1006 at 37°46'45.94" S 175°16'34.52" E, core 21-0437 at 37°47'00.14" S 175°16'47.68" E, and core Ferrybank at 37°47'20" S 175°17'12.31" E.

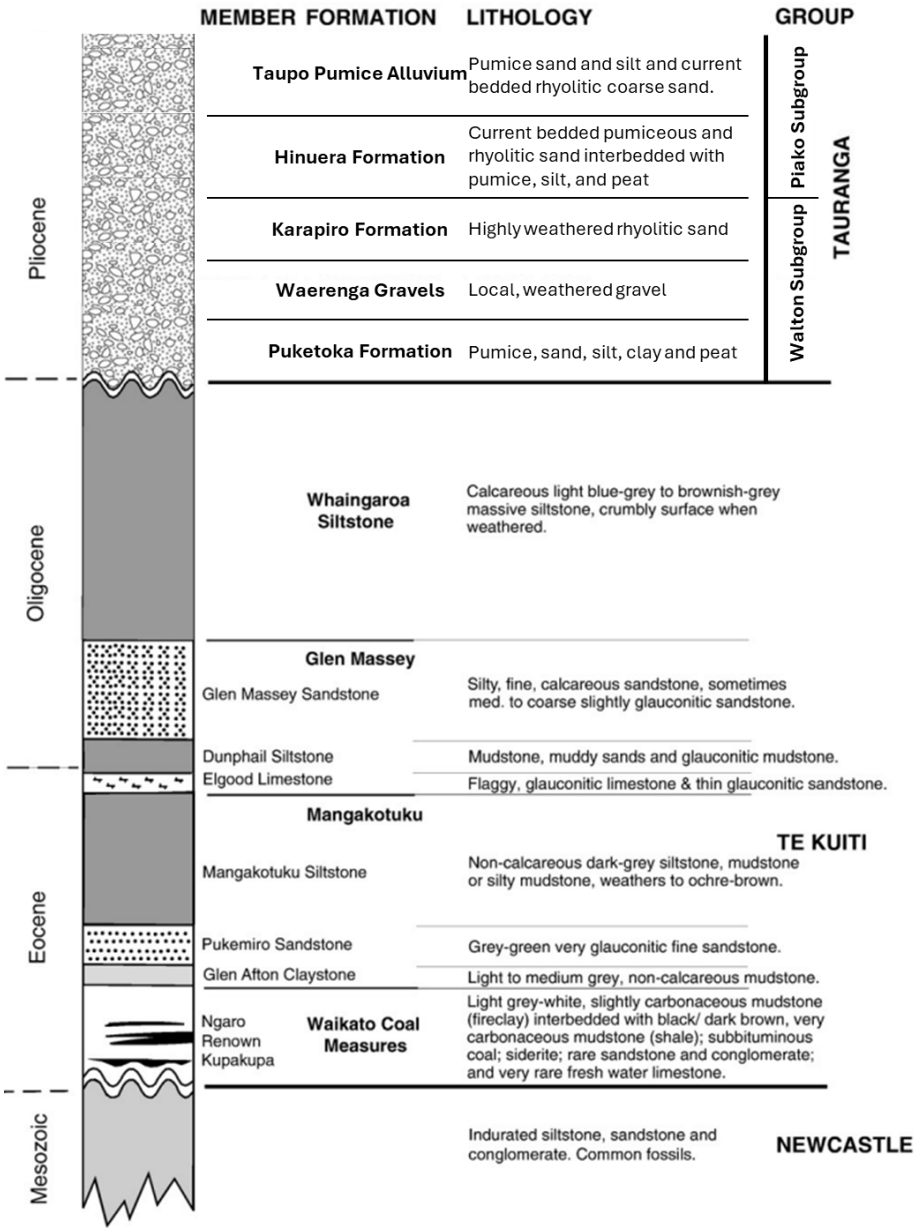

Figure 2.1. Stratigraphic Column of the Hamilton Basin (modified from Sherwood, 1972, and Mares *et al*., 2009).

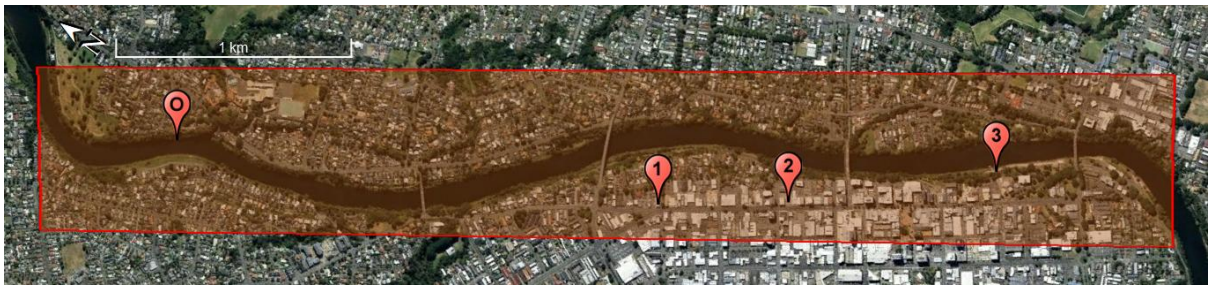

Figure 2.2. Study area, focusing on the Hamilton CBD, located atop the Hamilton Basin. 1) 20-1006. 2) 21-0437. 3) Ferrybank. O) Outcrop.

2.1.3. The Problem.

Quality and abundant data must be obtained to facilitate the creation of a representative geologically derived three dimensional (3D) seismic model, which will likely need to be upscaled using the methods discussed. One potential data source to be considered is publicly available geotechnical borehole data from the New Zealand Geotechnical Society (NZGS) database. Accurate classification of a sediment's physical characteristics is important when modelling a soil's response to seismic stress, as soils with differing characteristics will behave differently; thus, the characteristics of the shallow stratigraphy must be defined. The current seismic hazard and potential for seismic amplification will also be discussed, along with whether any recent assessments are considering newly identified faults and fault zones.

2.2. Dataset and Methods.

This study focused on three sediment cores and one outcrop, which were examined using particle size analysis, X-ray diffraction (XRD), radiocarbon dating, structural analysis, and structure-from-motion 3D models. Facies-driven descriptions were determined using samples derived from the three sediment cores, and the outcrop was profiled using an Unmanned Aerial Vehicle (UAV).

2.2.1. Facies.

The facies descriptions presented in this study were based on the physical characteristics observed in each core, including grain size, colour (Munsell Colour Chart), mineralogy, and sedimentary structures. Clast sizes were obtained by a Mastersizer 3000 after pre-treatment that included oven-drying, sieving finer particles (<2 mm), and H_2O_2 to remove organics. Field-moist samples were then defined using the Munsell Colour Chart, noting their hue, value, and chroma. A Cubex-50 X-ray was utilised to examine the cores' structure; note that the core box showed linear lines, which were disregarded. After further pre-treatment, including oven-drying and pulverisation, XRD was used to determine the mineralogical composition, with peaks assigned using HighScore Plus. Where no peaks were identified, the sample was defined as non-crystalline/amorphous.

2.2.2. Outcrop.

Prior to field investigation, an extensive desktop study utilised ArcGIS and Google Earth to determine safe and legal survey locations; one section was identified, and a Notice to Airmen (NOTAM) was issued for two surveys conducted in November 2024 and January 2025. Manual flight paths with sufficient image overlap (>80%) allowed a Phantom 4 UAV to conduct the survey.

Pix4D created 3D orthomosaics from the georeferenced images; these images were key to the classification and measurement of the strata encountered. Polylines were selected as the best measurement tool due to the ability to consider variations in the face of a bluff's topography.

2.2.3. Radiocarbon Dating.

Several samples that showed high organic matter, e.g. rootlets, peat, wood, and charcoal, were subsampled for radiocarbon dating. Samples were oven-dried at 105 °C for 24 to 48 hours at the request of the University of Waikato Radiocarbon Dating Laboratory. After processing, samples were dated by accelerator mass spectrometry (AMS). Due to the half-life of C^{14}, samples deposited more than ~50,000 years ago cannot be dated using this method.

2.3. Results and Interpretations.

2.3.1. Facies.

Structureless sediments were most commonly observed during analysis; when structure was present, it included cross-bedding, current-ripple lamination, and planar bedding (Figure 2.3). As noted earlier, the boxes housing the cores showed fine horizontal lines during X-ray analysis and should thus be ignored. All textural groups included structureless beds; sand and mud variants also included cross-bedding, current-ripple lamination, and planar bedding, while organic units were observed as either structureless or planar-bedded (Table 2.1). Sediment contacts were abrupt, erosional and gradational. All facies, save for the organic F6A/B, included pumice, ranging from highly weathered pumiceous sand to unweathered to slightly weathered pebbles. The sedimentary environments interpreted from these facies were typical of a braided river system and are discussed in depth below.

2.3.1.1. Facies One (F1).

Facies 1 presents as a structureless muddy to sandy gravel. Granules and pebbles dominate; mud and sand are also present. No structure was observed. These structureless layers are 0.30 to 2.50 m thick; the basal contact is typically abrupt, and the upper contact is a normal gradational boundary. Gravel composition is both pumiceous and rhyolitic. No lithological accessories or fossils were identified. Occurs abruptly over F2 (structureless sandy mud to muddy sand) and F6A (structureless to planar-bedded coal) and gradationally under F2.

Strong currents are required to move coarse-grained materials, like those observed in this facies. During high-energy events, finer particles can be eroded from the channel base, leaving coarser

Table 2.1. Detailed descriptions and interpretations of the seven facies observed within the Hinuera Formation and Walton Subgroup.

Facies Association	Facies	Grain Size	Package Thickness	Contact(s)	Physical Structures	Physical Accessories	Sedimentary Environment
FA1: Braided River System	**F1:** Structureless, muddy sandy gravel	Granules to pebbles, medium to coarse-grained sand.	0.30-2.50 m	Abrupt, gradational	Structureless	Pumice	Lag deposit or channel base
	F2: Structureless, sandy mud to muddy sand	Fine to coarse-grained silt, very fine to coarse-grained sand; occasional to some granules and pebbles	0.05-5.00 m	Abrupt, gradational, erosional	Structureless	Pumice	Abandoned channel
	F3: Current-ripple laminated to cross-bedded muddy sand	Very fine to medium-grained sand; occasional granules and pebbles	0.05-0.65 m	Abrupt, erosional	Current ripple lamination, cross-bedded	Pumice	Fluvial channel
	F4: Planar-bedded, sandy mud to muddy sand, organic sand	Medium to coarse-grained silt, very fine to medium-grained sand; occasional granules and pebbles	0.30-0.70 m	Abrupt, gradational	Planar-bedded, rarely interbedded with planar-bedded organic sand	Pumice	Levee deposit or floodplain
	F5: Current-ripple laminated to cross-bedded sandy mud	Fine to coarse-grained silt, very fine to fine-grained sand; occasional granules and pebbles	0.05-0.45 m	Abrupt, erosional	Current ripple lamination, cross-bedded	Pumice	Fluvial bar
	F6A: Peat	Very fine-grained silt to medium-grained sand	0.15-0.20 m	Abrupt, gradational	Structureless, planar-bedded	Rootlets, charcoal, wood	Floodplain or floodplain lake
	F6B: Coal	Coarse-grained silt to very fine-grained sand	0.05-0.70 m	Abrupt, gradational	Structureless, planar-bedded	-	Floodplain or floodplain lake
FA2: Volcanic Eruption	**F7:** Ignimbrite	Very fine to fine-grained sand, pumiceous granules and pebbles	10.40 m	Abrupt	Massive	Pumice, lithics, glass	-

Note: Colour present is defined for each unique facies.

material. Where the flow strength is sufficiently strong, coarse-grained sediments will also move. The coarse-grained material in this facies suggests deposition in an area of high energy, while the fine-grained material suggests periods of lower energy that allowed these finer sediments to accumulate in the gravel's pore space. Miall (1977) notes that structureless gravel with a sand and mud matrix, similar to this facies, would be deposited as a channel lag deposit.

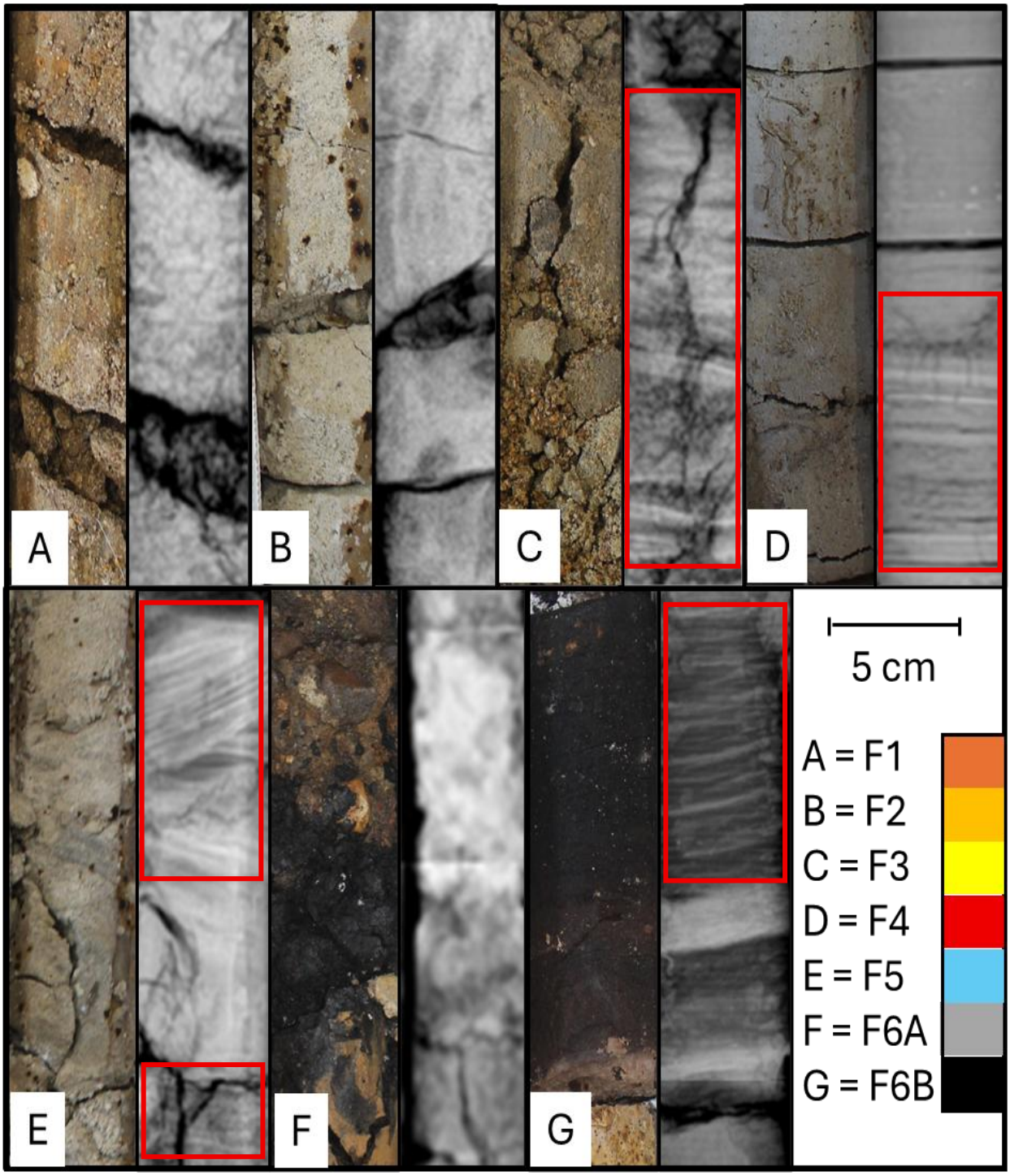

Figure 2.3. Examples of the six, excluding F7, recurring sedimentary facies observed in cores 20-1006, 21-0437, and Ferrybank. Structure, where present, is shown in red boxes.

2.3.1.2. Facies Two (F2).

Facies 2 occurs as structureless layers of sandy mud to muddy sand. Structureless layers of fine to coarse-grained silt and very fine to coarse-grained sand with uncommon granules and pebbles. Thickness ranges from sub-decimetre (~0.05 cm) to meter-scale (<5.00 m), with abrupt, gradational, and erosional contacts. Occasional gravels are both pumiceous and rhyolitic. No lithological accessories or fossils were identified. Facies 2 was the dominant facies encountered and shared boundaries with all other facies encountered.

The sandy mud and muddy sand observed in this facies lack internal structure and would thus have been dumped rapidly as a channel flow winnowed or ceased, either permanently, as observed in channel abandonment, or temporarily, as a channel avulsion in flooding events (Bridge, 2006). As the channel is abandoned, through one of the processes above, bedload sediments would be rapidly deposited due to the slowing of the river's flow; where the flow winnows or ceases for sufficient time, suspended finer sediments would also be deposited. Abandoned channels are known to alternate between abandonment and activity (Ferguson & Werritty, 1983; Bridge, 2003), allowing for the repeated deposition of structureless sediments similar to those in this facies (Bridge, 2006).

2.3.1.3. Facies Three (F3).

Facies 3 consists of prominent cross-bedded and current-ripple laminated sand. This facies is dominated by very fine to medium-grained sand with occasional granules and pebbles. Thickness ranges from sub-decimetre (~0.05 cm) to half metre scale (0.65 m) with abrupt and erosional contacts. Current ripple laminations are millimetre- to centimetre-scale; cross-bed thickness ranges from millimetre-scale to less than 10 cm. Occasional gravels are both pumiceous and rhyolitic. No lithological accessories or fossils were identified. Occurs as erosional and abrupt over and under F2 (structureless sandy mud to muddy sand) and F5 (current-ripple laminated to cross-bedded sandy mud) and abrupt over F7 (ignimbrite).

The coarse-grained, fine to medium-grained sand and granules and pebbles, sediment indicate that this facies was deposited in a high-energy environment; this is further reinforced by the cross-bedding observed. The channels' flow would have needed to be strong enough to move coarse sediment and to incise existing deposits as channel migration occurs. The current-ripple lamination provides further confidence in these observations, as Sing (1972) notes that cross-bedded sediments are often observed with or transitioning to ripple-laminated sediments, typically as channel flow winnows (Bridge, 2006). These sediments were likely deposited in a

fluvial channel during a high-water event (Sing, 1972), and continued to be deposited as flow winnowed and water levels receded (Bridge, 2006).

2.3.1.4. Facies Four (F4).

Facies 4 displays planar-parallel laminated sandy mud and muddy sand, with rare interbedded planar-bedded organic sand. Sandy mud layers present as a medium to coarse-grained silt, the muddy sand as a very fine to medium-grained; rare granules and pebbles. Thickness ranges from 0.30 to 0.70 m thick with abrupt basal contacts and the upper contacts as either abrupt or gradational. Parallel laminations are millimetre-scale. Occasional gravels are both pumiceous and rhyolitic. No lithological accessories or fossils were identified. Occurs as erosional and abrupt over and under F2 (structureless sandy mud to muddy sand).

The compositional material that F4 consists of is likely derived from the erosion of volcanic formations further upstream, as suggested by the presence of rhyolite and pumice, and deposited near the river channel. The coarse-grained sediments suggest that the channel would need to have had a strong enough flow to move them, while the planar bedding suggests that this flow would have slowed quickly. This change in flow velocity would be observed on a channel's levee or on the floodplain proximal to the river channel, as flow velocity decreases when leaving the channel and again when the floodwaters recede. Successive flooding events would allow for the build-up of these planar-bedded deposits on the channel levee (Singh, 1972; Bridge, 2006) or the floodplain (Miall, 1977).

2.3.1.5. Facies Five (F5).

Facies 5 consists of prominent cross-bedded and current-ripple laminated mud. The sandy mud observed ranges from fine to coarse-grained silt and very fine to fine-grained sand with occasional granules and pebbles. Thickness ranges from sub-decimetre (~0.05 cm) to half a metre (0.45 m) thick with abrupt and erosional contacts. Current ripple laminations are millimetre- to centimetre-scale; cross-bed thickness ranges from millimetre-scale to less than 10 cm. Occasional gravels are both pumiceous and rhyolitic. No lithological accessories or fossils were identified. Occurs as abrupt over and under F2 (structureless sandy mud to muddy sand) and over F3 (cross-bedded and current-ripple laminated sand) and as erosional over and under F3 and over F2.

The fine-grained sediment, fine to coarse-grained silt and very fine to fine-grained sand, and the physical structures, cross-bedding and current-ripple lamination, indicate a depositional environment of varying flow velocities and water levels. Bridge (2006) has previously observed similar cross-bedding and current-ripple laminations in sandy rivers in the upper plane bed and

near the edges of a river's channel, noting that ripples are typically restricted to low-velocity water flow. Sing (1972) observed that current-ripple lamination and cross-bedding in fine-grained material can be found in a fluvial bar. Sediments were likely deposited as water level and flow speed increased, initially incising the tops of existing fluvial bars, forming cross-beds, and later as flow velocity decreased, depositing the finer suspended sediment, forming current-ripple laminations. Successive cycles would gradually build up the upper fluvial bar, resulting in the deposits observed in this facies.

2.3.1.6. Facies Six (F6A/B).

Two sub-facies make up F6: F6A (peat) and F6B (coal). As both sub-units share the same contacts, abrupt and gradational, and physical structures, structureless and planar-bedded, the presence or absence of visible plant material and the strength of the layers were used to differentiate them. F6A presented very fine-grained silt to medium-grained sand. Thickness ranged from 0.15 to 0.20 m. Parallel laminations are millimetre-scale. Lithological accessories included rootlets, charcoal, and wood. No fossils were identified. Occurs as gradational over and under F1 (structureless muddy to sandy gravel) and gradational under F2 (structureless sandy mud to muddy sand) and abrupt under F2. F6B presented as coarse-grained silt to very fine-grained sand. Thickness ranged from 0.05 to 0.70 m. Parallel laminations are millimetre-scale. No lithological accessories or fossils were identified. Occurs as abrupt over and under F2 (structureless sandy mud to muddy sand) and gradational under F2 and abrupt under F7 (ignimbrite).

During a flood, the water table exceeds the riverbanks and covers the floodplain. As water levels decline and recede into the river channel, sediment-laden water can be trapped, leading to deposition of fine suspended sediments. The still water allows for the suspended fine sediments to be deposited as a uniform bed, which, after successive flooding events, results in the planar bedding observed in this facies (Sherwood, 1972). The inclusion of dead organic matter in these still waters leads to the formation of peat and, later, coal (Miall, 1977). The fine-grained composition, high organic content, and structureless to planar-bedded appearance suggest that the depositional environment for these facies is likely a floodplain or floodplain lake (Miall, 1977).

2.3.1.7. Facies Seven (F7).

Facies 7 appears to be a completely weathered ignimbrite. Structureless, the ignimbrite consists of very fine to fine-grained sand and pumiceous granules and pebbles. The thickness of this unit is 10.40 m. No lithological accessories or fossils were identified. This facies occurs abruptly over

F6B (as coarse-grained silt to very fine-grained sand coal) and abruptly below F3 (cross-bedded and current-ripple laminated sand).

2.3.2. Stratigraphy.

2.3.2.1. Outcrop.

The lowermost layer(s) in Section 1 (S1) (Figure 2.4), above the river water line, are covered by vegetation and recent mud and could therefore not be interpreted. An erosional boundary separates the undefinable section from a ~0.25 m muddy-sandy-gravel layer (F1) that grades normally into a ~0.10 to 0.20 m layer of cross-bedded muddy sand (F3). Atop F3 is an abrupt boundary that sees a ~0.30 m layer of organic material, likely a sandy coal product (F6B), that is separated by an erosional boundary from the overlying, ~2.50 m, structureless sandy mud to muddy sand layer (F2). Within the uppermost layer (F2), ~1.2 m above the F6B to F2 interface, is one, possibly two, liquefied layers and an injection structure protruding down towards, but not entering, F6B. The liquefied layer, ~0.10 to 0.15 m thick, pinches out, or reduces in thickness to ~0.02 m, before increasing to ~0.10 m.

Directly aside the entrenched channel of the Waikato River, S1 is likely to share characteristics with a classic meandering river channel deposit. A typical meander channel deposit begins with a gravel-dominated base, followed by a cross-bedded to current-ripple laminated point bar, then a package of interbedded sand and mud as the channel is abandoned, and is concluded by a mud layer (Swan *et al.*, 2018). This typical structure is observed in S1, as the outcrop begins with a gravel-dominated layer, followed by a cross-bedded sand, current ripples were not observed due to the distance from the outcrop, but are assumed to be present, before a layer of organic mud, coal, and is finished with a muddy to sandy package. As such, the geological history of S1 is likely to have begun as a meandering river that was later abandoned at the most upstream end, allowing fine mud and organic matter to settle before fine sand and mud were deposited from the downstream channel end. Sometime after the deposition ceased, a high-energy stress, likely an earthquake, caused a thin layer of the upper F2 package to liquify.

As in S1, the most immediately exposed strata above the river waterline in Section 2 (S2) (Figure 2.5) were covered in vegetation and could not be interpreted. Residing on an abrupt boundary atop the undefinable is a ~0.5 m layer of structureless muddy sandy gravel (F1). An erosional contact separates a ~2.0 m layer of F2, followed by an abrupt contact to a ~5.0 m planar-bedded sandy mud to muddy sand (F4). Within F4, ~1.0 atop the F2 to F4 contact, appears to show evidence of deformation and liquefaction.

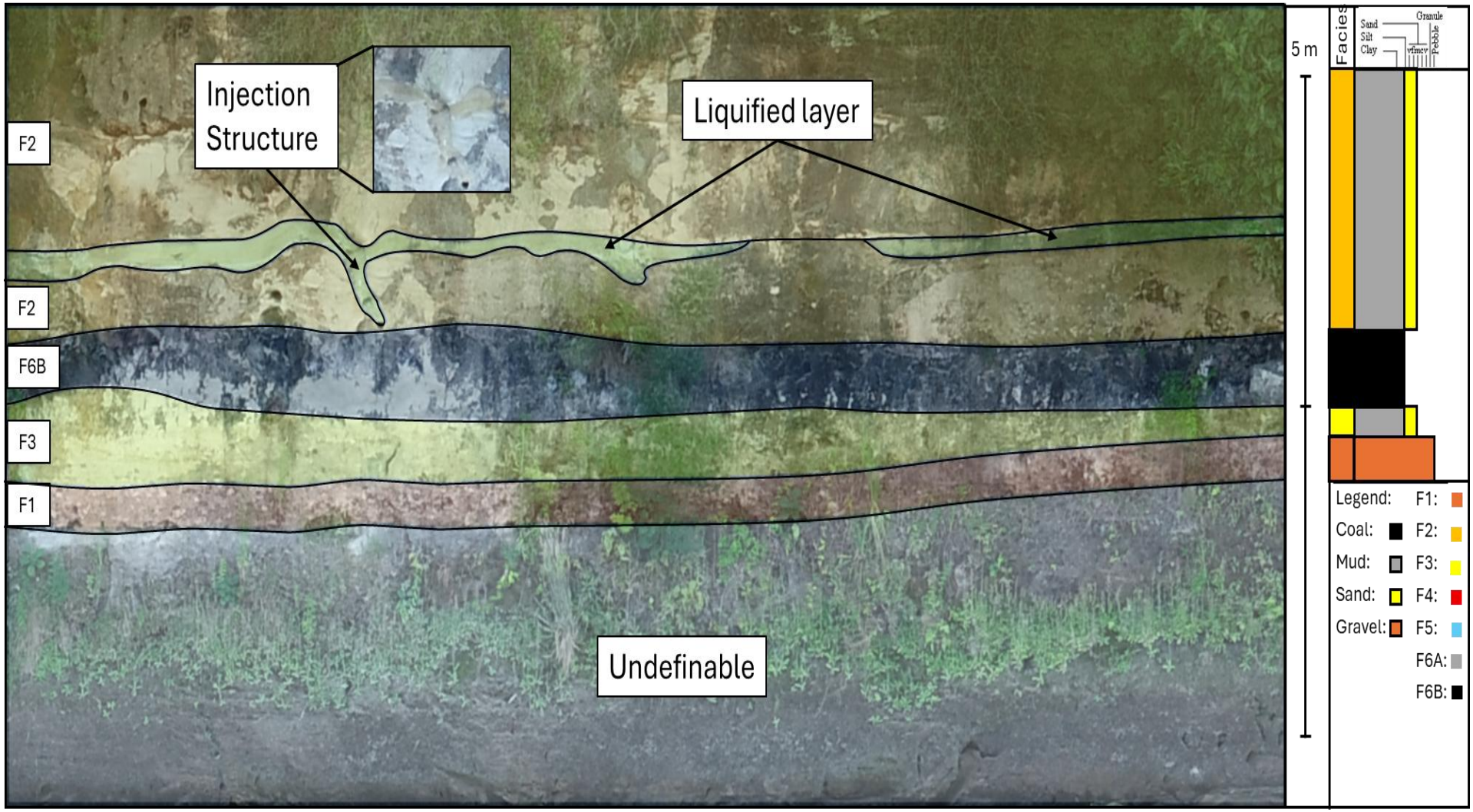

Figure 2.4. Outcrop: Section 1 (Waikato River) with facies identified and possible liquefaction and injection structure noted.

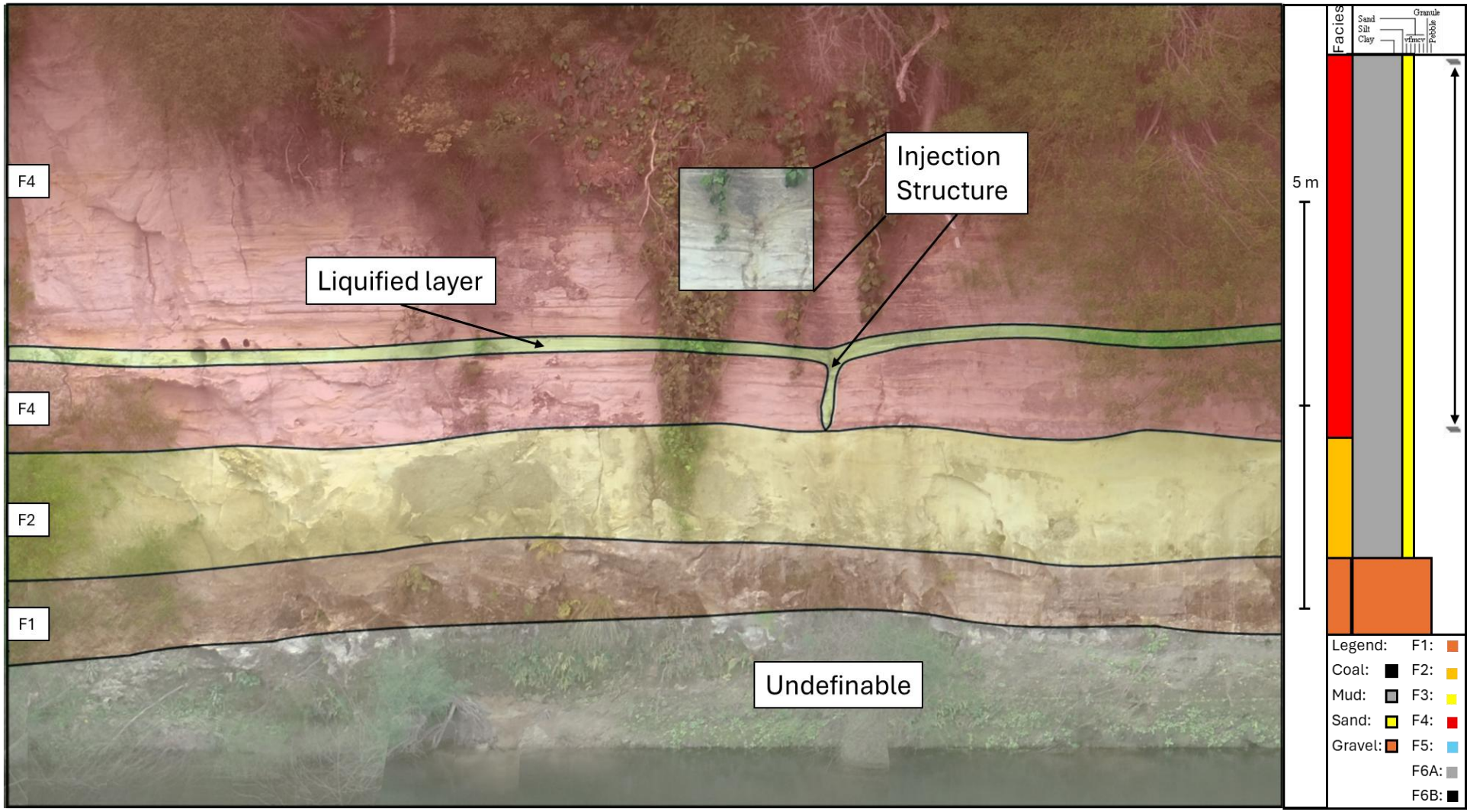

Figure 2.5. Outcrop: Section 2 (Waikato River) with facies identified and possible liquefaction and injection structure noted.

The geological history of S2 is both similar to and different from that of S1, with some elements of a classic meandering river deposit, but not all. The base of the outcrop sees a structureless gravel (F1), consistent with a channel base, followed by an erosional contact that indicates a period of time where the sediment budget was negative. After this, the facies indicate that the channel was abandoned for a period before sedimentation resumed, producing a series of interbedded mud and sand (F4) that was deposited on either the channel levee or a floodplain. The influx/reduction in available sediment could be linked to the volcanism at the time, from which the majority of this sediment is derived. As with S1, a seismic event triggered a thin layer of liquefaction in F4, which, despite forming an injection structure, did not cross into the lower F2.

2.3.2.2. Core 20-1006

Core 20-1006 (Figure 2.6) is 30.00 meters thick. From the base at 30.00 to 25.00 metres below ground level (mbgl), the core is characterised by repeating packages of structureless (F2) to cross-bedded sand (F3) and mud (F5) ~1.0 to 2.0 m thick that are separated by ~0.25 to 0.50 m thick structureless to planar-bedded coal layers (F6B). Deposits from 25.00 to 18.50 mbgl consist of two packages of structureless mud/sand (F2) that are topped with <0.50 m thick planar bedded mud/sand (F4). From 18.50 to 2.00 mbgl, are two packages (18.50 to 11.00 and 11.00 to 2.00 mbgl) of F2 followed by alternating F2 to F3 successions ~0.50 to 1.00 m thick and are each capped by 0.50 m thick organic layer (F6A); occasional ~0.25 m cross-bedded and current-ripple laminated sandy mud (F5) and one gravel bar, 0.50 and 1.50 m thick, are observed within each package. From 2.00 mbgl to ground level, the core is characterised as F2.

The base of core 20-1006 appears to be an abandoned channel. A new channel then cut through, as evidenced by the cross-bedding, beginning with a thin layer of fluvial channel deposits and ending with fluvial bar deposits, before being abandoned again. The succession ends with a floodplain or floodplain lake deposit forming, before the succession repeats and ends at 25.00 mbgl. From here on, the channel is abandoned, only receiving ~0.50 m planar-bedded levee or floodplain deposits every few metres. The channel remains abandoned until ~15.50 mbgl, whereupon a new channel briefly appears before re-abandoning until 14.50 mbgl. From 14.50 to 11.00 mbgl, there is a package of fining upwards sediments similar to a classic meandering river (Swan *et al*., 2018), with a layer of gravel at the channel base, cross-bedded mud and sand representing the fluvial channel and bar deposits, and ending with a layer of planar-bedded organic muds. From 11.00 to 10.25 mbgl, the channel remains abandoned, after which a small, ~0.75 m thick, package of alternating current ripple laminated mud and sands is deposited; after deposition, the channel is abandoned once more at 9.50 mbgl and remains so until 5.50 mbgl. Layers ~0.50 m thick of current-ripple laminated and cross-bedded sand begin at 5.50 mbgl,

indicating that a fluvial channel has once again returned, before abandoning once more and leaving behind a lag deposit in the form of a structureless gravel and sand until ground level.

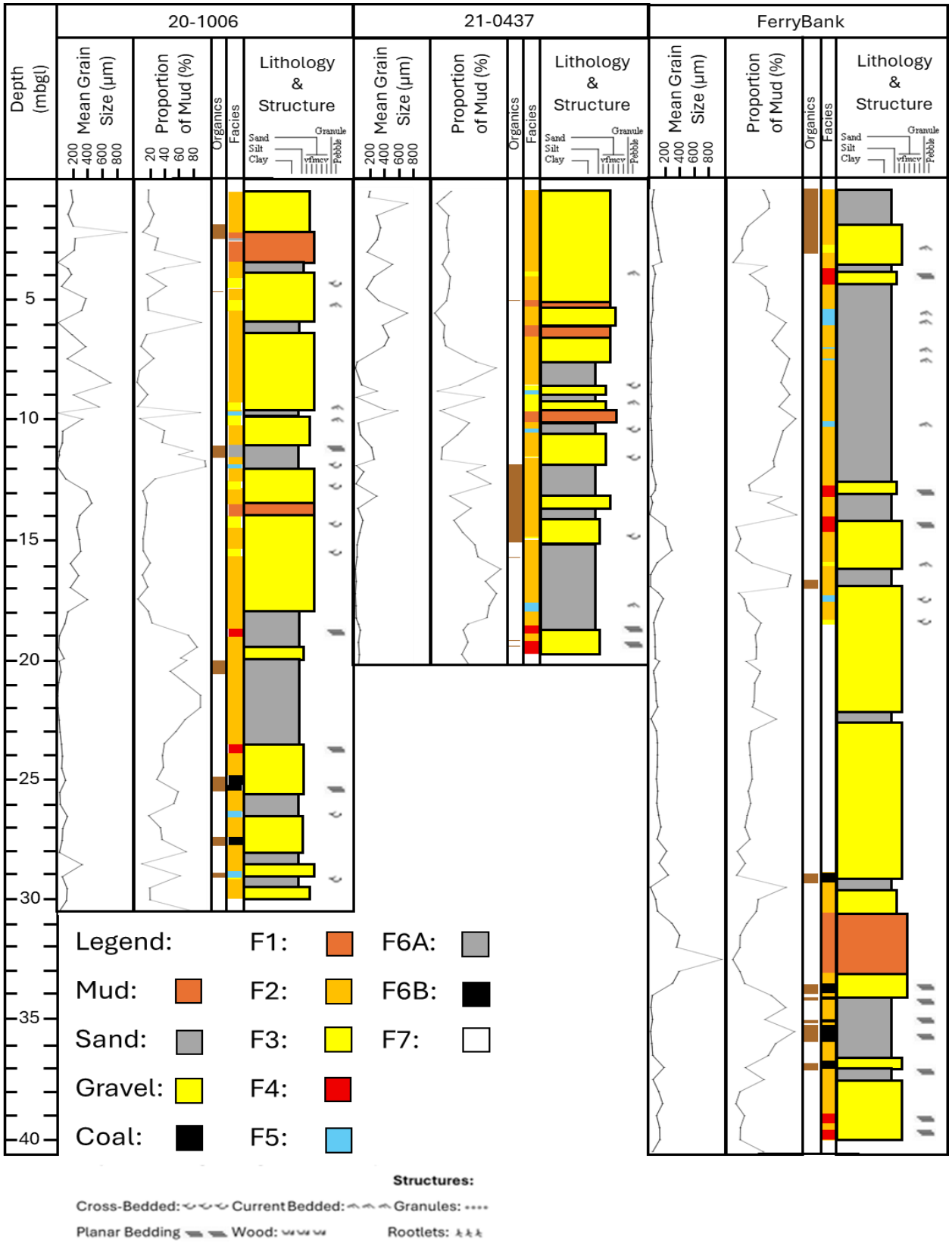

Figure 2.6. Facies driven stratigraphic log; 21-0437, 20-1006, Ferrybank.

2.3.2.3. Core 21-0437.

Core 21-0437 (Figure 2.6) is 19.50 meters thick. From the base at 19.50 to 18.50 mbgl, the core is characterised by ~0.50 m thick alternating planar bedded mud/sand (F4) and structureless mud/sand layers (F2). Deposits from 18.50 to 10.50 mbgl consist of ~0.50 to 3.50 m thick layers of F2 with thin, <0.25 to 0.50 m thick, layers of cross-bedded sand (F3) and current-ripple laminated and cross-bedded mud (F5) interbedding the F2 layers. From 10.50 to 8.50 mbgl, sediments present begin with a ~0.25 m layer of F5, followed by a ~0.25 m thick layer of F2, then a ~0.50 m thick structureless gravel (F1), topped by ~0.25 to 1.00 m thick interbedded F3 and F2 layers. From 8.50 to 5.00 mbgl, sediments appear as a repeating coarsening-upwards package, ~1.00 to 2.50 m thick, beginning with F2 and topped by F1. Sediments from 5.00 mbgl to ground level are characterised as F2, except for one ~0.25 m thick layer of F3 at 4.00 mbgl.

The basal deposits from 19.50 to 18.50 mbgl are planar-bedded mud/sand and were deposited as either a levee or a floodplain deposit, most likely a levee deposit, as an abandoned channel overlies the deposits. Planar-bedded deposits are present at similar depths in core 20-1006 and could indicate a large flooding event. From 18.50 to 10.50 mbgl, the channel largely remains abandoned, with only brief instances of activity, including cross-bedded fluvial channel deposits at ~14.50 and ~11.50 mbgl. From 10.50 to 8.50 mbgl, a fining-upward package suggests depositional environments associated with a classic meandering river (Swan *et al.*, 2018), including the channel base or lag deposit, fluvial channel, and fluvial bar. The channel is once again abandoned from 8.50 to 6.45 mbgl. Two gravel layers <0.50 m thick are observed after channel abandonment at 6.45 to 6.15 and 5.05 to 5.00 mbgl, potentially indicating a lag deposit left behind after volcanic activity led to pumiceous breakout floods. From 5.00 mbgl to ground level, the channel is abandoned with only a brief period of activity indicated by a ~0.25 m thick layer of current-rippled sand at 4.00 mbgl.

2.3.2.4. Core Ferrybank.

Core Ferrybank (Figure 2.6) is 40.50 meters thick. From the base at 40.50 to 38.50 mbgl, the core is characterised as a series of planar-bedded mud/sand (F4) layers ~0.50 m thick, interbedded with a structureless mud/sand (F2) layer ~0.50 m thick. Sediments from 38.50 to 33.00 mbgl consist of several packages, ~0.25 to 2.00 m thick, of F2 topped with coal (F6B). From 33.00 to 29.10 mbgl, a ~2.50 m thick structureless muddy sandy gravel (F1) layer is present that fines upward to F1 then to F2 and is capped by a 0.30 m thick layer of F6B. An ignimbrite is present from 29.10 to 18.70 mbgl. From 18.70 to 14.65 mbgl, we see F2 with several ~0.25 m layers of cross-bedded mud (F5) and current-ripple laminated to cross-bedded sand (F3). From 14.65 to 12.90

mbgl, the core consists of interbedded F2 and F4 facies. Sediments from 12.90 to 2.60 mbgl are dominated by F2, with ~0.05 to 0.50 m thick layers of F5 and end with a 0.35 m layer of F3; one 0.75 m thick layer of F4 is present at 4.50 mbgl. The core is characterised as F2 from 2.60 mbgl to ground level.

The basal deposits from 40.50 to 39.00 mbgl were deposited at either the channel levee or on a floodplain. A levee deposit seems most fitting for these deposits, given that the overlying abandoned channel deposits are capped by planar-bedded coal, which suggests a potential floodplain lake. From 39.00 to 33.00 mbgl, multiple successive cycles of inactive channel deposits and planar-bedded coal are observed, potentially suggesting that the abandoned channel was flooded several times and that water receded slowly, promoting organic decomposition and swamp conditions. From 33.00 to 29.10 mbgl, a fining upwards succession suggests that a fluvial channel was present. From 29.10 to 18.70 mbgl, an ignimbrite is present. Deposits ranging from 18.70 to 14.65 mbgl suggest the channel alternates between active and abandoned stages. Flooding is evident at 14.65 and 13.25 mbgl, with the current planar-bedded sandy mud and muddy sand. From 13.25 to 4.50 mbgl, the channel alternates between active and abandoned states. One final flooding event is represented by levee/floodplain deposits at 4.50 mbgl, as well as a brief fluvial channel at 2.75 mbgl. From 2.75 mbgl to ground level, the channel remains abandoned.

2.3.3. X-Ray Diffraction (XRD).

Samples from all cores were dominated by quartz and feldspars, with less common cristobalite and tridymite inclusions. Augite was observed in core 21-0437 (Table 2.2) at 2.00 mbgl, as well as clay minerals, potentially halloysite and kaolinite, from 13.00 to 16.00 mbgl. The majority of samples analysed were crystalline and showed strong peaks (Figure 2.7A), though some were non-crystalline minerals and showed an amorphous hump. Both 21-0437 and Ferrybank displayed amorphous humps at various depths, indicating a high presence of organic/non-crystalline materials (Figure 2.7B). The overall homogeneity of the samples was expected, as discussed in Section 1.3. The Hinuera Formation and the Walton Subgroup, especially the Karapiro Formation, are comprised of nearly identical material, with the main difference being the degree of weathering (Kear & Schofield, 1978).

2.3.4. Radiocarbon Dating.

The radiocarbon ages obtained by AMS C^{14} dating ranged from recent (204±16 BP) to exceeding the dating method's limits (>50,000 BP). Radiocarbon ages >50,000 BP could still provide

information on the depositional history, as the Hinuera Formation was deposited between ~24 to 19 ka (Selby & Lowe, 1992) and 16 to 12 ka (Schofield, 1965); thus, samples greater than this range, despite sharing similar physical characteristics, would likely be either the Karapiro or Puketoka Formation. Based on radiocarbon ages (Table 2.3), the sediments within our cores are from both the Piako and Walton Subgroups. One interesting age was obtained in core 21-0437 at 5.03 mbgl, as the age for this sample, 23,125±116 BP, was older than the nearest deeper age, 18,417±65 BP at 11.90 mbgl. Following the law of superposition, this should not occur as units deposited higher in the stratigraphy must be younger than those below. When this occurs, the change in age is defined as a stratigraphic age reversal. One possible reason shallower sediment appears younger is that braided river systems' channels are not static; rather, they are constantly moving, incising, and eroding their paleochannels while simultaneously depositing freshly eroded material. Older radiocarbon could mix with the more recently eroded sediments and be deposited together; thus, these sediments could yield an older radiocarbon age than layers deposited below. For the reasons observed above, 21-0437 at 5.03 mbgl can be disregarded.

Table 2.2. Minerals present in core 21-0437.

ID	Feldspar	Quartz	Cristobalite	Halite	Tridymite	Clay	Augite	Amorphous
1.00	*	*						
2.00	*	*					*	
4.00	*	*						
6.00	*	*						
6.85	*	*						
8.00	*	*						
8.25	*	*						
8.50	*	*	*					
9.00	*	*						
10.00	*	*						
11.50	*	*						
12.00	*	*						
13.00		*				*		
15.00	*	*				*		
16.00			*			*		
18.00	*							
19.00								*
19.50								*

*Note: Sample IDs are presented in mbgl. An * indicates minerals were present in the sample during analysis. Samples that include clay minerals may include Kaolinite and Halloysite.*

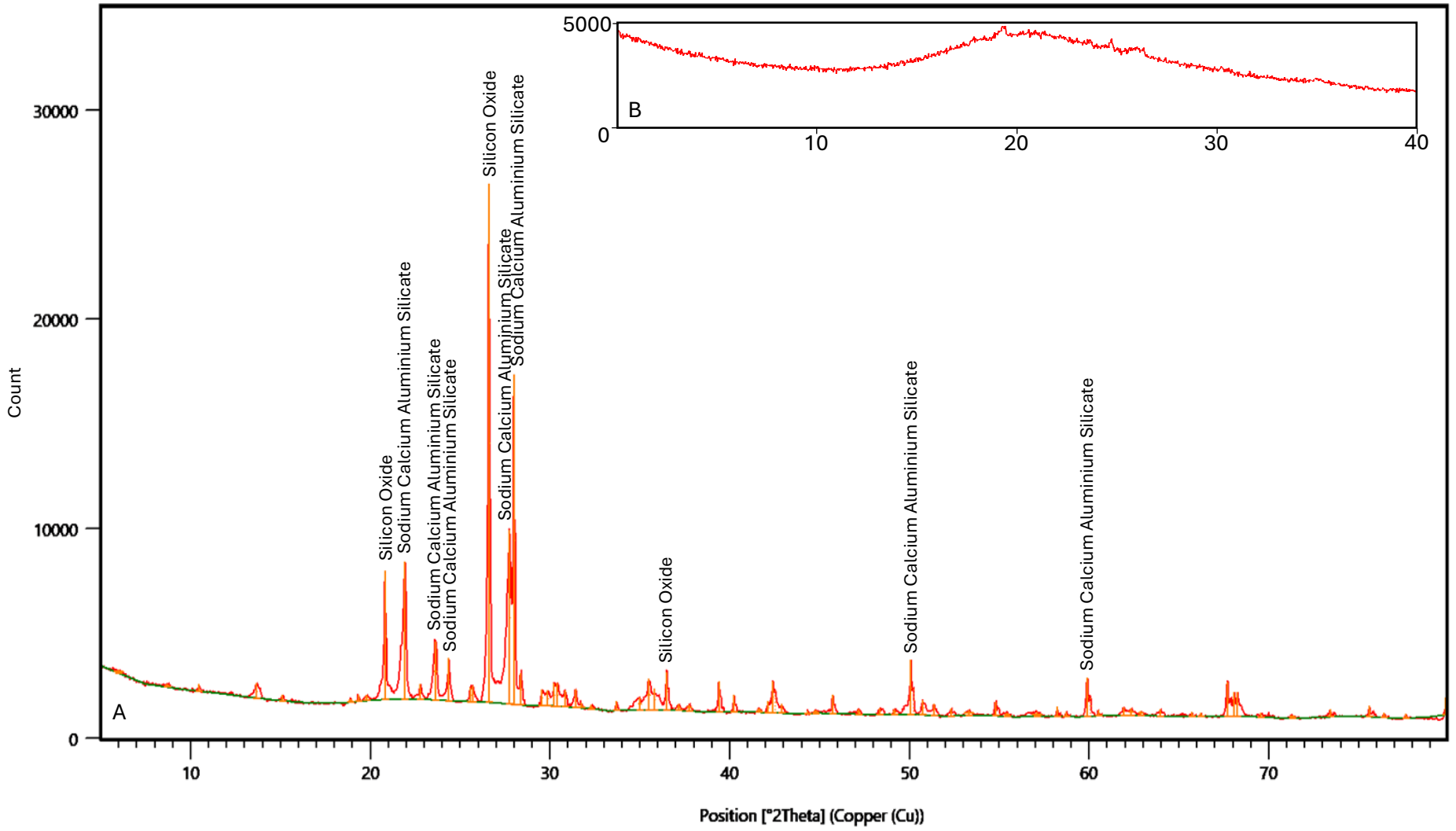

Figure 2.7. Diffractogram of two contrasting XRD Results. A) Core 21-0437 at 6.00 mbgl shows clear, intense peaks that indicate a highly crystalline sample (ten most intense peaks labelled). B) Core Ferrybank at 9.00 mbgl shows an amorphous hump with no identifiable peaks.

Table 2.3. Radiocarbon dates (BP) of samples from cores 20-1006, 21-0437, and Ferrybank.

Core	Depth (mbgl)	FC^{14} (%)	FC^{14} Error (%)	Result (years BP)	Result Error (years)
20-1006	2.75	97.49	0.19	204	16
20-1006	11.45	9.48	0.08	18,925	69
20-1006	25.05	0.08	0.07	>49,200	N/A
20-1006	27.45	0.09	0.07	>48,800	N/A
21-0437	5.03	5.62	0.08	23,125	116
21-0437	11.90	10.1	0.08	18,417	65
Ferrybank	15.95	0.02	0.07	>49,900	N/A
Ferrybank	29.20	0.06	0.07	>51,700	N/A

Note: FC^{14} = Fraction of C^{14} comparative to the modern C^{14} standard. BP = before present. Samples that were at the limit of the dating are displayed as greater than (>) the age displayed.

2.4. Discussion.

2.4.1. Geological History of the Hamilton CBD.

The core and outcrop analysis presented (Figure 2.8) in this investigation has shown that the depositional environments and facies associated are typical of those found within a braided river system, with one section being derived from volcanic processes. Radiocarbon dating and depth suggest that the ignimbrite was deposited >50 ka and would likely be part of the Walton Subgroup (Figure 2.1).

Multiple successive cycles and partial cycles of active channels, channel abandonment, and flooding were observed. Sediments were deposited in the upper levels and the base of active channels at high flow velocities, before winnowing flow or sudden abandonment due to avulsion allowed the deposition of fine-grained suspended sediment. The repeated nature of channel abandonment and adoption led to successive cycles of fining upward packages, with the basal structures typically massive or cross-bedded, and the upper structures presenting as cross-bedded or current-ripple laminated. The processes and sediment composition were defined as seven unique facies and were used to interpret the paleoenvironments presented (Table 2.1). These successive cycles of channel meandering and positive sediment budget have resulted in the formation of the Hinuera Formation and the present-day geomorphology of the Hamilton Basin. Floodplains were the primary means of distinguishing packages because of their reliability as stratigraphic datums. The identification of these paleoenvironments, which were typical of

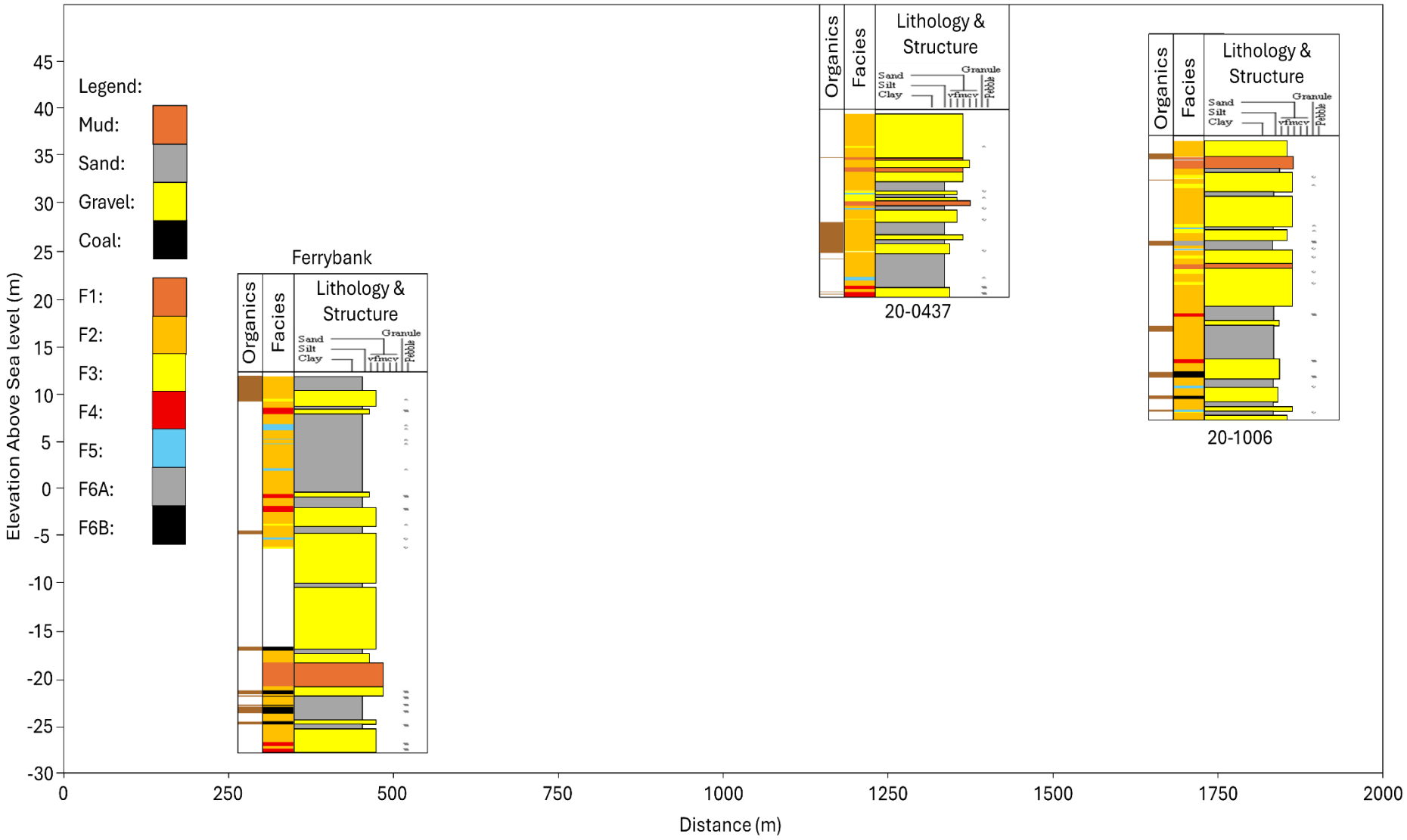

Figure 2.8. Lithological cross-section of examined cores.

those found in a braided river atop an alluvial fan, were important as they provided insight into why it may be challenging to create a 3D model of the upper stratigraphy of the Hamilton Basin; these issues are discussed further (Section 2.4.2). Depositional material was exclusively volcaniclastic gravel, sand, and mud, with peat/coal formation occurring between deposition events. The observations of the sediments and the corresponding formations, the Karapiro and Hinuera Formations, are consistent with previous investigations in similar areas (Healy, 1946; Kear & Schofield, 1978; Kamp & Lowe, 1981).

Previous research into the Canterbury Basin by Wotherspoon *et al*. (2014) has identified the velocities at which shear waves travel through strata with different grain sizes (Table 2.4); it is important to note that these velocities can vary depending on the strata's compactness, porosity, weathering, saturation, age, and depth (Paoletti, 2012). The V_{S30} variances between grain size identified in the study by Wotherspoon *et al*. (2014) reinforce the importance of accurately defining and modelling unique sedimentary layers, as these values show that misclassified units, or where a unit's physical properties are not accurately upscaled, could result in the over- or under-estimation of seismic activity during an earthquake. As the geometry of a braided river system is highly variable and can span tens of metres to kilometres horizontally, with channel deposits typically centimetre to less than two metres thick (Bridge, 2006; Lunt *et al*, 2013), there will be challenges associated with classifying the area between data points (Section 2.4.2).

No reliable tephra deposits were identified during this investigation, though the presence of peat/coal layers could have preserved small amounts of sediment as cryptotephras. Potential liquefaction was observed in multiple sections across the outcrop. As this was observed in the shallow stratigraphy downstream of the Hinuera disjunction, it is assumed that the sediments belong to the younger Hinuera-2 surface and were thus deposited within the last ~24 ka (Selby & Lowe, 1992). If this instance of liquefaction were produced by seismic stress rather than depositional deformation, it would provide evidence that a seismic event of sufficient intensity to produce liquefaction occurred within the last ~24 ka. It is important to consider whether further deformation could occur under a new seismic stress or whether the deformation occurred during deposition, especially given that the observed layers in the shallow stratigraphy are highly proximal to a free face and thus at a higher risk of lateral spread (Bartlett & Youd, 1995).

The nature of a braided river system and the spatial variation in available data increase the complexity when building geological models. The correlation of individual units/layers would not be feasible, as the sedimentary and structural homogeneity would make it impossible to distinguish and define each layer. Linking packages of sediments defined by their unique facies

and successions would make more sense; however, this would require significantly more data points and, even then, may not be accurate because previous deposits were eroded as the river channels moved. These complications are scaling issues that can be, at least partially, remediated. For these reasons, accurate classification of the physical properties of the shallow stratigraphy is important when creating 3D geological models.

Table 2.4. Shear wave velocity (V_{S30}) ranges for grain sizes in the shallow stratigraphy of the Christchurch Basin.

Grain Size	V_{S30} range (ms^{-1})
Gravel	150 to 600
Sand	110 to 240
Silt	100 to 140
Peat	80

Note: Grain size shear wave velocity (V_S) ranges obtained from Wotherspoon et al. (2014).

2.4.2. The Challenge of Scale in Geological Models.

One of the biggest challenges when developing a representative geological model of a large area is linking areas with data to those without, and accurately predicting the geology between data points without making the model so large as to be computationally infeasible. Seismic and geological modelling is best undertaken using a stochastic approach, thus necessitating the construction of a large number of models to capture uncertainty. This is often achieved by balancing model grid resolution and computation time (Durlofsky, 2005); thus, upscaling is necessary when considering large areas or regions. The significant issues with upscaling become evident when the scale of a typical simulation is considered: reservoir simulations can incorporate 10^5-10^6 cells, and geological models can contain 10^7-10^8 cells (Durlofsky, 2005). Data is "upscaled" in order to bridge the gap between data-points, a process that sees the coarsening of fine-scale data across set intervals, e.g. the petrological characteristics of sediments recovered are averaged together to form one value (deterministic), or a statistical distribution of potential values (stochastic) (Blöschl & Sivapalan, 1995).

The process of upscaling fine-scale data within a braided river system is particularly difficult due to the diversity of geological processes across a large horizontal area; e.g. processes and sediments within an active channel will differ significantly from those on a floodplain. Models that are not upscaled correctly may yield skewed or biased data and may not be representative of the site's actual geology (Pickup & Hern, 2002). Previous studies (Ding, 2004; Durlofsky, 2005)

have encountered significant challenges when modelling channelised deposits compared to the overlying non-channelised deposits. To improve model accuracy, a combination of near-well upscaling and border cells is needed. Near-well upscaling is the process of defining the surrounding area near the borehole with the same petrological properties. Border cells are fine-scale data points that surround the coarser upscaled block. Ding (2004) noted that coarse-scale model errors were reduced tenfold where near-well upscaling was incorporated.

The results of this investigation show thin layers of sediment that have differing physical properties, typically structure and clast-size, from the overlying or underlying layers; thus, these lenses and layers will behave uniquely relative to each other during a seismic event. Deterministic upscaling would be inadvisable for a model derived from the data in this investigation, given the interbedded nature of some sediment packages and differences in facies structure. A stochastic upscale would be better suited to the data presented, as this method considers a series of potential values, allowing models to account for numerous outcomes and to present the most likely. Pickup and Hern (2002) achieved success by employing stochastic modelling and defining two levels of heterogeneity: lamina- and bed-scale. A similar approach could be utilised for models derived from our datasets. Near-well upscaling of the data could be utilised during model creation; however, more data points would likely be needed to be truly representative, as such few data points could lead to an oversimplification of the site. There is also the potential for the near-well upscaling to misrepresent the areas immediately surrounding the borehole due to a braided river system's lateral discontinuity, e.g. an area within the borehole may be defined as a channel, but that does not necessarily result in the area ten metres away being a channel. Based on the successes of previous researchers (Ding, 2004; Durlofsky, 2005), border cells would ideally be incorporated into future models; unfortunately, no such data were available for this investigation.

The horizontal and vertical extent, metre to kilometre scale and centimetre to metre scale (Bridge, 2006; Lunt *et al.*, 2013), of the depositional environments in a typical braided river are highly variable, as evidenced in this study (Figure 2.8). As coarse-scale geological models can include cells ranging from 25 to 100 m horizontally and 1 to 10 m vertically (Ringrose & Bentley, 2021), units encountered through borehole analysis alone would therefore be upscaled to a minimum of 25 m horizontally, regardless of whether such evidence is present. Some of the facies identified in this investigation, F3 to F6B, are thinner than a typical vertical cell size and would be over-represented in a geological model. Without more data points, results from any geological modelling may not accurately reflect the shallow stratigraphy in Hamilton Basin. Due to the horizontal discontinuity of the facies encountered, well-to-well linking of units is unlikely to

correlate accurately. One method of obtaining subsurface data that would complement this investigation would be to add seismic reflection profiles or ground penetrating radar (GPR) data proximal to borehole locations to determine the horizontal extent of the encountered units.

Publicly available geotechnical borehole logs could be used to increase model certainty or to sense-check any models produced; however, such data is not always collected by geologists/researchers and may have been defined incorrectly. As noted further when discussing the study's limitations (Section 3.3), geotechnical borehole records can miss important structural and package cycle data where Standard Penetration Tests (SPTs) are used. The missing data from SPTs can be attributed to the compaction of 0.45 m of sediment under repeated blows from a 63.5 kg hammer; this process results in soil compaction, blending of different strata, and destruction of unit boundaries and structure. All of this lost data is very important when defining facies and interpreting a site's paleoenvironment. This lost data leads to further complications with upscaling and would be most evident in averaging. For example, if 45% (0.45 m) of a 1 m section is lost, the physical properties in the remaining 55% (0.55 m) section would be overestimated. Further issues arise when considering the cyclic nature of rivers; if key layers are not observed, the proper succession of paleoenvironments may be misinterpreted.

The quality of an upscaled seismic model will be crucial for informing seismic risk assessments, building consents, and the local geology's response to seismic stress. Upscaled models could lead to the over- or underestimation of a site's response to a seismic event, with consequences ranging from higher than necessary expenditure in the case of overestimation to building or landform failure resulting in injury and death when underestimation occurs. Because of the potential for generalisation errors, interpretations derived from large-scale seismic or geological models should be taken with caution. Such large-scale coarse models should be used in tandem with finer-scale models, known as a nested approach, in which a coarse model identifies areas where the seismic hazard risk is intolerable, allowing researchers to target them with finer-scale models. It is also important that the correct modelling methodology is utilised, as discussed in this study, as different methodologies can lead to varying accuracies and outcomes from the models produced. This discussion has suggested a series of methodologies based on the shallow stratigraphy analysed, and noted that certain data sources, such as geotechnical boreholes, should be used with caution, if at all.

2.4.3. Seismic Hazard Applications - Hamilton Basin.

Despite the apparent lack of many major faults in Hamilton Basin, recent developments continue to find evidence of fault movement in deposits as recent as the Hinuera Formation (Moon & de

Lange, 2017; Spinardi *et al.*, 2017). Despite high confidence in these fault zones, the depths and recurrence intervals remain unknown; thus, if they were to rupture, the impact on surrounding areas is unknown. As these faults are observed in the shallow stratigraphy, it is reasonable to conclude that if a rupture were to occur, vertical displacement could impact proximal infrastructure and developments. Hamilton Basin is also proximal to the Kerepehi Fault, which has a recurrence interval of approximately 1,000 years and is predicted to be able to cause a M_W5.5 to M_W7.0 earthquake to occur, or a M_W7.2 to M_W7.4 earthquake if all onshore sections ruptured simultaneously (Persaud *et al.*, 2016). As previously mentioned, shaking during a seismic event would be more complex in the Hamilton Basin due to the basin effect; that is, shaking could be more intense in some areas and less intense in others. This investigation has confirmed the presence of significant layers of unconsolidated soft sediments that are known to be amplified under certain conditions, e.g. a concave basin-floor topography and sediment physical characteristics. When subjected to seismic stresses, basins with similar grain size sedimentary infill (Canterbury Basin 2010/2011 and Mexico City Basin 1985) have exhibited significant seismic amplification. The composition of the shallow stratigraphy, especially the interbedded silt and sand layers, was important to accurately define so that these properties could be reflected in the development of future geological models. The interbedded nature of these sediments is also important as seismic amplification potential increases when a seismic wave travels through impedance contrasts between differing media.

The evidence of liquefaction observed and discussed during this investigation, and in previous studies discussed in Chapter One that assessed liquefaction potential, indicates that areas with high water tables in Hamilton City are at risk of liquefaction (Hume *et al.*, 1975; Kleyburg *et al.*, 2015; McKay, 2017). Current lake sediments are understandably most at risk due to their saturation and fine-particle content, with Kluger *et al*. (2023) noting that liquefaction triggered by the Kerepehi Fault occurred in lake sediments deposited from 17.5 to 14.0 ka, and that local faults triggered liquefaction in sediments deposited from 10.0 to 7.6 ka. McKay (2017) observed a highly variable water table in their CPT investigations, ranging from 0.60 to 4.00 mbgl, and found varying degrees of liquefaction risk based on depth: a low to moderate risk at 3.00 mbgl and a low to high risk at 5.00 and 10.00 mbgl, with the average depth at which liquefaction occurred at 1.20 mbgl. A paleoseismic study by Chaneva (2024) identified several high magnitude (>M7.2) paleoearthquakes resulting from movement in the Hikurangi Trough that had the potential to cause liquefaction in the Hamilton Basin, reinforcing that, despite the relatively low recurrence interval of the Kerepehi Fault, there is still a risk of liquefaction to Hamilton City. If the sandy mud

and muddy sand sediments, less than 10 mbgl, encountered during this investigation are below the water table, it would be reasonable to assume liquefaction could occur under seismic stress.

The creation of a geological model of the Hamilton Basin will require analysis of significant quantities of geological and geophysical data that must be upscaled. Scaling issues are likely to arise during modelling due to the variable nature of braided river systems, the heterogeneity of sedimentary strata, and limited data availability. Upscaling will still need to be utilised, despite its potential drawbacks, as it would not be feasible to use fine-scale data to build a large model. A combination of stochastic upscaling, near-well upscaling, and the use of border cells to confine upscaled channel deposits would be crucial to reducing the margin of error in any models produced. The models produced will be used to identify the most sensitive areas within the Hamilton Basin, where finer-scale models could be developed to better assess at-risk zones and provide a deeper understanding of the basin's history and heterogeneity. Where areas are identified as exceeding tolerable risk levels, measures could be put in place to reduce the risk to tolerable levels. Such measures could include draining high water tables in areas with a high liquefaction potential, ensuring that buildings in at-risk areas are built to a sufficient structural standard, or excluding developments in certain areas.

2.5. References.

Bartlett, S. F., Youd, T. L. (1995). Empirical Predication of Liquefaction-Induced Lateral Spread. *Journal of Geotechnical Engineering, 121*(4), 316-331. doi.org/10.1061/(ASCE)0733-9410(1995)121:4(316)

Blöschl, G., Sivapalan, M. (1995). Scale Issues in Hydrological Modelling: A Review. *Hydrological Processes, 9*(3-4), 251-290. doi.org/10.1002/hyp.3360090305

Bridge, J. S. (2003). *Rivers and Floodplains: Forms, Processes, and Sedimentary Record*. Wiley-Blackwell.

Bridge, J. S. (2006). Fluvial Facies Models: Recent Developments. In H. W. Posamentier & R. G. Walker (Eds.), Facies Models Revisited (SEPM Special Publication 84, pp. 85-117). Society for Sedimentary Geology. doi.org/10.2110/pec.06.84.0085

Chaneva, J. (2024). *Estimating Pre-Historic Earthquake Parameters in the Hamilton Lowlands Using Laboratory Geotechnical Analyses of Seismically Liquefied Volcanic-Ash Layers in Lakes* (Doctoral dissertation, University of Waikato). University of Waikato Research Commons.

Ding, D. Y. (2004). Near-Well Upscaling for Reservoir Simulations. *Oil & Gas Science and Technology – Revision. IFP, 59*(2), 157-165. doi.org/10.2516/ogst:2004012

Durlofsky, L. J. (2005). Upscaling and Gridding of Fine Scale Geological Models for Flow Simulation. [Paper presented at the 8th International Forum on Reservoir Simulation, Iles Borromées, Stresa, Italy]. Stanford University.

Ferguson, R.I. and Werritty, A. (1983). Bar Development and Channel Changes in the Gravelly River Feshie, Scotland. *In Modern and Ancient Fluvial Systems* (eds J.D. Collinson and J. Lewin). doi.org/10.1002/9781444303773.ch14

Healy, J. (1946). Geology of the Karapiro District, Cambridge. *New Zealand Journal of Science and Technology, B27*(3), 199-217.

Henderson, J., Bartrum, J. A. (1913). The Geology of the Aroha Subdivision Hauraki, Auckland. *Bulletin (New Zealand Geological Survey), 16*.

Hume, T. M., Sherwood, A. M., Nelson, C. S. (1975). Alluvial Sedimentology of the Upper Pleistocene Hinuera Formation, Hamilton Basin, New Zealand. *Journal of the Royal Society of New Zealand, 5*(4), 461-462.

Kamp, P. J., Lowe, D. J. (1981). Quaternary Stratigraphic, Landscape, and Soils of the Hamilton Basin. *Geological Society of New Zealand Miscellaneous Publication 29B*, pp. 14-28.

Kear, D., Schofield, J. C. (1978). Geology of the Ngāruawāhia Subdivision. *New Zealand Geological Survey Bulletin, 88*, 1-168.

Kleyburg, M. A., Moon, V. G., Lowe, D. J., Nelson, C. S. (2015). Paleoliquefaction in Late Pleistocene Alluvial Sediments in Hauraki and Hamilton Basins, and Implications for Paleoseismicity. *Proceedings, 12th Australia New Zealand Conference on Geomechanics (ANZ 2015), 22-25 February, 2015, Wellington, pp. 524-531*.

Kluger, M. O., Lowe, D. J., Moon, V. G., Chaneva, J., Johnston, R., Villamor, P., Ilanko, T., Melchert, R. A., Orense, R. P., Loame, R. C., Ross. R. (2023). Seismically-Induced Down-Sagging Structures in Tephra Layers (Tephra-Seismites) Preserved in Lakes Since 17.5 cal ka, Hamilton Lowlands, New Zealand. *Sedimentary Geology*, *445*, 1-23. doi.org/10.1016/j.sedgeo.2022.106327

Lowe, D.J. (2010). Introduction to the Landscapes and Soils of the Hamilton Basin. *In*: Lowe, D. J., Neall, V. E., Hedley, M., Clothier, B., Mackay, A. 2010. Guidebook for Pre-conference North Island, New Zealand 'Volcanoes to Oceans' field tour (27- 30 July). 19th World Soils Congress, International Union of Soil Sciences, Brisbane. *Soil and Earth Sciences Occasional Publication No. 3*, Massey University, Palmerston North, pp. 1.24-1.61.

Lunt, I. A., Smith, G. H. S., Best, J. L., Ashworth, P. J., Lane, S. N., Simpson, C. J. (2013). Deposits of the Sandy Braided South Saskatchewan River: Implications for the Use of Modern Analogues in Reconstructing Channel Dimensions in Reservoir Characterisation. *American Association of Petroleum Geologists Bulletin, 97*(4), 553-576. doi.org/10.1306/09251211152

Mares, T. E., Radliński, A. P., Moore, T. A., Cookson, D., Thiyagarajan, T., Ilavsky, J. Klepp, J. (2009). Assessing the Potential for CO_2 Adsorption in a Subbituminous Coal, Huntly Coalfield, New Zealand, Using Small Angle Scattering Techniques. *International Journal of Coal Geology, 77*, 54-68. doi/10.1016/j.coal.2008.07.007

McKay, A. M. (2017). Evaluating Soil Landscape Models to Predict Liquefaction Susceptibility in the Hinuera Formation, Hamilton Basin (Thesis, Master of Science (MSc)). The University of Waikato, Hamilton, New Zealand. hdl.handle.net/10289/11635

Miall, A. D. (1977). A Review of the Braided-River Depositional Environment. *Earth-Science Reviews, 13*(1), 1-62. doi.org/10.1016/0012-8252(77)90055-1

Moon, V., De Lange, W. EQC. (2017). *Potential Shallow Seismic Sources in the Hamilton Basin*. (EQC 16/717).

Paoletti, V. (2012). Remarks on Factors Influencing Shear Wave Velocities and Their Role in Evaluating Susceptibilities to Earthquake-Triggered Slope Instability: Case Study for the Campania Area (Italy). *Natural Hazards and Earth Systems Sciences, 12*, 2147-2158. doi.org/10.5194/nhess-12-2147-2012

Persaud, M., Villamor, P., Berryman, K. R., Ries, W., Litchfield, N., Alloway, B. V. (2016). The Kerepehi Fault, Hauraki Rift, North Island, New Zealand: Active Fault Characterisation and Hazard. *New Zealand Journal of Geology and Geophysics, 59*(1), 117-135. doi.org/10.1080/00288306.2015.1127826

Pickup, G. E., Hern, C. Y. (2002). The Development of Appropriate Upscaling Procedures. *Transport in Porous Media, 46*, 119-138. doi.org/10.1023/A:1015055515059

Ringrose, P., & Bentley, M. (2021). *Reservoir Model Design: A Practitioner's Guide* (2nd ed.). Springer. doi.org/10.1007/978-3-030-70163-5

Schofield, J. C. (1965). The Hinuera Formation and Associated Quaternary Events. *New Zealand Journal of Geology and Geophysics, 8*(5), 772-791. doi.org/10.1080/00288306.1965.10422116

Selby, M. J., Lowe, D. J. (1992). The Middle Waikato Basin and Hills. *Landforms Of New Zealand, 2*, 233-255.

Sherwood, A. M. (1972). Sedimentary Structures, Features, and Paleoenvironments of the Hinuera Formation. [Thesis, University of Waikato]. Research Commons.

Singh, I. B. (1972). On the Bedding in the Natural-Levee and the Point-Bar Deposits of the Gomti River, Uttar Pradesh, India. *Sedimentary Geology, 7*(4), 309-317.

Spinardi, F., Campbell, B. R., Moon, V., Pittari, A., Fox, B. R. S., de Lange, W. (2017). Unravelling Fault Structures of the Hamilton Basin. *Proc. 20th NZGS Geotechnical Symposium*. Eds. GJ Alexander & CY Chin, Napier.

Swan, A., Hartley, A. J., Owen, A., Howell, J. (2018). Reconstruction of a Sandy Point-Bar Deposit: Implications for Fluvial Facies Analysis. *International Association of Sedimentologists Special Publications, 48*, 445-474. doi.org/10.1002/9781119424437.ch17

Wotherspoon, L., Orense, R., Bradley, B., Cox, B., Wood, C., Green, R., & Techi, V. (2014). *Geotechnical Characterisation of Christchurch Strong Motion Stations* (Version 2.0). Earthquake Commission.

3. Chapter Three – Summary and Conclusions.

3.1. Conclusions.

This thesis aimed to investigate the shallow stratigraphy of the Hamilton Central Business District (CDB) to better understand the physical and chemical characteristics of the geological units and assist in the development of future three dimensional (3D) geological models. This study has achieved the goals defined in Chapter One through numerous data collection techniques, grain size analysis, X-ray diffraction (XRD), use of the Munsell colour chart, facies analysis, radiocarbon dating, and 3D outcrop modelling. The continual identification of new faults and the ever-increasing population in Hamilton City show that even areas previously thought to be safe from seismic activity may be susceptible to earthquake-induced damage. The data derived from this investigation have the potential to assist in developing 3D geological models to interpret the strata throughout Hamilton Basin. Such future models may be able to provide information on the areas most at risk to seismic activity and on how to mitigate that risk. This final chapter will summarise the key findings of this investigation, identify any limitations encountered, and suggest areas for further research.

Due to the variable nature of braided rivers, the few available data points, and the high spatial variability of drill sites for the cores, sophisticated stratigraphic analysis would not be feasible. Instead, a simple lithostratigraphic cross-section (Figure 2.8) was developed to show the variability and similarities in the sediments recovered from the cores. There are multiple factors that are challenging to the mapping and modelling the study area and the wider Hamilton Basin. These challenge include the high degree of spatial and temporal facies variability inherent to braided river systems. Braided and meandering rivers are consistently changing by eroding older deposits and depositing new sediment; in this case, both the older and younger sediments are typically derived from similar sources.

One issue considered is scaling, specifically upscaling, and the potential benefits and issues associated with a change in model scale. The process of upscaling a set of data, typically a highly detailed but narrow investigation similar to what has been discussed in this paper, involves simplifying a dataset, often averaging the properties of similar points/packages over a defined distance interval, in order to better represent an overall area and reduce the computational power required to derive a model. When done correctly, and sometimes combined with stochastic modelling, an upscaled model can provide a reasonably accurate representation of an area's geology as a whole, which, in terms of seismic modelling, could help define safe development

standards. The problem with an upscaled seismic model that is based on narrow data points is that some areas will be given a seismic hazard rating that overestimates the effect of a seismic event, while others will be given an underestimate, the consequences for these include the over engineering, and thus higher cost of developments, as well as the under engineering that could lead to building failure.

3.2. Key Findings.

3.2.1. Hamilton CBD – Paleoenvironments.

This investigation found evidence that most of the shallow stratigraphy was deposited in a braided river system, consistent with previous studies (Sherwood, 1972; Kear & Schofield, 1978; Lowe, 2010). Braided river systems and the associated lateral heterogeneity and discontinuity will need to be considered in future geological modelling efforts. Paleoenvironment and facies extent identified in borehole cores could be supported further with the addition of seismic reflection data or ground penetrating radar (GRP).

3.2.2. Geological Modelling.

Creating a complete 3D geological model of the basin is possible, but scaling issues will need to be carefully managed. Numerous methods exist that, when combined, could be used to create a detailed and representative model of the Hamilton Basin. The vertical aspect of a grid cell size presents the biggest challenge in upscaling due to the thin nature of several facies identified in this investigation (F3 to F6B). The variance in shear wave velocity in the upper stratigraphy (V_{S30}) also poses issues as the units defined, e.g. gravel, sand, contain proportions of differing grain size. Researchers should embrace stochasticity in their efforts to reduce statistical uncertainty and better reflect the data being upscaled.

3.2.3. Seismic Hazard – Hamilton City.

While the Kerepehi Fault Zone has a low recurrence interval, new faults have been found in Hamilton City in recent years. There is potential for a M_W5.5 to M_W7.0 earthquake to occur, or M_W7.2 to M_W7.4 earthquake if all onshore Kerepehi Fault sections rupture (Persaud *et al*., 2016), where seismic amplification could result in significantly stronger, or weaker, seismic activity (Moon & de Lange, 2017), up to two to three times more intense than other cities (Dempsey *et al*., 2021). Liquefaction risk, observed in the Hinuera Formation (McKay, 2017), would be greatest in areas of high water tables (Kleyburg *et al*., 2015). Where seismic amplification is present, damage could be similar to that observed during the 2010/2011 Christchurch earthquake sequence

(Dempsey *et al.*, 2021). Kluger *et al.* (2023) identified liquefaction in lake sediments triggered by seismic activity proximal to the Kerepehi Fault and by local faulting in Hamilton Basin.

3.2.4. Data Sources.

For the reasons discussed (Section 2.4.2), geotechnical borehole data should be used with caution in the creation of any 3D geological models; specifically, boreholes that are not logged by qualified workers should be limited or excluded. A potential use of geotechnical borehole data could be to sense-check the results of any models produced. Data derived should include a combination of petrological boreholes, outcrop analysis, horizontal vertical spectral ratio (HVSR), and seismic reflection profiles. As the above methods will also be subject to their own error margins, statistical modelling should be utilised to increase accuracy by identifying the statistical medians and means.

3.3. Limitations and Future Studies.

As in any study, certain limitations were encountered. One of the biggest limitations in this study was the availability of data. The Waikato River's banks are covered with significant amounts of native vegetation throughout Hamilton City, making it difficult to find accessible outcrops to examine. This challenge increased further when considering the requirements for operating a UAV safely and legally. Only one outcrop satisfied these requirements, which, unfortunately, was quite distal from the nearest core location. Future studies investigating outcrops adjacent to the Waikato River would benefit from collecting samples from exposed outcrops by boat.

Core quality was also a limiting factor. The cores were subjected to numerous standard penetration tests (SPTs), which resulted in core compression, data loss when the SPT ran through strata with different physical characteristics, and the destruction of key unit contacts. Due to this limitation, there is the potential for over- or under-representation of packages in each core. Where layers of a different facies were present but had been disturbed, they may not have been recovered properly and would thus not be observed during logging.

The number available data points was another limitation. Further investigations or modelling should attempt to obtain and interpret more cores or alternative data sources. As mentioned, incorporating publicly available geotechnical borehole data may be useful, though verifying their accuracy may pose challenges.

One final limitation discussed is the difficulty encountered in dating the sediments recovered. Of the samples sent for radiocarbon dating, four were too old to date, one was aged as recent (<250

yr), and one was disregarded because its age was older than the sediments below; only two could be interpreted with confidence.

Other areas that may be of interest for future research include the presence of highly weathered ignimbrite, the liquefied layer observed in the outcrop, and the creation of 3D geological models, the latter of which is currently underway. The creation of any 3D models will be subject to their own limitations, many of which were discussed in this thesis and are likely to raise further questions and spark future studies.

3.4. References.

Dempsey, D., Eccles, J. D., Huang, J., Jeong, S., Nicolin, E., Stolte, A., Wotherspoon, L., Bradley, B. A. (2021). Ground Motion Simulation of Hypothetical Earthquakes in the Upper North Island of New Zealand. *New Zealand Journal of Geology and Geophysics, 64*(4), 570-588. doi.org/10.1080/00288306.2020.1842469

Kear, D., Schofield, J. C. (1978). Geology of the Ngāruawāhia Subdivision. *New Zealand Geological Survey Bulletin, 88*, 1-168.

Kleyburg, M. A., Moon, V. G., Lowe, D. J., Nelson, C. S. (2015). Paleoliquefaction in Late Pleistocene Alluvial Sediments in Hauraki and Hamilton Basins, and Implications for Paleoseismicity. *Proceedings, 12th Australia New Zealand Conference on Geomechanics (ANZ 2015), 22-25 February, 2015, Wellington, pp. 524-531*.

Kluger, M. O., Lowe, D. J., Moon, V. G., Chaneva, J., Johnston, R., Villamor, P., Ilanko, T., Melchert, R. A., Orense, R. P., Loame, R. C., Ross. R. (2023). Seismically-Induced Down-Sagging Structures in Tephra Layers (Tephra-Seismites) Preserved in Lakes Since 17.5 cal ka, Hamilton Lowlands, New Zealand. *Sedimentary Geology*, *445*, 1-23. doi.org/10.1016/j.sedgeo.2022.106327

Lowe, D.J. (2010). Introduction to the Landscapes and Soils of the Hamilton Basin. *In*: Lowe, D. J., Neall, V. E., Hedley, M., Clothier, B., Mackay, A. 2010. Guidebook for Pre-conference North Island, New Zealand 'Volcanoes to Oceans' field tour (27- 30 July). 19th World Soils Congress, International Union of Soil Sciences, Brisbane. *Soil and Earth Sciences Occasional Publication No. 3*, Massey University, Palmerston North, pp. 1.24-1.61.

McKay, A. M. (2017). Evaluating Soil Landscape Models to Predict Liquefaction Susceptibility in the Hinuera Formation, Hamilton Basin (Thesis, Master of Science (MSc)). The University of Waikato, Hamilton, New Zealand. hdl.handle.net/10289/11635

Moon, V., De Lange, W. EQC. (2017). *Potential Shallow Seismic Sources in the Hamilton Basin*. (EQC 16/717).

Persaud, M., Villamor, P., Berryman, K. R., Ries, W., Litchfield, N., Alloway, B. V. (2016). The Kerepehi Fault, Hauraki Rift, North Island, New Zealand: Active Fault Characterisation and Hazard. *New Zealand Journal of Geology and Geophysics, 59*(1), 117-135. doi.org/10.1080/00288306.2015.1127826

Sherwood, A. M. (1972). Sedimentary Structures, Features, and Paleoenvironments of the Hinuera Formation. [Thesis, University of Waikato]. Research Commons.

4. Appendices.

Appendix 1. Munsell Colour Chart.

Brownish yellow, brown, strong brown, greyish brown, grey, dark grey, black, were the most common colours observed across the cores. Strong brown & brownish yellow mottling was present across various depths and textures, most likely due to the weathering of ferromagnesian minerals and pumice clasts, the latter of which were typically observed between the layers. White, pale orange yellow (creamy in appearance), and black mottles were present less frequently, where the white and pale orange yellow were likely from weathered pumice clasts and the black from organic inclusions. Examples of interbedded layers with organic inclusions (very dark brown), ferromagnesian mottles, and pumiceous mottles are shown in Figure 4.1.

Figure 4.1. Examples of Sediment Colours Observed. A) 10YR 7/2 Light Grey Interbedded with 10YR 2/2 Very Dark Brown Organic Layers. B) 7.5YR 2.5/2 Very Dark Brown Oxidised Gravel Resulting in Mottling. C) 10YR 7/1 Light Grey Pumiceous Mottling.

Appendix 2. Grainsize.

- 20-1006.

SAMPLE STATISTICS

		20-1006_0.50mbgl	20-1006_1.00mbgl	20-1006_1.50mbgl
	ANALYST AND DATE:	, 11/29/2024	, 11/29/2024	, 11/29/2024
	LOCATION:	175°17'12.32" E 37°47'20.83" S	175°17'12.32" E 37°47'20.83" S	175°17'12.32" E 37°47'20.83" S
	SIEVING ERROR:	0.0%	0.0%	0.0%
	SAMPLE TYPE:	Bimodal, Very Poorly Sorted	Bimodal, Very Poorly Sorted	Bimodal, Very Poorly Sorted
	TEXTURAL GROUP:	Gravelly Muddy Sand	Gravelly Muddy Sand	Gravelly Muddy Sand
	SEDIMENT NAME:	he Gravelly Very Coarse Silty Mediu	Fine Gravelly Very Coarse Silty Fine	Fine Gravelly Very Coarse Silty Fine
FOLK AND WARD METHOD (μm)	MEAN (M_G):	193.2	216.6	150.1
	SORTING (σ_G):	5.202	5.243	6.994
	SKEWNESS (Sk_G):	-0.222	0.084	-0.063
	KURTOSIS (K_G):	1.553	1.382	1.407
FOLK AND WARD METHOD (ϕ)	MEAN (M_Z):	2.372	2.207	2.736
	SORTING (σ_I):	2.379	2.390	2.806
	SKEWNESS (Sk_I):	0.222	-0.084	0.063
	KURTOSIS (K_G):	1.553	1.382	1.407
FOLK AND WARD METHOD (Description)	MEAN:	Fine Sand	Fine Sand	Fine Sand
	SORTING:	Very Poorly Sorted	Very Poorly Sorted	Very Poorly Sorted
	SKEWNESS:	Fine Skewed	Symmetrical	Symmetrical
	KURTOSIS:	Very Leptokurtic	Leptokurtic	Leptokurtic
	MODE 1 (μm):	275.0	163.0	163.0
	MODE 1 (ϕ):	1.868	2.622	2.622
	D_{10} (μm):	15.72	27.02	10.21
	D_{50} (μm):	236.2	182.1	158.8
	D_{90} (μm):	985.1	2533.3	2655.5
	(D_{90} / D_{10}) (μm):	62.67	93.77	260.2
	(D_{90} - D_{10}) (μm):	969.4	2506.3	2645.3
	(D_{75} / D_{25}) (μm):	5.287	5.900	7.539
	(D_{75} - D_{25}) (μm):	401.1	409.4	370.0
	D_{10} (ϕ):	0.022	-1.341	-1.409
	D_{50} (ϕ):	2.082	2.457	2.654
	D_{90} (ϕ):	5.992	5.210	6.614
	(D_{90} / D_{10}) (ϕ):	276.2	-3.885	-4.694
	(D_{90} - D_{10}) (ϕ):	5.970	6.551	8.023
	(D_{75} / D_{25}) (ϕ):	3.366	3.509	3.371
	(D_{75} - D_{25}) (ϕ):	2.403	2.561	2.914
	% GRAVEL:	6.7%	12.4%	13.8%
	% SAND:	74.0%	68.9%	59.7%
	% MUD:	19.2%	18.7%	26.6%
	% V COARSE GRAVEL:	0.0%	0.0%	0.0%
	% COARSE GRAVEL:	0.0%	0.0%	0.0%
	% MEDIUM GRAVEL:	0.0%	0.0%	0.0%
	% FINE GRAVEL:	0.0%	0.0%	0.0%
	% V FINE GRAVEL:	6.7%	12.4%	13.8%
	% V COARSE SAND:	3.0%	4.2%	1.3%
	% COARSE SAND:	14.9%	8.3%	7.4%
	% MEDIUM SAND:	23.4%	15.0%	14.5%
	% FINE SAND:	21.0%	23.2%	20.3%
	% V FINE SAND:	11.8%	18.3%	16.3%
	% V COARSE SILT:	5.5%	7.9%	8.6%
	% COARSE SILT:	3.8%	3.8%	5.5%
	% MEDIUM SILT:	3.2%	2.5%	4.1%
	% FINE SILT:	2.7%	1.9%	3.3%
	% V FINE SILT:	2.1%	1.4%	2.6%
	% CLAY:	2.0%	1.2%	2.6%

Figure 4.2. 20-1006 GRADISTAT Grainsize Analysis (1/17).

20-1006_2.00mbgl	20-1006_2.25mbgl	20-1006_2.50mbgl	20-1006_3.00mbgl
, 11/29/2024	, 11/29/2024	, 11/22/2024	, 11/22/2024
175°17'12.32" E 37°47'20.83" S	175°17'12.32" E 37°47'20.83" S	175°17'12.32" E 37°47'20.83" S	175°17'12.32" E 37°47'20.83" S
0.0%	0.0%	0.0%	0.0%
Unimodal, Very Poorly Sorted	Trimodal, Poorly Sorted	Trimodal, Very Poorly Sorted	Unimodal, Very Poorly Sorted
Gravelly Muddy Sand	Muddy Sandy Gravel	Muddy Sandy Gravel	Muddy Sandy Gravel
he Gravelly Very Coarse Silty Mediu	Coarse Silty Sandy Very Fine Grave	ry Coarse Silty Sandy Very Fine Gra	ry Coarse Silty Sandy Very Fine Gra
224.7	956.8	250.4	235.7
5.334	3.273	8.495	5.514
-0.168	-1.582	-0.396	-0.057
1.268	-8.824	0.522	0.517
2.154	0.064	1.998	2.085
2.415	1.711	3.087	2.463
0.168	1.582	0.396	0.057
1.268	-8.824	0.522	0.517
Fine Sand	Coarse Sand	Medium Sand	Fine Sand
Very Poorly Sorted	Poorly Sorted	Very Poorly Sorted	Very Poorly Sorted
Fine Skewed	Very Fine Skewed	Very Fine Skewed	Symmetrical
Leptokurtic	Very Platykurtic	Very Platykurtic	Very Platykurtic
275.0	3000.0	34.00	68.50
1.868	-1.500	4.884	3.872
19.18	42.48	8.966	21.28
248.5	2846.8	363.4	197.7
1497.4	377770675.2	16948.9	59436.0
78.06	8893212.7	1890.3	2793.1
1478.2	377770632.8	16939.9	59414.7
6.900	0.801	107.8	45.45
526.8	-419.034	3831.9	2487.6
-0.582	-18.527	-4.083	-5.893
2.009	-1.509	1.460	2.338
5.704	4.557	6.801	5.554
-9.793	-0.246	-1.666	-0.942
6.287	23.08	10.88	11.45
4.987	1.424	-2.460	-3.088
2.787	-0.320	6.752	5.506
6.3%	75.7%	33.4%	39.7%
74.3%	13.0%	34.4%	32.5%
19.4%	11.3%	32.2%	27.8%
0.0%	0.0%	0.0%	0.0%
0.0%	0.0%	0.0%	0.0%
0.0%	0.0%	0.0%	0.0%
0.0%	0.0%	0.0%	0.0%
6.3%	75.7%	33.4%	39.7%
9.6%	2.0%	4.1%	1.3%
14.0%	2.7%	8.9%	3.0%
19.9%	3.1%	7.4%	4.0%
18.3%	2.7%	6.4%	7.8%
12.4%	2.5%	7.6%	16.4%
6.6%	2.4%	9.1%	14.2%
4.1%	2.4%	8.5%	6.5%
3.0%	2.1%	5.7%	3.1%
2.4%	1.5%	3.4%	1.5%
1.8%	1.3%	2.4%	1.0%
1.7%	1.7%	3.1%	1.5%

Figure 4.3. 20-1006 GRADISTAT Grainsize Analysis (2/17).

20-1006_3.50mbgl	20-1006_3.75mbgl	20-1006_4.00mbgl	20-1006_4.50mbgl
, 11/22/2024	, 11/29/2024	, 11/29/2024	, 11/29/2024
175°17'12.32" E 37°47'20.83" S	175°17'12.32" E 37°47'20.83" S	175°17'12.32" E 37°47'20.83" S	175°17'12.32" E 37°47'20.83" S
0.0%	0.0%	0.0%	0.0%
Bimodal, Very Poorly Sorted	Unimodal, Very Poorly Sorted	Bimodal, Poorly Sorted	Bimodal, Very Poorly Sorted
Gravelly Mud	Gravelly Mud	Muddy Sand	Slightly Gravelly Muddy Sand
Very Fine Gravelly Fine Silt	Very Fine Gravelly Very Coarse Silt	Very Coarse Silty Medium Sand	Fine Gravelly Very Coarse Silty Ver
8.941	149.8	197.1	58.90
6.251	9.366	3.176	4.741
0.248	0.044	-0.445	-0.269
1.670	0.532	1.403	1.201
6.805	2.739	2.343	4.085
2.644	3.227	1.667	2.245
-0.248	-0.044	0.445	0.269
1.670	0.532	1.403	1.201
Medium Silt	Fine Sand	Fine Sand	Very Coarse Silt
Very Poorly Sorted	Very Poorly Sorted	Poorly Sorted	Very Poorly Sorted
Coarse Skewed	Symmetrical	Very Fine Skewed	Fine Skewed
Very Leptokurtic	Very Platykurtic	Leptokurtic	Leptokurtic
5.850	81.00	325.0	115.0
7.502	3.631	1.626	3.126
1.595	6.967	31.45	5.997
8.555	97.77	262.9	77.79
68.12	17109.8	596.3	304.8
42.71	2456.0	18.96	50.82
66.53	17102.9	564.9	298.8
6.413	119.7	3.260	6.544
18.93	3058.7	288.2	134.1
3.876	-4.097	0.746	1.714
6.869	3.354	1.927	3.684
9.292	7.165	4.991	7.382
2.398	-1.749	6.691	4.306
5.417	11.26	4.245	5.667
1.489	-3.248	2.346	2.019
2.681	6.903	1.705	2.710
5.2%	25.9%	0.0%	0.8%
5.4%	32.9%	83.1%	55.7%
89.4%	41.2%	16.9%	43.5%
0.0%	0.0%	0.0%	0.0%
0.0%	0.0%	0.0%	0.0%
0.0%	0.0%	0.0%	0.0%
0.0%	0.0%	0.0%	0.0%
5.2%	25.9%	0.0%	0.8%
0.0%	0.3%	1.1%	1.6%
0.3%	3.0%	15.3%	3.7%
0.6%	5.6%	36.3%	7.0%
1.2%	10.4%	22.7%	20.1%
3.4%	13.6%	7.7%	23.3%
7.4%	13.1%	6.9%	14.7%
14.7%	10.9%	4.3%	10.3%
19.9%	6.5%	2.4%	6.8%
20.0%	3.9%	1.4%	4.5%
15.0%	3.1%	0.9%	3.4%
12.4%	3.6%	1.0%	3.8%

Figure 4.4. 20-1006 GRADISTAT Grainsize Analysis (3/17).

20-1006_5.00mbgl	20-1006_5.50mbgl	20-1006_6.00mbgl	20-1006_6.50mbgl
, 11/29/2024	, 11/29/2024	, 11/22/2024	, 11/29/2024
175°17'12.32" E 37°47'20.83" S	175°17'12.32" E 37°47'20.83" S	175°17'12.32" E 37°47'20.83" S	175°17'12.32" E 37°47'20.83" S
0.0%	0.0%	0.0%	0.0%
Bimodal, Very Poorly Sorted	Bimodal, Very Poorly Sorted	Unimodal, Poorly Sorted	Unimodal, Very Poorly Sorted
Gravelly Muddy Sand	Gravelly Muddy Sand	Slightly Gravelly Mud	Slightly Gravelly Muddy Sand
ne Gravelly Very Coarse Silty Mediu	ne Gravelly Very Coarse Silty Coars	lightly Very Fine Gravelly Medium Sy	Fine Gravelly Very Coarse Silty Me
398.3	337.0	10.75	205.1
6.415	5.799	3.731	4.072
-0.193	-0.100	-0.071	-0.176
0.886	0.908	1.058	1.382
1.328	1.569	6.540	2.286
2.681	2.536	1.900	2.026
0.193	0.100	0.071	0.176
0.886	0.908	1.058	1.382
Medium Sand	Medium Sand	Medium Silt	Fine Sand
Very Poorly Sorted	Very Poorly Sorted	Poorly Sorted	Very Poorly Sorted
Fine Skewed	Fine Skewed	Symmetrical	Fine Skewed
Platykurtic	Mesokurtic	Mesokurtic	Leptokurtic
325.0	650.0	11.70	275.0
1.626	0.628	6.502	1.868
21.13	29.22	1.909	26.86
358.1	324.0	11.71	223.7
7441.6	3427.1	55.23	897.1
352.3	117.3	28.94	33.40
7420.4	3397.9	53.32	870.2
11.43	10.91	5.613	4.783
1260.7	912.4	21.50	370.7
-2.896	-1.777	4.178	0.157
1.481	1.626	6.417	2.161
5.565	5.097	9.033	5.218
-1.922	-2.868	2.162	33.30
8.461	6.874	4.855	5.062
-6.537	-540.410	1.473	3.065
3.515	3.448	2.489	2.258
24.5%	18.3%	0.7%	4.9%
57.7%	62.8%	7.9%	78.3%
17.8%	18.9%	91.4%	16.8%
0.0%	0.0%	0.0%	0.0%
0.0%	0.0%	0.0%	0.0%
0.0%	0.0%	0.0%	0.0%
0.0%	0.0%	0.0%	0.0%
24.5%	18.3%	0.7%	4.9%
3.2%	6.8%	0.0%	3.5%
13.3%	15.4%	0.0%	14.7%
19.1%	15.1%	0.6%	23.0%
14.4%	14.0%	2.3%	22.7%
7.6%	11.6%	4.9%	14.4%
5.4%	8.4%	11.1%	6.0%
4.3%	4.7%	21.0%	3.5%
3.1%	2.4%	22.4%	2.6%
2.1%	1.5%	16.0%	2.0%
1.5%	1.0%	10.7%	1.4%
1.5%	0.9%	10.2%	1.3%

Figure 4.5. 20-1006 GRADISTAT Grainsize Analysis (4/17).

20-1006_7.00mbgl	20-1006_7.50mbgl	20-1006_8.00mbgl	20-1006_8.50mbgl
, 11/29/2024	, 11/29/2024	, 11/29/2024	, 11/29/2024
175°17'12.32" E 37°47'20.83" S	175°17'12.32" E 37°47'20.83" S	175°17'12.32" E 37°47'20.83" S	175°17'12.32" E 37°47'20.83" S
0.0%	0.0%	0.0%	0.0%
Bimodal, Poorly Sorted	Bimodal, Very Poorly Sorted	Unimodal, Poorly Sorted	Unimodal, Poorly Sorted
Gravelly Sand	Slightly Gravelly Muddy Sand	Slightly Gravelly Sand	Gravelly Sand
Very Fine Gravelly Medium Sand	y Fine Gravelly Very Coarse Silty M	ghtly Very Fine Gravelly Coarse Sa	Very Fine Gravelly Coarse Sand
395.6	139.7	451.6	737.7
3.540	5.721	2.587	2.698
-0.091	-0.322	-0.313	-0.014
1.654	1.140	1.623	0.906
1.338	2.840	1.147	0.439
1.824	2.516	1.371	1.432
0.091	0.322	0.313	0.014
1.654	1.140	1.623	0.906
Medium Sand	Fine Sand	Medium Sand	Coarse Sand
Poorly Sorted	Very Poorly Sorted	Poorly Sorted	Poorly Sorted
Symmetrical	Very Fine Skewed	Very Fine Skewed	Symmetrical
Very Leptokurtic	Leptokurtic	Very Leptokurtic	Mesokurtic
385.0	325.0	545.0	545.0
1.383	1.626	0.881	0.881
79.29	9.441	111.4	192.6
393.0	195.6	492.9	623.7
1798.3	862.4	1099.8	4302.1
22.68	91.34	9.871	22.34
1719.0	853.0	988.4	4109.5
3.476	8.331	2.592	3.607
527.1	403.3	466.3	910.0
-0.847	0.214	-0.137	-2.105
1.347	2.354	1.021	0.681
3.657	6.727	3.166	2.377
-4.319	31.50	-23.062	-1.129
4.503	6.513	3.303	4.482
5.137	3.717	4.458	-4.569
1.798	3.058	1.374	1.851
9.3%	4.3%	2.4%	17.9%
81.9%	69.1%	90.8%	78.5%
8.8%	26.6%	6.9%	3.6%
0.0%	0.0%	0.0%	0.0%
0.0%	0.0%	0.0%	0.0%
0.0%	0.0%	0.0%	0.0%
0.0%	0.0%	0.0%	0.0%
9.3%	4.3%	2.4%	17.9%
8.1%	3.4%	10.3%	13.3%
21.9%	14.9%	36.5%	28.8%
30.2%	20.4%	30.6%	25.1%
16.8%	18.4%	9.5%	9.1%
4.9%	12.1%	3.9%	2.2%
2.5%	7.5%	1.9%	1.0%
2.0%	5.8%	1.5%	0.8%
1.6%	4.6%	1.3%	0.8%
1.2%	3.5%	1.0%	0.6%
0.8%	2.6%	0.7%	0.4%
0.7%	2.6%	0.5%	0.0%

Figure 4.6. 20-1006 GRADISTAT Grainsize Analysis (5/17).

20-1006_9.00mbgl	20-1006_9.50mbgl	20-1006_9.75mbgl	20-1006_10.00mbgl
, 11/29/2024	, 11/29/2024	, 11/29/2024	, 11/29/2024
175°17'12.32" E 37°47'20.83" S	175°17'12.32" E 37°47'20.83" S	175°17'12.32" E 37°47'20.83" S	175°17'12.32" E 37°47'20.83" S
0.0%	0.0%	0.0%	0.0%
Bimodal, Very Poorly Sorted	Unimodal, Poorly Sorted	Unimodal, Very Poorly Sorted	Unimodal, Poorly Sorted
Gravelly Muddy Sand	Gravelly Sand	Sandy Mud	Slightly Gravelly Sand
ne Gravelly Very Coarse Silty Mediu	Very Fine Gravelly Coarse Sand	Very Fine Sandy Fine Silt	ghtly Very Fine Gravelly Medium Sa
224.1	581.4	8.358	351.8
5.157	2.676	4.276	2.557
-0.204	-0.043	0.134	-0.276
1.465	1.493	1.047	1.658
2.157	0.782	6.903	1.507
2.366	1.420	2.096	1.354
0.204	0.043	-0.134	0.276
1.465	1.493	1.047	1.658
Fine Sand	Coarse Sand	Medium Silt	Medium Sand
Very Poorly Sorted	Poorly Sorted	Very Poorly Sorted	Poorly Sorted
Fine Skewed	Symmetrical	Coarse Skewed	Fine Skewed
Leptokurtic	Leptokurtic	Mesokurtic	Very Leptokurtic
325.0	650.0	5.850	385.0
1.626	0.628	7.502	1.383
19.76	177.8	1.460	108.2
268.9	590.7	7.731	370.4
1362.5	1826.4	64.80	843.3
68.93	10.27	44.39	7.796
1342.7	1648.6	63.34	735.1
5.598	2.842	6.942	2.564
473.5	639.0	18.48	351.8
-0.446	-0.869	3.948	0.246
1.895	0.759	7.015	1.433
5.661	2.492	9.420	3.209
-12.686	-2.867	2.386	13.05
6.107	3.361	5.472	2.963
4.128	73.81	1.505	2.710
2.485	1.507	2.795	1.359
8.7%	9.0%	0.0%	0.9%
73.1%	86.7%	10.3%	91.5%
18.2%	4.3%	89.7%	7.5%
0.0%	0.0%	0.0%	0.0%
0.0%	0.0%	0.0%	0.0%
0.0%	0.0%	0.0%	0.0%
0.0%	0.0%	0.0%	0.0%
8.7%	9.0%	0.0%	0.9%
4.4%	15.4%	0.0%	5.0%
16.0%	34.3%	0.2%	26.5%
23.3%	25.8%	2.1%	38.2%
18.9%	8.4%	3.5%	18.0%
10.5%	2.8%	4.4%	3.7%
5.6%	1.3%	7.5%	1.8%
3.9%	0.9%	13.7%	1.7%
3.0%	0.9%	18.3%	1.5%
2.3%	0.7%	19.9%	1.2%
1.7%	0.4%	16.3%	0.8%
1.7%	0.0%	14.2%	0.5%

Figure 4.7. 20-1006 GRADISTAT Grainsize Analysis (6/17).

20-1006_10.50mbgl	20-1006_11.00mbgl	20-1006_11.35mbgl	20-1006_11.50mbgl
, 11/29/2024	, 11/29/2024	, 11/29/2024	, 11/29/2024
175°17'12.32" E 37°47'20.83" S	175°17'12.32" E 37°47'20.83" S	175°17'12.32" E 37°47'20.83" S	175°17'12.32" E 37°47'20.83" S
0.0%	0.0%	0.0%	0.0%
Unimodal, Poorly Sorted	Unimodal, Poorly Sorted	Unimodal, Poorly Sorted	Unimodal, Very Poorly Sorted
Muddy Sand	Muddy Sand	Sandy Mud	Sandy Mud
Very Coarse Silty Very Fine Sand	Very Coarse Silty Very Fine Sand	Very Fine Sandy Very Coarse Silt	Very Fine Sandy Very Coarse Silt
77.28	70.47	27.71	31.91
3.733	3.061	2.955	5.534
-0.152	-0.313	-0.308	-0.226
1.102	1.355	1.227	0.989
3.694	3.827	5.174	4.970
1.900	1.614	1.563	2.468
0.152	0.313	0.308	0.226
1.102	1.355	1.227	0.989
Very Fine Sand	Very Fine Sand	Coarse Silt	Very Coarse Silt
Poorly Sorted	Poorly Sorted	Poorly Sorted	Very Poorly Sorted
Fine Skewed	Very Fine Skewed	Very Fine Skewed	Fine Skewed
Mesokurtic	Leptokurtic	Leptokurtic	Mesokurtic
68.50	96.50	40.50	68.50
3.872	3.379	4.631	3.872
12.15	12.94	5.287	2.528
82.03	82.76	32.72	40.70
344.5	220.9	85.27	228.4
28.35	17.07	16.13	90.36
332.3	207.9	79.98	225.9
5.299	3.406	3.554	9.863
155.1	99.59	40.41	97.22
1.538	2.179	3.552	2.130
3.608	3.595	4.934	4.619
6.363	6.272	7.563	8.628
4.138	2.879	2.129	4.050
4.825	4.093	4.012	6.498
2.008	1.626	1.441	2.029
2.406	1.768	1.829	3.302
0.0%	0.0%	0.0%	0.0%
59.1%	62.2%	20.5%	39.2%
40.9%	37.8%	79.5%	60.8%
0.0%	0.0%	0.0%	0.0%
0.0%	0.0%	0.0%	0.0%
0.0%	0.0%	0.0%	0.0%
0.0%	0.0%	0.0%	0.0%
0.0%	0.0%	0.0%	0.0%
0.1%	0.0%	0.0%	0.0%
3.6%	0.4%	0.0%	1.3%
14.2%	6.9%	0.5%	7.3%
18.9%	23.0%	2.5%	12.9%
22.3%	32.0%	17.5%	17.6%
19.2%	18.5%	31.6%	17.1%
9.9%	8.1%	23.3%	14.0%
5.0%	4.3%	11.3%	9.3%
3.0%	2.8%	5.8%	6.7%
1.9%	2.0%	3.5%	6.0%
1.9%	2.0%	3.9%	7.8%

Figure 4.8. 20-1006 GRADISTAT Grainsize Analysis (7/17).

20-1006_11.75mbgl	20-1006_12.00mbgl	20-1006_12.50mbgl	20-1006_13.00mbgl
, 11/22/2024	, 11/29/2024	, 11/29/2024	, 11/29/2024
175°17'12.32" E 37°47'20.83" S	175°17'12.32" E 37°47'20.83" S	175°17'12.32" E 37°47'20.83" S	175°17'12.32" E 37°47'20.83" S
0.0%	0.0%	0.0%	0.0%
Unimodal, Poorly Sorted	Unimodal, Poorly Sorted	Bimodal, Very Poorly Sorted	Unimodal, Poorly Sorted
Mud	Mud	Slightly Gravelly Muddy Sand	Slightly Gravelly Muddy Sand
Coarse Silt	Medium Silt	ery Fine Gravelly Medium Silty Med	ery Fine Gravelly Medium Silty Med
9.699	7.439	123.8	403.9
3.273	2.879	6.889	3.006
-0.152	-0.114	-0.556	-0.392
0.940	1.043	0.933	2.482
6.688	7.071	3.014	1.308
1.711	1.526	2.784	1.588
0.152	0.114	0.556	0.392
0.940	1.043	0.933	2.482
Medium Silt	Fine Silt	Very Fine Sand	Medium Sand
Poorly Sorted	Poorly Sorted	Very Poorly Sorted	Poorly Sorted
Fine Skewed	Fine Skewed	Very Fine Skewed	Very Fine Skewed
Mesokurtic	Mesokurtic	Mesokurtic	Very Leptokurtic
23.30	11.70	460.0	460.0
5.507	6.502	1.126	1.126
1.883	1.738	5.237	30.95
10.86	7.985	263.8	431.3
39.74	26.78	798.2	885.6
21.10	15.41	152.4	28.62
37.86	25.04	792.9	854.6
5.322	3.892	13.84	2.311
18.96	11.04	476.6	360.9
4.653	5.223	0.325	0.175
6.524	6.968	1.922	1.213
9.053	9.168	7.577	5.014
1.945	1.755	23.30	28.60
4.399	3.946	7.252	4.839
1.445	1.323	4.945	2.852
2.412	1.960	3.791	1.209
0.0%	0.0%	0.3%	1.6%
3.5%	2.5%	71.1%	86.8%
96.5%	97.5%	28.6%	11.5%
0.0%	0.0%	0.0%	0.0%
0.0%	0.0%	0.0%	0.0%
0.0%	0.0%	0.0%	0.0%
0.0%	0.0%	0.0%	0.0%
0.0%	0.0%	0.3%	1.6%
0.0%	0.0%	4.5%	4.8%
0.0%	0.4%	21.2%	33.6%
0.0%	0.6%	25.7%	38.8%
0.6%	0.5%	13.1%	8.4%
2.9%	0.9%	6.5%	1.2%
12.0%	3.9%	4.7%	1.5%
22.6%	16.6%	4.9%	1.9%
22.6%	27.9%	5.8%	2.6%
17.1%	23.6%	5.5%	2.4%
11.8%	14.1%	4.1%	1.7%
10.4%	11.4%	3.6%	1.4%

Figure 4.9. 20-1006 GRADISTAT Grainsize Analysis (8/17).

20-1006_13.50mbgl	20-1006_14.00mbgl	20-1006_14.50mbgl	20-1006_15.00mbgl
, 11/29/2024	, 11/29/2024	, 11/29/2024	, 11/29/2024
175°17'12.32" E 37°47'20.83" S	175°17'12.32" E 37°47'20.83" S	175°17'12.32" E 37°47'20.83" S	175°17'12.32" E 37°47'20.83" S
0.0%	0.0%	0.0%	0.0%
Trimodal, Very Poorly Sorted	Bimodal, Very Poorly Sorted	Unimodal, Poorly Sorted	Bimodal, Poorly Sorted
Muddy Sandy Gravel	Gravelly Muddy Sand	Slightly Gravelly Muddy Sand	Gravelly Muddy Sand
ry Coarse Silty Sandy Very Fine Grave	Gravelly Very Coarse Silty Mediu	y Fine Gravelly Very Coarse Silty Me	Gravelly Very Coarse Silty Mediu
478.3	312.4	272.6	306.2
6.642	5.400	3.741	3.795
-0.470	-0.209	-0.403	-0.200
0.878	1.456	1.831	1.945
1.064	1.679	1.875	1.708
2.732	2.433	1.903	1.924
0.470	0.209	0.403	0.200
0.878	1.456	1.831	1.945
Medium Sand	Medium Sand	Medium Sand	Medium Sand
Very Poorly Sorted	Very Poorly Sorted	Poorly Sorted	Poorly Sorted
Very Fine Skewed	Fine Skewed	Very Fine Skewed	Fine Skewed
Platykurtic	Leptokurtic	Very Leptokurtic	Very Leptokurtic
545.0	460.0	385.0	385.0
0.881	1.126	1.383	1.383
15.36	24.87	25.62	48.30
649.2	375.8	341.4	348.7
8400.4	2292.6	907.7	2469.7
547.0	92.17	35.42	51.14
8385.0	2267.8	882.1	2421.4
14.13	5.679	3.162	3.163
2621.0	668.2	385.9	397.8
-3.070	-1.197	0.140	-1.304
0.623	1.412	1.551	1.520
6.025	5.329	5.286	4.372
-1.962	-4.452	37.85	-3.352
9.095	6.526	5.147	5.676
-1.554	9.294	3.012	3.125
3.820	2.506	1.661	1.661
31.1%	11.2%	1.7%	11.7%
51.9%	72.9%	84.1%	76.7%
17.0%	15.9%	14.3%	11.6%
0.0%	0.0%	0.0%	0.0%
0.0%	0.0%	0.0%	0.0%
0.0%	0.0%	0.0%	0.0%
0.0%	0.0%	0.0%	0.0%
31.1%	11.2%	1.7%	11.7%
8.2%	9.0%	6.4%	0.8%
18.0%	19.7%	22.4%	19.1%
15.0%	23.4%	34.1%	33.8%
6.6%	13.7%	16.2%	16.6%
4.1%	7.2%	5.0%	6.4%
3.5%	4.7%	3.5%	3.6%
3.4%	3.6%	2.9%	2.4%
3.3%	2.9%	2.7%	2.1%
2.8%	2.1%	2.3%	1.6%
2.1%	1.4%	1.6%	1.1%
2.0%	1.1%	1.3%	0.8%

Figure 4.10. 20-1006 GRADISTAT Grainsize Analysis (9/17).

20-1006_15.50mbgl	20-1006_16.00mbgl	20-1006_16.50mbgl	20-1006_17.00mbgl
, 11/29/2024	, 11/29/2024	, 11/29/2024	, 11/29/2024
175°17'12.32" E 37°47'20.83" S	175°17'12.32" E 37°47'20.83" S	175°17'12.32" E 37°47'20.83" S	175°17'12.32" E 37°47'20.83" S
0.0%	0.0%	0.0%	0.0%
Unimodal, Poorly Sorted	Bimodal, Very Poorly Sorted	Unimodal, Poorly Sorted	Unimodal, Poorly Sorted
Slightly Gravelly Muddy Sand	Gravelly Muddy Sand	Slightly Gravelly Muddy Sand	Slightly Gravelly Muddy Sand
y Fine Gravelly Very Coarse Silty Me	ne Gravelly Very Coarse Silty Mediu	y Fine Gravelly Very Coarse Silty Me	y Fine Gravelly Very Coarse Silty Me
325.7	183.1	296.8	182.2
3.410	5.238	3.205	3.915
-0.361	-0.180	-0.262	-0.321
1.604	1.364	1.554	1.501
1.618	2.450	1.752	2.456
1.770	2.389	1.680	1.969
0.361	0.180	0.262	0.321
1.604	1.364	1.554	1.501
Medium Sand	Fine Sand	Medium Sand	Fine Sand
Poorly Sorted	Very Poorly Sorted	Poorly Sorted	Poorly Sorted
Very Fine Skewed	Fine Skewed	Fine Skewed	Very Fine Skewed
Very Leptokurtic	Leptokurtic	Very Leptokurtic	Very Leptokurtic
460.0	325.0	385.0	275.0
1.126	1.626	1.383	1.868
44.20	17.28	52.62	20.12
386.3	223.9	324.0	224.1
1033.9	997.1	942.5	701.7
23.39	57.72	17.91	34.87
989.7	979.8	889.9	681.5
3.328	6.335	3.314	4.030
461.0	419.4	394.6	305.0
-0.048	0.004	0.085	0.511
1.372	2.159	1.626	2.158
4.500	5.855	4.248	5.635
-93.482	1404.1	49.72	11.02
4.548	5.851	4.163	5.124
3.883	3.648	3.099	2.545
1.735	2.663	1.729	2.011
0.7%	7.4%	1.8%	3.1%
87.3%	71.2%	87.2%	78.8%
12.0%	21.4%	10.9%	18.1%
0.0%	0.0%	0.0%	0.0%
0.0%	0.0%	0.0%	0.0%
0.0%	0.0%	0.0%	0.0%
0.0%	0.0%	0.0%	0.0%
0.7%	7.4%	1.8%	3.1%
10.1%	2.5%	6.9%	2.5%
26.7%	14.9%	21.2%	12.3%
31.0%	21.8%	31.7%	27.4%
14.1%	18.9%	20.4%	24.9%
5.5%	13.0%	7.0%	11.7%
3.6%	7.3%	3.1%	5.6%
2.6%	4.8%	2.5%	3.9%
2.1%	3.6%	2.1%	3.0%
1.6%	2.6%	1.6%	2.4%
1.1%	1.7%	1.0%	1.7%
0.9%	1.4%	0.7%	1.5%

Figure 4.11. 20-1006 GRADISTAT Grainsize Analysis (10/17).

20-1006_17.50mbgl	20-1006_18.00mbgl	20-1006_18.50mbgl	20-1006_19.00mbgl
, 11/29/2024	, 11/29/2024	, 11/29/2024	, 11/29/2024
175°17'12.32" E 37°47'20.83" S	175°17'12.32" E 37°47'20.83" S	175°17'12.32" E 37°47'20.83" S	175°17'12.32" E 37°47'20.83" S
0.0%	0.0%	0.0%	0.0%
Unimodal, Poorly Sorted	Unimodal, Poorly Sorted	Unimodal, Poorly Sorted	Unimodal, Poorly Sorted
Slightly Gravelly Sand	Slightly Gravelly Muddy Sand	Muddy Sand	Sandy Mud
ghtly Very Fine Gravelly Medium Sa	ery Fine Gravelly Very Coarse Silty F	Very Coarse Silty Fine Sand	Very Fine Sandy Very Coarse Silt
419.1	148.2	105.8	30.81
2.054	3.080	3.008	3.099
-0.147	-0.258	-0.368	-0.281
1.245	1.342	1.451	1.190
1.254	2.754	3.241	5.020
1.039	1.623	1.589	1.632
0.147	0.258	0.368	0.281
1.245	1.342	1.451	1.190
Medium Sand	Fine Sand	Very Fine Sand	Coarse Silt
Poorly Sorted	Poorly Sorted	Poorly Sorted	Poorly Sorted
Fine Skewed	Fine Skewed	Very Fine Skewed	Fine Skewed
Leptokurtic	Leptokurtic	Leptokurtic	Leptokurtic
460.0	193.5	163.0	48.50
1.126	2.375	2.622	4.372
169.8	28.87	17.68	5.644
427.0	165.4	125.2	35.99
935.3	473.6	301.1	102.1
5.508	16.40	17.04	18.09
765.5	444.7	283.5	96.43
2.377	3.561	3.188	3.890
377.2	210.3	141.0	48.08
0.096	1.078	1.732	3.292
1.228	2.596	2.997	4.796
2.558	5.114	5.822	7.469
26.52	4.743	3.362	2.269
2.461	4.036	4.090	4.177
3.018	2.033	1.733	1.496
1.249	1.832	1.673	1.960
0.1%	0.9%	0.0%	0.0%
95.5%	80.1%	75.8%	26.4%
4.5%	19.0%	24.2%	73.6%
0.0%	0.0%	0.0%	0.0%
0.0%	0.0%	0.0%	0.0%
0.0%	0.0%	0.0%	0.0%
0.0%	0.0%	0.0%	0.0%
0.1%	0.9%	0.0%	0.0%
7.8%	0.8%	0.0%	0.0%
32.1%	7.0%	1.0%	0.0%
39.2%	22.8%	15.5%	0.4%
14.3%	30.2%	33.6%	5.3%
2.0%	19.4%	25.7%	20.7%
1.1%	8.5%	10.0%	29.4%
0.9%	4.0%	5.1%	21.2%
1.0%	2.3%	3.2%	10.5%
0.9%	1.8%	2.4%	5.4%
0.5%	1.3%	1.8%	3.4%
0.0%	1.1%	1.7%	3.7%

Figure 4.12. 20-1006 GRADISTAT Grainsize Analysis (11/17).

20-1006_19.50mbgl	20-1006_19.95mbgl	20-1006_20.05mbgl	20-1006_20.50mbgl
, 11/22/2024	, 11/22/2024	, 11/22/2024	, 11/29/2024
175°17'12.32" E 37°47'20.83" S	175°17'12.32" E 37°47'20.83" S	175°17'12.32" E 37°47'20.83" S	175°17'12.32" E 37°47'20.83" S
0.0%	0.0%	0.0%	0.0%
Unimodal, Poorly Sorted	Unimodal, Very Poorly Sorted	Trimodal, Very Poorly Sorted	Unimodal, Poorly Sorted
Sandy Mud	Gravelly Mud	Gravelly Mud	Muddy Sand
Very Fine Sandy Very Coarse Silt	Very Fine Gravelly Very Coarse Silt	Very Fine Gravelly Very Coarse Silt	Very Coarse Silty Very Fine Sand
20.74	96.50	25.81	52.98
3.249	11.85	6.752	2.733
-0.285	0.298	0.060	-0.398
1.113	1.065	1.471	1.485
5.591	3.373	5.276	4.239
1.700	3.566	2.755	1.451
0.285	-0.298	-0.060	0.398
1.113	1.065	1.471	1.485
Coarse Silt	Very Fine Sand	Coarse Silt	Very Coarse Silt
Poorly Sorted	Very Poorly Sorted	Very Poorly Sorted	Poorly Sorted
Fine Skewed	Coarse Skewed	Symmetrical	Very Fine Skewed
Leptokurtic	Mesokurtic	Leptokurtic	Leptokurtic
34.00	34.00	40.50	81.00
4.884	4.884	4.631	3.631
3.510	4.373	2.976	10.16
24.97	37.53	28.63	63.70
73.00	10524.1	517.5	137.3
20.80	2406.7	173.9	13.51
69.49	10519.7	514.5	127.2
4.389	12.13	7.828	2.775
35.64	152.8	62.68	62.80
3.776	-3.396	0.950	2.864
5.323	4.736	5.126	3.973
8.154	7.837	8.392	6.620
2.159	-2.308	8.829	2.311
4.378	11.23	7.442	3.756
1.481	2.392	1.781	1.440
2.134	3.600	2.969	1.472
0.0%	21.8%	6.1%	0.0%
14.2%	14.9%	22.3%	51.1%
85.8%	63.3%	71.6%	48.9%
0.0%	0.0%	0.0%	0.0%
0.0%	0.0%	0.0%	0.0%
0.0%	0.0%	0.0%	0.0%
0.0%	0.0%	0.0%	0.0%
0.0%	21.8%	6.1%	0.0%
0.0%	0.0%	1.0%	0.0%
0.0%	0.6%	3.0%	0.0%
0.2%	1.4%	1.6%	0.3%
2.2%	2.7%	3.6%	12.9%
11.7%	10.2%	13.0%	37.9%
27.6%	18.5%	19.4%	27.1%
25.2%	17.6%	17.3%	8.8%
13.9%	11.2%	13.0%	4.8%
8.2%	7.0%	9.5%	3.4%
5.3%	4.5%	6.3%	2.4%
5.6%	4.4%	6.2%	2.4%

Figure 4.13. 20-1006 GRADISTAT Grainsize Analysis (12/17).

20-1006_20.95mbgl	20-1006_21.50mbgl	20-1006_22.00mbgl	20-1006_22.50mbgl
, 11/22/2024	, 11/22/2024	, 11/22/2024	, 11/29/2024
175°17'12.32" E 37°47'20.83" S	175°17'12.32" E 37°47'20.83" S	175°17'12.32" E 37°47'20.83" S	175°17'12.32" E 37°47'20.83" S
0.0%	0.0%	0.0%	0.0%
Polymodal, Very Poorly Sorted	Unimodal, Very Poorly Sorted	Unimodal, Very Poorly Sorted	Unimodal, Very Poorly Sorted
Sandy Mud	Mud	Mud	Sandy Mud
Medium Sandy Coarse Silt	Very Fine Silt	Fine Silt	Very Fine Sandy Very Coarse Silt
21.07	7.879	10.35	27.60
9.626	4.589	4.095	4.173
0.036	0.097	-0.014	-0.240
0.773	0.886	0.933	1.020
5.569	6.988	6.595	5.179
3.267	2.198	2.034	2.061
-0.036	-0.097	0.014	0.240
0.773	0.886	0.933	1.020
Coarse Silt	Medium Silt	Medium Silt	Coarse Silt
Very Poorly Sorted	Very Poorly Sorted	Very Poorly Sorted	Very Poorly Sorted
Symmetrical	Symmetrical	Symmetrical	Fine Skewed
Platykurtic	Platykurtic	Mesokurtic	Mesokurtic
385.0	2.950	5.850	58.00
1.383	8.484	7.502	4.113
1.089	1.176	1.621	3.632
19.07	7.116	10.34	35.16
405.1	60.23	61.16	138.1
372.1	51.23	37.72	38.03
404.0	59.05	59.54	134.5
33.72	9.428	7.367	6.794
109.9	21.85	24.97	62.51
1.304	4.053	4.031	2.856
5.713	7.135	6.595	4.830
9.843	9.732	9.269	8.105
7.550	2.401	2.299	2.838
8.539	5.679	5.237	5.249
2.615	1.605	1.563	1.733
5.075	3.237	2.881	2.764
0.0%	0.0%	0.0%	0.0%
32.4%	9.5%	9.6%	30.5%
67.6%	90.5%	90.4%	69.5%
0.0%	0.0%	0.0%	0.0%
0.0%	0.0%	0.0%	0.0%
0.0%	0.0%	0.0%	0.0%
0.0%	0.0%	0.0%	0.0%
0.0%	0.0%	0.0%	0.0%
0.0%	0.0%	0.0%	0.0%
6.4%	0.1%	0.0%	0.2%
10.8%	1.6%	1.5%	3.9%
6.7%	2.2%	1.9%	7.3%
8.5%	5.6%	6.3%	19.1%
9.8%	10.8%	13.5%	22.9%
10.9%	13.3%	16.2%	15.2%
10.2%	14.2%	17.8%	11.9%
9.5%	17.0%	17.9%	8.9%
10.1%	17.2%	13.0%	5.5%
17.1%	18.1%	11.9%	5.1%

Figure 4.14. 20-1006 GRADISTAT Grainsize Analysis (13/17).

20-1006_23.00mbgl	20-1006_23.50mbgl	20-1006_24.00mbgl	20-1006_24.50mbgl
, 11/22/2024	, 11/22/2024	, 11/22/2024	, 11/29/2024
175°17'12.32" E 37°47'20.83" S	175°17'12.32" E 37°47'20.83" S	175°17'12.32" E 37°47'20.83" S	175°17'12.32" E 37°47'20.83" S
0.0%	0.0%	0.0%	0.0%
Unimodal, Poorly Sorted	Unimodal, Poorly Sorted	Unimodal, Poorly Sorted	Unimodal, Very Poorly Sorted
Sandy Mud	Muddy Sand	Muddy Sand	Muddy Sand
Very Fine Sandy Very Coarse Silt	Very Coarse Silty Very Fine Sand	Very Coarse Silty Fine Sand	Very Coarse Silty Fine Sand
39.07	59.16	71.77	63.39
3.558	3.604	3.790	4.713
-0.399	-0.415	-0.387	-0.384
1.073	1.107	0.984	1.067
4.678	4.079	3.801	3.980
1.831	1.849	1.922	2.237
0.399	0.415	0.387	0.384
1.073	1.107	0.984	1.067
Very Coarse Silt	Very Coarse Silt	Very Fine Sand	Very Fine Sand
Poorly Sorted	Poorly Sorted	Poorly Sorted	Very Poorly Sorted
Very Fine Skewed	Very Fine Skewed	Very Fine Skewed	Very Fine Skewed
Mesokurtic	Mesokurtic	Mesokurtic	Mesokurtic
81.00	115.0	163.0	137.0
3.631	3.126	2.622	2.873
5.189	7.800	8.891	5.396
52.87	80.80	97.24	90.92
141.4	211.8	280.1	312.9
27.26	27.15	31.51	57.98
136.3	204.0	271.2	307.5
5.045	4.963	6.223	7.182
75.62	113.6	156.3	160.7
2.822	2.239	1.836	1.676
4.242	3.630	3.362	3.459
7.590	7.002	6.813	7.534
2.690	3.127	3.711	4.494
4.769	4.763	4.978	5.858
1.685	1.822	2.088	2.175
2.335	2.311	2.638	2.844
0.0%	0.0%	0.0%	0.0%
43.2%	59.0%	61.6%	60.5%
56.8%	41.0%	38.4%	39.5%
0.0%	0.0%	0.0%	0.0%
0.0%	0.0%	0.0%	0.0%
0.0%	0.0%	0.0%	0.0%
0.0%	0.0%	0.0%	0.0%
0.0%	0.0%	0.0%	0.0%
0.0%	0.0%	0.0%	0.0%
0.0%	0.0%	0.2%	2.3%
0.8%	5.8%	13.3%	13.5%
12.9%	25.0%	27.8%	23.4%
29.5%	28.2%	20.3%	21.4%
22.7%	14.8%	12.7%	12.3%
12.2%	9.4%	10.2%	8.2%
8.3%	6.7%	6.7%	6.3%
6.0%	4.5%	4.2%	5.0%
3.9%	2.9%	2.5%	3.8%
3.6%	2.7%	2.0%	3.9%

Figure 4.15. 20-1006 GRADISTAT Grainsize Analysis (14/17).

20-1006_25.00mbgl	20-1006_25.50mbgl	20-1006_26.00mbgl	20-1006_26.50mbgl
, 11/29/2024	, 11/29/2024	, 11/22/2024	, 11/22/2024
175°17'12.32" E 37°47'20.83" S	175°17'12.32" E 37°47'20.83" S	175°17'12.32" E 37°47'20.83" S	175°17'12.32" E 37°47'20.83" S
0.0%	0.0%	0.0%	0.0%
Bimodal, Very Poorly Sorted	Bimodal, Very Poorly Sorted	Unimodal, Poorly Sorted	Bimodal, Very Poorly Sorted
Muddy Sand	Sandy Mud	Sandy Mud	Gravelly Muddy Sand
Very Coarse Silty Medium Sand	Very Fine Sandy Very Coarse Silt	Very Fine Sandy Very Coarse Silt	Fine Gravelly Very Coarse Silty Fine
115.6	36.45	42.45	141.0
4.481	6.708	3.570	4.298
-0.513	-0.063	-0.378	-0.108
0.950	0.869	1.076	2.118
3.113	4.778	4.558	2.826
2.164	2.746	1.836	2.104
0.513	0.063	0.378	0.108
0.950	0.869	1.076	2.118
Very Fine Sand	Very Coarse Silt	Very Coarse Silt	Fine Sand
Very Poorly Sorted	Very Poorly Sorted	Poorly Sorted	Very Poorly Sorted
Very Fine Skewed	Symmetrical	Very Fine Skewed	Fine Skewed
Mesokurtic	Platykurtic	Mesokurtic	Very Leptokurtic
325.0	68.50	81.00	163.0
1.626	3.872	3.631	2.622
10.38	2.817	5.747	19.12
188.6	38.18	56.13	156.7
485.3	398.9	155.6	1114.2
46.75	141.6	27.08	58.27
474.9	396.1	149.9	1095.1
8.222	16.15	5.106	3.277
297.2	132.2	82.28	188.2
1.043	1.326	2.684	-0.156
2.407	4.711	4.155	2.674
6.590	8.472	7.443	5.709
6.318	6.389	2.773	-36.583
5.547	7.146	4.759	5.865
2.944	2.419	1.715	1.909
3.040	4.013	2.352	1.712
0.0%	0.0%	0.0%	7.4%
69.4%	40.1%	46.0%	73.1%
30.6%	59.9%	54.0%	19.4%
0.0%	0.0%	0.0%	0.0%
0.0%	0.0%	0.0%	0.0%
0.0%	0.0%	0.0%	0.0%
0.0%	0.0%	0.0%	0.0%
0.0%	0.0%	0.0%	7.4%
0.0%	0.1%	0.0%	3.1%
8.9%	6.4%	0.0%	2.6%
30.3%	10.5%	1.6%	14.7%
20.8%	9.8%	15.4%	33.0%
9.4%	13.3%	29.0%	19.8%
9.2%	13.6%	21.1%	6.6%
8.1%	11.8%	12.4%	4.0%
5.5%	11.2%	8.2%	2.9%
3.3%	10.0%	5.5%	2.4%
2.2%	6.8%	3.6%	1.8%
2.3%	6.5%	3.4%	1.8%

Figure 4.16. 20-1006 GRADISTAT Grainsize Analysis (15/17).

20-1006_27.00mbgl	20-1006_27.50mbgl	20-1006_28.00mbgl	20-1006_28.50mbgl
, 11/22/2024	, 11/22/2024	, 11/22/2024	, 11/22/2024
175°17'12.32" E 37°47'20.83" S	175°17'12.32" E 37°47'20.83" S	175°17'12.32" E 37°47'20.83" S	175°17'12.32" E 37°47'20.83" S
0.0%	0.0%	0.0%	0.0%
Unimodal, Poorly Sorted	Unimodal, Very Poorly Sorted	Unimodal, Poorly Sorted	Unimodal, Poorly Sorted
Muddy Sand	Muddy Sand	Sandy Mud	Slightly Gravelly Muddy Sand
Very Coarse Silty Very Fine Sand	Very Coarse Silty Very Fine Sand	Very Fine Sandy Very Coarse Silt	y Fine Gravelly Very Coarse Silty C
77.33	69.50	30.79	345.3
2.993	4.611	3.313	3.031
-0.246	-0.261	-0.277	-0.434
1.291	1.264	1.118	1.430
3.693	3.847	5.021	1.534
1.582	2.205	1.728	1.600
0.246	0.261	0.277	0.434
1.291	1.264	1.118	1.430
Very Fine Sand	Very Fine Sand	Coarse Silt	Medium Sand
Poorly Sorted	Very Poorly Sorted	Poorly Sorted	Poorly Sorted
Fine Skewed	Fine Skewed	Fine Skewed	Very Fine Skewed
Leptokurtic	Leptokurtic	Leptokurtic	Leptokurtic
96.50	115.0	58.00	545.0
3.379	3.126	4.113	0.881
15.68	7.223	5.014	60.27
88.17	89.61	36.48	434.1
251.7	407.1	111.5	963.2
16.05	56.37	22.24	15.98
236.0	399.9	106.5	903.0
3.457	5.504	4.460	3.210
108.9	144.4	54.10	471.9
1.990	1.296	3.165	0.054
3.504	3.480	4.777	1.204
5.995	7.113	7.640	4.052
3.012	5.487	2.414	74.97
4.004	5.817	4.475	3.998
1.661	1.983	1.561	4.088
1.790	2.460	2.157	1.682
0.0%	0.0%	0.0%	1.4%
64.4%	62.2%	29.1%	88.4%
35.6%	37.8%	70.9%	10.2%
0.0%	0.0%	0.0%	0.0%
0.0%	0.0%	0.0%	0.0%
0.0%	0.0%	0.0%	0.0%
0.0%	0.0%	0.0%	0.0%
0.0%	0.0%	0.0%	1.4%
0.7%	0.8%	0.0%	7.2%
1.8%	6.7%	0.0%	33.9%
7.6%	9.3%	0.2%	29.0%
23.5%	19.9%	7.0%	11.6%
30.8%	25.4%	21.9%	6.7%
17.6%	13.1%	26.4%	3.6%
8.0%	7.8%	19.5%	2.5%
4.6%	6.4%	11.0%	1.8%
2.5%	4.7%	6.2%	1.1%
1.4%	3.1%	3.9%	0.7%
1.4%	2.8%	3.9%	0.6%

Figure 4.17. 20-1006 GRADISTAT Grainsize Analysis (16/17).

20-1006_29.00mbgl	20-1006_29.50mbgl	20-1006_30.00mbgl	20-1006_30.45mbgl
, 11/22/2024	, 11/18/2024	, 11/18/2024	, 11/18/2024
175°17'12.32" E 37°47'20.83" S	175°17'12.32" E 37°47'20.83" S	175°17'12.32" E 37°47'20.83" S	175°17'12.32" E 37°47'20.83" S
0.0%	0.0%	0.0%	0.0%
Polymodal, Very Poorly Sorted	Unimodal, Poorly Sorted	Unimodal, Poorly Sorted	Unimodal, Poorly Sorted
Gravelly Mud	Slightly Gravelly Muddy Sand	Slightly Gravelly Muddy Sand	Sandy Mud
Very Fine Gravelly Medium Silt	ery Fine Gravelly Very Coarse Silty S	ery Fine Gravelly Very Coarse Silty S	Very Fine Sandy Very Coarse Silt
70.48	138.4	127.3	27.38
14.35	3.397	3.201	3.064
0.289	-0.401	-0.340	-0.200
0.737	1.401	1.377	1.102
3.827	2.854	2.973	5.191
3.843	1.764	1.679	1.616
-0.289	0.401	0.340	0.200
0.737	1.401	1.377	1.102
Very Fine Sand	Fine Sand	Fine Sand	Coarse Silt
Very Poorly Sorted	Poorly Sorted	Poorly Sorted	Poorly Sorted
Coarse Skewed	Very Fine Skewed	Very Fine Skewed	Fine Skewed
Platykurtic	Leptokurtic	Leptokurtic	Mesokurtic
34.00	230.0	193.5	40.50
4.884	2.126	2.375	4.631
2.911	18.39	18.79	5.471
31.67	180.7	153.9	30.21
3403.0	451.3	409.3	96.13
1169.0	24.55	21.79	17.57
3400.1	432.9	390.5	90.66
60.01	3.614	3.482	4.183
493.7	214.8	188.0	44.15
-1.767	1.148	1.289	3.379
4.981	2.468	2.700	5.049
8.424	5.765	5.734	7.514
-4.768	5.022	4.450	2.224
10.19	4.617	4.446	4.135
6.943	2.058	1.936	1.503
5.907	1.854	1.800	2.065
18.4%	3.9%	1.4%	0.0%
19.2%	75.2%	77.3%	22.3%
62.5%	20.9%	21.3%	77.7%
0.0%	0.0%	0.0%	0.0%
0.0%	0.0%	0.0%	0.0%
0.0%	0.0%	0.0%	0.0%
0.0%	0.0%	0.0%	0.0%
18.4%	3.9%	1.4%	0.0%
0.9%	0.0%	0.0%	0.0%
5.7%	3.7%	4.4%	0.0%
2.8%	25.9%	21.4%	0.3%
1.8%	31.5%	32.0%	4.7%
7.9%	14.1%	19.5%	17.4%
12.7%	7.1%	7.5%	26.5%
13.0%	5.0%	5.1%	23.8%
13.0%	3.7%	3.8%	14.1%
10.8%	2.5%	2.4%	6.5%
6.8%	1.5%	1.4%	3.3%
6.1%	1.2%	1.1%	3.5%

Figure 4.18. 20-1006 GRADISTAT Grainsize Analysis (17/17).

- 21-0437.

SAMPLE STATISTICS

		21-0437_0.50mbgl	21-0437_0.75mbgl	21-0437_1.00mbgl
	ANALYST AND DATE:	, 11/18/2024	, 11/18/2024	, 11/18/2024
	LOCATION:	175°16'47.95" E 37°46.59.65" S	175°16'47.95" E 37°46.59.65" S	175°16'47.95" E 37°46.59.65" S
	SIEVING ERROR:	0.0%	0.0%	0.0%
	SAMPLE TYPE:	Trimodal, Very Poorly Sorted	Unimodal, Poorly Sorted	Bimodal, Poorly Sorted
	TEXTURAL GROUP:	Gravelly Muddy Sand	Slightly Gravelly Muddy Sand	Gravelly Muddy Sand
	SEDIMENT NAME:	he Gravelly Very Coarse Silty Mediu	y Fine Gravelly Very Coarse Silty Me	ne Gravelly Very Coarse Silty Mediu
FOLK AND WARD METHOD (μm)	MEAN (M_G):	206.8	191.9	713.1
	SORTING (σ_G):	5.368	3.355	3.961
	SKEWNESS (Sk_G):	-0.091	-0.298	-0.083
	KURTOSIS (K_G):	0.927	1.245	1.062
FOLK AND WARD METHOD (ϕ)	MEAN (M_Z):	2.273	2.381	0.488
	SORTING (σ_I):	2.424	1.746	1.986
	SKEWNESS (Sk_I):	0.091	0.298	0.083
	KURTOSIS (K_G):	0.927	1.245	1.062
FOLK AND WARD METHOD (Description)	MEAN:	Fine Sand	Fine Sand	Coarse Sand
	SORTING:	Very Poorly Sorted	Poorly Sorted	Poorly Sorted
	SKEWNESS:	Symmetrical	Fine Skewed	Symmetrical
	KURTOSIS:	Mesokurtic	Leptokurtic	Mesokurtic
	MODE 1 (μm):	325.0	325.0	460.0
	MODE 1 (ϕ):	1.626	1.626	1.126
	D_{10} (μm):	20.62	33.47	88.90
	D_{50} (μm):	209.5	244.1	525.5
	D_{90} (μm):	4454.6	656.7	5892.7
	(D_{90} / D_{10}) (μm):	216.0	19.62	66.29
	(D_{90} - D_{10}) (μm):	4434.0	623.3	5803.8
	(D_{75} / D_{25}) (μm):	10.02	4.109	4.634
	(D_{75} - D_{25}) (μm):	505.8	312.7	978.1
	D_{10} (ϕ):	-2.155	0.607	-2.559
	D_{50} (ϕ):	2.255	2.034	0.928
	D_{90} (ϕ):	5.600	4.901	3.492
	(D_{90} / D_{10}) (ϕ):	-2.598	8.079	-1.365
	(D_{90} - D_{10}) (ϕ):	7.755	4.294	6.051
	(D_{75} / D_{25}) (ϕ):	4.998	2.599	-5.939
	(D_{75} - D_{25}) (ϕ):	3.325	2.039	2.212
	% GRAVEL:	15.2%	4.9%	22.6%
	% SAND:	57.6%	77.5%	69.4%
	% MUD:	27.2%	17.7%	8.1%
	% V COARSE GRAVEL:	0.0%	0.0%	0.0%
	% COARSE GRAVEL:	0.0%	0.0%	0.0%
	% MEDIUM GRAVEL:	0.0%	0.0%	0.0%
	% FINE GRAVEL:	0.0%	0.0%	0.0%
	% V FINE GRAVEL:	15.2%	4.9%	22.6%
	% V COARSE SAND:	1.9%	0.4%	6.1%
	% COARSE SAND:	10.4%	12.0%	23.4%
	% MEDIUM SAND:	18.2%	31.7%	25.1%
	% FINE SAND:	14.2%	22.1%	10.5%
	% V FINE SAND:	12.9%	11.3%	4.2%
	% V COARSE SILT:	12.9%	8.3%	2.9%
	% COARSE SILT:	7.2%	4.4%	1.9%
	% MEDIUM SILT:	3.2%	2.2%	1.3%
	% FINE SILT:	1.7%	1.3%	0.9%
	% V FINE SILT:	1.1%	0.8%	0.6%
	% CLAY:	1.1%	0.6%	0.5%

Figure 4.19. 21-0437 GRADISTAT Grainsize Analysis (1/12).

21-0437_1.50mbgl	21-0437_2.00mbgl	21-0437_2.50mbgl	21-0437_3.00mbgl
, 11/18/2024	, 11/18/2024	, 11/18/2024	, 11/18/2024
175°16'47.95" E 37°46.59.65" S	175°16'47.95" E 37°46.59.65" S	175°16'47.95" E 37°46.59.65" S	175°16'47.95" E 37°46.59.65" S
0.0%	0.0%	0.0%	0.0%
Bimodal, Very Poorly Sorted	Bimodal, Very Poorly Sorted	Bimodal, Very Poorly Sorted	Unimodal, Very Poorly Sorted
Gravelly Muddy Sand	Gravelly Muddy Sand	Gravelly Muddy Sand	Slightly Gravelly Muddy Sand
he Gravelly Very Coarse Silty Mediu	he Gravelly Very Coarse Silty Mediu	he Gravelly Very Coarse Silty Mediu	y Fine Gravelly Very Coarse Silty Me
297.2	349.9	305.7	169.6
8.938	7.490	8.156	5.957
-0.247	-0.279	-0.346	-0.322
0.744	0.733	0.690	1.259
1.751	1.515	1.710	2.560
3.160	2.905	3.028	2.575
0.247	0.279	0.346	0.322
0.744	0.733	0.690	1.259
Medium Sand	Medium Sand	Medium Sand	Fine Sand
Very Poorly Sorted	Very Poorly Sorted	Very Poorly Sorted	Very Poorly Sorted
Fine Skewed	Fine Skewed	Very Fine Skewed	Very Fine Skewed
Platykurtic	Platykurtic	Platykurtic	Leptokurtic
385.0	385.0	460.0	325.0
1.383	1.383	1.126	1.626
9.034	13.50	9.790	10.74
301.7	366.4	374.4	240.8
7754.9	8268.7	10780.5	1140.3
858.4	612.4	1101.1	106.2
7745.9	8255.2	10770.7	1129.5
30.47	25.85	36.27	7.629
2049.3	2231.2	2681.4	447.0
-2.955	-3.048	-3.430	-0.189
1.729	1.448	1.418	2.054
6.790	6.211	6.674	6.541
-2.298	-2.038	-1.946	-34.546
9.745	9.258	10.10	6.731
-3.550	-2.863	-2.541	4.057
4.929	4.692	5.181	2.931
25.7%	26.7%	28.8%	4.8%
50.5%	52.3%	48.1%	71.1%
23.8%	20.9%	23.0%	24.1%
0.0%	0.0%	0.0%	0.0%
0.0%	0.0%	0.0%	0.0%
0.0%	0.0%	0.0%	0.0%
0.0%	0.0%	0.0%	0.0%
25.7%	26.7%	28.8%	4.8%
1.1%	2.0%	1.7%	6.8%
10.6%	13.1%	12.4%	14.1%
17.1%	17.4%	15.9%	23.1%
13.0%	11.6%	10.5%	17.1%
8.7%	8.3%	7.5%	10.0%
6.1%	5.9%	5.8%	6.9%
4.7%	4.3%	4.7%	5.1%
3.8%	3.4%	3.8%	3.9%
3.2%	2.7%	3.1%	3.1%
2.7%	2.1%	2.6%	2.5%
3.3%	2.5%	3.0%	2.6%

Figure 4.20. 21-0437 GRADISTAT Grainsize Analysis (2/12).

21-0437_3.50mbgl	21-0437_4.00mbgl	21-0437_4.50mbgl	21-0437_5.00mbgl
, 11/18/2024	, 11/18/2024	, 11/18/2024	, 11/18/2024
175°16'47.95" E 37°46.59.65" S	175°16'47.95" E 37°46.59.65" S	175°16'47.95" E 37°46.59.65" S	175°16'47.95" E 37°46.59.65" S
0.0%	0.0%	0.0%	0.0%
Bimodal, Very Poorly Sorted	Bimodal, Very Poorly Sorted	Unimodal, Very Poorly Sorted	Bimodal, Very Poorly Sorted
Gravelly Muddy Sand	Gravelly Muddy Sand	Gravelly Muddy Sand	Muddy Sandy Gravel
ne Gravelly Very Coarse Silty Coarse	ne Gravelly Very Coarse Silty Mediu	ne Gravelly Very Coarse Silty Mediu	ry Coarse Silty Sandy Very Fine Gra
513.3	263.5	161.1	327.6
6.275	9.927	5.934	7.086
-0.282	-0.303	-0.208	-0.395
1.158	0.873	1.416	0.644
0.962	1.924	2.634	1.610
2.650	3.311	2.569	2.825
0.282	0.303	0.208	0.395
1.158	0.873	1.416	0.644
Coarse Sand	Medium Sand	Fine Sand	Medium Sand
Very Poorly Sorted	Very Poorly Sorted	Very Poorly Sorted	Very Poorly Sorted
Fine Skewed	Very Fine Skewed	Fine Skewed	Very Fine Skewed
Leptokurtic	Platykurtic	Leptokurtic	Very Platykurtic
545.0	325.0	325.0	325.0
0.881	1.626	1.626	1.626
24.70	6.547	13.08	12.10
499.6	319.3	211.2	421.9
6398.0	5920.8	903.6	17521.8
259.0	904.3	69.09	1448.1
6373.3	5914.2	890.5	17509.7
6.827	20.66	7.004	42.24
1025.7	1134.8	398.1	3879.3
-2.678	-2.566	0.146	-4.131
1.001	1.647	2.244	1.245
5.339	7.255	6.257	6.369
-1.994	-2.828	42.77	-1.542
8.017	9.821	6.110	10.50
-9.451	-16.203	3.538	-1.713
2.771	4.369	2.808	5.401
20.5%	20.4%	7.6%	35.9%
64.2%	53.9%	68.3%	43.4%
15.3%	25.7%	24.1%	20.7%
0.0%	0.0%	0.0%	0.0%
0.0%	0.0%	0.0%	0.0%
0.0%	0.0%	0.0%	0.0%
0.0%	0.0%	0.0%	0.0%
20.5%	20.4%	7.6%	35.9%
7.9%	7.0%	1.2%	2.0%
21.6%	12.8%	13.9%	9.1%
19.7%	15.0%	22.2%	13.1%
9.0%	11.7%	18.4%	11.4%
6.0%	7.3%	12.6%	7.9%
4.2%	5.5%	8.0%	5.3%
3.2%	4.9%	5.2%	4.2%
2.5%	4.3%	3.6%	3.3%
2.0%	3.9%	2.8%	2.7%
1.6%	3.3%	2.2%	2.3%
1.8%	3.7%	2.3%	2.9%

Figure 4.21. 21-0437 GRADISTAT Grainsize Analysis (3/12).

21-0437_5.50mbgl	21-0437_6.00mbgl	21-0437_6.50mbgl	21-0437_6.85mbgl
, 11/18/2024	, 11/18/2024	, 11/18/2024	, 11/18/2024
175°16'47.95" E 37°46.59.65" S	175°16'47.95" E 37°46.59.65" S	175°16'47.95" E 37°46.59.65" S	175°16'47.95" E 37°46.59.65" S
0.0%	0.0%	0.0%	0.0%
Unimodal, Poorly Sorted	Bimodal, Very Poorly Sorted	Bimodal, Very Poorly Sorted	Bimodal, Very Poorly Sorted
Gravelly Sand	Muddy Sandy Gravel	Gravelly Muddy Sand	Gravelly Muddy Sand
Very Fine Gravelly Coarse Sand	ry Coarse Silty Sandy Very Fine Grane	Gravelly Very Coarse Silty Coarsne	Gravelly Very Coarse Silty Coars
712.7	378.1	461.4	401.4
2.572	6.163	6.360	7.503
-0.108	-0.319	-0.443	-0.312
1.978	0.656	0.780	0.852
0.489	1.403	1.116	1.317
1.363	2.624	2.669	2.907
0.108	0.319	0.443	0.312
1.978	0.656	0.780	0.852
Coarse Sand	Medium Sand	Medium Sand	Medium Sand
Poorly Sorted	Very Poorly Sorted	Very Poorly Sorted	Very Poorly Sorted
Fine Skewed	Very Fine Skewed	Very Fine Skewed	Very Fine Skewed
Very Leptokurtic	Very Platykurtic	Platykurtic	Platykurtic
775.0	325.0	775.0	650.0
0.373	1.626	0.373	0.628
270.1	19.10	18.06	14.89
719.9	416.7	598.1	436.6
1705.0	12301.0	9397.7	6928.3
6.313	644.1	520.3	465.2
1435.0	12281.9	9379.7	6913.4
2.335	29.64	18.80	16.06
626.4	3256.3	2527.0	1596.9
-0.770	-3.621	-3.232	-2.793
0.474	1.263	0.742	1.196
1.889	5.710	5.791	6.069
-2.453	-1.577	-1.792	-2.173
2.658	9.331	9.023	8.862
-8.296	-1.790	-1.989	-4.216
1.224	4.889	4.233	4.005
7.5%	31.6%	28.5%	24.1%
87.5%	50.3%	54.5%	56.3%
5.0%	18.1%	17.0%	19.7%
0.0%	0.0%	0.0%	0.0%
0.0%	0.0%	0.0%	0.0%
0.0%	0.0%	0.0%	0.0%
0.0%	0.0%	0.0%	0.0%
7.5%	31.6%	28.5%	24.1%
21.9%	3.0%	9.6%	7.7%
42.7%	11.6%	15.8%	15.2%
18.7%	15.0%	12.8%	14.8%
2.3%	12.6%	9.9%	11.2%
1.8%	8.3%	6.5%	7.3%
1.3%	5.3%	4.2%	5.3%
1.3%	3.9%	3.5%	4.2%
1.0%	3.0%	2.9%	3.3%
0.8%	2.3%	2.4%	2.6%
0.5%	1.8%	2.0%	2.1%
0.1%	1.9%	2.0%	2.2%

Figure 4.22. 21-0437 GRADISTAT Grainsize Analysis (4/12).

21-0437_7.50mbgl	21-0437_7.75mbgl	21-0437_8.45mbgl	21-0437_8.70mbgl
, 11/22/2024	, 11/22/2024	, 11/18/2024	, 11/18/2024
175°16'47.95" E 37°46.59.65" S	175°16'47.95" E 37°46.59.65" S	175°16'47.95" E 37°46.59.65" S	175°16'47.95" E 37°46.59.65" S
0.0%	0.0%	0.0%	0.0%
Unimodal, Poorly Sorted	Unimodal, Very Poorly Sorted	Trimodal, Very Poorly Sorted	Unimodal, Poorly Sorted
Sandy Mud	Sandy Mud	Gravelly Muddy Sand	Gravelly Sand
Very Fine Sandy Very Coarse Silt	Very Fine Sandy Medium Silt	e Gravelly Very Coarse Silty Very Fi	Very Fine Gravelly Medium Sand
35.47	10.66	96.71	303.9
3.959	4.498	7.668	3.225
-0.312	0.025	-0.107	-0.044
1.006	0.915	1.004	1.752
4.817	6.552	3.370	1.718
1.985	2.169	2.939	1.689
0.312	-0.025	0.107	0.044
1.006	0.915	1.004	1.752
Very Coarse Silt	Medium Silt	Very Fine Sand	Medium Sand
Poorly Sorted	Very Poorly Sorted	Very Poorly Sorted	Poorly Sorted
Very Fine Skewed	Symmetrical	Fine Skewed	Symmetrical
Mesokurtic	Mesokurtic	Mesokurtic	Very Leptokurtic
81.00	11.70	96.50	275.0
3.631	6.502	3.379	1.868
4.272	1.522	5.818	77.52
45.72	10.41	110.1	295.1
154.9	78.02	3341.8	2172.6
36.26	51.26	574.4	28.03
150.6	76.50	3336.0	2095.1
6.375	8.583	15.44	3.053
79.72	26.99	376.6	352.2
2.691	3.680	-1.741	-1.119
4.451	6.586	3.183	1.761
7.871	9.360	7.425	3.689
2.925	2.543	-4.266	-3.296
5.180	5.680	9.166	4.809
1.785	1.616	4.009	2.726
2.672	3.101	3.948	1.610
0.0%	0.0%	11.9%	10.2%
39.9%	13.0%	49.5%	80.9%
60.1%	87.0%	38.7%	8.8%
0.0%	0.0%	0.0%	0.0%
0.0%	0.0%	0.0%	0.0%
0.0%	0.0%	0.0%	0.0%
0.0%	0.0%	0.0%	0.0%
0.0%	0.0%	11.9%	10.2%
0.0%	0.0%	0.9%	2.0%
0.0%	0.0%	8.3%	14.2%
2.5%	0.6%	13.1%	32.0%
13.1%	4.2%	13.3%	25.7%
24.3%	8.2%	13.9%	7.0%
20.2%	11.6%	11.4%	2.5%
14.1%	15.6%	8.5%	1.9%
9.9%	16.8%	6.6%	1.6%
6.7%	16.2%	4.9%	1.3%
4.7%	13.8%	3.6%	0.9%
4.4%	13.0%	3.6%	0.6%

Figure 4.23. 21-0437 GRADISTAT Grainsize Analysis (5/12).

21-0437_8.90mbgl	21-0437_9.45mbgl	21-0437_9.50mbgl	21-0437_10.00mbgl
, 11/22/2024	, 11/18/2024	, 11/18/2024	, 11/22/2024
175°16'47.95" E 37°46.59.65" S	175°16'47.95" E 37°46.59.65" S	175°16'47.95" E 37°46.59.65" S	175°16'47.95" E 37°46.59.65" S
0.0%	0.0%	0.0%	0.0%
Bimodal, Very Poorly Sorted	Bimodal, Very Poorly Sorted	Bimodal, Very Poorly Sorted	Unimodal, Very Poorly Sorted
Slightly Gravelly Sandy Mud	Gravelly Muddy Sand	Muddy Sandy Gravel	Slightly Gravelly Sandy Mud
Fine Gravelly Very Fine Sandy Verne	Gravelly Very Coarse Silty Mediury	Coarse Silty Sandy Very Fine Grav	Fine Gravelly Very Fine Sandy Very
24.08	406.4	578.7	48.41
4.383	6.686	4.328	4.074
-0.120	-0.203	-0.591	-0.270
0.918	0.981	0.828	1.085
5.376	1.299	0.789	4.368
2.132	2.741	2.114	2.026
0.120	0.203	0.591	0.270
0.918	0.981	0.828	1.085
Coarse Silt	Medium Sand	Coarse Sand	Very Coarse Silt
Very Poorly Sorted	Very Poorly Sorted	Very Poorly Sorted	Very Poorly Sorted
Fine Skewed	Fine Skewed	Very Fine Skewed	Fine Skewed
Mesokurtic	Mesokurtic	Platykurtic	Mesokurtic
68.50	385.0	545.0	96.50
3.872	1.383	0.881	3.379
3.115	19.11	36.96	6.079
26.39	362.7	812.3	60.11
139.8	7198.5	26286.4	222.4
44.89	376.6	711.3	36.58
136.7	7179.4	26249.4	216.3
8.361	10.000	11.57	6.085
64.48	1133.1	2785.7	104.1
2.838	-2.848	-4.716	2.169
5.244	1.463	0.300	4.056
8.326	5.709	4.758	7.362
2.934	-2.005	-1.009	3.394
5.488	8.557	9.474	5.193
1.812	-8.998	-1.196	1.867
3.064	3.322	3.533	2.605
0.3%	23.9%	39.6%	1.3%
28.9%	58.5%	48.1%	47.5%
70.9%	17.6%	12.3%	51.2%
0.0%	0.0%	0.0%	0.0%
0.0%	0.0%	0.0%	0.0%
0.0%	0.0%	0.0%	0.0%
0.0%	0.0%	0.0%	0.0%
0.3%	23.9%	39.6%	1.3%
0.0%	2.7%	6.3%	0.0%
0.2%	13.5%	15.6%	0.8%
2.6%	21.2%	14.3%	5.8%
9.0%	13.9%	7.6%	16.9%
17.1%	7.3%	4.2%	23.9%
16.8%	4.9%	2.9%	18.4%
16.5%	3.8%	2.6%	12.8%
15.0%	3.0%	2.2%	8.2%
10.4%	2.3%	1.8%	4.9%
6.4%	1.8%	1.4%	3.4%
5.8%	1.8%	1.4%	3.5%

Figure 4.24. 21-0437 GRADISTAT Grainsize Analysis (6/12).

21-0437_10.50mbgl	21-0437_11.00mbgl	21-0437_11.50mbgl	21-0437_11.75mbgl
, 11/18/2024	, 11/18/2024	, 11/18/2024	, 11/18/2024
175°16'47.95" E 37°46.59.65" S	175°16'47.95" E 37°46.59.65" S	175°16'47.95" E 37°46.59.65" S	175°16'47.95" E 37°46.59.65" S
0.0%	0.0%	0.0%	0.0%
Unimodal, Very Poorly Sorted	Unimodal, Very Poorly Sorted	Unimodal, Very Poorly Sorted	Trimodal, Very Poorly Sorted
Muddy Sand	Gravelly Muddy Sand	Gravelly Muddy Sand	Gravelly Mud
Very Coarse Silty Fine Sand	he Gravelly Very Coarse Silty Mediu	he Gravelly Very Coarse Silty Mediu	Very Fine Gravelly Medium Silt
80.64	229.4	263.1	22.12
4.656	4.290	4.316	8.198
-0.378	-0.200	-0.155	0.225
1.086	1.748	1.602	1.133
3.632	2.124	1.926	5.498
2.219	2.101	2.110	3.035
0.378	0.200	0.155	-0.225
1.086	1.748	1.602	1.133
Very Fine Sand	Fine Sand	Medium Sand	Coarse Silt
Very Poorly Sorted	Very Poorly Sorted	Very Poorly Sorted	Very Poorly Sorted
Very Fine Skewed	Fine Skewed	Fine Skewed	Coarse Skewed
Mesokurtic	Very Leptokurtic	Very Leptokurtic	Leptokurtic
193.5	325.0	325.0	11.70
2.375	1.626	1.626	6.502
7.011	30.03	34.90	2.146
113.1	270.0	290.8	17.67
388.9	959.9	1431.9	4715.3
55.47	31.96	41.03	2197.2
381.9	929.8	1397.0	4713.2
7.055	3.933	4.265	13.60
199.7	365.6	433.2	69.59
1.363	0.059	-0.518	-2.237
3.144	1.889	1.782	5.822
7.156	5.057	4.841	8.864
5.252	85.59	-9.346	-3.962
5.794	4.998	5.359	11.10
2.340	2.921	3.547	2.008
2.819	1.976	2.093	3.766
0.0%	8.5%	8.2%	14.4%
64.8%	76.3%	77.6%	13.2%
35.2%	15.2%	14.2%	72.3%
0.0%	0.0%	0.0%	0.0%
0.0%	0.0%	0.0%	0.0%
0.0%	0.0%	0.0%	0.0%
0.0%	0.0%	0.0%	0.0%
0.0%	8.5%	8.2%	14.4%
0.2%	1.0%	5.2%	0.0%
5.0%	14.7%	15.5%	0.0%
17.3%	29.1%	27.2%	0.5%
24.4%	21.6%	20.3%	3.7%
17.9%	9.8%	9.5%	9.0%
10.9%	5.0%	4.8%	10.3%
8.0%	3.2%	3.0%	14.6%
5.6%	2.3%	2.2%	15.9%
4.2%	1.8%	1.7%	13.0%
3.2%	1.4%	1.3%	9.7%
3.2%	1.5%	1.2%	8.8%

Figure 4.25. 21-0437 GRADISTAT Grainsize Analysis (7/12).

21-0437_12.00mbgl	21-0437_12.50mbgl	21-0437_13.00mbgl	21-0437_13.50mbgl
, 11/22/2024	, 11/22/2024	, 11/22/2024	, 11/18/2024
175°16'47.95" E 37°46.59.65" S	175°16'47.95" E 37°46.59.65" S	175°16'47.95" E 37°46.59.65" S	175°16'47.95" E 37°46.59.65" S
0.0%	0.0%	0.0%	0.0%
Bimodal, Very Poorly Sorted	Bimodal, Very Poorly Sorted	Unimodal, Very Poorly Sorted	Unimodal, Very Poorly Sorted
Gravelly Mud	Sandy Mud	Gravelly Muddy Sand	Sandy Mud
Very Fine Gravelly Very Coarse Silt	Very Fine Sandy Coarse Silt	ne Gravelly Very Coarse Silty Mediu	Very Fine Sandy Very Coarse Silt
122.9	16.78	298.8	44.49
9.146	5.367	7.489	6.775
0.196	-0.164	-0.012	-0.184
0.934	1.057	1.036	0.999
3.024	5.897	1.743	4.490
3.193	2.424	2.905	2.760
-0.196	0.164	0.012	0.184
0.934	1.057	1.036	0.999
Very Fine Sand	Coarse Silt	Medium Sand	Very Coarse Silt
Very Poorly Sorted	Very Poorly Sorted	Very Poorly Sorted	Very Poorly Sorted
Coarse Skewed	Fine Skewed	Symmetrical	Fine Skewed
Mesokurtic	Mesokurtic	Mesokurtic	Mesokurtic
48.50	34.00	325.0	68.50
4.372	4.884	1.626	3.872
7.606	1.670	17.85	2.780
67.40	21.02	204.1	54.36
5186.4	124.4	6361.7	419.4
681.9	74.49	356.3	150.9
5178.8	122.8	6343.8	416.6
15.35	8.874	8.954	12.51
328.2	45.30	484.9	155.7
-2.375	3.007	-2.669	1.254
3.891	5.572	2.293	4.201
7.039	9.226	5.808	8.491
-2.964	3.068	-2.176	6.773
9.413	6.219	8.477	7.237
3.609	1.734	4.621	2.422
3.940	3.150	3.163	3.645
16.2%	0.0%	17.9%	0.0%
35.6%	20.3%	56.7%	46.6%
48.2%	79.7%	25.5%	53.4%
0.0%	0.0%	0.0%	0.0%
0.0%	0.0%	0.0%	0.0%
0.0%	0.0%	0.0%	0.0%
0.0%	0.0%	0.0%	0.0%
16.2%	0.0%	17.9%	0.0%
0.4%	0.0%	0.3%	0.8%
4.6%	1.1%	8.5%	6.8%
7.7%	3.9%	18.1%	10.7%
8.8%	5.0%	15.9%	12.5%
14.0%	10.3%	13.8%	15.9%
17.4%	18.6%	10.7%	15.6%
12.7%	19.4%	5.8%	11.2%
7.8%	12.7%	3.1%	7.8%
4.6%	9.1%	2.0%	6.0%
2.8%	8.7%	1.7%	5.6%
2.8%	11.2%	2.1%	7.2%

Figure 4.26. 21-0437 GRADISTAT Grainsize Analysis (8/12).

21-0437_14.00mbgl	21-0437_14.50mbgl	21-0437_15.00mbgl	21-0437_15.50mbgl
, 11/29/2024	, 11/29/2024	, 11/22/2024	, 11/29/2024
175°16'47.95" E 37°46.59.65" S	175°16'47.95" E 37°46.59.65" S	175°16'47.95" E 37°46.59.65" S	175°16'47.95" E 37°46.59.65" S
0.0%	0.0%	0.0%	0.0%
Unimodal, Very Poorly Sorted	Bimodal, Very Poorly Sorted	Bimodal, Very Poorly Sorted	Unimodal, Very Poorly Sorted
Muddy Sand	Muddy Sand	Sandy Mud	Slightly Gravelly Sandy Mud
Very Coarse Silty Fine Sand	Very Coarse Silty Fine Sand	Very Fine Sandy Very Coarse Silt	Fine Gravelly Very Fine Sandy Very
111.4	71.66	33.35	33.17
4.198	4.653	7.187	4.857
-0.251	-0.237	-0.171	-0.219
1.138	1.058	0.879	1.111
3.166	3.803	4.906	4.914
2.070	2.218	2.845	2.280
0.251	0.237	0.171	0.219
1.138	1.058	0.879	1.111
Very Fine Sand	Very Fine Sand	Very Coarse Silt	Very Coarse Silt
Very Poorly Sorted	Very Poorly Sorted	Very Poorly Sorted	Very Poorly Sorted
Fine Skewed	Fine Skewed	Fine Skewed	Fine Skewed
Leptokurtic	Mesokurtic	Platykurtic	Leptokurtic
275.0	230.0	68.50	58.00
1.868	2.126	3.872	4.113
13.11	6.935	2.105	3.581
129.0	83.28	41.06	42.85
509.9	377.9	346.8	218.2
38.89	54.48	164.7	60.94
496.8	370.9	344.7	214.6
6.068	7.495	17.41	7.299
247.1	187.3	134.6	78.50
0.972	1.404	1.528	2.196
2.955	3.586	4.606	4.545
6.253	7.172	8.892	8.125
6.436	5.108	5.820	3.700
5.281	5.768	7.364	5.929
2.481	2.315	2.468	1.829
2.601	2.906	4.122	2.868
0.0%	0.0%	0.0%	2.2%
69.4%	57.6%	41.3%	35.1%
30.6%	42.4%	58.7%	62.7%
0.0%	0.0%	0.0%	0.0%
0.0%	0.0%	0.0%	0.0%
0.0%	0.0%	0.0%	0.0%
0.0%	0.0%	0.0%	0.0%
0.0%	0.0%	0.0%	2.2%
1.0%	0.0%	0.0%	0.0%
9.4%	4.4%	4.6%	1.0%
20.0%	16.4%	10.8%	5.5%
20.5%	18.7%	11.8%	8.5%
18.5%	18.0%	14.0%	20.1%
13.1%	16.3%	13.9%	21.4%
6.5%	9.7%	11.3%	13.1%
3.9%	5.8%	9.2%	9.9%
2.6%	3.9%	7.9%	7.7%
2.1%	3.2%	7.2%	5.1%
2.3%	3.6%	9.3%	5.5%

Figure 4.27. 21-0437 GRADISTAT Grainsize Analysis (9/12).

21-0437_16.00mbgl	21-0437_16.50mbgl	21-0437_17.00mbgl	21-0437_17.50mbgl
, 11/22/2024	, 11/22/2024	, 11/22/2024	, 11/22/2024
175°16'47.95" E 37°46.59.65" S	175°16'47.95" E 37°46.59.65" S	175°16'47.95" E 37°46.59.65" S	175°16'47.95" E 37°46.59.65" S
0.0%	0.0%	0.0%	0.0%
Unimodal, Very Poorly Sorted	Unimodal, Very Poorly Sorted	Trimodal, Very Poorly Sorted	Unimodal, Very Poorly Sorted
Mud	Sandy Mud	Sandy Mud	Sandy Mud
Coarse Silt	Very Fine Sandy Very Coarse Silt	Very Fine Sandy Coarse Silt	Very Fine Sandy Very Coarse Silt
9.123	20.04	10.16	16.66
4.205	4.948	4.873	5.027
-0.115	-0.297	-0.020	-0.212
0.853	0.878	0.877	0.872
6.776	5.641	6.621	5.907
2.072	2.307	2.285	2.330
0.115	0.297	0.020	0.212
0.853	0.878	0.877	0.872
Medium Silt	Coarse Silt	Medium Silt	Coarse Silt
Very Poorly Sorted	Very Poorly Sorted	Very Poorly Sorted	Very Poorly Sorted
Fine Skewed	Fine Skewed	Symmetrical	Fine Skewed
Platykurtic	Platykurtic	Platykurtic	Platykurtic
23.30	58.00	34.00	48.50
5.507	4.113	4.884	4.372
1.212	1.902	1.236	1.670
10.08	27.79	10.44	21.40
51.42	116.6	73.37	105.0
42.42	61.30	59.39	62.86
50.21	114.7	72.14	103.3
8.742	10.55	10.63	11.07
24.32	60.69	30.27	51.64
4.282	3.101	3.769	3.252
6.632	5.169	6.581	5.546
9.688	9.038	9.661	9.226
2.263	2.915	2.563	2.837
5.407	5.938	5.892	5.974
1.603	1.872	1.695	1.838
3.128	3.399	3.409	3.468
0.0%	0.0%	0.0%	0.0%
6.7%	27.3%	12.5%	22.2%
93.3%	72.7%	87.5%	77.8%
0.0%	0.0%	0.0%	0.0%
0.0%	0.0%	0.0%	0.0%
0.0%	0.0%	0.0%	0.0%
0.0%	0.0%	0.0%	0.0%
0.0%	0.0%	0.0%	0.0%
0.0%	0.0%	0.0%	0.0%
0.1%	0.0%	0.2%	0.2%
1.1%	1.7%	2.1%	2.6%
0.8%	6.9%	2.8%	4.6%
4.7%	18.7%	7.4%	14.7%
14.9%	20.4%	14.0%	19.7%
18.1%	13.7%	15.0%	14.9%
16.3%	10.9%	14.7%	11.8%
14.9%	9.5%	14.7%	10.7%
12.9%	8.1%	13.2%	9.3%
16.2%	10.2%	16.0%	11.5%

Figure 4.28. 21-0437 GRADISTAT Grainsize Analysis (10/12).

21-0437_18.00mbgl	21-0437_18.25mbgl	21-0437_18.50mbgl	21-0437_19.00mbgl
, 11/22/2024	, 11/29/2024	, 11/29/2024	, 11/29/2024
175°16'47.95" E 37°46.59.65" S	175°16'47.95" E 37°46.59.65" S	175°16'47.95" E 37°46.59.65" S	175°16'47.95" E 37°46.59.65" S
0.0%	0.0%	0.0%	0.0%
Unimodal, Very Poorly Sorted	Unimodal, Very Poorly Sorted	Bimodal, Very Poorly Sorted	Unimodal, Very Poorly Sorted
Sandy Mud	Slightly Gravelly Sandy Mud	Muddy Sand	Muddy Sand
Very Fine Sandy Very Coarse Silt	Fine Gravelly Very Fine Sandy Very	Very Coarse Silty Very Fine Sand	Very Coarse Silty Very Fine Sand
20.91	51.56	77.02	50.31
4.642	4.443	6.990	4.440
-0.229	-0.243	-0.157	-0.262
0.934	1.091	0.917	1.202
5.579	4.278	3.699	4.313
2.215	2.151	2.805	2.151
0.229	0.243	0.157	0.262
0.934	1.091	0.917	1.202
Coarse Silt	Very Coarse Silt	Very Fine Sand	Very Coarse Silt
Very Poorly Sorted	Very Poorly Sorted	Very Poorly Sorted	Very Poorly Sorted
Fine Skewed	Fine Skewed	Fine Skewed	Fine Skewed
Mesokurtic	Mesokurtic	Mesokurtic	Leptokurtic
48.50	96.50	81.00	81.00
4.372	3.379	3.631	3.631
2.332	5.569	4.539	5.373
26.89	63.04	88.20	63.80
121.0	268.4	738.6	251.7
51.90	48.19	162.7	46.83
118.7	262.8	734.1	246.3
8.911	6.650	15.88	5.910
55.96	119.8	317.0	108.4
3.047	1.898	0.437	1.990
5.217	3.988	3.503	3.970
8.745	7.488	7.783	7.540
2.870	3.946	17.81	3.788
5.698	5.591	7.346	5.549
1.791	1.967	3.551	1.872
3.156	2.733	3.989	2.563
0.0%	2.6%	0.0%	0.0%
25.3%	47.7%	56.8%	50.7%
74.7%	49.7%	43.2%	49.3%
0.0%	0.0%	0.0%	0.0%
0.0%	0.0%	0.0%	0.0%
0.0%	0.0%	0.0%	0.0%
0.0%	0.0%	0.0%	0.0%
0.0%	2.6%	0.0%	0.0%
0.0%	0.0%	5.1%	1.0%
0.0%	0.7%	12.4%	3.2%
2.7%	8.0%	13.1%	5.9%
6.7%	17.3%	12.6%	16.2%
15.8%	21.8%	13.6%	24.4%
21.4%	18.1%	12.7%	18.7%
15.4%	11.9%	9.8%	11.1%
11.5%	7.3%	6.6%	6.9%
10.4%	5.1%	5.1%	4.9%
8.1%	3.7%	4.2%	3.7%
8.0%	3.7%	4.7%	4.1%

Figure 4.29. 21-0437 GRADISTAT Grainsize Analysis (11/12).

21-0437_19.50mbgl	21-0437_19.95mbgl
, 11/29/2024	, 11/29/2024
175°16'47.95" E 37°46.59.65" S	175°16'47.95" E 37°46.59.65" S
0.0%	0.0%
Unimodal, Poorly Sorted	Unimodal, Very Poorly Sorted
Slightly Gravelly Muddy Sand	Sandy Mud
Fine Gravelly Very Coarse Silty Ver	Very Fine Sandy Very Coarse Silt
63.49	51.83
3.813	4.585
-0.329	-0.181
1.309	1.073
3.977	4.270
1.931	2.197
0.329	0.181
1.309	1.073
Very Fine Sand	Very Coarse Silt
Poorly Sorted	Very Poorly Sorted
Very Fine Skewed	Fine Skewed
Leptokurtic	Mesokurtic
96.50	81.00
3.379	3.631
7.581	5.830
79.18	59.80
249.5	305.9
32.92	52.47
242.0	300.1
4.443	7.076
114.1	122.3
2.003	1.709
3.659	4.064
7.043	7.422
3.517	4.344
5.041	5.714
1.779	2.004
2.152	2.823
0.7%	0.0%
58.1%	48.7%
41.2%	51.3%
0.0%	0.0%
0.0%	0.0%
0.0%	0.0%
0.0%	0.0%
0.7%	0.0%
0.0%	0.0%
1.0%	3.6%
8.3%	9.6%
21.3%	15.1%
27.6%	20.4%
17.3%	18.0%
8.6%	13.0%
5.1%	8.1%
3.8%	5.2%
3.1%	3.5%
3.3%	3.5%

Figure 4.30. 21-0437 GRADISTAT Grainsize Analysis (12/12).

- Ferrybank.

SAMPLE STATISTICS

		FB_0.10mbgl	FB_0.50mbgl	FB_1.00mbgl
	ANALYST AND DATE:	, 2/27/2025 2:27:36 PM	, 2/27/2025 2:39:41 PM	, 2/27/2025 2:48:02 PM
	LOCATION:	175°17'12.32" E 37°47'20.83" S	175°17'12.32" E 37°47'20.83" S	175°17'12.32" E 37°47'20.83" S
	SIEVING ERROR:	0.0%	0.0%	0.0%
	SAMPLE TYPE:	Unimodal, Poorly Sorted	Bimodal, Very Poorly Sorted	Unimodal, Poorly Sorted
	TEXTURAL GROUP:	Muddy Sand	Gravelly Mud	Slightly Gravelly Sandy Mud
	SEDIMENT NAME:	Very Coarse Silty Fine Sand	Very Fine Gravelly Very Coarse Silt	Fine Gravelly Very Fine Sandy Very
FOLK AND WARD METHOD (μm)	MEAN (M_G):	86.69	65.08	40.88
	SORTING (σ_G):	3.383	6.524	3.934
	SKEWNESS (Sk_G):	-0.420	0.063	-0.264
	KURTOSIS (K_G):	1.235	1.434	1.054
FOLK AND WARD METHOD (ϕ)	MEAN (M_Z):	3.528	3.942	4.612
	SORTING (σ_I):	1.758	2.706	1.976
	SKEWNESS (Sk_I):	0.420	-0.063	0.264
	KURTOSIS (K_G):	1.235	1.434	1.054
FOLK AND WARD METHOD (Description)	MEAN:	Very Fine Sand	Very Fine Sand	Very Coarse Silt
	SORTING:	Poorly Sorted	Very Poorly Sorted	Poorly Sorted
	SKEWNESS:	Very Fine Skewed	Symmetrical	Fine Skewed
	KURTOSIS:	Leptokurtic	Leptokurtic	Mesokurtic
	MODE 1 (μm):	163.0	58.00	81.00
	MODE 1 (ϕ):	2.622	4.113	3.631
	D_{10} (μm):	12.00	6.443	5.341
	D_{50} (μm):	114.3	62.23	50.12
	D_{90} (μm):	284.5	477.2	184.3
	(D_{90} / D_{10}) (μm):	23.72	74.07	34.51
	(D_{90} - D_{10}) (μm):	272.5	470.8	179.0
	(D_{75} / D_{25}) (μm):	4.051	7.788	5.967
	(D_{75} - D_{25}) (μm):	147.5	166.7	87.22
	D_{10} (ϕ):	1.813	1.067	2.440
	D_{50} (ϕ):	3.130	4.006	4.318
	D_{90} (ϕ):	6.381	7.278	7.549
	(D_{90} / D_{10}) (ϕ):	3.519	6.819	3.094
	(D_{90} - D_{10}) (ϕ):	4.568	6.211	5.109
	(D_{75} / D_{25}) (ϕ):	1.858	2.241	1.792
	(D_{75} - D_{25}) (ϕ):	2.018	2.961	2.577
	% GRAVEL:	0.0%	5.9%	0.3%
	% SAND:	70.0%	44.0%	42.5%
	% MUD:	30.0%	50.1%	57.2%
	% V COARSE GRAVEL:	0.0%	0.0%	0.0%
	% COARSE GRAVEL:	0.0%	0.0%	0.0%
	% MEDIUM GRAVEL:	0.0%	0.0%	0.0%
	% FINE GRAVEL:	0.0%	0.0%	0.0%
	% V FINE GRAVEL:	0.0%	5.9%	0.3%
	% V COARSE SAND:	0.0%	0.0%	0.0%
	% COARSE SAND:	0.1%	3.5%	0.0%
	% MEDIUM SAND:	14.3%	11.0%	4.6%
	% FINE SAND:	31.7%	11.9%	14.5%
	% V FINE SAND:	23.8%	17.5%	23.4%
	% V COARSE SILT:	11.2%	20.9%	20.3%
	% COARSE SILT:	7.0%	12.2%	14.2%
	% MEDIUM SILT:	4.8%	6.1%	9.4%
	% FINE SILT:	3.2%	3.7%	5.8%
	% V FINE SILT:	2.0%	3.1%	3.7%
	% CLAY:	1.8%	4.3%	3.7%

Figure 4.31. Ferrybank GRADISTAT Grainsize Analysis (1/22).

FB_1.25mbgl	FB_2.00mbgl	FB_2.50mbgl	FB_3.00mbgl
, 2/27/2025 2:56:17 PM	, 2/27/2025 3:04:10 PM	, 2/27/2025 3:11:45 PM	, 2/27/2025 3:19:46 PM
175°17'12.32" E 37°47'20.83" S	175°17'12.32" E 37°47'20.83" S	175°17'12.32" E 37°47'20.83" S	175°17'12.32" E 37°47'20.83" S
0.0%	0.0%	0.0%	0.0%
Unimodal, Poorly Sorted	Unimodal, Poorly Sorted	Unimodal, Poorly Sorted	Unimodal, Poorly Sorted
Slightly Gravelly Sandy Mud	Muddy Sand	Slightly Gravelly Muddy Sand	Slightly Gravelly Muddy Sand
Fine Gravelly Very Fine Sandy Very	Very Coarse Silty Fine Sand	ery Fine Gravelly Very Coarse Silty F	ery Fine Gravelly Very Coarse Silty F
44.40	88.89	118.2	131.7
3.072	3.145	2.971	3.506
-0.298	-0.382	-0.346	-0.250
1.130	1.291	1.453	1.434
4.493	3.492	3.081	2.925
1.619	1.653	1.571	1.810
0.298	0.382	0.346	0.250
1.130	1.291	1.453	1.434
Very Coarse Silt	Very Fine Sand	Very Fine Sand	Fine Sand
Poorly Sorted	Poorly Sorted	Poorly Sorted	Poorly Sorted
Fine Skewed	Very Fine Skewed	Very Fine Skewed	Fine Skewed
Leptokurtic	Leptokurtic	Leptokurtic	Leptokurtic
68.50	137.0	163.0	193.5
3.872	2.873	2.622	2.375
8.166	14.39	18.75	20.57
52.71	111.3	138.0	159.4
144.6	277.2	339.7	493.8
17.70	19.26	18.11	24.01
136.4	262.8	320.9	473.2
4.100	3.592	3.125	3.727
70.60	134.9	155.2	203.3
2.790	1.851	1.558	1.018
4.246	3.167	2.858	2.650
6.936	6.119	5.737	5.603
2.486	3.306	3.683	5.504
4.146	4.268	4.179	4.585
1.595	1.763	1.771	2.027
2.036	1.845	1.644	1.898
0.2%	0.0%	0.0%	2.9%
42.4%	70.9%	78.5%	75.2%
57.4%	29.1%	21.5%	22.0%
0.0%	0.0%	0.0%	0.0%
0.0%	0.0%	0.0%	0.0%
0.0%	0.0%	0.0%	0.0%
0.0%	0.0%	0.0%	0.0%
0.2%	0.0%	0.0%	2.9%
0.0%	0.0%	0.0%	1.7%
0.0%	0.6%	2.4%	5.3%
1.4%	12.6%	18.5%	19.4%
12.4%	31.5%	34.0%	31.2%
28.6%	26.3%	23.6%	17.7%
25.7%	11.7%	8.1%	8.4%
14.4%	6.8%	4.7%	5.8%
7.7%	4.5%	3.6%	3.5%
4.4%	2.8%	2.5%	2.1%
2.6%	1.7%	1.5%	1.2%
2.5%	1.5%	1.2%	0.9%

Figure 4.32. Ferrybank GRADISTAT Grainsize Analysis (2/22).

FB_3.50mbgl	FB_3.65mbgl	FB_4.00mbgl	FB_4.50mbgl
, 2/27/2025 3:27:17 PM	, 2/27/2025 3:34:59 PM	, 2/27/2025 3:42:37 PM	, 2/27/2025 3:50:43 PM
175°17'12.32" E 37°47'20.83" S	175°17'12.32" E 37°47'20.83" S	175°17'12.32" E 37°47'20.83" S	175°17'12.32" E 37°47'20.83" S
0.0%	0.0%	0.0%	0.0%
Unimodal, Poorly Sorted	Unimodal, Poorly Sorted	Unimodal, Poorly Sorted	Unimodal, Poorly Sorted
Slightly Gravelly Sand	Slightly Gravelly Sandy Mud	Muddy Sand	Sandy Mud
Slightly Very Fine Gravelly Fine Sand	Fine Gravelly Very Fine Sandy Very	Very Coarse Silty Very Fine Sand	Very Fine Sandy Very Coarse Silt
169.6	49.91	84.08	52.17
2.076	3.216	2.982	2.451
-0.294	-0.185	-0.260	-0.321
1.606	1.391	1.443	1.309
2.560	4.324	3.572	4.261
1.054	1.685	1.576	1.293
0.294	0.185	0.260	0.321
1.606	1.391	1.443	1.309
Fine Sand	Very Coarse Silt	Very Fine Sand	Very Coarse Silt
Poorly Sorted	Poorly Sorted	Poorly Sorted	Poorly Sorted
Fine Skewed	Fine Skewed	Fine Skewed	Very Fine Skewed
Very Leptokurtic	Leptokurtic	Leptokurtic	Leptokurtic
193.5	68.50	115.0	68.50
2.375	3.872	3.126	3.872
64.71	9.624	15.99	13.89
178.2	57.21	95.20	59.70
334.1	169.9	261.4	129.7
5.162	17.66	16.35	9.338
269.4	160.3	245.4	115.8
2.112	3.612	3.183	2.718
132.6	71.80	109.7	58.46
1.582	2.557	1.936	2.946
2.489	4.128	3.393	4.066
3.950	6.699	5.967	6.170
2.497	2.620	3.082	2.094
2.368	4.142	4.031	3.223
1.542	1.556	1.632	1.420
1.079	1.853	1.670	1.442
0.9%	4.0%	0.0%	0.0%
89.4%	42.0%	68.4%	47.4%
9.7%	54.1%	31.6%	52.6%
0.0%	0.0%	0.0%	0.0%
0.0%	0.0%	0.0%	0.0%
0.0%	0.0%	0.0%	0.0%
0.0%	0.0%	0.0%	0.0%
0.9%	4.0%	0.0%	0.0%
0.0%	0.1%	1.0%	0.0%
0.3%	0.6%	2.2%	0.0%
24.2%	1.5%	7.6%	0.2%
47.5%	10.6%	25.4%	10.9%
17.3%	29.2%	32.2%	36.3%
3.3%	26.6%	15.3%	30.2%
2.4%	12.9%	6.5%	11.5%
1.5%	6.5%	4.0%	5.1%
1.3%	3.8%	2.6%	2.7%
0.8%	2.3%	1.7%	1.6%
0.4%	2.0%	1.4%	1.5%

Figure 4.33. Ferrybank GRADISTAT Grainsize Analysis (3/22).

FB_5.00mbgl	FB_5.50mbgl	FB_6.00mbgl	FB_6.75mbgl
, 2/27/2025 3:58:25 PM	, 2/27/2025 4:06:15 PM	, 2/27/2025 4:13:55 PM	, 2/27/2025 4:21:20 PM
175°17'12.32" E 37°47'20.83" S	175°17'12.32" E 37°47'20.83" S	175°17'12.32" E 37°47'20.83" S	175°17'12.32" E 37°47'20.83" S
0.0%	0.0%	0.0%	0.0%
Unimodal, Poorly Sorted	Unimodal, Poorly Sorted	Unimodal, Poorly Sorted	Unimodal, Poorly Sorted
Sandy Mud	Slightly Gravelly Sandy Mud	Slightly Gravelly Sandy Mud	Sandy Mud
Very Fine Sandy Very Coarse Silt	Fine Gravelly Very Fine Sandy Very	Fine Gravelly Very Fine Sandy Very	Very Fine Sandy Very Coarse Silt
47.37	53.08	28.41	44.73
2.561	2.261	2.715	2.527
-0.335	-0.275	-0.218	-0.296
1.298	1.268	1.120	1.238
4.400	4.236	5.137	4.483
1.356	1.177	1.441	1.337
0.335	0.275	0.218	0.296
1.298	1.268	1.120	1.238
Very Coarse Silt	Very Coarse Silt	Coarse Silt	Very Coarse Silt
Poorly Sorted	Poorly Sorted	Poorly Sorted	Poorly Sorted
Very Fine Skewed	Fine Skewed	Fine Skewed	Fine Skewed
Leptokurtic	Leptokurtic	Leptokurtic	Leptokurtic
68.50	68.50	40.50	58.00
3.872	3.872	4.631	4.113
11.15	16.57	6.920	11.12
55.09	58.75	31.86	50.71
122.5	124.8	86.46	116.8
10.99	7.532	12.49	10.51
111.4	108.3	79.54	105.7
2.876	2.542	3.466	2.984
56.41	54.37	39.60	53.73
3.029	3.002	3.532	3.097
4.182	4.089	4.972	4.302
6.487	5.915	7.175	6.491
2.142	1.970	2.032	2.096
3.458	2.913	3.643	3.394
1.432	1.387	1.430	1.435
1.524	1.346	1.793	1.577
0.0%	0.0%	0.1%	0.0%
43.0%	46.3%	20.2%	38.6%
57.0%	53.7%	79.7%	61.4%
0.0%	0.0%	0.0%	0.0%
0.0%	0.0%	0.0%	0.0%
0.0%	0.0%	0.0%	0.0%
0.0%	0.0%	0.0%	0.0%
0.0%	0.0%	0.1%	0.0%
0.0%	0.0%	0.0%	0.0%
0.0%	0.0%	0.0%	0.0%
0.2%	0.1%	0.6%	0.3%
9.0%	9.8%	2.8%	7.5%
33.8%	36.4%	16.8%	30.8%
31.1%	32.8%	30.5%	33.2%
12.9%	11.8%	25.1%	15.2%
6.0%	4.5%	13.0%	6.2%
3.3%	2.2%	5.9%	3.2%
1.9%	1.2%	2.8%	1.9%
1.7%	1.2%	2.4%	1.7%

Figure 4.34. Ferrybank GRADISTAT Grainsize Analysis (4/22).

FB_7.00mbgl	FB_7.50mbgl	FB_8.50mbgl	FB_9.00mbgl
, 2/27/2025 4:28:40 PM	, 2/27/2025 4:36:06 PM	, 2/27/2025 4:44:22 PM	, 2/27/2025 4:52:16 PM
175°17'12.32" E 37°47'20.83" S	175°17'12.32" E 37°47'20.83" S	175°17'12.32" E 37°47'20.83" S	175°17'12.32" E 37°47'20.83" S
0.0%	0.0%	0.0%	0.0%
Unimodal, Poorly Sorted	Unimodal, Poorly Sorted	Unimodal, Poorly Sorted	Unimodal, Poorly Sorted
Slightly Gravelly Sandy Mud	Sandy Mud	Slightly Gravelly Sandy Mud	Sandy Mud
Fine Gravelly Very Fine Sandy Very	Very Fine Sandy Very Coarse Silt	Fine Gravelly Very Fine Sandy Very	Very Fine Sandy Very Coarse Silt
37.84	25.63	33.39	25.40
2.751	2.680	2.829	2.626
-0.310	-0.235	-0.230	-0.203
1.183	1.161	1.170	1.127
4.724	5.286	4.904	5.299
1.460	1.422	1.500	1.393
0.310	0.235	0.230	0.203
1.183	1.161	1.170	1.127
Very Coarse Silt	Coarse Silt	Very Coarse Silt	Coarse Silt
Poorly Sorted	Poorly Sorted	Poorly Sorted	Poorly Sorted
Very Fine Skewed	Fine Skewed	Fine Skewed	Fine Skewed
Leptokurtic	Leptokurtic	Leptokurtic	Leptokurtic
58.00	34.00	48.50	34.00
4.113	4.884	4.372	4.884
8.049	6.171	7.772	6.472
44.14	28.59	37.96	27.90
107.8	75.16	103.6	74.75
13.39	12.18	13.32	11.55
99.75	68.99	95.78	68.28
3.450	3.331	3.576	3.325
51.62	34.62	47.17	34.03
3.214	3.734	3.272	3.742
4.502	5.128	4.719	5.163
6.957	7.340	7.008	7.272
2.165	1.966	2.142	1.943
3.743	3.606	3.736	3.530
1.472	1.400	1.467	1.397
1.787	1.736	1.838	1.733
0.1%	0.0%	0.5%	0.0%
32.3%	15.7%	26.4%	15.4%
67.6%	84.3%	73.1%	84.6%
0.0%	0.0%	0.0%	0.0%
0.0%	0.0%	0.0%	0.0%
0.0%	0.0%	0.0%	0.0%
0.0%	0.0%	0.0%	0.0%
0.1%	0.0%	0.5%	0.0%
0.0%	0.0%	1.2%	0.0%
0.0%	0.0%	0.7%	0.0%
0.4%	0.0%	0.5%	0.2%
5.8%	1.7%	3.6%	1.7%
26.1%	14.1%	20.4%	13.5%
32.7%	30.7%	31.6%	30.0%
17.4%	27.5%	21.3%	28.2%
7.9%	14.0%	10.1%	14.7%
4.5%	6.1%	5.0%	6.3%
2.7%	3.1%	2.7%	2.9%
2.5%	2.9%	2.4%	2.5%

Figure 4.35. Ferrybank GRADISTAT Grainsize Analysis (5/22).

FB_9.50mbgl	FB_10.00mbgl	FB_10.50mbgl	FB_11.75mbgl
, 3/4/2025 9:12:49 AM	, 3/4/2025 9:29:11 AM	, 3/4/2025 9:46:12 AM	, 3/4/2025 9:53:47 AM
175°17'12.32" E 37°47'20.83" S	175°17'12.32" E 37°47'20.83" S	175°17'12.32" E 37°47'20.83" S	175°17'12.32" E 37°47'20.83" S
0.0%	0.0%	0.0%	0.0%
Unimodal, Poorly Sorted	Unimodal, Poorly Sorted	Unimodal, Poorly Sorted	Unimodal, Poorly Sorted
Slightly Gravelly Sandy Mud	Slightly Gravelly Mud	Sandy Mud	Sandy Mud
Fine Gravelly Very Fine Sandy Ver	Slightly Very Fine Gravelly Coarse Si	Very Fine Sandy Very Coarse Silt	Very Fine Sandy Very Coarse Silt
35.92	19.74	32.87	43.96
2.762	2.464	2.589	2.489
-0.196	-0.150	-0.256	-0.262
1.130	1.131	1.141	1.186
4.799	5.663	4.927	4.508
1.465	1.301	1.372	1.316
0.196	0.150	0.256	0.262
1.130	1.131	1.141	1.186
Very Coarse Silt	Coarse Silt	Very Coarse Silt	Very Coarse Silt
Poorly Sorted	Poorly Sorted	Poorly Sorted	Poorly Sorted
Fine Skewed	Fine Skewed	Fine Skewed	Fine Skewed
Leptokurtic	Leptokurtic	Leptokurtic	Leptokurtic
48.50	23.30	48.50	58.00
4.372	5.507	4.372	4.113
8.648	5.467	8.319	11.52
39.72	20.81	36.98	49.03
112.0	55.46	91.57	115.9
12.95	10.15	11.01	10.06
103.3	50.00	83.25	104.4
3.613	3.170	3.287	3.041
50.43	24.01	42.71	53.09
3.159	4.172	3.449	3.108
4.654	5.586	4.757	4.350
6.853	7.515	6.909	6.440
2.170	1.801	2.003	2.072
3.694	3.343	3.460	3.331
1.482	1.344	1.426	1.438
1.853	1.665	1.717	1.605
0.0%	0.5%	0.0%	0.0%
29.5%	7.0%	24.1%	37.1%
70.5%	92.5%	75.9%	62.9%
0.0%	0.0%	0.0%	0.0%
0.0%	0.0%	0.0%	0.0%
0.0%	0.0%	0.0%	0.0%
0.0%	0.0%	0.0%	0.0%
0.0%	0.5%	0.0%	0.0%
0.1%	0.0%	0.0%	0.0%
0.9%	0.0%	0.0%	0.0%
1.3%	0.4%	0.6%	0.7%
5.3%	0.9%	3.0%	7.0%
21.9%	5.7%	20.5%	29.3%
30.7%	22.5%	33.8%	33.4%
21.2%	34.1%	22.9%	16.6%
10.0%	21.8%	10.0%	6.5%
4.4%	7.9%	4.6%	3.1%
2.2%	3.3%	2.3%	1.7%
2.0%	2.9%	2.2%	1.6%

Figure 4.36. Ferrybank GRADISTAT Grainsize Analysis (6/22).

FB_12.00mbgl	FB_12.75mbgl	FB_13.00mbgl	FB_13.25mbgl
, 3/4/2025 11:25:21 AM	, 3/4/2025 10:01:16 AM	, 3/4/2025 10:08:56 AM	, 3/4/2025 10:16:23 AM
175°17'12.32" E 37°47'20.83" S	175°17'12.32" E 37°47'20.83" S	175°17'12.32" E 37°47'20.83" S	175°17'12.32" E 37°47'20.83" S
0.0%	0.0%	0.0%	0.0%
Bimodal, Very Poorly Sorted	Unimodal, Very Poorly Sorted	Unimodal, Poorly Sorted	Unimodal, Poorly Sorted
Slightly Gravelly Sandy Mud	Slightly Gravelly Muddy Sand	Muddy Sand	Sandy Mud
ery Fine Gravelly Very Fine Sandy C	ery Fine Gravelly Very Coarse Silty F	Very Coarse Silty Fine Sand	Very Fine Sandy Very Coarse Silt
34.76	91.92	80.46	25.07
5.618	4.157	3.739	3.768
0.048	-0.364	-0.417	-0.302
1.025	1.205	1.213	0.981
4.846	3.443	3.636	5.318
2.490	2.056	1.903	1.914
-0.048	0.364	0.417	0.302
1.025	1.205	1.213	0.981
Very Coarse Silt	Very Fine Sand	Very Fine Sand	Coarse Silt
Very Poorly Sorted	Very Poorly Sorted	Poorly Sorted	Poorly Sorted
Symmetrical	Very Fine Skewed	Very Fine Skewed	Very Fine Skewed
Mesokurtic	Leptokurtic	Leptokurtic	Mesokurtic
23.30	163.0	163.0	58.00
5.507	2.622	2.622	4.113
3.947	9.660	9.306	3.410
32.43	124.1	109.3	31.97
388.3	398.3	294.5	104.7
98.39	41.23	31.64	30.71
384.4	388.6	285.2	101.3
9.843	5.254	4.603	6.135
96.42	191.4	153.0	54.41
1.365	1.328	1.764	3.255
4.946	3.011	3.194	4.967
7.985	6.694	6.748	8.196
5.851	5.040	3.826	2.518
6.620	5.366	4.984	4.941
2.025	2.150	1.935	1.664
3.299	2.393	2.203	2.617
0.1%	0.0%	0.0%	0.0%
35.8%	69.5%	67.7%	26.4%
64.1%	30.5%	32.3%	73.6%
0.0%	0.0%	0.0%	0.0%
0.0%	0.0%	0.0%	0.0%
0.0%	0.0%	0.0%	0.0%
0.0%	0.0%	0.0%	0.0%
0.1%	0.0%	0.0%	0.0%
0.8%	0.3%	0.0%	0.0%
6.6%	5.6%	0.9%	0.0%
6.4%	17.1%	14.4%	0.7%
8.4%	26.8%	29.3%	5.6%
13.6%	19.8%	23.2%	20.1%
15.0%	10.1%	11.4%	24.3%
17.0%	6.9%	7.1%	17.4%
13.8%	5.1%	5.1%	12.3%
8.5%	3.7%	3.8%	8.5%
5.2%	2.5%	2.6%	5.6%
4.7%	2.3%	2.3%	5.5%

Figure 4.37. Ferrybank GRADISTAT Grainsize Analysis (7/22).

FB_13.50mbgl	FB_14.00mbgl	FB_14.50mbgl	FB_15.00mbgl
, 3/4/2025 10:24:13 AM	, 3/4/2025 10:39:53 AM	, 3/4/2025 10:47:22 AM	, 3/4/2025 10:54:48 AM
175°17'12.32" E 37°47'20.83" S	175°17'12.32" E 37°47'20.83" S	175°17'12.32" E 37°47'20.83" S	175°17'12.32" E 37°47'20.83" S
0.0%	0.0%	0.0%	0.0%
Unimodal, Poorly Sorted	Unimodal, Poorly Sorted	Unimodal, Poorly Sorted	Unimodal, Very Poorly Sorted
Sandy Mud	Mud	Slightly Gravelly Muddy Sand	Slightly Gravelly Muddy Sand
Very Fine Sandy Very Coarse Silt	Medium Silt	y Fine Gravelly Very Coarse Silty Me	y Fine Gravelly Very Coarse Silty C
47.69	9.466	220.0	246.3
2.880	3.496	2.946	5.031
-0.280	-0.016	-0.432	-0.433
1.135	1.005	1.794	1.111
4.390	6.723	2.184	2.022
1.526	1.806	1.559	2.331
0.280	0.016	0.432	0.433
1.135	1.005	1.794	1.111
Very Coarse Silt	Medium Silt	Fine Sand	Fine Sand
Poorly Sorted	Poorly Sorted	Poorly Sorted	Very Poorly Sorted
Fine Skewed	Symmetrical	Very Fine Skewed	Very Fine Skewed
Leptokurtic	Mesokurtic	Very Leptokurtic	Leptokurtic
68.50	11.70	325.0	650.0
3.872	6.502	1.626	0.628
9.754	1.912	37.16	17.07
54.73	9.551	266.3	363.4
145.4	47.51	566.9	1180.9
14.90	24.85	15.26	69.18
135.6	45.60	529.7	1163.9
3.808	5.380	2.631	7.610
70.61	18.34	248.6	652.0
2.782	4.395	0.819	-0.240
4.191	6.710	1.909	1.460
6.680	9.031	4.750	5.872
2.401	2.055	5.801	-24.477
3.897	4.635	3.931	6.112
1.570	1.444	2.059	8.074
1.929	2.428	1.396	2.928
0.0%	0.0%	0.2%	0.5%
44.2%	6.5%	86.2%	79.9%
55.8%	93.5%	13.6%	19.6%
0.0%	0.0%	0.0%	0.0%
0.0%	0.0%	0.0%	0.0%
0.0%	0.0%	0.0%	0.0%
0.0%	0.0%	0.0%	0.0%
0.0%	0.0%	0.2%	0.5%
0.0%	0.0%	1.9%	14.4%
0.0%	0.0%	12.2%	24.9%
1.3%	0.4%	39.7%	19.8%
13.3%	1.1%	25.4%	12.1%
29.7%	4.9%	7.1%	8.6%
26.1%	10.5%	4.5%	5.9%
14.9%	17.0%	2.8%	4.3%
7.1%	22.5%	2.2%	3.4%
3.4%	20.5%	1.7%	2.7%
2.1%	12.7%	1.3%	1.9%
2.2%	10.2%	1.1%	1.5%

Figure 4.38. Ferrybank GRADISTAT Grainsize Analysis (8/22).

FB_15.50mbgl	FB_16.00mbgl	FB_16.50mbgl	FB_17.00mbgl
, 3/4/2025 11:02:21 AM	, 3/4/2025 11:10:41 AM	, 3/4/2025 11:17:58 AM	, 3/4/2025 11:36:06 AM
175°17'12.32" E 37°47'20.83" S	175°17'12.32" E 37°47'20.83" S	175°17'12.32" E 37°47'20.83" S	175°17'12.32" E 37°47'20.83" S
0.0%	0.0%	0.0%	0.0%
Unimodal, Poorly Sorted	Unimodal, Very Poorly Sorted	Unimodal, Poorly Sorted	Unimodal, Poorly Sorted
Slightly Gravelly Muddy Sand	Slightly Gravelly Muddy Sand	Sandy Mud	Sandy Mud
y Fine Gravelly Very Coarse Silty Me	Fine Gravelly Very Coarse Silty Ver	Very Fine Sandy Very Coarse Silt	Very Fine Sandy Coarse Silt
307.1	111.0	21.55	20.23
3.700	4.827	3.064	3.579
-0.337	-0.028	-0.267	-0.153
1.716	1.005	1.081	1.010
1.703	3.171	5.536	5.627
1.887	2.271	1.615	1.840
0.337	0.028	0.267	0.153
1.716	1.005	1.081	1.010
Medium Sand	Very Fine Sand	Coarse Silt	Coarse Silt
Poorly Sorted	Very Poorly Sorted	Poorly Sorted	Poorly Sorted
Very Fine Skewed	Symmetrical	Fine Skewed	Fine Skewed
Very Leptokurtic	Mesokurtic	Mesokurtic	Mesokurtic
385.0	96.50	34.00	34.00
1.383	3.379	4.884	4.884
34.24	14.02	4.025	3.380
364.8	109.3	25.20	22.51
1101.1	790.9	72.16	89.78
32.16	56.41	17.93	26.56
1066.9	776.9	68.14	86.40
3.324	8.190	4.222	5.519
444.7	290.9	35.47	40.61
-0.139	0.338	3.793	3.477
1.455	3.194	5.310	5.473
4.868	6.156	7.957	8.209
-35.029	18.20	2.098	2.360
5.007	5.818	4.164	4.731
3.654	2.904	1.469	1.569
1.733	3.034	2.078	2.464
1.6%	2.9%	0.0%	0.0%
85.1%	62.2%	14.1%	18.4%
13.4%	34.9%	85.9%	81.6%
0.0%	0.0%	0.0%	0.0%
0.0%	0.0%	0.0%	0.0%
0.0%	0.0%	0.0%	0.0%
0.0%	0.0%	0.0%	0.0%
1.6%	2.9%	0.0%	0.0%
10.3%	3.9%	0.0%	0.0%
23.0%	10.7%	0.0%	0.0%
32.0%	13.0%	0.1%	1.3%
15.0%	15.9%	1.6%	3.8%
4.8%	18.7%	12.5%	13.3%
3.8%	14.7%	27.9%	21.2%
2.9%	9.4%	25.6%	22.0%
2.5%	5.4%	14.6%	16.8%
1.9%	2.6%	8.1%	10.3%
1.3%	1.5%	5.0%	6.0%
1.0%	1.4%	4.7%	5.2%

Figure 4.39. Ferrybank GRADISTAT Grainsize Analysis (9/22).

FB_17.25mbgl	FB_17.50mbgl	FB_18.00mbgl	FB_18.50mbgl
, 3/4/2025 11:43:51 AM	, 3/4/2025 11:52:18 AM	, 3/4/2025 12:00:02 PM	, 3/4/2025 12:07:40 PM
175°17'12.32" E 37°47'20.83" S	175°17'12.32" E 37°47'20.83" S	175°17'12.32" E 37°47'20.83" S	175°17'12.32" E 37°47'20.83" S
0.0%	0.0%	0.0%	0.0%
Unimodal, Poorly Sorted	Bimodal, Very Poorly Sorted	Unimodal, Very Poorly Sorted	Unimodal, Very Poorly Sorted
Muddy Sand	Gravelly Muddy Sand	Slightly Gravelly Muddy Sand	Slightly Gravelly Muddy Sand
Very Coarse Silty Fine Sand	e Gravelly Very Coarse Silty Very Fi	ery Fine Gravelly Very Coarse Silty F	Fine Gravelly Very Coarse Silty Ver
122.4	192.2	116.7	62.92
2.402	6.125	4.451	6.232
-0.333	0.027	-0.205	-0.139
1.637	1.003	1.204	0.992
3.030	2.379	3.099	3.990
1.264	2.615	2.154	2.640
0.333	-0.027	0.205	0.139
1.637	1.003	1.204	0.992
Very Fine Sand	Fine Sand	Very Fine Sand	Very Fine Sand
Poorly Sorted	Very Poorly Sorted	Very Poorly Sorted	Very Poorly Sorted
Very Fine Skewed	Symmetrical	Fine Skewed	Fine Skewed
Very Leptokurtic	Mesokurtic	Leptokurtic	Mesokurtic
163.0	115.0	137.0	96.50
2.622	3.126	2.873	3.379
32.26	16.41	12.88	4.834
132.2	165.4	134.3	72.66
271.4	1642.9	621.6	571.0
8.411	100.1	48.26	118.1
239.1	1626.4	608.7	566.2
2.410	11.93	5.861	11.77
115.4	706.2	254.0	199.3
1.882	-0.716	0.686	0.808
2.919	2.596	2.897	3.783
4.954	5.929	6.279	7.692
2.633	-8.278	9.153	9.516
3.072	6.645	5.593	6.884
1.542	10.52	2.495	2.618
1.269	3.577	2.551	3.558
0.0%	6.3%	0.3%	2.6%
83.0%	69.4%	71.1%	50.7%
17.0%	24.3%	28.6%	46.6%
0.0%	0.0%	0.0%	0.0%
0.0%	0.0%	0.0%	0.0%
0.0%	0.0%	0.0%	0.0%
0.0%	0.0%	0.0%	0.0%
0.0%	6.3%	0.3%	2.6%
0.0%	14.2%	3.7%	1.4%
0.1%	10.3%	9.7%	7.8%
12.8%	9.6%	17.0%	10.7%
40.7%	17.6%	21.6%	14.6%
29.4%	17.8%	19.1%	16.4%
7.1%	9.4%	11.1%	13.4%
3.1%	5.3%	6.3%	10.9%
2.4%	3.8%	4.3%	8.3%
1.9%	2.7%	3.1%	5.8%
1.4%	1.7%	2.1%	4.0%
1.0%	1.4%	1.8%	4.2%

Figure 4.40. Ferrybank GRADISTAT Grainsize Analysis (10/22).

FB_19.00mbgl	FB_19.50mbgl	FB_20.00mbgl	FB_20.10mbgl
, 3/4/2025 12:15:09 PM	, 3/4/2025 12:23:17 PM	, 3/4/2025 12:30:50 PM	, 3/4/2025 12:38:12 PM
175°17'12.32" E 37°47'20.83" S	175°17'12.32" E 37°47'20.83" S	175°17'12.32" E 37°47'20.83" S	175°17'12.32" E 37°47'20.83" S
0.0%	0.0%	0.0%	0.0%
Unimodal, Very Poorly Sorted	Unimodal, Very Poorly Sorted	Unimodal, Very Poorly Sorted	Unimodal, Very Poorly Sorted
Slightly Gravelly Muddy Sand	Slightly Gravelly Muddy Sand	Slightly Gravelly Muddy Sand	Slightly Gravelly Muddy Sand
Fine Gravelly Very Coarse Silty Ver	Fine Gravelly Very Coarse Silty Ver	Fine Gravelly Very Coarse Silty Ver	ery Fine Gravelly Very Coarse Silty F
77.65	80.27	84.12	139.3
4.719	5.074	5.242	5.098
-0.190	-0.132	-0.124	-0.181
1.138	1.103	1.063	1.173
3.687	3.639	3.571	2.844
2.239	2.343	2.390	2.350
0.190	0.132	0.124	0.181
1.138	1.103	1.063	1.173
Very Fine Sand	Very Fine Sand	Very Fine Sand	Fine Sand
Very Poorly Sorted	Very Poorly Sorted	Very Poorly Sorted	Very Poorly Sorted
Fine Skewed	Fine Skewed	Fine Skewed	Fine Skewed
Leptokurtic	Mesokurtic	Mesokurtic	Leptokurtic
96.50	96.50	96.50	193.5
3.379	3.379	3.379	2.375
8.128	8.070	8.115	12.86
89.89	87.51	90.54	158.2
463.7	561.9	605.9	919.3
57.05	69.62	74.67	71.49
455.5	553.8	597.8	906.5
6.646	7.612	8.355	7.020
179.7	199.5	223.0	336.2
1.109	0.832	0.723	0.121
3.476	3.514	3.465	2.660
6.943	6.953	6.945	6.281
6.261	8.360	9.608	51.77
5.834	6.121	6.222	6.160
2.219	2.380	2.546	3.081
2.732	2.928	3.063	2.812
0.2%	0.2%	0.3%	0.4%
60.6%	59.3%	59.8%	72.6%
39.2%	40.5%	39.9%	27.0%
0.0%	0.0%	0.0%	0.0%
0.0%	0.0%	0.0%	0.0%
0.0%	0.0%	0.0%	0.0%
0.0%	0.0%	0.0%	0.0%
0.2%	0.2%	0.3%	0.4%
1.4%	2.6%	3.0%	8.3%
7.2%	8.8%	9.7%	11.2%
12.5%	11.6%	12.2%	16.6%
18.1%	16.3%	15.7%	20.2%
21.4%	19.9%	19.1%	16.3%
14.5%	15.0%	14.5%	9.8%
9.0%	9.5%	9.5%	6.0%
6.1%	6.3%	6.3%	4.2%
4.2%	4.2%	4.2%	3.0%
2.9%	2.9%	2.8%	2.1%
2.6%	2.6%	2.6%	1.8%

Figure 4.41. Ferrybank GRADISTAT Grainsize Analysis (11/22).

FB_20.50mbgl	FB_20.60mbgl	FB_21.00mbgl	FB_21.75mbgl
, 3/5/2025 9:24:42 AM	, 3/5/2025 9:32:05 AM	, 3/5/2025 9:39:34 AM	, 3/5/2025 9:47:00 AM
175°17'12.32" E 37°47'20.83" S	175°17'12.32" E 37°47'20.83" S	175°17'12.32" E 37°47'20.83" S	175°17'12.32" E 37°47'20.83" S
0.0%	0.0%	0.0%	0.0%
Unimodal, Very Poorly Sorted	Unimodal, Very Poorly Sorted	Unimodal, Very Poorly Sorted	Bimodal, Very Poorly Sorted
Slightly Gravelly Muddy Sand	Slightly Gravelly Muddy Sand	Slightly Gravelly Muddy Sand	Slightly Gravelly Muddy Sand
Fine Gravelly Very Coarse Silty Ver	Fine Gravelly Very Coarse Silty Ver	Fine Gravelly Very Coarse Silty Very	Fine Gravelly Very Coarse Silty Me
63.83	63.63	86.42	98.14
5.067	4.884	4.997	6.325
-0.174	-0.192	-0.152	-0.180
1.052	1.066	1.091	0.908
3.970	3.974	3.532	3.349
2.341	2.288	2.321	2.661
0.174	0.192	0.152	0.180
1.052	1.066	1.091	0.908
Very Fine Sand	Very Fine Sand	Very Fine Sand	Very Fine Sand
Very Poorly Sorted	Very Poorly Sorted	Very Poorly Sorted	Very Poorly Sorted
Fine Skewed	Fine Skewed	Fine Skewed	Fine Skewed
Mesokurtic	Mesokurtic	Mesokurtic	Mesokurtic
96.50	96.50	96.50	545.0
3.379	3.379	3.379	0.881
6.232	6.505	8.610	6.969
73.74	75.17	95.91	116.0
430.3	397.9	575.9	805.9
69.04	61.17	66.89	115.6
424.0	391.4	567.3	798.9
8.127	7.705	7.516	14.29
164.3	159.6	216.0	376.8
1.217	1.330	0.796	0.311
3.761	3.734	3.382	3.108
7.326	7.264	6.860	7.165
6.021	5.464	8.618	23.01
6.109	5.935	6.064	6.853
2.251	2.204	2.452	3.943
3.023	2.946	2.910	3.837
0.0%	0.6%	0.4%	2.8%
54.6%	54.6%	61.6%	59.8%
45.4%	44.8%	38.0%	37.5%
0.0%	0.0%	0.0%	0.0%
0.0%	0.0%	0.0%	0.0%
0.0%	0.0%	0.0%	0.0%
0.0%	0.0%	0.0%	0.0%
0.0%	0.6%	0.4%	2.8%
0.6%	0.7%	2.1%	3.6%
7.1%	5.6%	9.7%	14.0%
11.5%	11.3%	12.6%	14.4%
15.6%	16.9%	17.2%	13.7%
19.8%	20.1%	19.9%	14.1%
15.7%	15.6%	14.0%	11.2%
10.7%	10.7%	8.9%	8.8%
7.4%	7.2%	6.0%	6.7%
5.0%	4.9%	4.0%	4.7%
3.4%	3.3%	2.7%	3.2%
3.2%	3.1%	2.4%	2.9%

Figure 4.42. Ferrybank GRADISTAT Grainsize Analysis (12/22).

FB_22.00mbgl	FB_22.50mbgl	FB_23.00mbgl	FB_23.50mbgl
, 3/5/2025 9:55:29 AM	, 3/5/2025 10:02:59 AM	, 3/5/2025 10:10:38 AM	, 3/5/2025 10:19:08 AM
175°17'12.32" E 37°47'20.83" S	175°17'12.32" E 37°47'20.83" S	175°17'12.32" E 37°47'20.83" S	175°17'12.32" E 37°47'20.83" S
0.0%	0.0%	0.0%	0.0%
Unimodal, Very Poorly Sorted	Unimodal, Very Poorly Sorted	Unimodal, Very Poorly Sorted	Unimodal, Very Poorly Sorted
Gravelly Muddy Sand	Sandy Mud	Slightly Gravelly Muddy Sand	Slightly Gravelly Muddy Sand
e Gravelly Very Coarse Silty Very Fi	Very Fine Sandy Very Coarse Silt	Fine Gravelly Very Coarse Silty Ver	Fine Gravelly Very Coarse Silty Ver
117.3	27.15	100.2	112.1
6.557	5.829	4.735	4.643
-0.033	-0.071	-0.129	-0.115
1.049	0.957	1.159	1.183
3.092	5.203	3.319	3.157
2.713	2.543	2.243	2.215
0.033	0.071	0.129	0.115
1.049	0.957	1.159	1.183
Very Fine Sand	Coarse Silt	Very Fine Sand	Very Fine Sand
Very Poorly Sorted	Very Poorly Sorted	Very Poorly Sorted	Very Poorly Sorted
Symmetrical	Symmetrical	Fine Skewed	Fine Skewed
Mesokurtic	Mesokurtic	Leptokurtic	Leptokurtic
96.50	34.00	115.0	115.0
3.379	4.884	3.126	3.126
9.417	2.478	10.97	12.90
117.0	29.35	107.5	118.7
1228.4	254.0	639.4	694.9
130.4	102.5	58.30	53.89
1219.0	251.5	628.4	682.0
11.53	11.36	6.442	6.214
385.4	85.09	228.3	248.5
-0.297	1.977	0.645	0.525
3.096	5.091	3.218	3.074
6.730	8.656	6.511	6.277
-22.675	4.379	10.09	11.95
7.027	6.679	5.866	5.752
3.834	2.025	2.424	2.501
3.527	3.506	2.688	2.635
5.2%	0.0%	0.3%	1.9%
59.7%	33.2%	65.9%	67.2%
35.1%	66.8%	33.8%	30.9%
0.0%	0.0%	0.0%	0.0%
0.0%	0.0%	0.0%	0.0%
0.0%	0.0%	0.0%	0.0%
0.0%	0.0%	0.0%	0.0%
5.2%	0.0%	0.3%	1.9%
7.2%	0.0%	3.5%	3.6%
9.8%	3.0%	10.1%	9.7%
12.0%	7.2%	12.7%	13.7%
14.2%	9.5%	18.6%	19.5%
16.4%	13.5%	21.1%	20.8%
12.6%	15.4%	13.5%	12.6%
8.4%	15.0%	7.7%	7.0%
5.7%	12.2%	5.1%	4.6%
3.8%	9.4%	3.4%	3.1%
2.5%	7.1%	2.2%	2.0%
2.2%	7.6%	1.9%	1.6%

Figure 4.43. Ferrybank GRADISTAT Grainsize Analysis (13/22).

FB_24.00mbgl	FB_24.50mbgl	FB_25.00mbgl	FB_25.50mbgl
, 3/5/2025 10:26:53 AM	, 3/5/2025 10:34:37 AM	, 3/5/2025 10:42:10 AM	, 3/5/2025 10:49:38 AM
175°17'12.32" E 37°47'20.83" S	175°17'12.32" E 37°47'20.83" S	175°17'12.32" E 37°47'20.83" S	175°17'12.32" E 37°47'20.83" S
0.0%	0.0%	0.0%	0.0%
Unimodal, Very Poorly Sorted	Unimodal, Very Poorly Sorted	Unimodal, Very Poorly Sorted	Unimodal, Very Poorly Sorted
Slightly Gravelly Muddy Sand	Gravelly Muddy Sand	Slightly Gravelly Muddy Sand	Slightly Gravelly Muddy Sand
Fine Gravelly Very Coarse Silty Ver	e Gravelly Very Coarse Silty Very Fi	Fine Gravelly Very Coarse Silty Ver	Fine Gravelly Very Coarse Silty Ver
114.1	110.8	99.56	116.9
5.177	6.339	4.986	4.395
-0.069	0.027	-0.109	-0.113
1.194	1.301	1.131	1.210
3.132	3.174	3.328	3.097
2.372	2.664	2.318	2.136
0.069	-0.027	0.109	0.113
1.194	1.301	1.131	1.210
Very Fine Sand	Very Fine Sand	Very Fine Sand	Very Fine Sand
Very Poorly Sorted	Very Poorly Sorted	Very Poorly Sorted	Very Poorly Sorted
Symmetrical	Symmetrical	Fine Skewed	Fine Skewed
Leptokurtic	Leptokurtic	Leptokurtic	Leptokurtic
115.0	96.50	96.50	115.0
3.126	3.379	3.379	3.126
11.89	10.84	10.43	14.39
116.4	110.4	105.6	120.7
858.4	937.7	683.2	666.4
72.20	86.48	65.53	46.31
846.5	926.8	672.8	652.0
6.926	8.186	7.133	5.744
269.1	294.6	243.3	243.4
0.220	0.093	0.550	0.585
3.103	3.179	3.243	3.051
6.394	6.527	6.584	6.119
29.03	70.32	11.98	10.45
6.174	6.434	6.034	5.533
2.673	2.925	2.556	2.431
2.792	3.033	2.835	2.522
2.9%	5.6%	1.0%	1.6%
65.1%	60.4%	64.2%	68.7%
31.9%	34.0%	34.8%	29.6%
0.0%	0.0%	0.0%	0.0%
0.0%	0.0%	0.0%	0.0%
0.0%	0.0%	0.0%	0.0%
0.0%	0.0%	0.0%	0.0%
2.9%	5.6%	1.0%	1.6%
5.3%	3.7%	4.2%	3.0%
9.1%	9.2%	9.6%	10.0%
12.3%	11.8%	12.7%	14.1%
18.2%	16.2%	17.4%	20.0%
20.3%	19.5%	20.3%	21.6%
12.9%	13.4%	13.7%	12.7%
7.2%	7.9%	8.0%	6.4%
4.7%	5.2%	5.3%	4.1%
3.2%	3.4%	3.6%	2.9%
2.1%	2.2%	2.3%	1.9%
1.8%	1.9%	1.9%	1.6%

Figure 4.44. Ferrybank GRADISTAT Grainsize Analysis (14/22).

FB_26.00mbgl	FB_26.50mbgl	FB_27.00mbgl	FB_27.50mbgl
, 3/5/2025 10:58:08 AM	, 3/5/2025 11:05:49 AM	, 3/5/2025 11:13:35 AM	, 3/5/2025 11:21:06 AM
175°17'12.32" E 37°47'20.83" S	175°17'12.32" E 37°47'20.83" S	175°17'12.32" E 37°47'20.83" S	175°17'12.32" E 37°47'20.83" S
0.0%	0.0%	0.0%	0.0%
Unimodal, Very Poorly Sorted	Unimodal, Very Poorly Sorted	Unimodal, Very Poorly Sorted	Unimodal, Very Poorly Sorted
Slightly Gravelly Muddy Sand	Slightly Gravelly Muddy Sand	Slightly Gravelly Muddy Sand	Slightly Gravelly Muddy Sand
Fine Gravelly Very Coarse Silty Ver	Fine Gravelly Very Coarse Silty Ver	Fine Gravelly Very Coarse Silty Ver	Fine Gravelly Very Coarse Silty Ver
103.7	128.4	158.5	108.5
4.647	4.486	5.083	4.731
-0.140	-0.112	-0.025	-0.103
1.160	1.138	1.191	1.211
3.270	2.962	2.658	3.205
2.216	2.165	2.346	2.242
0.140	0.112	0.025	0.103
1.160	1.138	1.191	1.211
Very Fine Sand	Fine Sand	Fine Sand	Very Fine Sand
Very Poorly Sorted	Very Poorly Sorted	Very Poorly Sorted	Very Poorly Sorted
Fine Skewed	Fine Skewed	Symmetrical	Fine Skewed
Leptokurtic	Leptokurtic	Leptokurtic	Leptokurtic
115.0	115.0	115.0	115.0
3.126	3.126	3.126	3.126
11.54	15.16	17.24	12.32
111.9	131.1	150.6	113.8
628.8	728.7	1162.0	691.2
54.50	48.07	67.42	56.11
617.3	713.5	1144.8	678.9
6.375	6.440	7.093	6.203
237.5	294.1	374.1	240.4
0.669	0.457	-0.217	0.533
3.160	2.932	2.731	3.135
6.438	6.044	5.858	6.343
9.619	13.24	-27.046	11.90
5.768	5.587	6.075	5.810
2.462	2.765	3.357	2.460
2.672	2.687	2.826	2.633
0.7%	1.5%	4.8%	1.4%
66.6%	70.3%	69.8%	66.7%
32.7%	28.3%	25.4%	31.9%
0.0%	0.0%	0.0%	0.0%
0.0%	0.0%	0.0%	0.0%
0.0%	0.0%	0.0%	0.0%
0.0%	0.0%	0.0%	0.0%
0.7%	1.5%	4.8%	1.4%
3.2%	3.8%	7.1%	4.4%
9.8%	12.0%	10.6%	8.9%
14.0%	15.1%	14.2%	13.3%
18.8%	19.0%	18.8%	19.0%
20.8%	20.3%	19.1%	21.2%
13.3%	12.0%	10.7%	13.3%
7.3%	6.1%	5.4%	7.0%
4.8%	4.0%	3.6%	4.6%
3.3%	2.8%	2.5%	3.1%
2.2%	1.8%	1.7%	2.1%
1.9%	1.6%	1.4%	1.8%

Figure 4.45. Ferrybank GRADISTAT Grainsize Analysis (15/22).

FB_28.00mbgl	FB_28.50mbgl	FB_29.00mbgl	FB_29.50mbgl
, 3/5/2025 11:29:00 AM	, 3/5/2025 11:36:55 AM	, 3/5/2025 11:45:24 AM	, 3/5/2025 11:52:52 AM
175°17'12.32" E 37°47'20.83" S	175°17'12.32" E 37°47'20.83" S	175°17'12.32" E 37°47'20.83" S	175°17'12.32" E 37°47'20.83" S
0.0%	0.0%	0.0%	0.0%
Unimodal, Poorly Sorted	Unimodal, Very Poorly Sorted	Unimodal, Poorly Sorted	Unimodal, Very Poorly Sorted
Slightly Gravelly Muddy Sand	Slightly Gravelly Muddy Sand	Slightly Gravelly Muddy Sand	Slightly Gravelly Sandy Mud
y Fine Gravelly Very Coarse Silty Me	ery Fine Gravelly Very Coarse Silty	ly Fine Gravelly Very Coarse Silty Me	Fine Gravelly Very Fine Sandy Very
237.5	135.1	258.4	19.45
3.943	4.227	3.832	4.442
-0.156	-0.110	-0.222	-0.304
1.195	1.230	1.371	1.088
2.074	2.888	1.953	5.684
1.979	2.080	1.938	2.151
0.156	0.110	0.222	0.304
1.195	1.230	1.371	1.088
Fine Sand	Fine Sand	Medium Sand	Coarse Silt
Poorly Sorted	Very Poorly Sorted	Poorly Sorted	Very Poorly Sorted
Fine Skewed	Fine Skewed	Fine Skewed	Very Fine Skewed
Leptokurtic	Leptokurtic	Leptokurtic	Mesokurtic
275.0	115.0	325.0	40.50
1.868	3.126	1.626	4.631
36.59	17.12	34.54	2.079
247.3	137.8	287.2	26.67
1099.2	726.5	1063.5	98.95
30.04	42.43	30.79	47.59
1062.6	709.4	1029.0	96.87
5.394	5.469	4.432	6.466
462.0	268.8	445.9	45.72
-0.136	0.461	-0.089	3.337
2.016	2.859	1.800	5.228
4.772	5.868	4.856	8.910
-34.968	12.73	-54.665	2.670
4.909	5.407	4.945	5.573
3.972	2.528	3.698	1.640
2.431	2.451	2.148	2.693
1.8%	1.9%	3.7%	0.2%
83.1%	72.3%	82.2%	20.1%
15.1%	25.8%	14.1%	79.7%
0.0%	0.0%	0.0%	0.0%
0.0%	0.0%	0.0%	0.0%
0.0%	0.0%	0.0%	0.0%
0.0%	0.0%	0.0%	0.0%
1.8%	1.9%	3.7%	0.2%
9.9%	3.7%	7.3%	0.0%
16.8%	10.7%	18.6%	0.0%
21.2%	15.5%	25.5%	1.5%
20.9%	21.4%	20.8%	5.2%
14.3%	20.9%	10.0%	13.3%
6.0%	11.2%	4.7%	25.2%
3.0%	5.4%	3.2%	19.6%
2.2%	3.6%	2.4%	11.0%
1.7%	2.5%	1.8%	7.6%
1.2%	1.7%	1.1%	6.9%
1.0%	1.4%	1.0%	9.4%

Figure 4.46. Ferrybank GRADISTAT Grainsize Analysis (16/22).

FB_30.00mbgl	FB_30.50mbgl	FB_31.00mbgl	FB_31.50mbgl
, 3/5/2025 12:00:21 PM	, 3/5/2025 12:07:44 PM	, 3/5/2025 12:15:14 PM	, 3/5/2025 12:24:06 PM
175°17'12.32" E 37°47'20.83" S	175°17'12.32" E 37°47'20.83" S	175°17'12.32" E 37°47'20.83" S	175°17'12.32" E 37°47'20.83" S
0.0%	0.0%	0.0%	0.0%
Bimodal, Very Poorly Sorted	Bimodal, Very Poorly Sorted	Trimodal, Very Poorly Sorted	Trimodal, Very Poorly Sorted
Slightly Gravelly Muddy Sand	Slightly Gravelly Muddy Sand	Muddy Sandy Gravel	Muddy Sandy Gravel
Fine Gravelly Very Coarse Silty Very	Fine Gravelly Very Coarse Silty Cry	Coarse Silty Sandy Very Fine Gra	y Coarse Silty Sandy Very Fine Gra
88.08	113.1	305.2	410.6
5.209	6.075	7.229	5.398
-0.050	-0.002	-0.583	-0.562
1.024	0.903	0.572	0.592
3.505	3.144	1.712	1.284
2.381	2.603	2.854	2.432
0.050	0.002	0.583	0.562
1.024	0.903	0.572	0.592
Very Fine Sand	Very Fine Sand	Medium Sand	Medium Sand
Very Poorly Sorted	Very Poorly Sorted	Very Poorly Sorted	Very Poorly Sorted
Symmetrical	Symmetrical	Very Fine Skewed	Very Fine Skewed
Mesokurtic	Mesokurtic	Very Platykurtic	Very Platykurtic
48.50	48.50	3000.0	460.0
4.372	4.372	-1.500	1.126
9.001	10.15	11.53	25.86
83.05	98.48	580.8	664.3
627.6	996.0	34434.6	22399.7
69.73	98.13	2985.5	866.1
618.6	985.8	34423.1	22373.9
9.272	14.43	60.56	30.36
268.4	461.5	2996.8	3107.1
0.672	0.006	-5.106	-4.485
3.590	3.344	0.784	0.590
6.796	6.622	6.438	5.273
10.11	1134.9	-1.261	-1.176
6.124	6.617	11.54	9.758
2.854	4.805	-2.683	-1.924
3.213	3.851	5.920	4.924
0.1%	0.2%	41.9%	41.4%
57.2%	59.3%	30.2%	39.7%
42.8%	40.5%	27.9%	18.9%
0.0%	0.0%	0.0%	0.0%
0.0%	0.0%	0.0%	0.0%
0.0%	0.0%	0.0%	0.0%
0.0%	0.0%	0.0%	0.0%
0.1%	0.2%	41.9%	41.4%
3.2%	9.7%	2.2%	3.5%
10.8%	14.9%	7.9%	10.1%
15.0%	12.4%	8.2%	12.1%
12.8%	9.2%	4.9%	6.4%
15.3%	13.1%	7.0%	7.6%
18.7%	17.7%	9.2%	7.7%
10.2%	10.0%	6.9%	4.3%
4.9%	4.6%	4.0%	2.5%
3.3%	3.1%	2.9%	1.7%
2.9%	2.6%	2.3%	1.4%
2.8%	2.6%	2.5%	1.3%

Figure 4.47. Ferrybank GRADISTAT Grainsize Analysis (17/22).

FB_32.00mbgl	FB_32.50mbgl	FB_33.00mbgl	FB_33.50mbgl
, 3/5/2025 12:32:08 PM	, 3/5/2025 12:39:51 PM	, 3/5/2025 12:47:38 PM	, 3/6/2025 12:56:12 PM
175°17'12.32" E 37°47'20.83" S	175°17'12.32" E 37°47'20.83" S	175°17'12.32" E 37°47'20.83" S	175°17'12.32" E 37°47'20.83" S
0.0%	0.0%	0.0%	0.0%
Trimodal, Very Poorly Sorted	Trimodal, Poorly Sorted	Bimodal, Very Poorly Sorted	Bimodal, Very Poorly Sorted
Muddy Sandy Gravel	Muddy Sandy Gravel	Muddy Sandy Gravel	Gravelly Muddy Sand
ry Coarse Silty Sandy Very Fine Gra	ry Coarse Silty Sandy Very Fine Gra	ry Coarse Silty Sandy Very Fine Grai	ne Gravelly Very Coarse Silty Mediu
369.1	976.9	404.2	314.3
5.275	2.886	5.312	7.703
-0.409	-1.707	-0.708	-0.213
0.591	1.035	0.694	0.796
1.438	0.034	1.307	1.670
2.399	1.529	2.409	2.945
0.409	1.707	0.708	0.213
0.591	1.035	0.694	0.796
Medium Sand	Coarse Sand	Medium Sand	Medium Sand
Very Poorly Sorted	Poorly Sorted	Very Poorly Sorted	Very Poorly Sorted
Very Fine Skewed	Very Fine Skewed	Very Fine Skewed	Fine Skewed
Very Platykurtic	Mesokurtic	Platykurtic	Platykurtic
385.0	460.0	325.0	545.0
1.383	1.126	1.626	0.881
26.64	70.75	20.98	14.83
481.4	3386.8	806.1	315.3
24317.7	1395790.6	110339.4	5730.8
912.7	19728.9	5260.4	386.4
24291.1	1395719.9	110318.4	5716.0
28.77	4.125	19.63	18.47
3010.8	1394.2	2282.6	1093.3
-4.604	-10.447	-6.786	-2.519
1.055	-1.760	0.311	1.665
5.230	3.821	5.575	6.075
-1.136	-0.366	-0.822	-2.412
9.834	14.27	12.36	8.594
-1.953	-1.323	-2.392	-19.127
4.846	2.045	4.295	4.207
37.1%	63.6%	46.7%	20.2%
44.3%	27.4%	34.7%	54.9%
18.6%	9.1%	18.6%	25.0%
0.0%	0.0%	0.0%	0.0%
0.0%	0.0%	0.0%	0.0%
0.0%	0.0%	0.0%	0.0%
0.0%	0.0%	0.0%	0.0%
37.1%	63.6%	46.7%	20.2%
2.2%	2.5%	1.6%	6.8%
9.9%	7.4%	7.4%	13.6%
15.1%	8.4%	10.6%	13.7%
9.3%	4.4%	8.5%	11.0%
7.9%	4.7%	6.6%	9.7%
7.6%	4.1%	5.9%	8.4%
4.4%	1.9%	4.6%	6.2%
2.5%	1.1%	3.0%	4.0%
1.7%	0.8%	2.1%	2.6%
1.3%	0.6%	1.5%	1.7%
1.2%	0.5%	1.5%	1.9%

Figure 4.48. Ferrybank GRADISTAT Grainsize Analysis (18/22).

FB_34.00mbgl	FB_34.50mbgl	FB_35.00mbgl	FB_35.50mbgl
, 3/6/2025 1:05:10 PM	, 3/6/2025 1:12:36 PM	, 3/6/2025 1:20:06 PM	, 3/6/2025 1:27:45 PM
175°17'12.32" E 37°47'20.83" S	175°17'12.32" E 37°47'20.83" S	175°17'12.32" E 37°47'20.83" S	175°17'12.32" E 37°47'20.83" S
0.0%	0.0%	0.0%	0.0%
Unimodal, Very Poorly Sorted	Unimodal, Poorly Sorted	Unimodal, Very Poorly Sorted	Unimodal, Poorly Sorted
Slightly Gravelly Sandy Mud	Sandy Mud	Sandy Mud	Mud
Fine Gravelly Very Fine Sandy Very	Very Fine Sandy Very Coarse Silt	Very Fine Sandy Very Coarse Silt	Coarse Silt
43.34	25.88	45.33	21.24
5.630	3.135	4.071	2.653
-0.045	-0.263	-0.324	-0.235
1.324	1.112	1.066	1.215
4.528	5.272	4.464	5.557
2.493	1.649	2.026	1.408
0.045	0.263	0.324	0.235
1.324	1.112	1.066	1.215
Very Coarse Silt	Coarse Silt	Very Coarse Silt	Coarse Silt
Very Poorly Sorted	Poorly Sorted	Very Poorly Sorted	Poorly Sorted
Symmetrical	Fine Skewed	Very Fine Skewed	Fine Skewed
Leptokurtic	Leptokurtic	Mesokurtic	Leptokurtic
48.50	40.50	81.00	34.00
4.372	4.631	3.631	4.884
4.131	4.586	5.226	4.918
44.73	30.13	59.47	23.33
379.7	88.34	202.9	60.14
91.91	19.26	38.82	12.23
375.6	83.75	197.6	55.22
6.763	4.260	6.033	3.259
98.02	42.57	99.26	27.37
1.397	3.501	2.301	4.056
4.482	5.053	4.072	5.422
7.919	7.769	7.580	7.668
5.669	2.219	3.294	1.891
6.522	4.268	5.279	3.612
1.884	1.502	1.844	1.366
2.758	2.091	2.593	1.705
0.6%	0.0%	0.0%	0.0%
39.2%	20.6%	48.4%	9.0%
60.2%	79.4%	51.6%	91.0%
0.0%	0.0%	0.0%	0.0%
0.0%	0.0%	0.0%	0.0%
0.0%	0.0%	0.0%	0.0%
0.0%	0.0%	0.0%	0.0%
0.6%	0.0%	0.0%	0.0%
3.2%	0.0%	0.0%	0.0%
4.1%	0.0%	0.1%	0.0%
6.0%	0.2%	5.9%	0.3%
9.5%	3.6%	17.2%	1.3%
16.4%	16.8%	25.1%	7.4%
21.2%	28.2%	19.1%	27.3%
16.0%	22.9%	11.3%	32.6%
8.4%	12.9%	7.8%	16.6%
5.0%	7.1%	5.9%	6.7%
4.0%	4.2%	3.9%	3.7%
5.5%	4.2%	3.6%	4.0%

Figure 4.49. Ferrybank GRADISTAT Grainsize Analysis (19/22).

FB_36.00mbgl	FB_36.50mbgl	FB_37.00mbgl	FB_37.50mbgl
, 3/6/2025 1:35:14 PM	, 3/6/2025 1:43:18 PM	, 3/6/2025 1:52:50 PM	, 3/6/2025 2:00:30 PM
175°17'12.32" E 37°47'20.83" S	175°17'12.32" E 37°47'20.83" S	175°17'12.32" E 37°47'20.83" S	175°17'12.32" E 37°47'20.83" S
0.0%	0.0%	0.0%	0.0%
Unimodal, Poorly Sorted	Unimodal, Poorly Sorted	Bimodal, Very Poorly Sorted	Unimodal, Poorly Sorted
Sandy Mud	Sandy Mud	Slightly Gravelly Muddy Sand	Sandy Mud
Very Fine Sandy Very Coarse Silt	Very Fine Sandy Very Coarse Silt	Fine Gravelly Very Coarse Silty Very	Very Fine Sandy Very Coarse Silt
36.80	50.18	202.6	52.44
3.375	2.420	5.498	2.625
-0.177	-0.283	-0.095	-0.357
1.113	1.310	0.786	1.359
4.764	4.317	2.303	4.253
1.755	1.275	2.459	1.392
0.177	0.283	0.095	0.357
1.113	1.310	0.786	1.359
Very Coarse Silt	Very Coarse Silt	Fine Sand	Very Coarse Silt
Poorly Sorted	Poorly Sorted	Very Poorly Sorted	Poorly Sorted
Fine Skewed	Fine Skewed	Symmetrical	Very Fine Skewed
Leptokurtic	Leptokurtic	Platykurtic	Leptokurtic
40.50	68.50	1300.0	81.00
4.631	3.872	-0.373	3.631
6.634	14.97	18.11	11.63
40.39	56.10	203.4	61.85
147.6	125.2	1482.8	136.5
22.25	8.365	81.90	11.73
141.0	110.3	1464.7	124.9
4.617	2.691	15.54	2.844
64.54	55.08	873.3	62.59
2.760	2.997	-0.568	2.873
4.630	4.156	2.297	4.015
7.236	6.062	5.787	6.426
2.622	2.022	-10.184	2.237
4.476	3.064	6.356	3.553
1.613	1.407	40.76	1.447
2.207	1.428	3.958	1.508
0.0%	0.0%	0.7%	0.0%
34.1%	43.9%	73.6%	49.4%
65.9%	56.1%	25.7%	50.6%
0.0%	0.0%	0.0%	0.0%
0.0%	0.0%	0.0%	0.0%
0.0%	0.0%	0.0%	0.0%
0.0%	0.0%	0.0%	0.0%
0.0%	0.0%	0.7%	0.0%
0.0%	0.0%	22.3%	0.0%
0.0%	0.0%	15.2%	0.0%
2.2%	0.5%	8.6%	0.4%
11.4%	9.5%	12.6%	12.4%
20.5%	33.8%	14.8%	36.6%
25.2%	32.6%	10.4%	27.8%
19.4%	13.2%	6.8%	10.4%
10.1%	4.7%	4.4%	5.4%
5.2%	2.4%	2.5%	3.2%
3.1%	1.5%	1.2%	1.9%
3.0%	1.7%	0.5%	1.8%

Figure 4.50. Ferrybank GRADISTAT Grainsize Analysis (20/22).

FB_38.00mbgl	FB_38.50mbgl	FB_39.00mbgl	FB_39.50mbgl
, 3/6/2025 2:08:15 PM	, 3/6/2025 3:13:56 PM	, 3/6/2025 3:24:18 PM	, 3/6/2025 3:31:41 PM
175°17'12.32" E 37°47'20.83" S	175°17'12.32" E 37°47'20.83" S	175°17'12.32" E 37°47'20.83" S	175°17'12.32" E 37°47'20.83" S
0.0%	0.0%	0.0%	0.0%
Unimodal, Poorly Sorted	Unimodal, Poorly Sorted	Unimodal, Poorly Sorted	Unimodal, Poorly Sorted
Muddy Sand	Slightly Gravelly Muddy Sand	Muddy Sand	Slightly Gravelly Muddy Sand
Very Coarse Silty Fine Sand	ery Fine Gravelly Very Coarse Silty F	Very Coarse Silty Fine Sand	ery Fine Gravelly Very Coarse Silty F
129.2	181.9	101.0	141.0
2.634	2.828	2.932	3.079
-0.327	-0.218	-0.402	-0.300
1.440	1.523	1.400	1.412
2.953	2.459	3.307	2.827
1.397	1.500	1.552	1.622
0.327	0.218	0.402	0.300
1.440	1.523	1.400	1.412
Fine Sand	Fine Sand	Very Fine Sand	Fine Sand
Poorly Sorted	Poorly Sorted	Poorly Sorted	Poorly Sorted
Very Fine Skewed	Fine Skewed	Very Fine Skewed	Fine Skewed
Leptokurtic	Very Leptokurtic	Leptokurtic	Leptokurtic
163.0	193.5	163.0	193.5
2.622	2.375	2.622	2.375
27.71	42.17	17.13	23.43
145.1	192.7	124.1	161.8
328.8	522.6	282.7	440.4
11.86	12.39	16.50	18.80
301.1	480.4	265.6	417.0
2.829	2.981	3.127	3.356
148.4	214.9	134.9	195.1
1.605	0.936	1.822	1.183
2.785	2.376	3.011	2.627
5.173	4.568	5.867	5.415
3.224	4.879	3.219	4.577
3.569	3.632	4.045	4.232
1.706	1.967	1.705	1.945
1.500	1.576	1.645	1.747
0.0%	3.3%	0.0%	0.1%
81.3%	83.4%	75.3%	80.7%
18.7%	13.2%	24.7%	19.2%
0.0%	0.0%	0.0%	0.0%
0.0%	0.0%	0.0%	0.0%
0.0%	0.0%	0.0%	0.0%
0.0%	0.0%	0.0%	0.0%
0.0%	3.3%	0.0%	0.1%
0.0%	0.2%	0.0%	0.7%
1.7%	7.4%	0.1%	6.5%
18.9%	25.9%	14.2%	22.2%
37.2%	33.3%	35.3%	32.1%
23.5%	16.7%	25.7%	19.2%
7.9%	4.8%	9.7%	7.4%
4.2%	2.8%	5.7%	4.4%
2.7%	2.1%	3.8%	3.0%
1.9%	1.6%	2.6%	2.1%
1.2%	1.1%	1.6%	1.3%
0.8%	0.8%	1.3%	1.0%

Figure 4.51. Ferrybank GRADISTAT Grainsize Analysis (21/22).

FB_40.00mbgl	FB_40.50mbgl	
, 3/6/2025 3:39:13 PM	, 3/6/2025 3:56:30 PM	
175°17'12.32" E 37°47'20.83" S	175°17'12.32" E 37°47'20.83" S	
0.0%	0.0%	
Unimodal, Poorly Sorted	Unimodal, Poorly Sorted	
Slightly Gravelly Muddy Sand	Slightly Gravelly Muddy Sand	
ery Fine Gravelly Very Coarse Silty F	Fine Gravelly Very Coarse Silty Very Fine Sand	
145.8	49.30	
3.154	3.552	
-0.285	-0.337	
1.434	1.082	
2.778	4.342	
1.657	1.829	
0.285	0.337	
1.434	1.082	
Fine Sand	Very Coarse Silt	
Poorly Sorted	Poorly Sorted	
Fine Skewed	Very Fine Skewed	
Leptokurtic	Mesokurtic	
193.5	96.50	
2.375	3.379	
24.05	7.125	
167.6	63.06	
468.1	185.4	
19.46	26.02	
444.0	178.2	
3.394	5.085	
203.5	94.19	
1.095	2.432	
2.577	3.987	
5.378	7.133	
4.910	2.933	
4.282	4.701	
1.983	1.759	
1.763	2.346	
0.2%	0.2%	
80.8%	50.1%	
18.9%	49.7%	
0.0%	0.0%	
0.0%	0.0%	
0.0%	0.0%	
0.0%	0.0%	
0.2%	0.2%	
2.1%	0.0%	
6.2%	0.5%	
22.6%	3.8%	
31.7%	18.0%	
18.3%	27.9%	
7.3%	19.4%	
4.4%	12.0%	
2.9%	7.6%	
2.0%	4.9%	
1.3%	3.0%	
1.0%	2.7%	

Figure 4.52. Ferrybank GRADISTAT Grainsize Analysis (22/22).

Appendix 3. XRD.

- Sample Mineralogy.

Table 4.1. Minerals Present in Samples from Core 20-1006.

ID	Feldspar	Quartz	Cristobalite	Halite	Tridymite	Clay	Augite	Amorphous
1.00	*	*						
2.50	*	*						
3.00	*	*	*					
3.75	*	*	*					
4.00	*	*						
5.00	*	*						
6.00	*	*	*					
7.00	*	*						
9.00	*	*						
9.75	*	*	*					
11.00	*	*	*					
11.35	*	*	*					
12.00	*	*	*					
14.00	*	*						
16.00	*	*						
18.00	*	*						
19.00	*	*	*					
20.95	*	*						
23.00	*	*						
24.00	*	*						
25.00	*							
27.00	*	*						
27.50	*	*						
28.00	*	*						
30.00	*	*						

*Note: An * indicates minerals were present in the sample during analysis. Sample ID's are presented in mbgl.*

Table 4.2. Minerals Present in Samples from Core 21-0437.

ID	Feldspar	Quartz	Cristobalite	Halite	Tridymite	Clay	Augite	Amorphous
1.00	*	*						
2.00	*	*					*	
4.00	*	*						
6.00	*	*						
6.85	*	*						
8.00	*	*						
8.25	*	*						
8.50	*	*	*					
9.00	*	*						
10.00	*	*						
11.50	*	*						
12.00	*	*						
13.00		*				*		
15.00	*	*				*		
16.00			*			*		
18.00	*							
19.00								*
19.50								*

*Note: An * indicates minerals were present in the sample during analysis. Sample ID's are presented in mbgl. Samples that include clay minerals may include Kaolinite and Halloysite.*

Table 4.3. Minerals Present in Samples from Core Ferrybank.

ID	Feldspar	Quartz	Cristobalite	Halite	Tridymite	Clay	Augite	Amorphous
0.10	*	*						
1.00	*	*						
3.00	*	*						
5.00								*
7.00								*
9.00								*
10.50								*
12.00	*	*						
13.00	*	*						
15.00	*	*						
17.00	*	*						
17.50	*	*						
18.50	*	*						
20.00	*	*						
22.00	*	*						
23.50	*	*						
24.00	*	*						
29.00	*	*						
29.50	*	*	*		*			
31.00	*	*	*		*			
33.00	*	*	*		*			
34.00	*							
36.00	*	*						
39.00	*	*						
40.50	*	*						

*Note: An * indicates minerals were present in the sample during analysis. Sample ID's are presented in mbgl.*

- 20-1006.

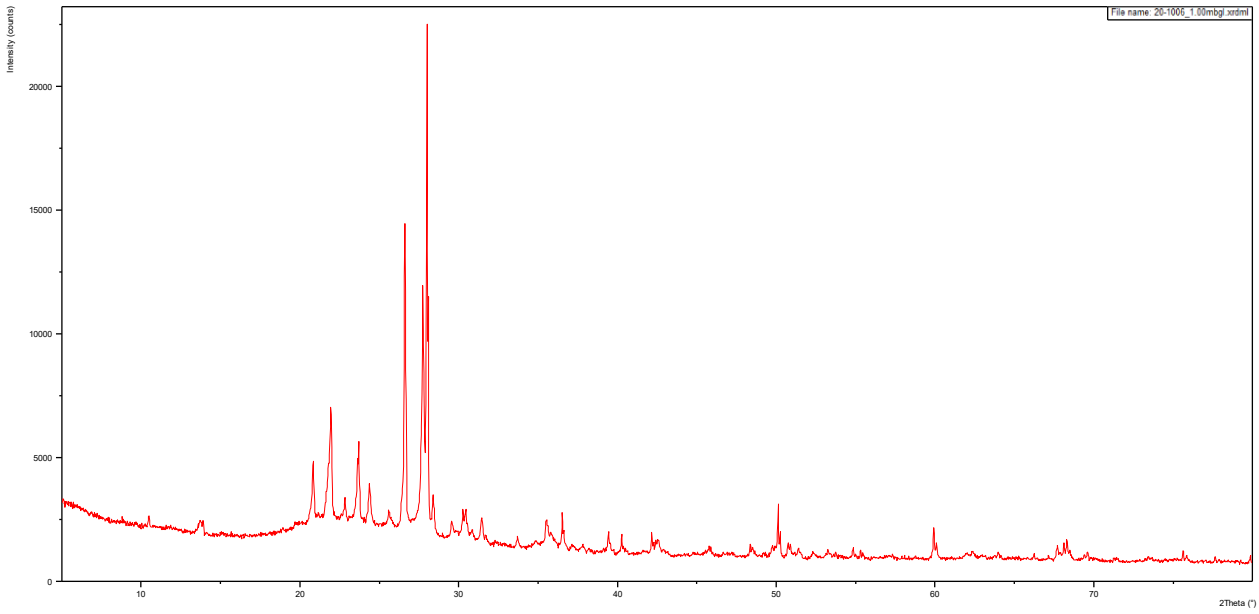

Figure 4.53. 20-1006 1.00mbgl XRD Diffractogram.

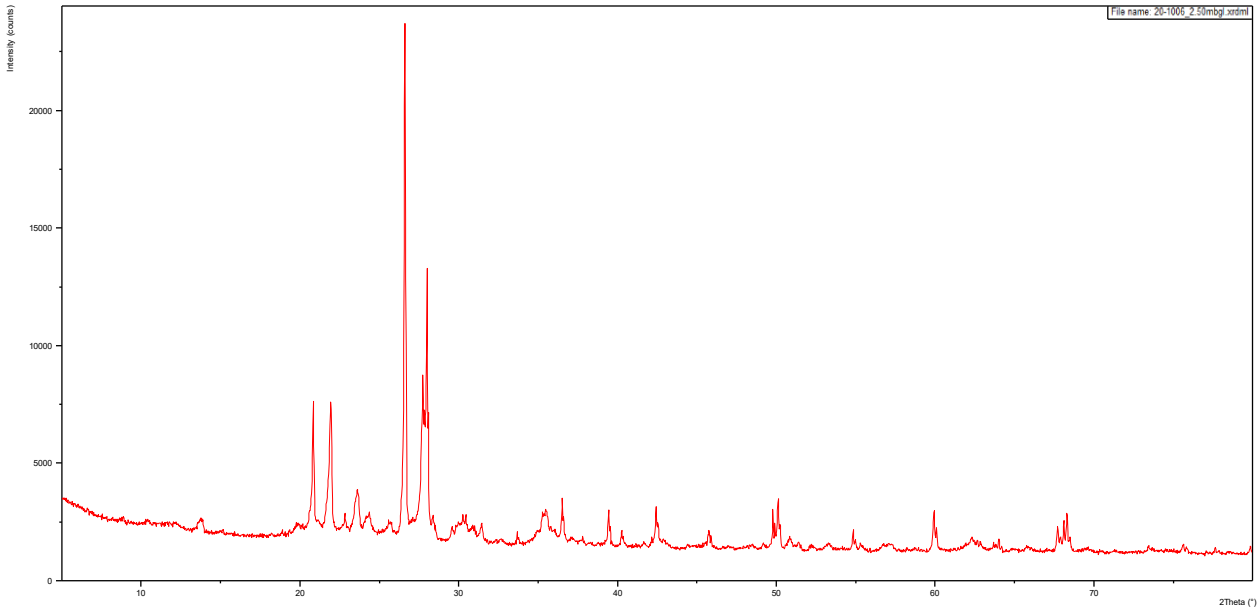

Figure 4.54. 20-1006 2.50mbgl XRD Diffractogram.

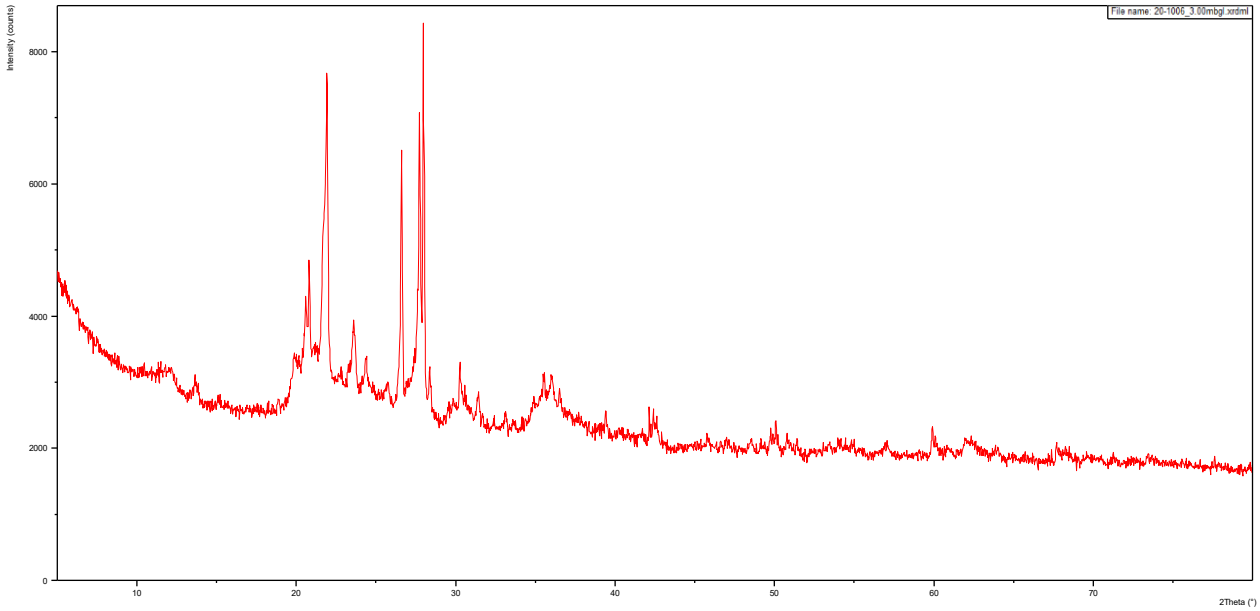

Figure 4.55. 20-1006 3.00mbgl XRD Diffractogram.

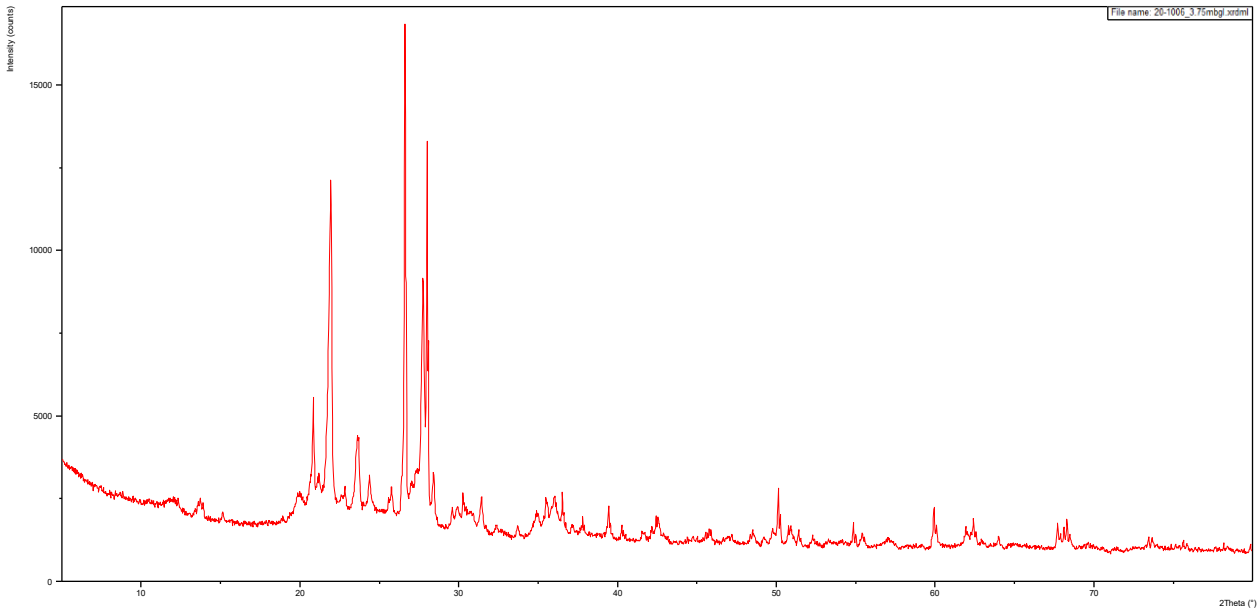

Figure 4.56. 20-1006 3.75mbgl XRD Diffractogram.

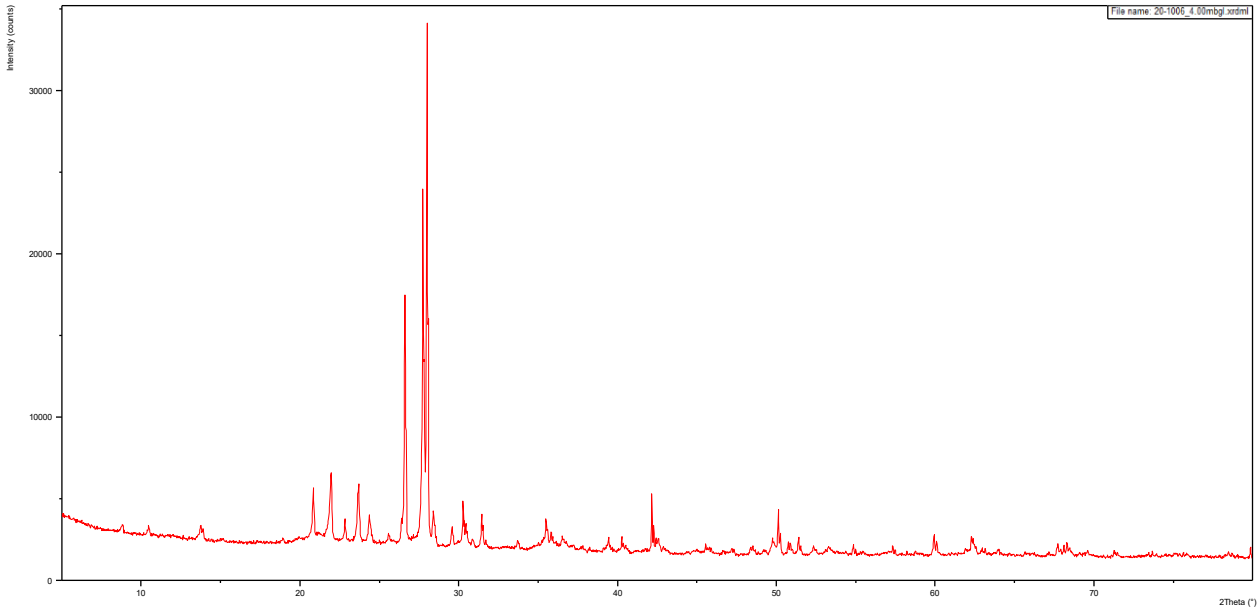

Figure 4.57. 20-1006 4.00mbgl XRD Diffractogram.

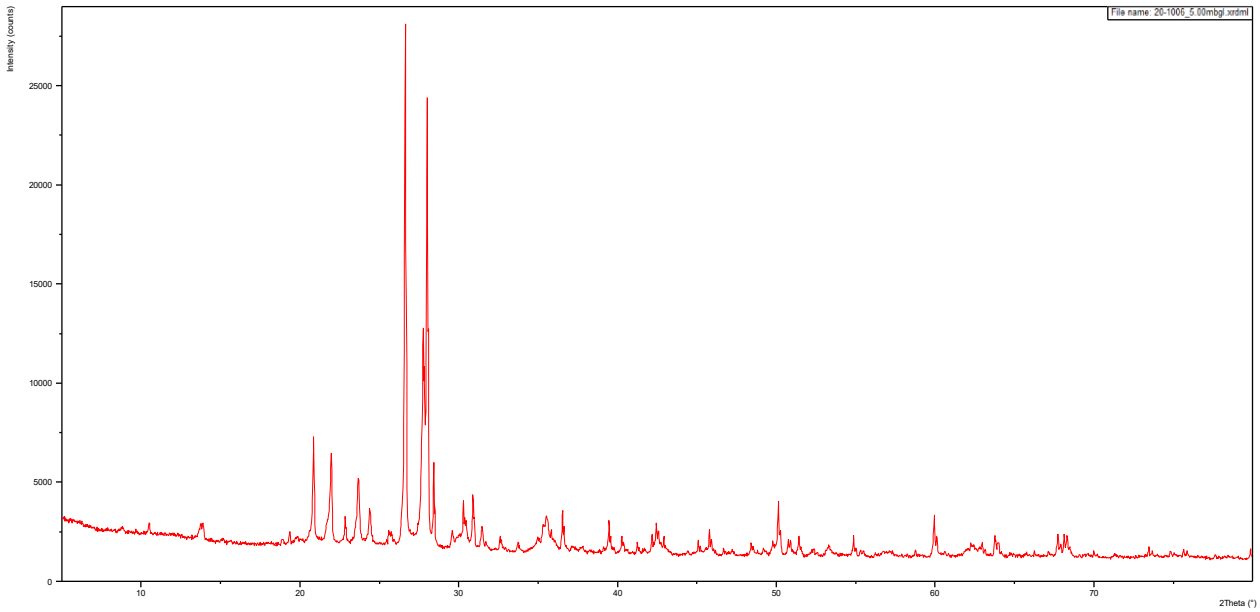

Figure 4.58. 20-1006 5.00mbgl XRD Diffractogram.

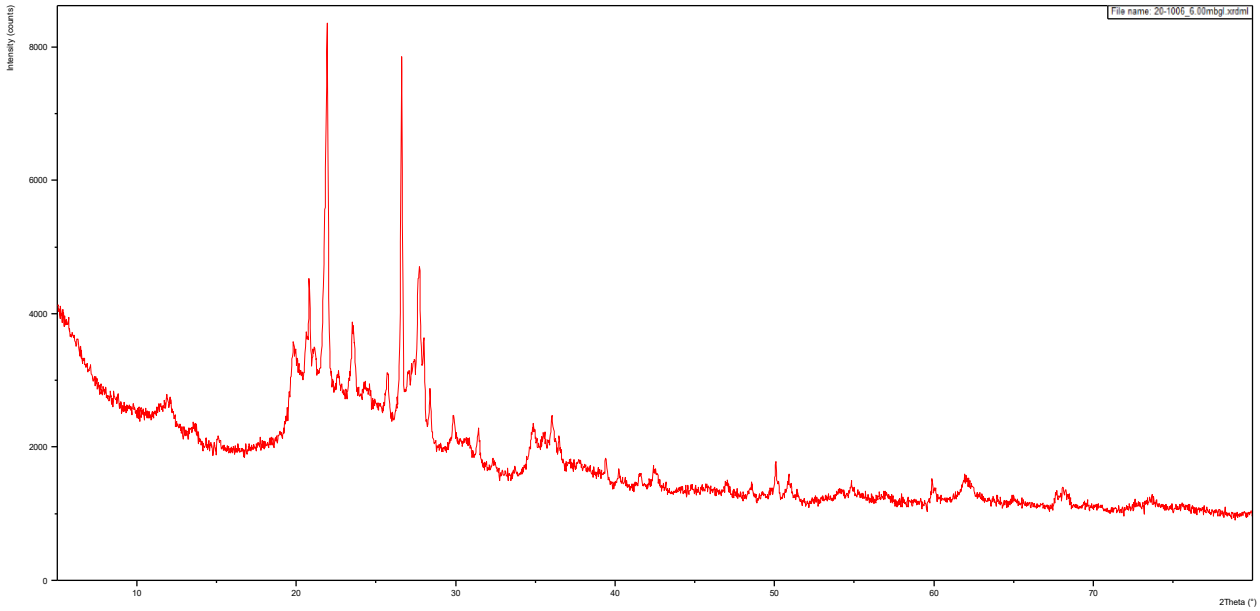

Figure 4.59. 20-1006 6.00mbgl XRD Diffractogram.

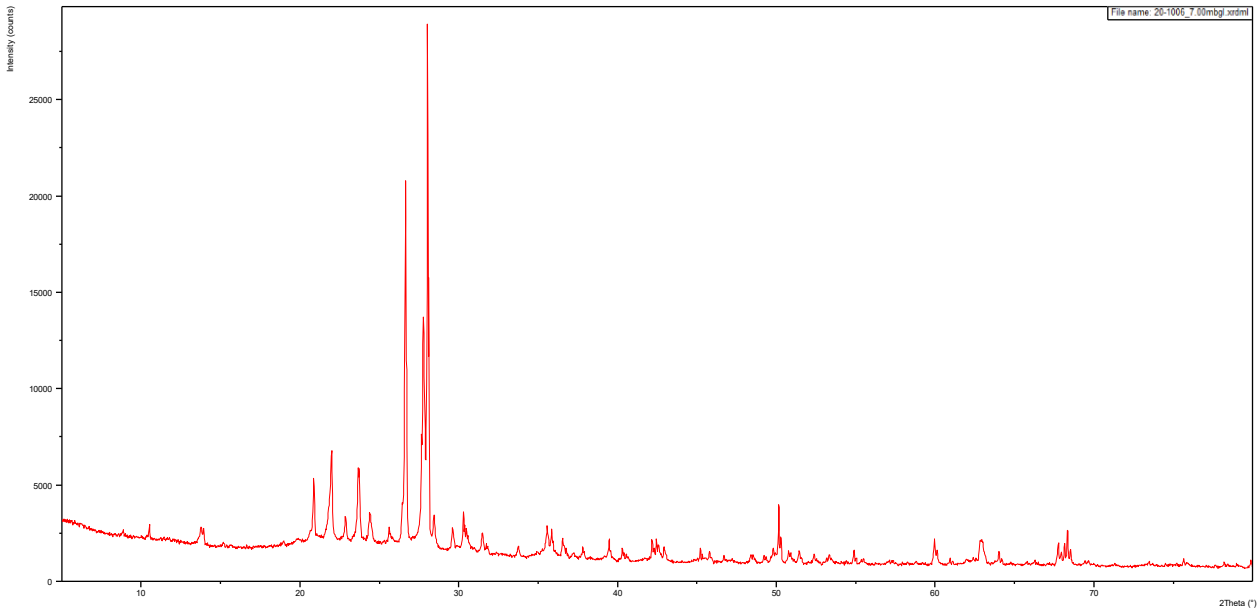

Figure 4.60. 20-1006 7.00mbgl XRD Diffractogram.

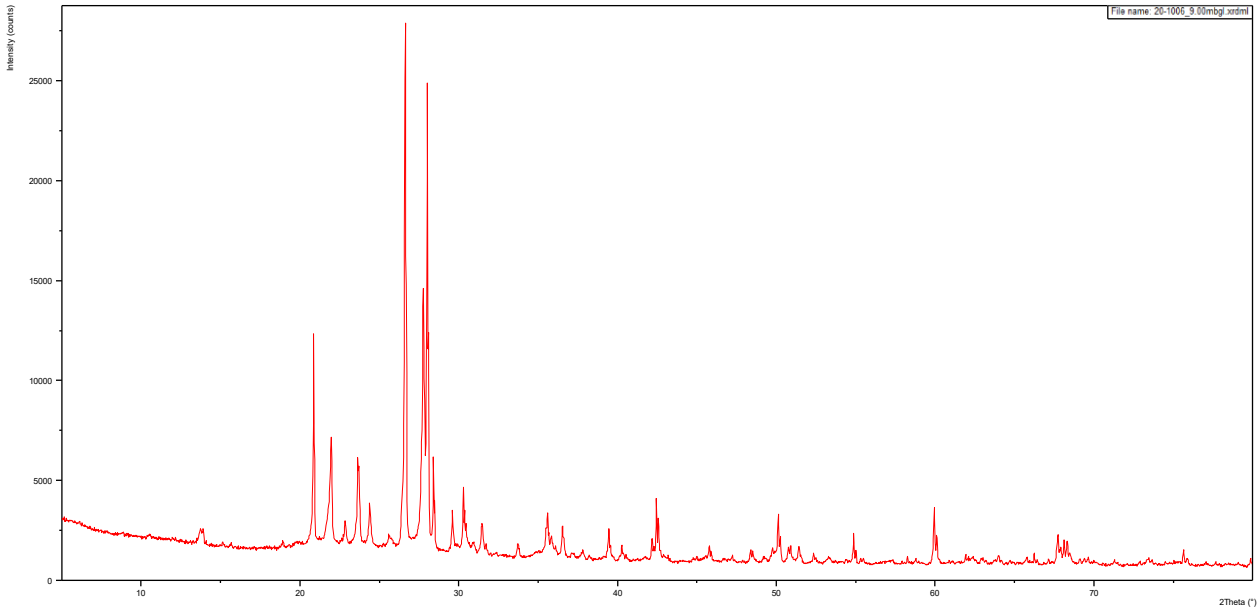

Figure 4.61. 20-1006 9.00mbgl XRD Diffractogram.

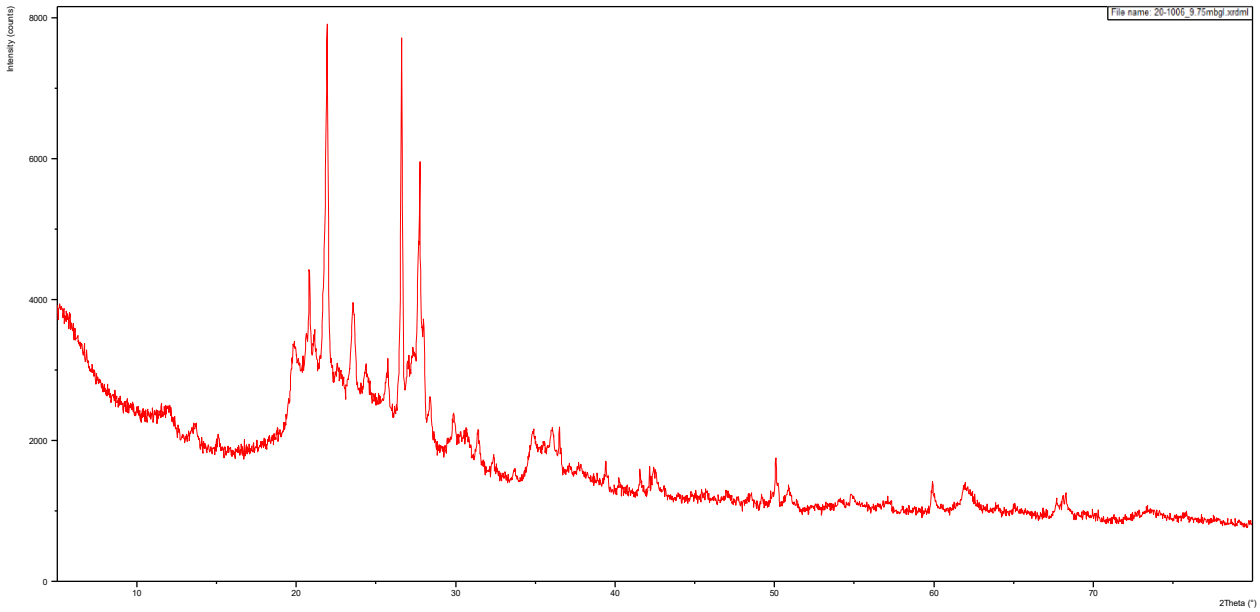

Figure 4.62. 20-1006 9.75mbgl XRD Diffractogram.

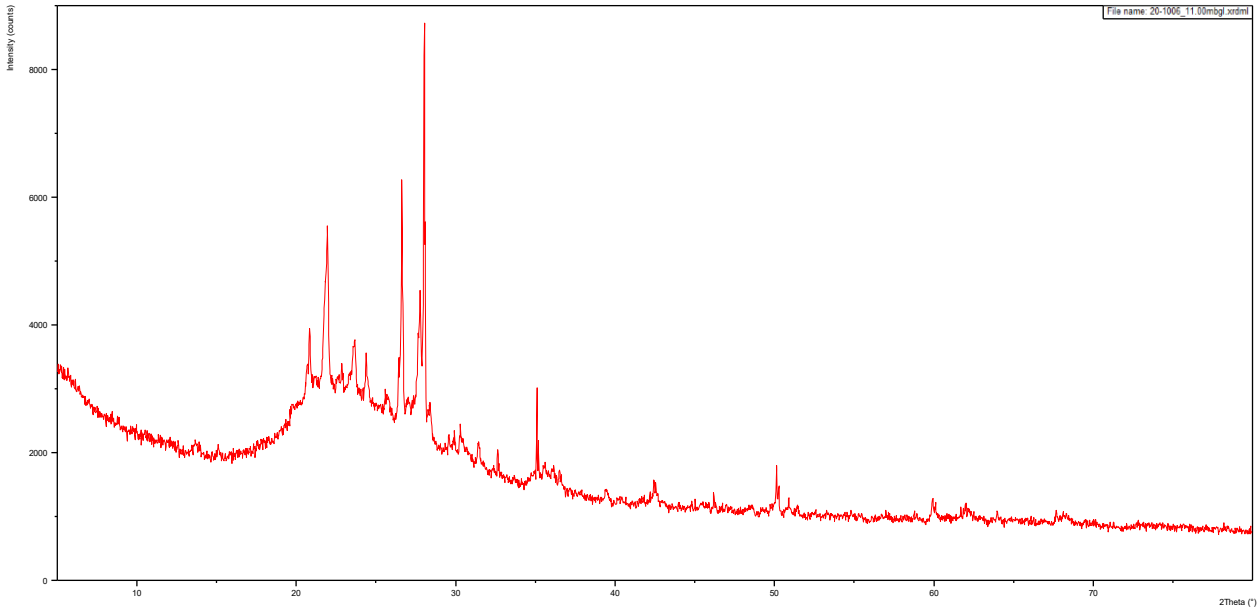

Figure 4.63. 20-1006 11.00mbgl XRD Diffractogram.

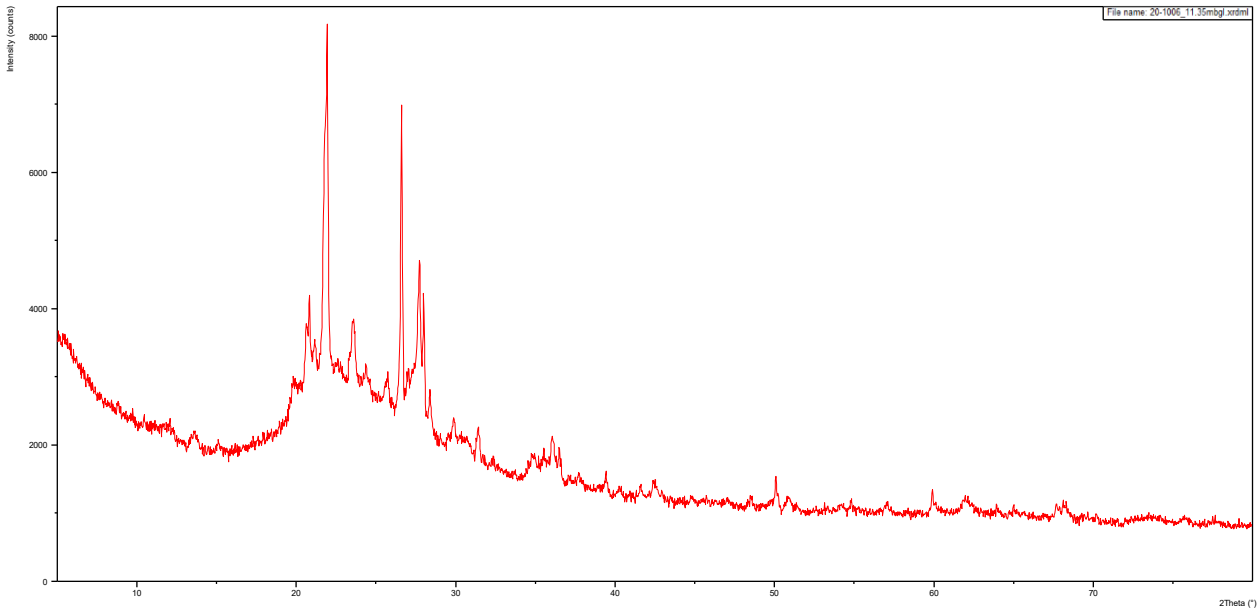

Figure 4.64. 20-1006 11.35mbgl XRD Diffractogram.

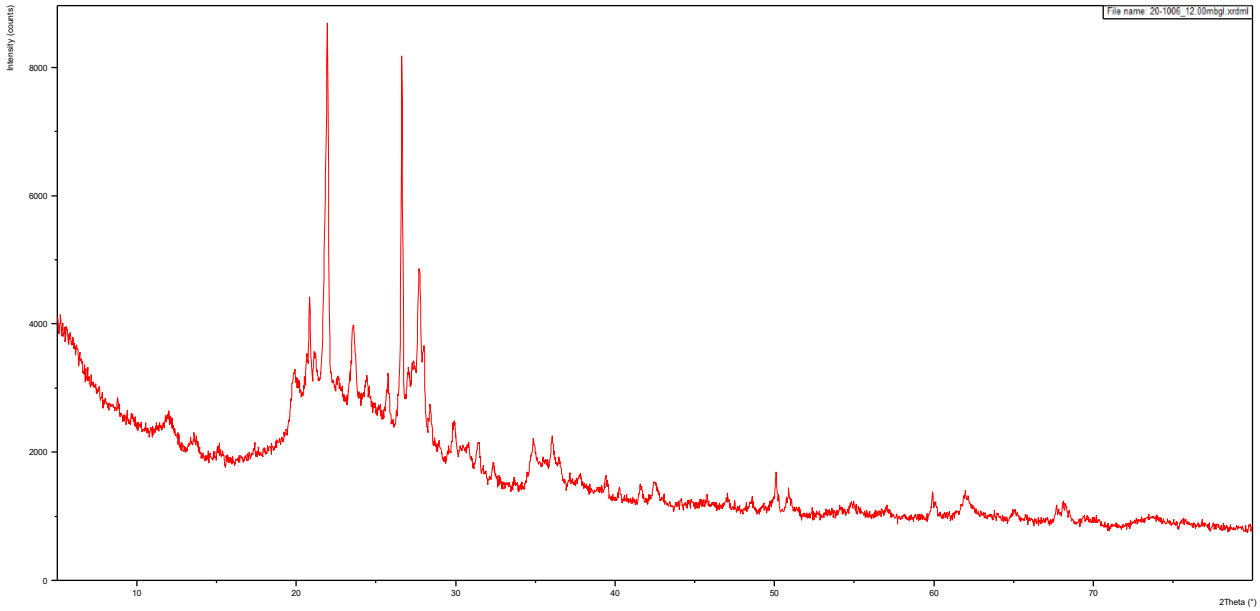

Figure 4.65. 20-1006 12.00mbgl XRD Diffractogram.

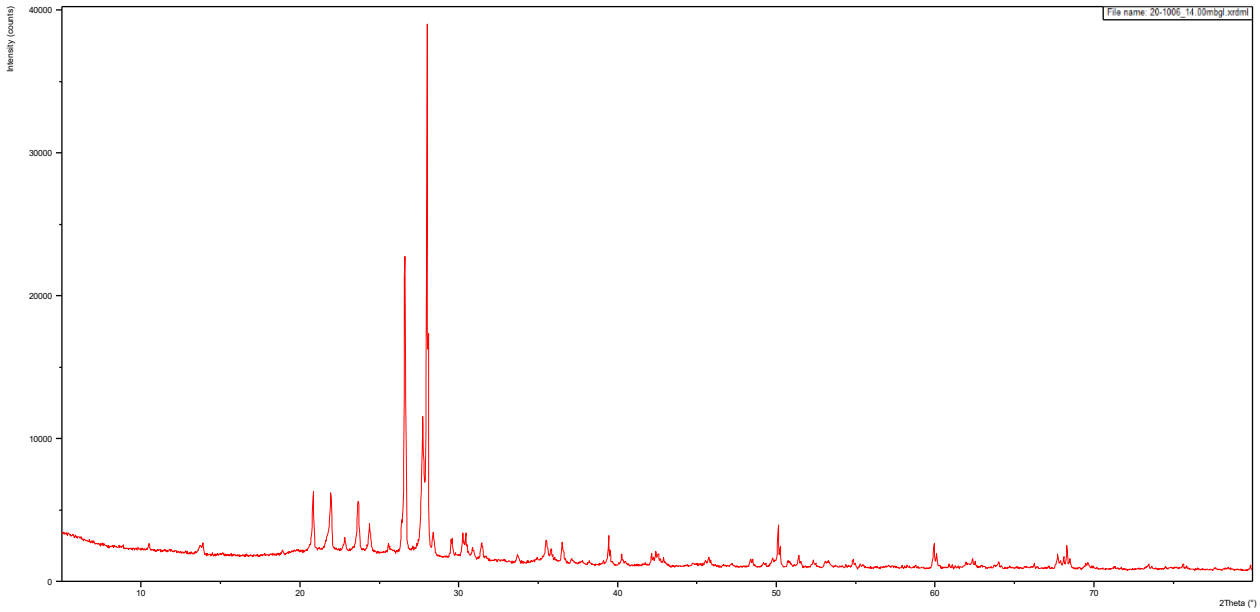

Figure 4.66. 20-1006 14.00mbgl XRD Diffractogram.

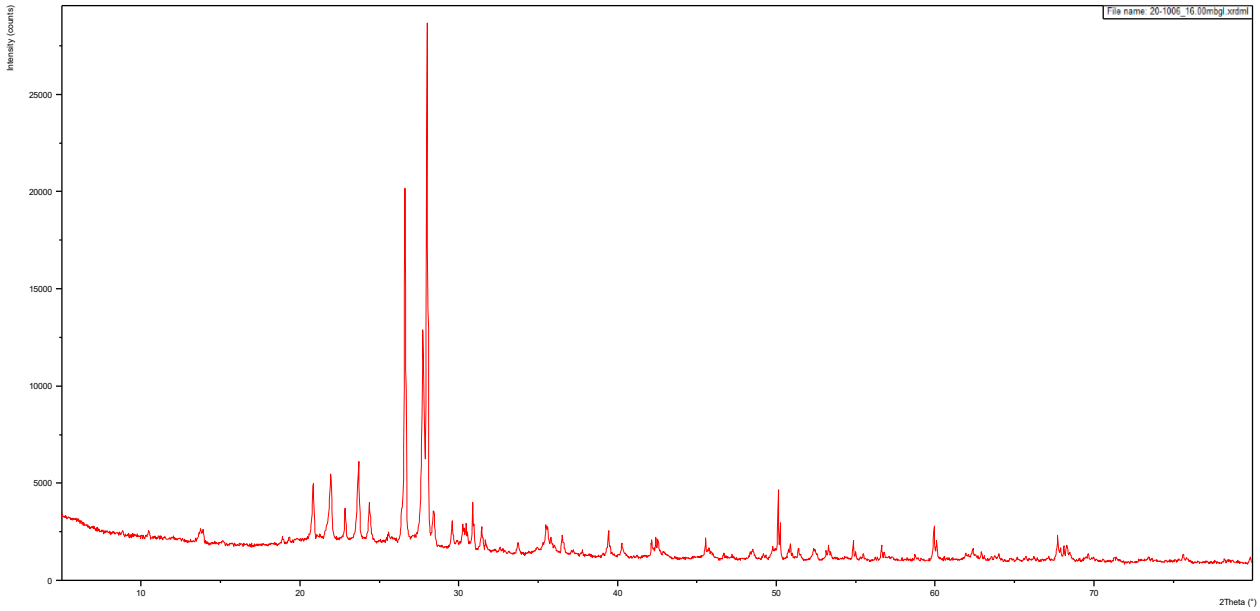

Figure 4.67. 20-1006 16.00mbgl XRD Diffractogram.

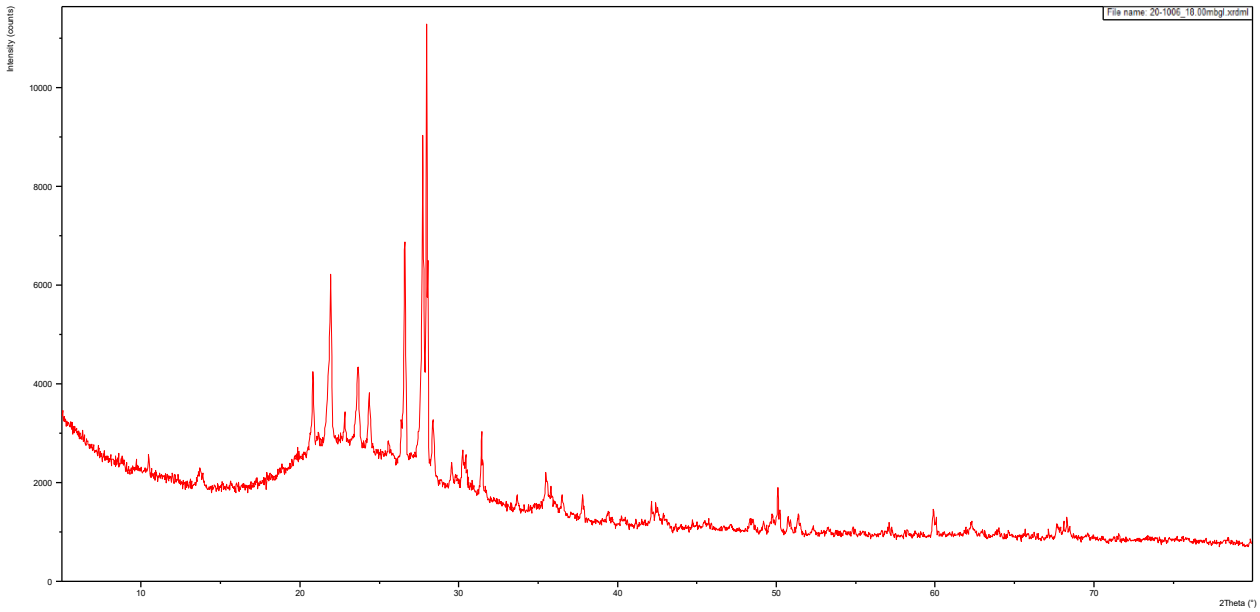

Figure 4.68. 20-1006 18.00mbgl XRD Diffractogram.

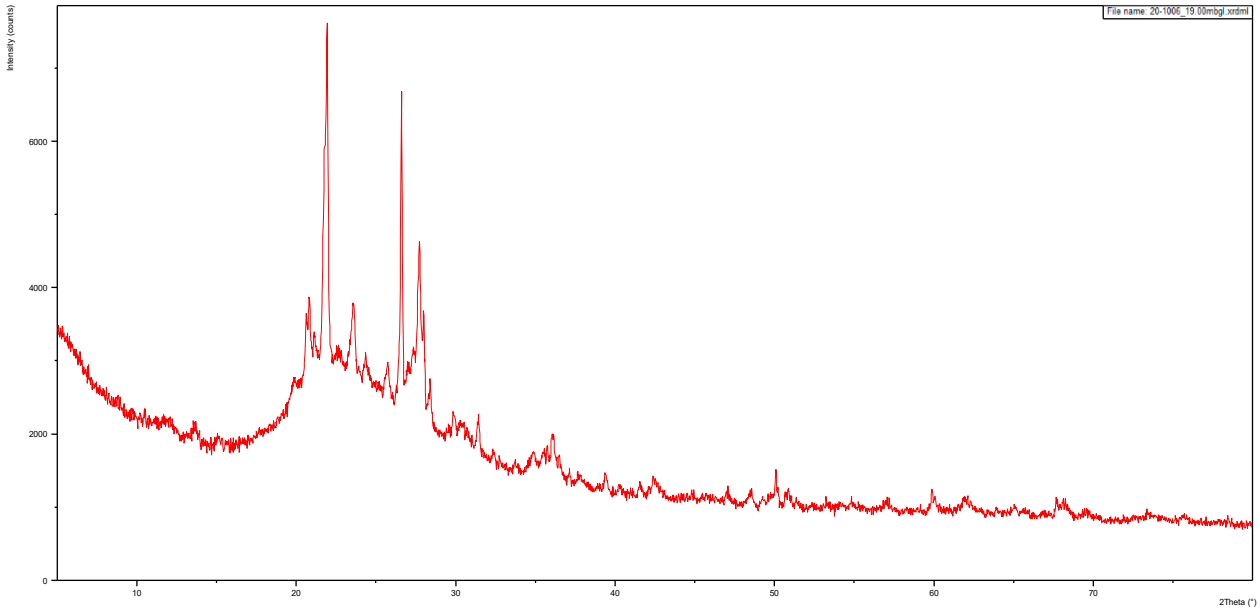

Figure 4.69. 20-1006 19.00mbgl XRD Diffractogram.

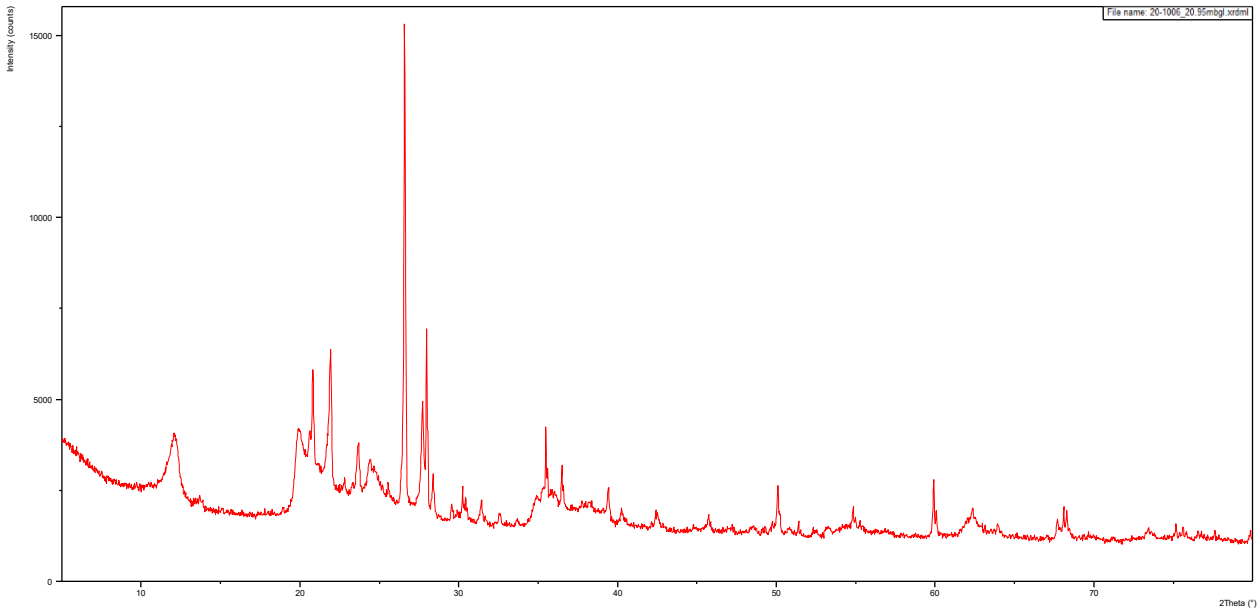

Figure 4.70. 20-1006 20.95mbgl XRD Diffractogram.

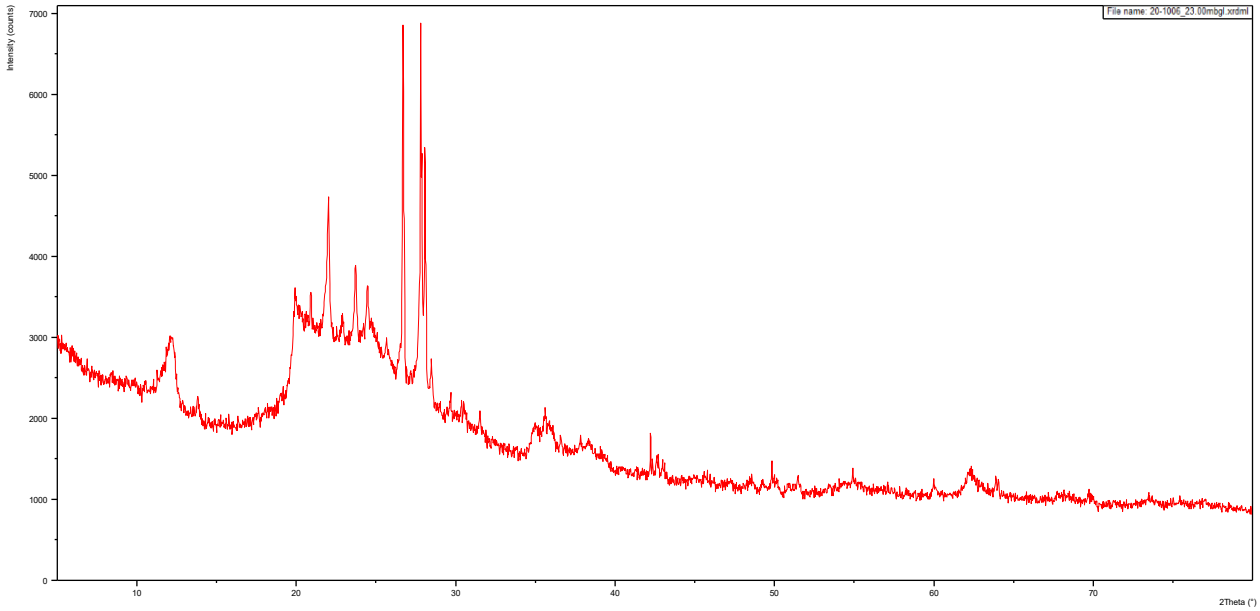

Figure 4.71. 20-1006 23.00mbgl XRD Diffractogram.

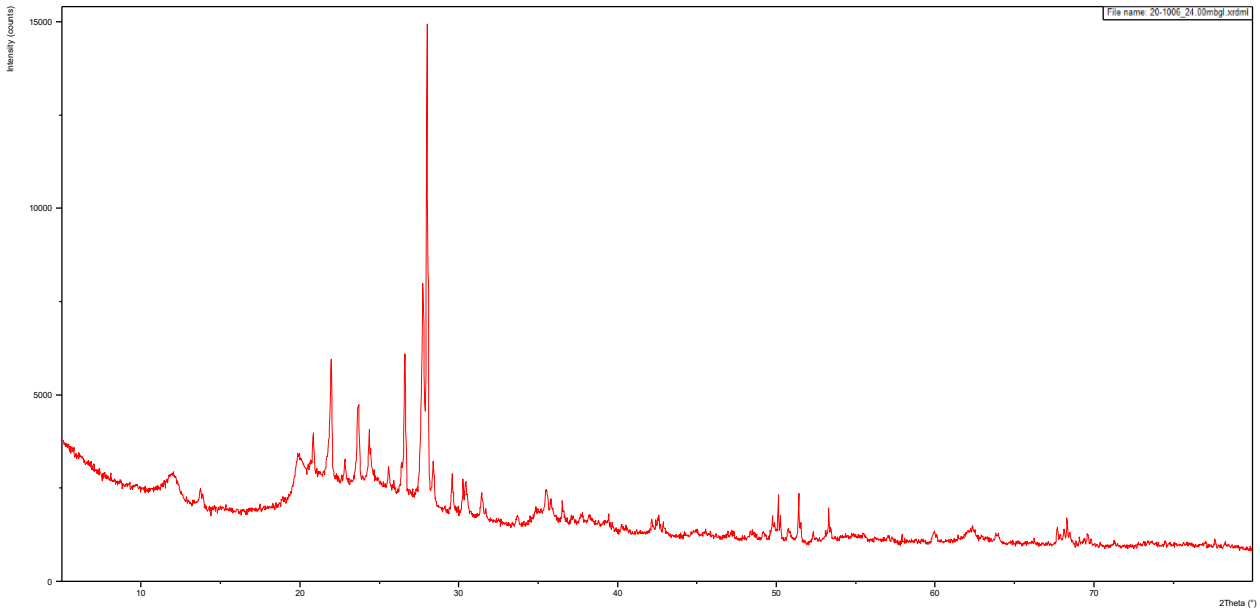

Figure 4.72. 20-1006 24.00mbgl XRD Diffractogram.

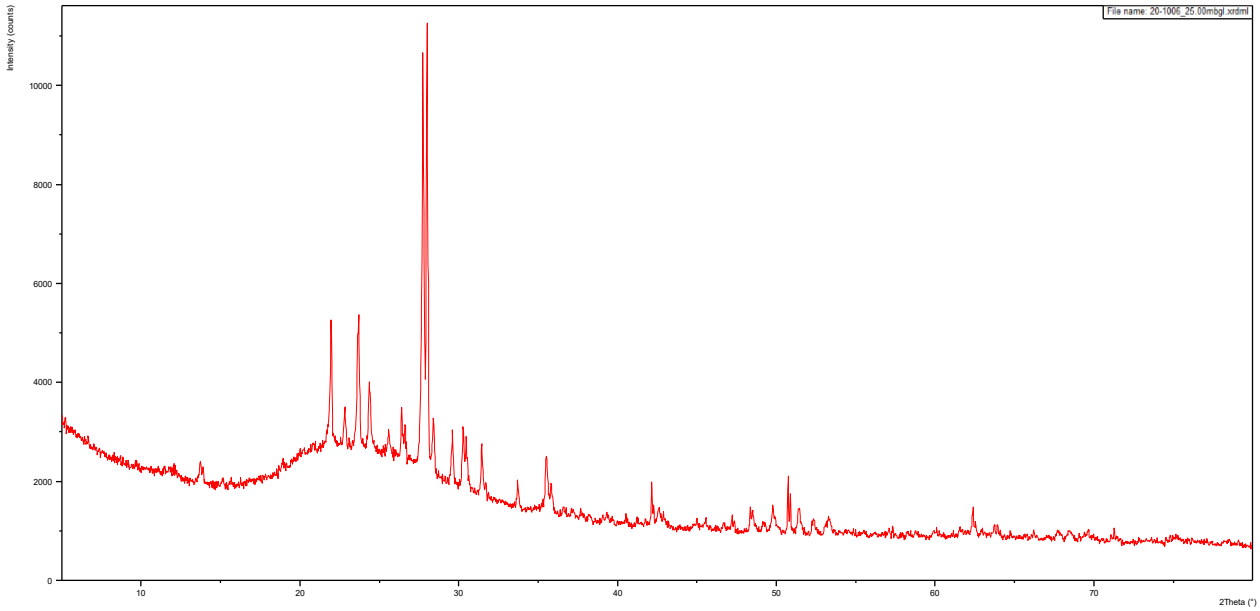

Figure 4.73. 20-1006 25.00mbgl XRD Diffractogram.

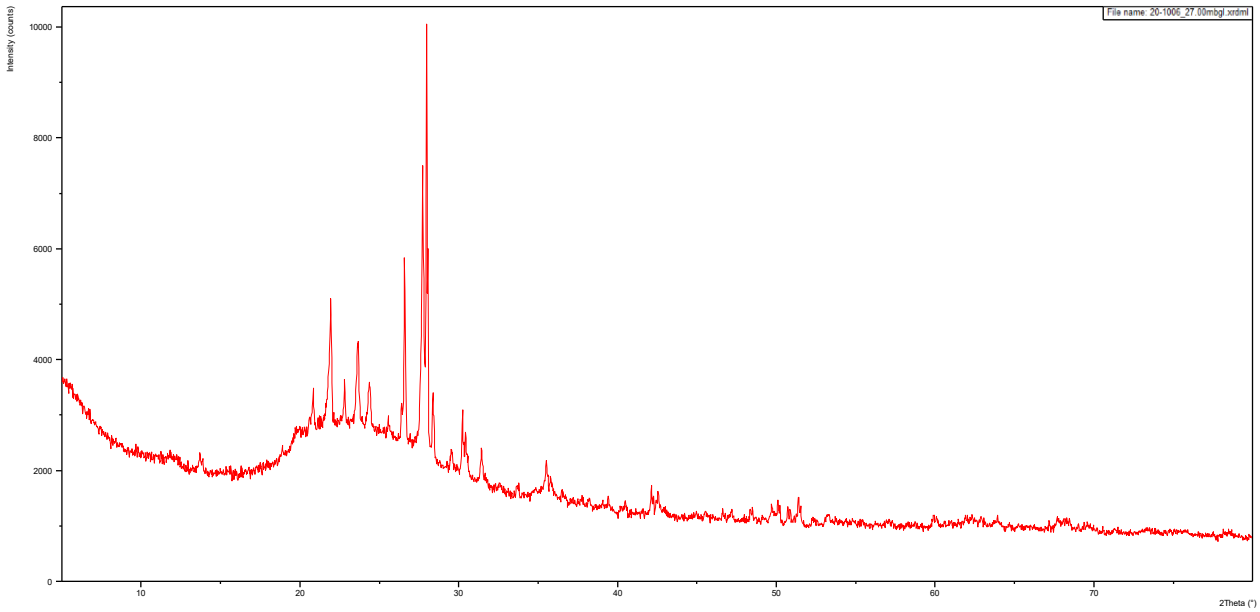

Figure 4.74. 20-1006 27.00mbgl XRD Diffractogram.

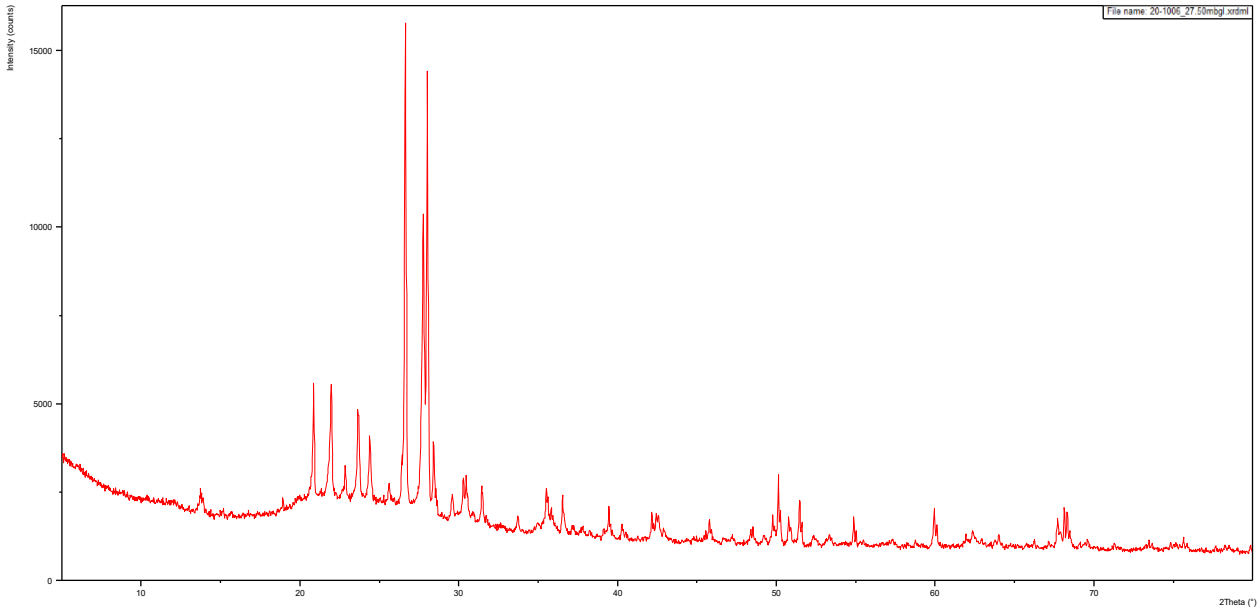

Figure 4.75. 20-1006 27.50mbgl XRD Diffractogram.

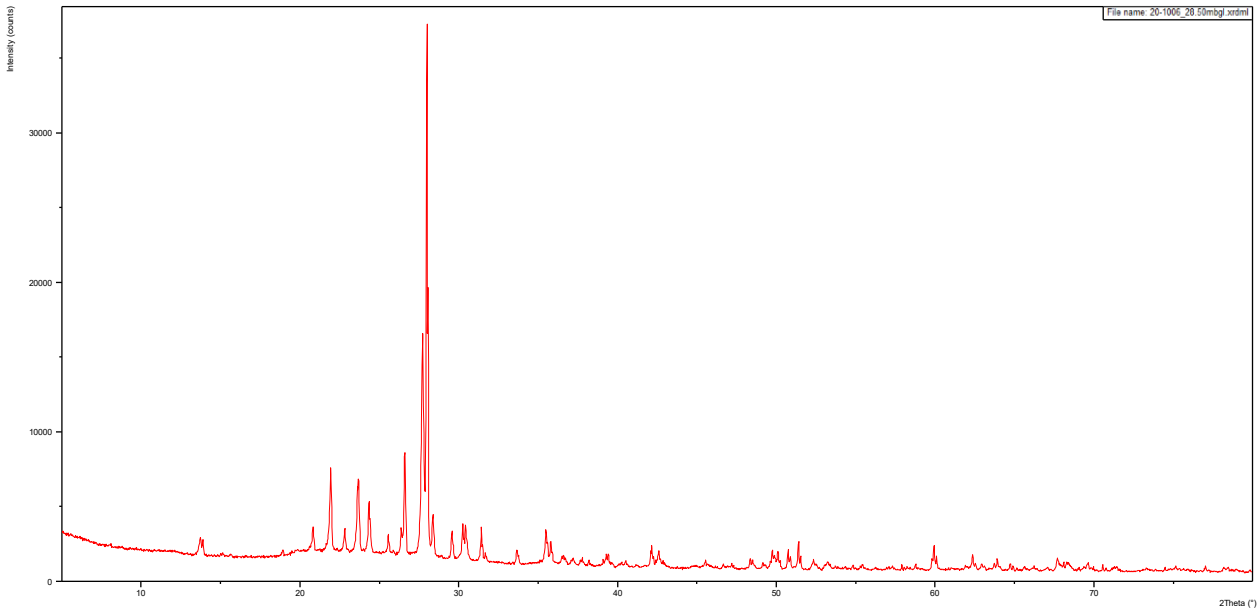

Figure 4.76. 20-1006 28.50mbgl XRD Diffractogram.

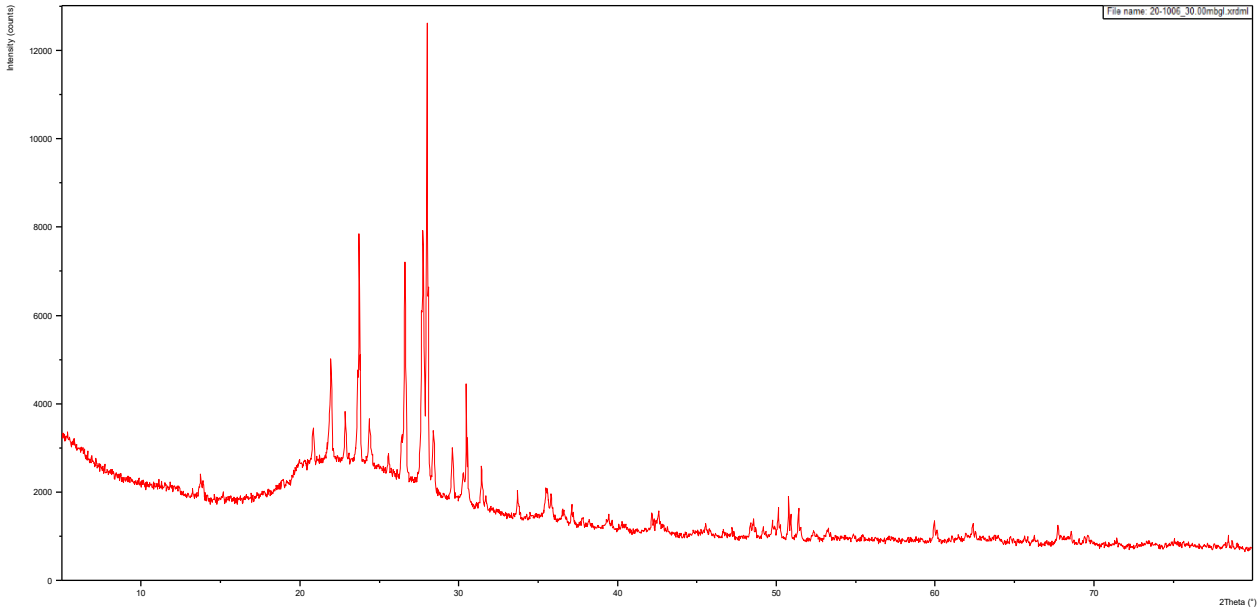

Figure 4.77. 20-1006 30.00mbgl XRD Diffractogram.

- 21-0437.

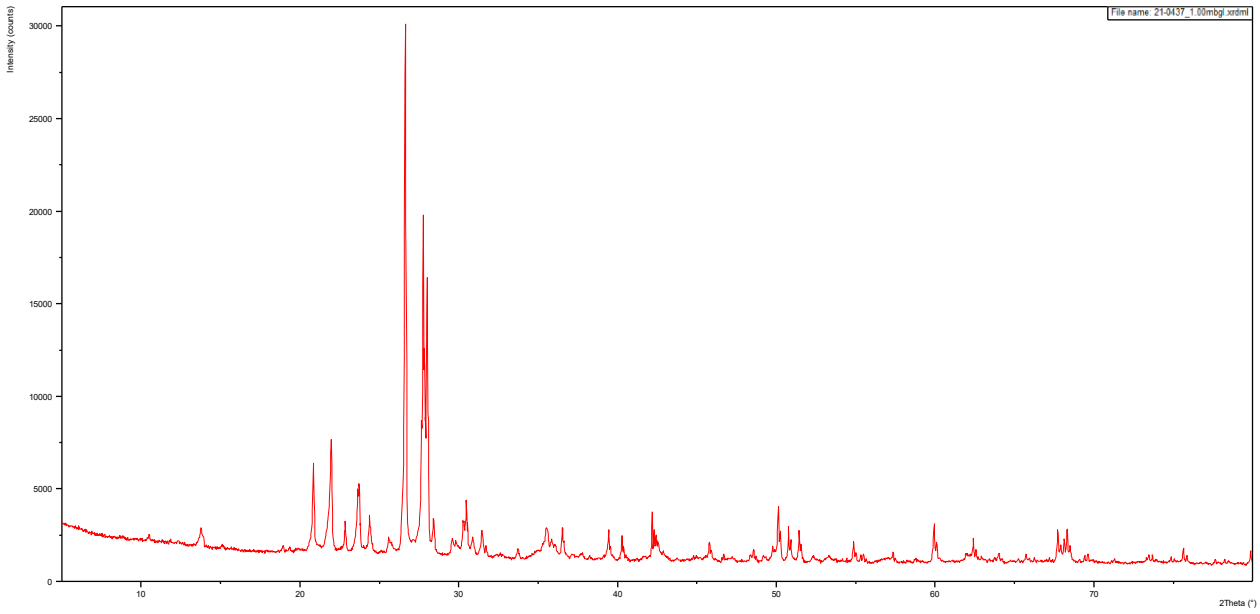

Figure 4.78. 21-0437 1.00mbgl XRD Diffractogram.

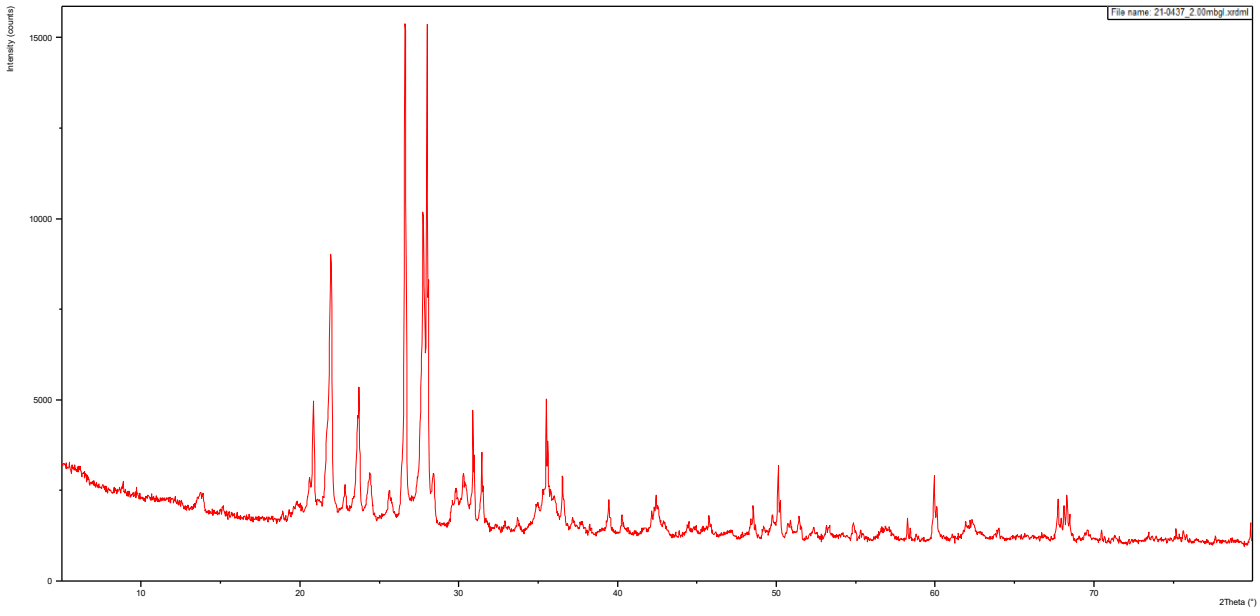

Figure 4.79. 21-0437 2.00mbgl XRD Diffractogram.

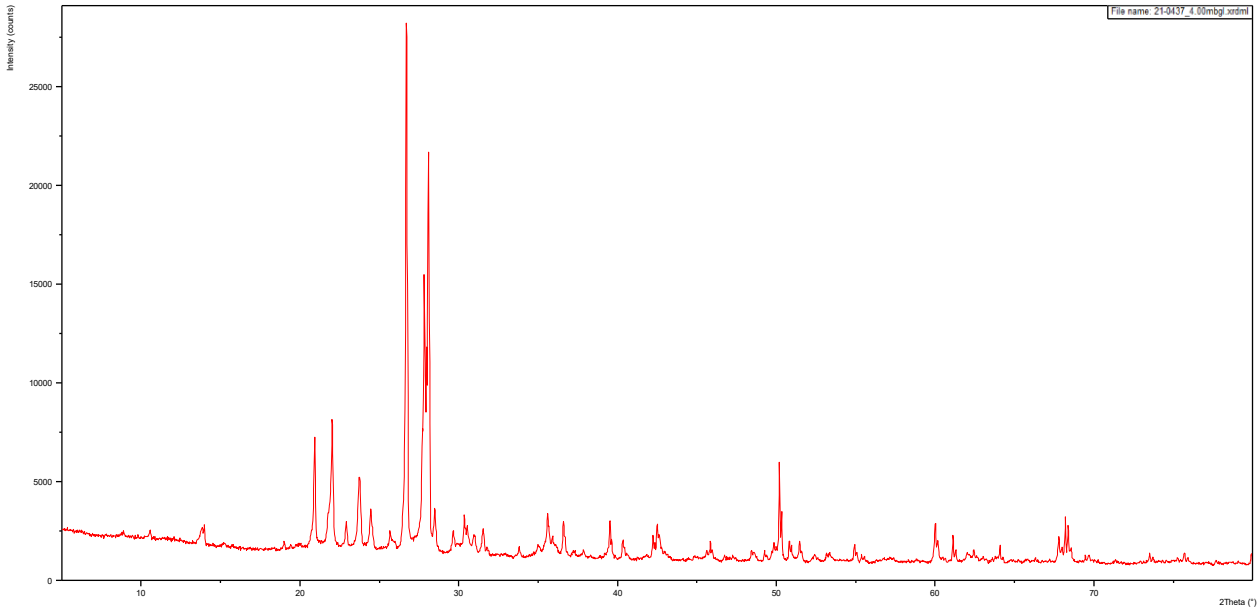

Figure 4.80. 21-0437 4.00mbgl XRD Diffractogram.

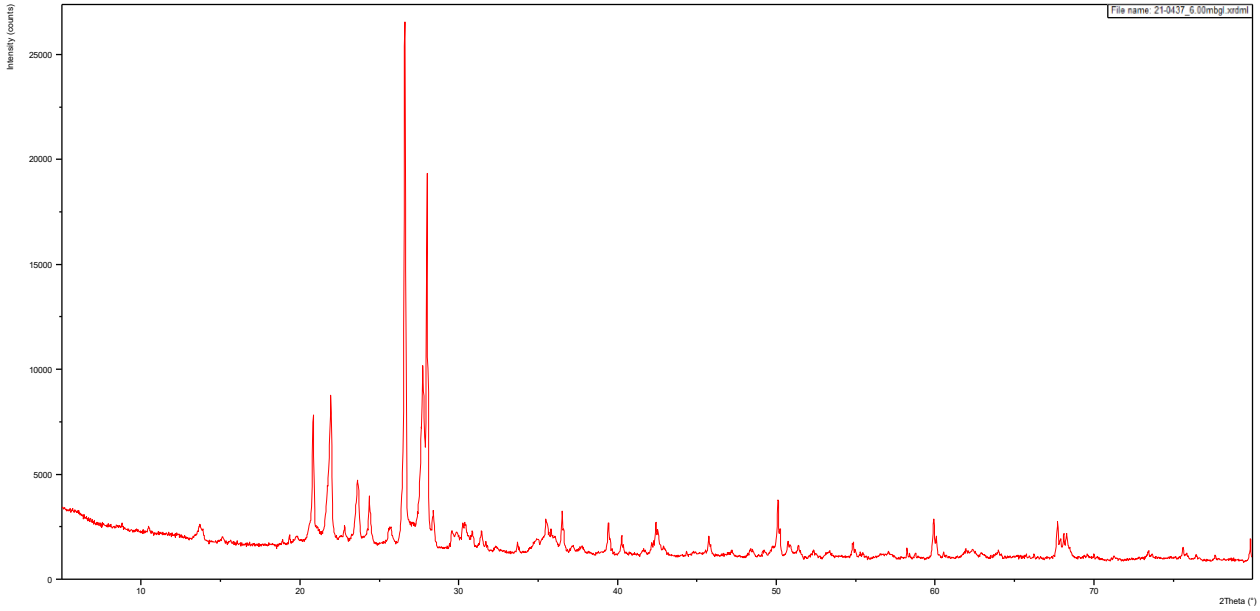

Figure 4.81. 21-0437 6.00mbgl XRD Diffractogram.

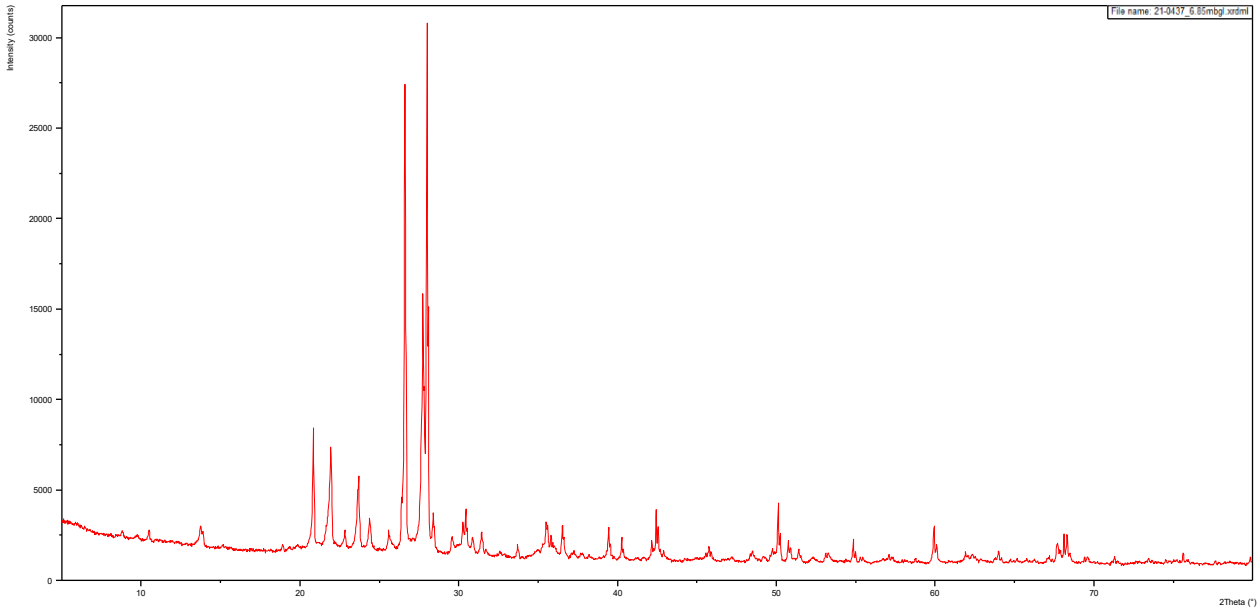

Figure 4.82. 21-0437 6.85mbgl XRD Diffractogram.

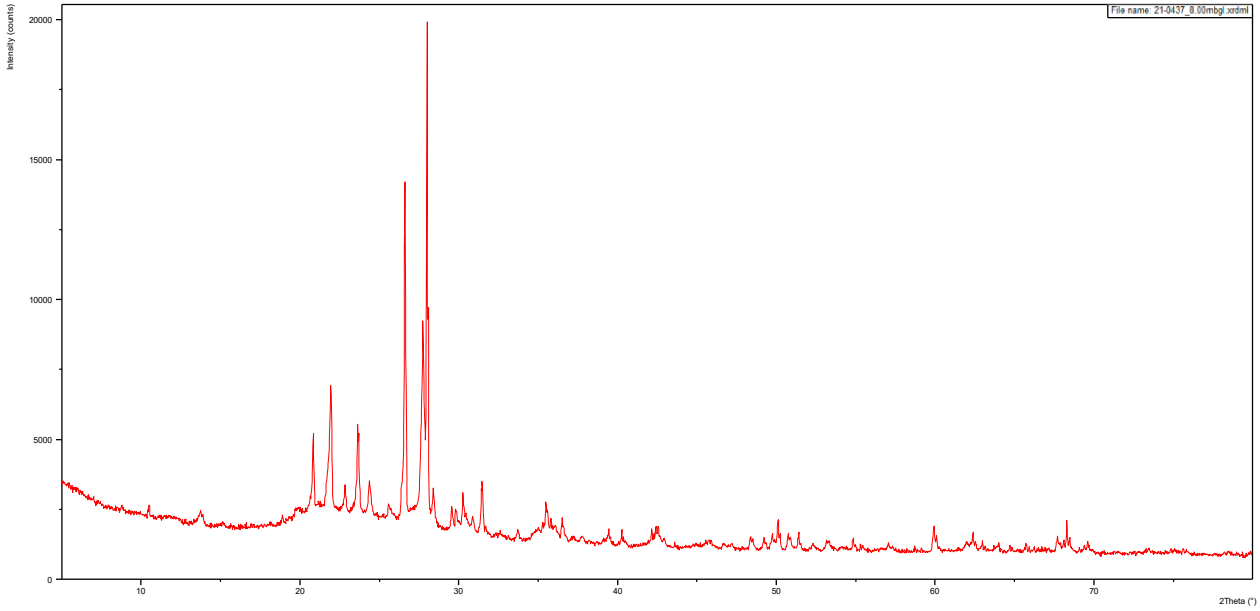

Figure 4.83. 21-0437 8.00mbgl XRD Diffractogram.

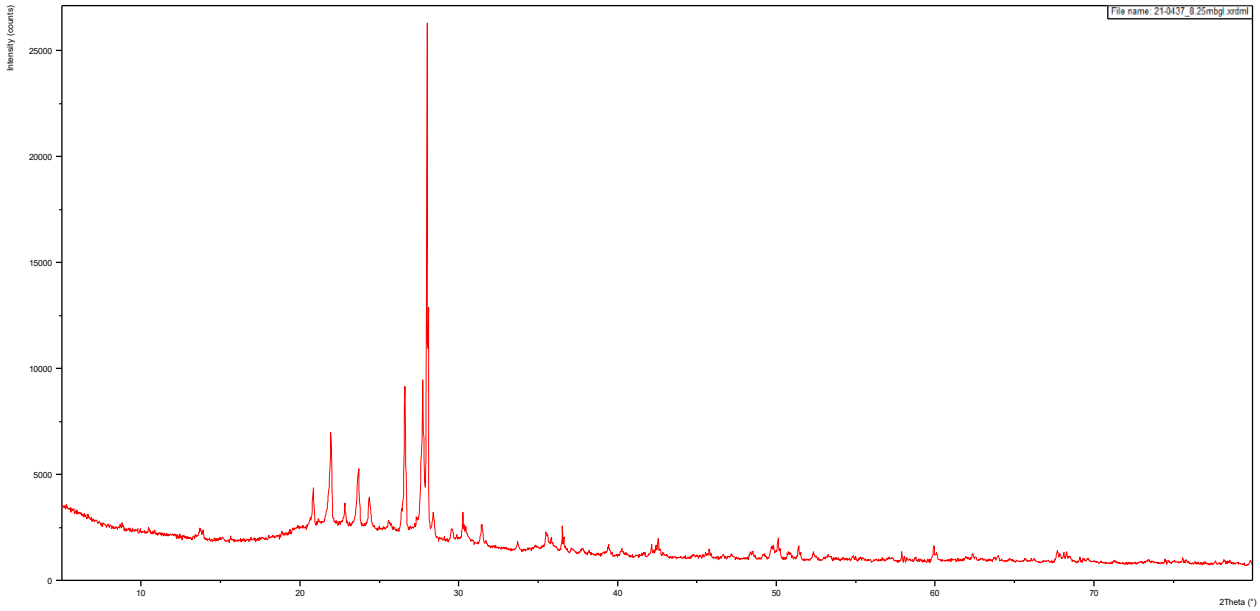

Figure 4.84. 21-0437 8.25mbgl XRD Diffractogram.

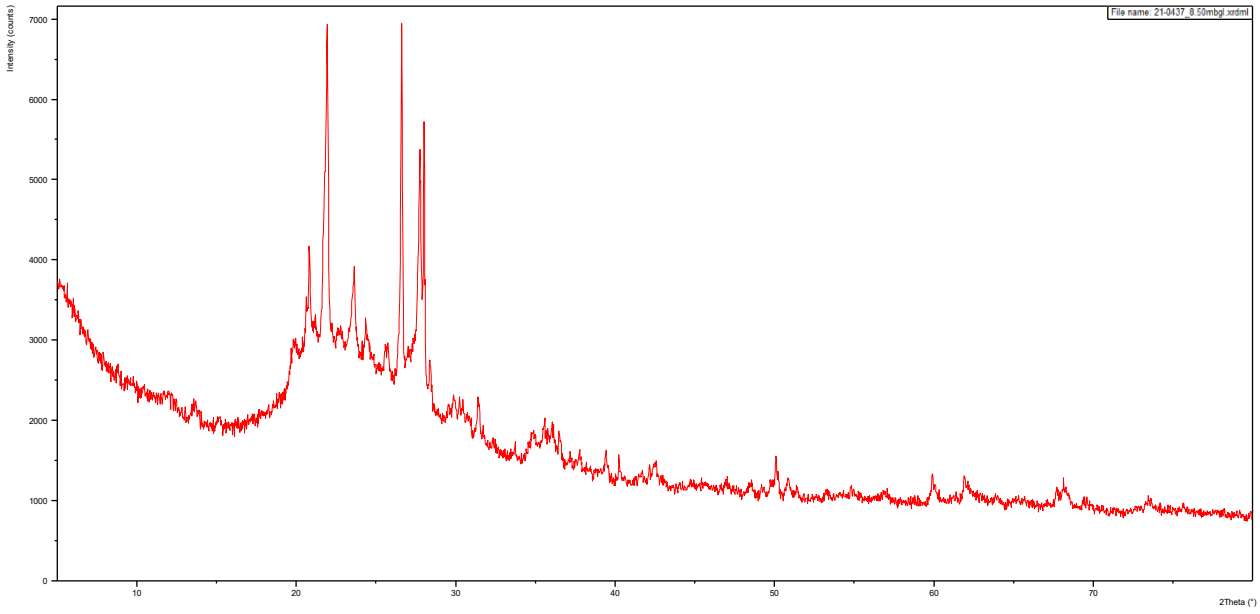

Figure 4.85. 21-0437 8.50mbgl XRD Diffractogram.

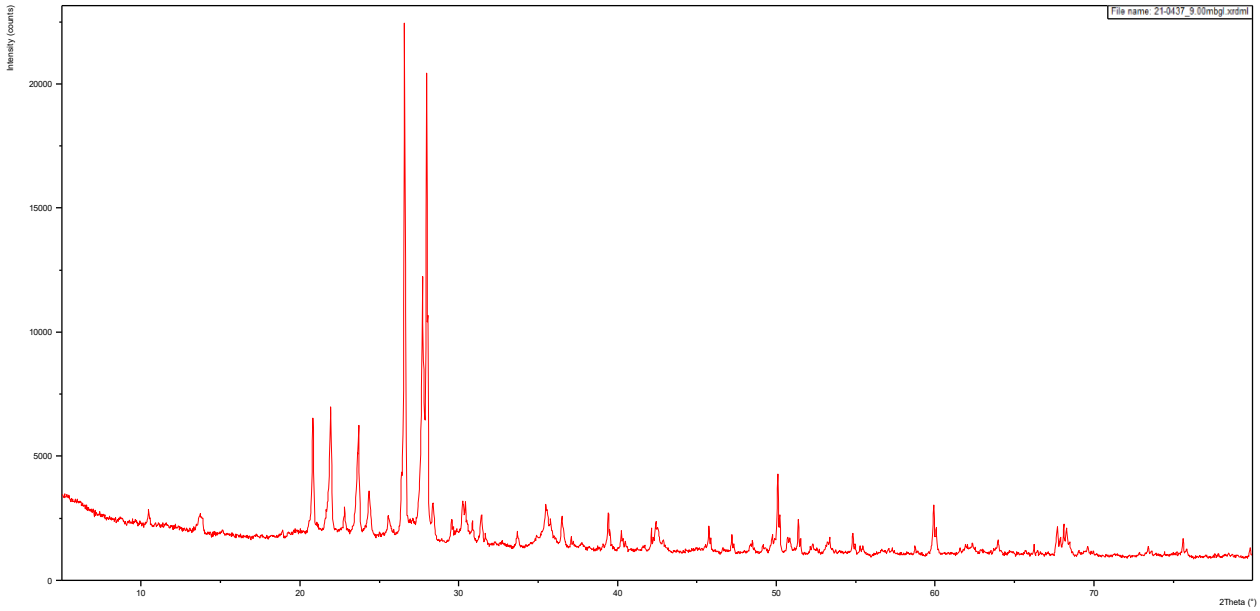

Figure 4.86. 21-0437 9.00mbgl XRD Diffractogram.

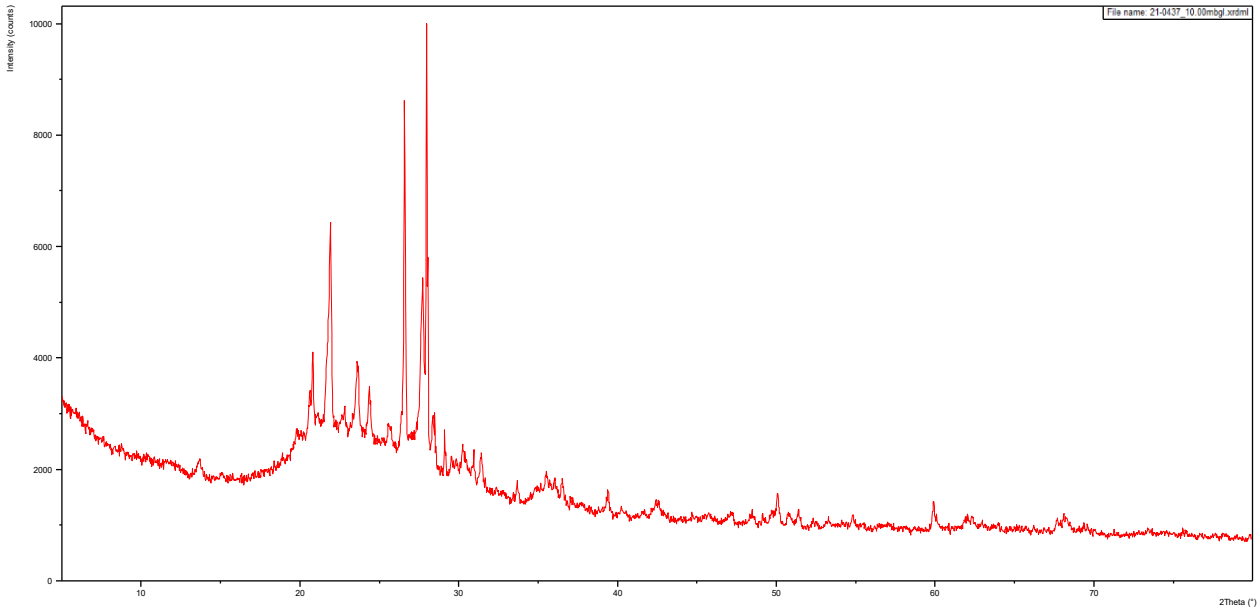

Figure 4.87. 21-0437 10.00mbgl XRD Diffractogram.

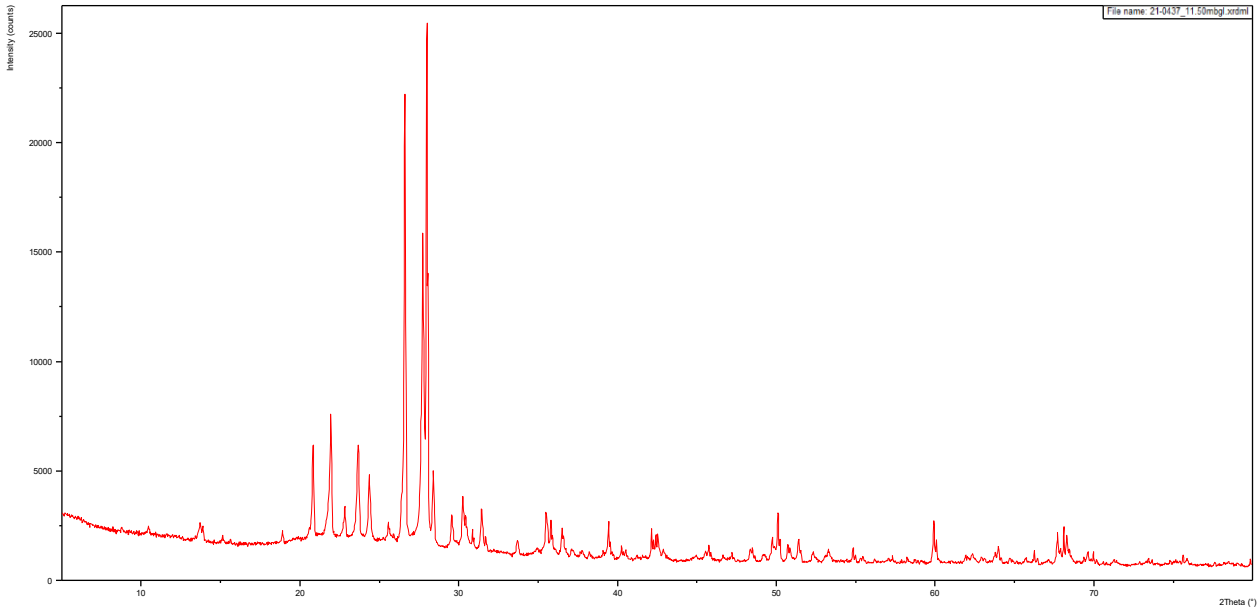

Figure 4.88. 21-0437 11.50mbgl XRD Diffractogram.

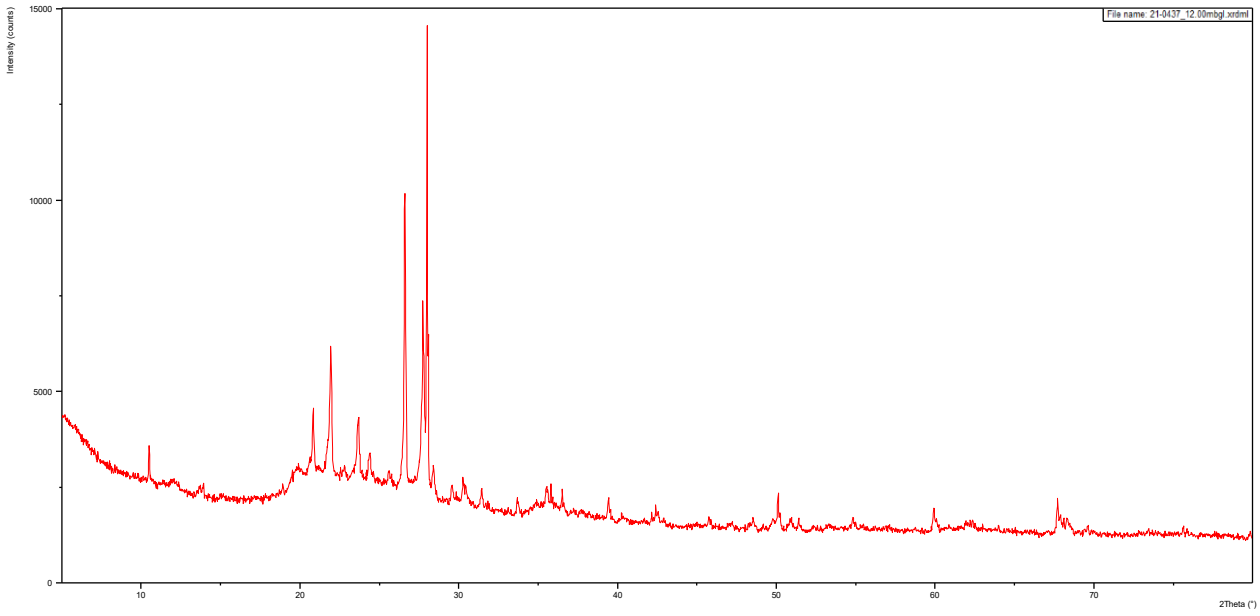

Figure 4.89. 21-0437 12.00mbgl XRD Diffractogram.

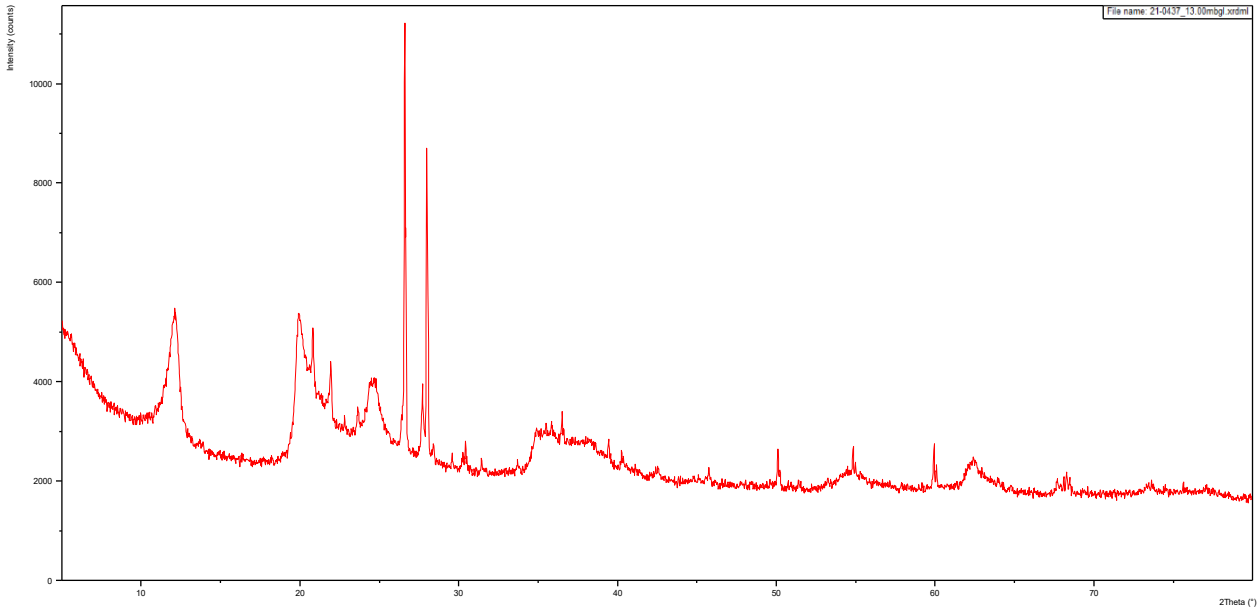

Figure 4.90. 21-0437 13.00mbgl XRD Diffractogram.

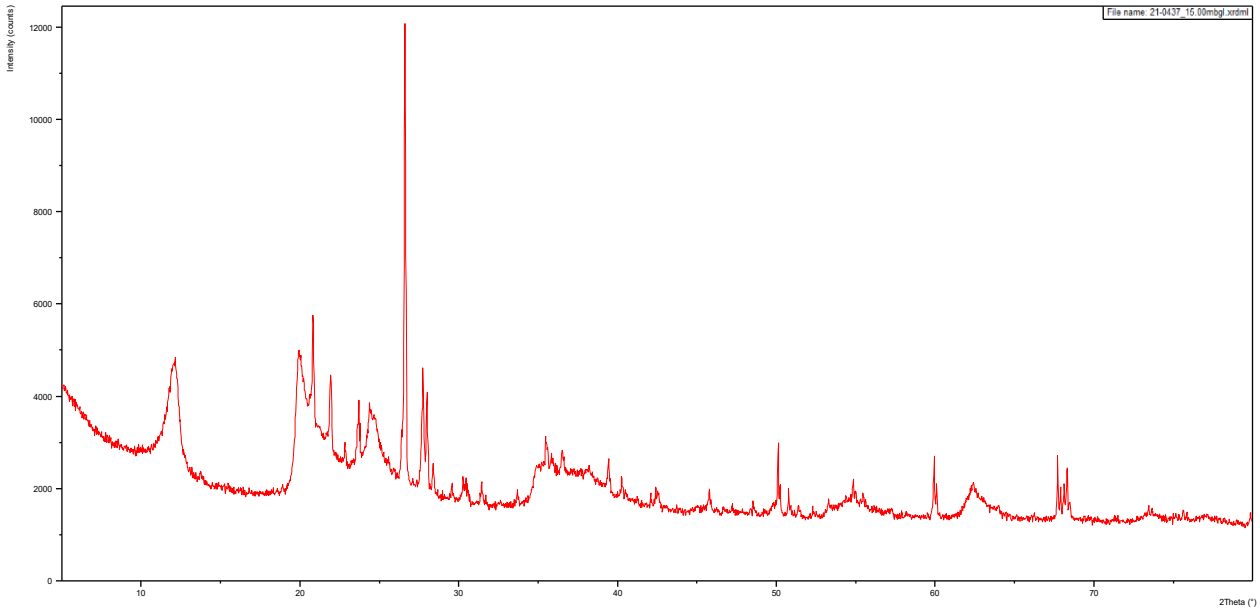

Figure 4.91. 21-0437 15.00mbgl XRD Diffractogram.

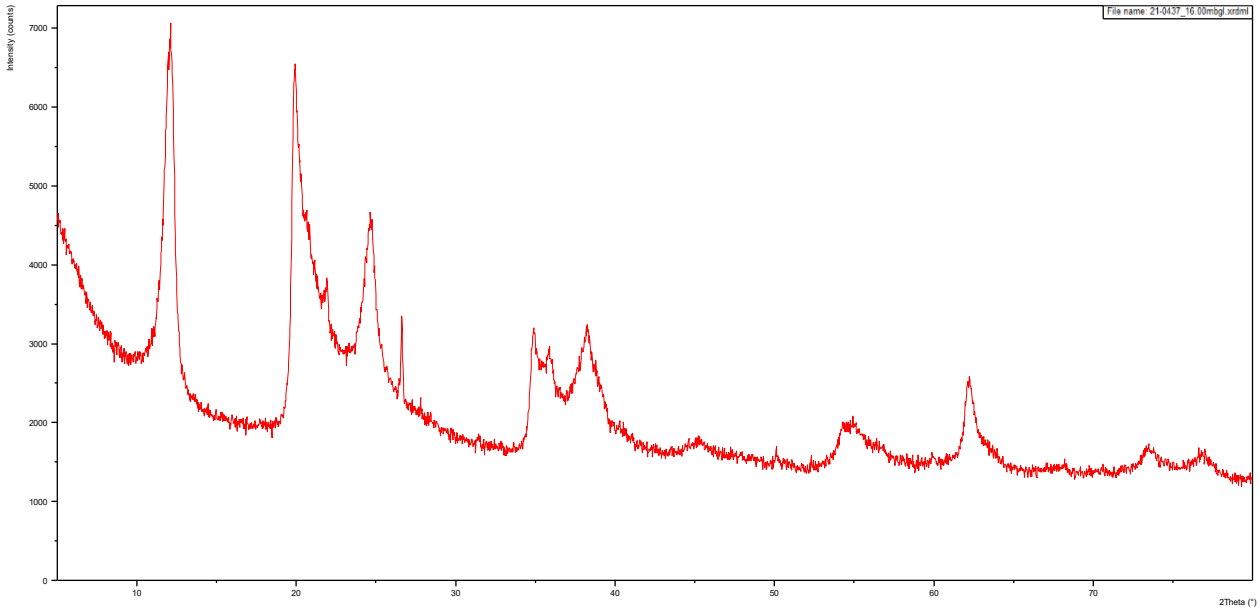

Figure 4.92. 21-0437 16.00mbgl XRD Diffractogram.

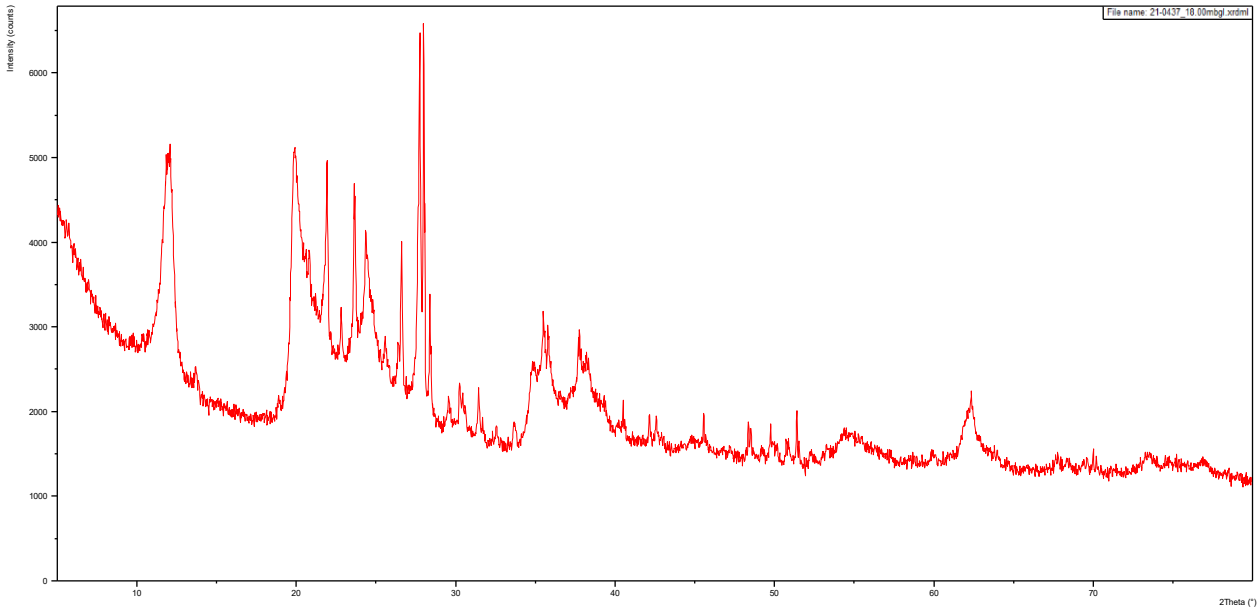

Figure 4.93. 21-0437 18.00mbgl XRD Diffractogram.

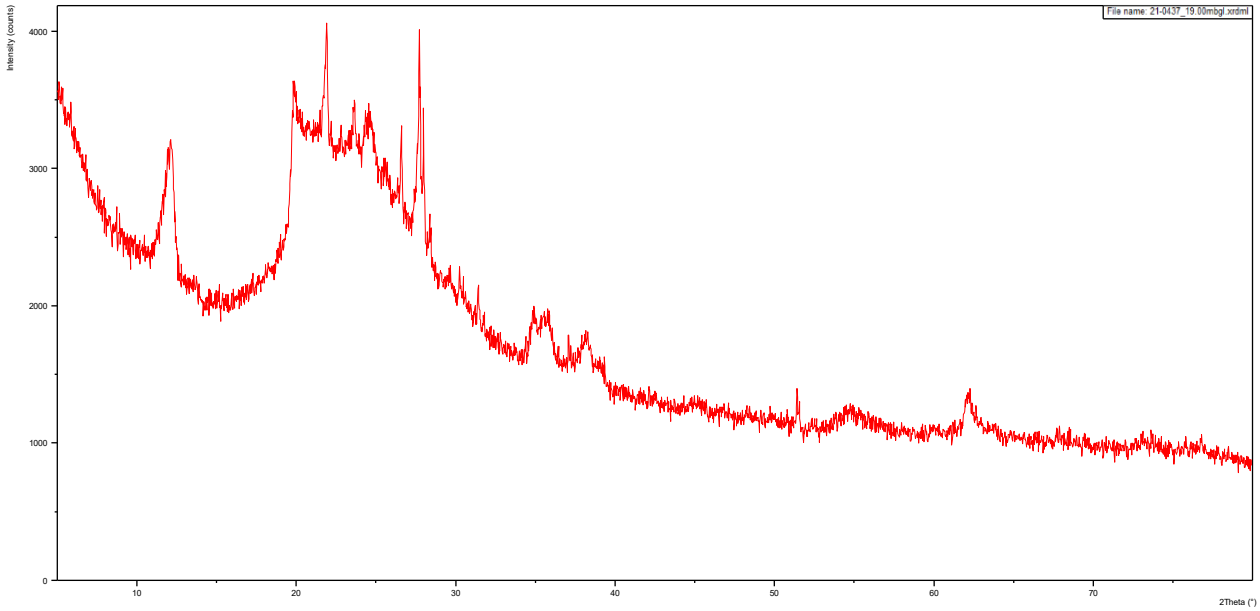

Figure 4.94. 21-0437 19.00mbgl XRD Diffractogram.

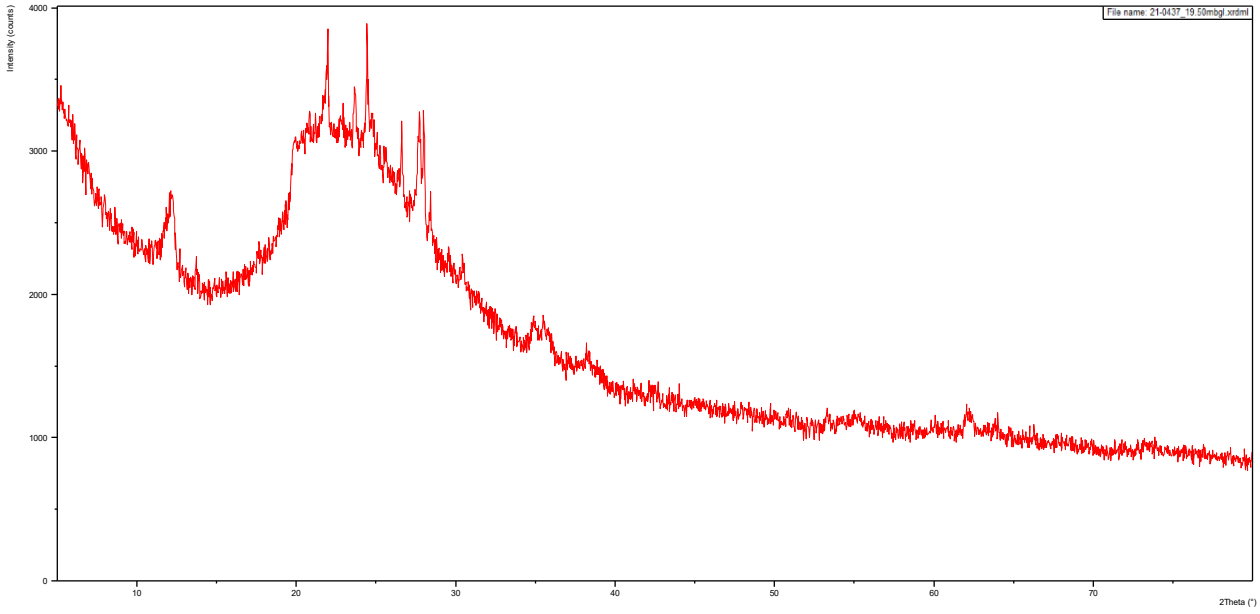

Figure 4.95. 21-0437 19.50mbgl XRD Diffractogram.

- Ferrybank.

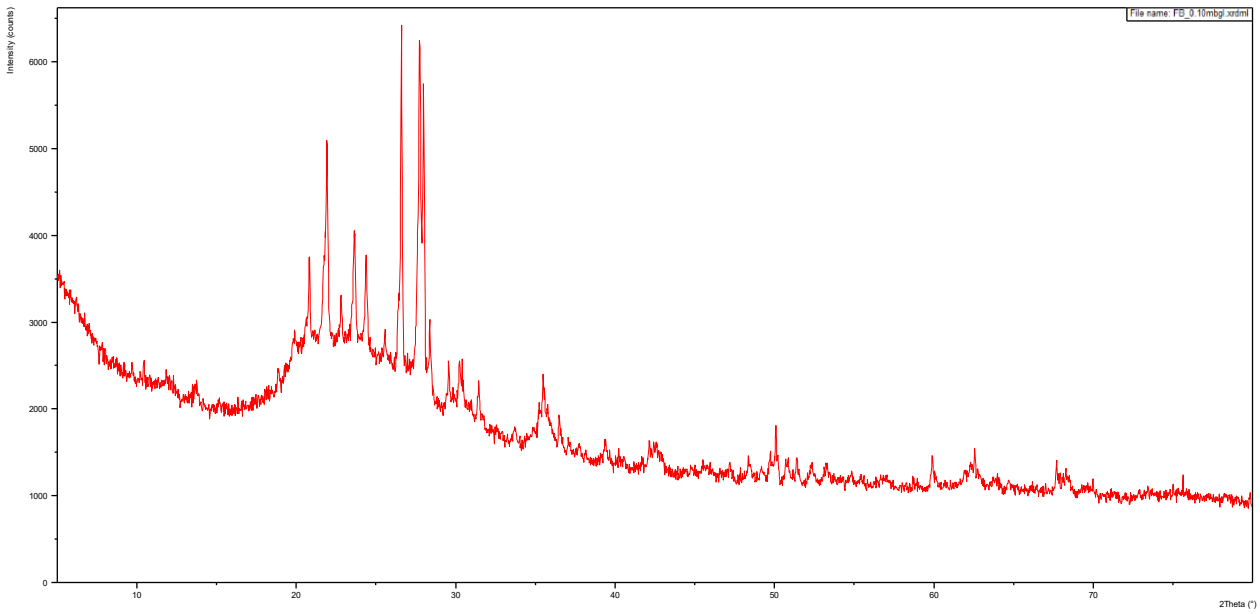

Figure 4.96. Ferrybank 0.10mbgl XRD Diffractogram.

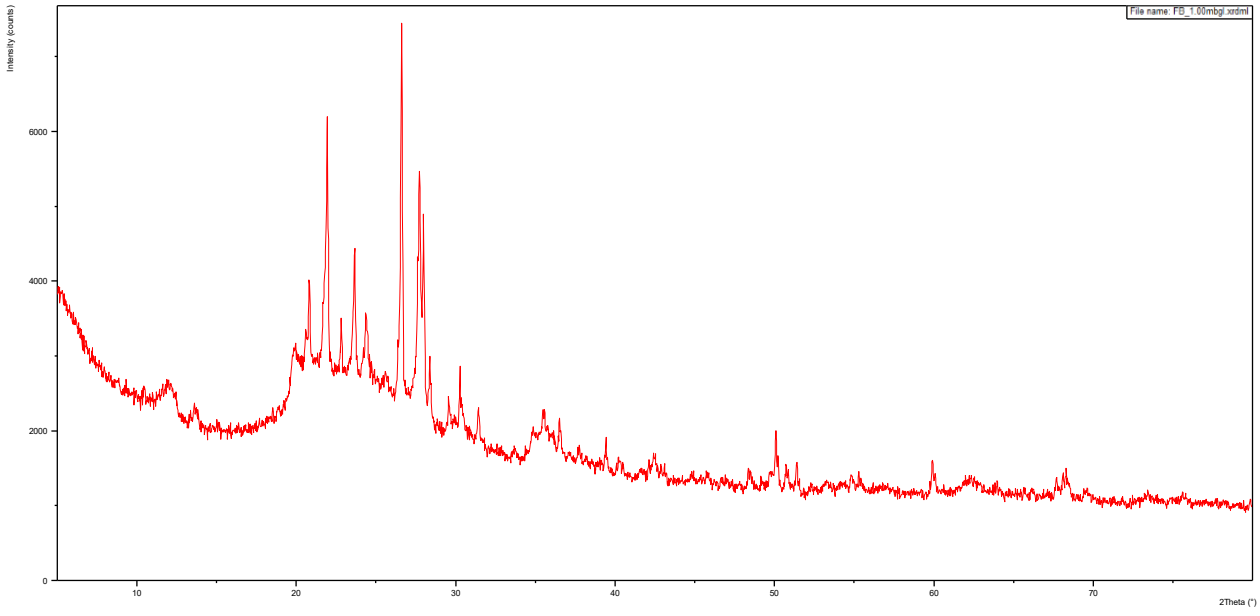

Figure 4.97. Ferrybank 1.00mbgl XRD Diffractogram.

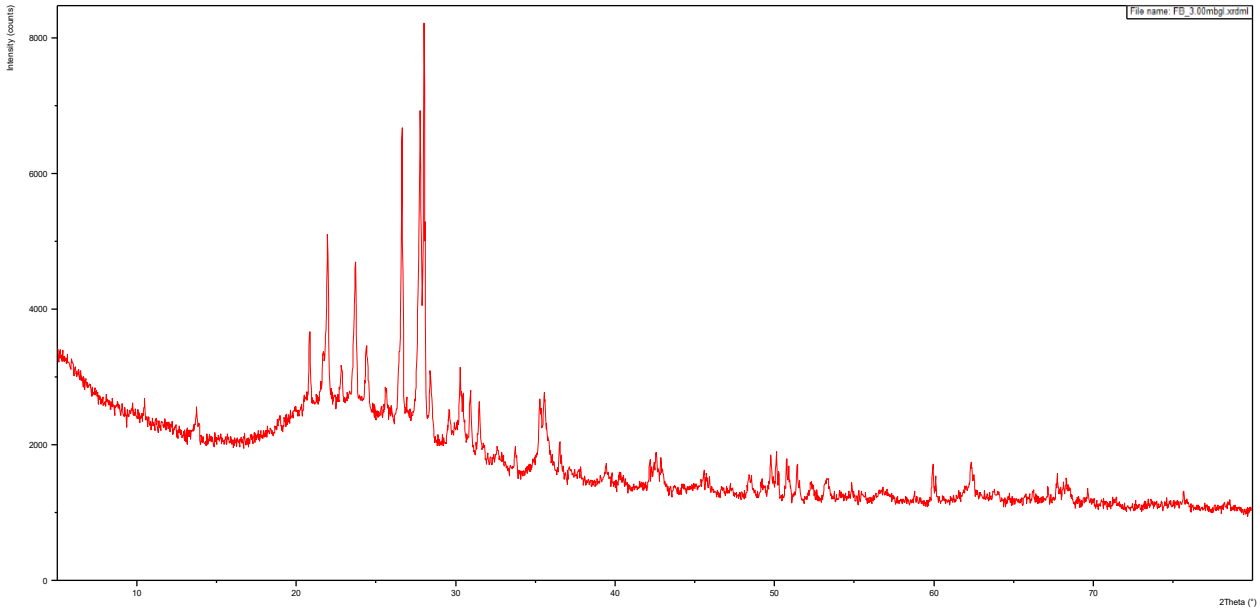

Figure 4.98. Ferrybank 3.00mbgl XRD Diffractogram.

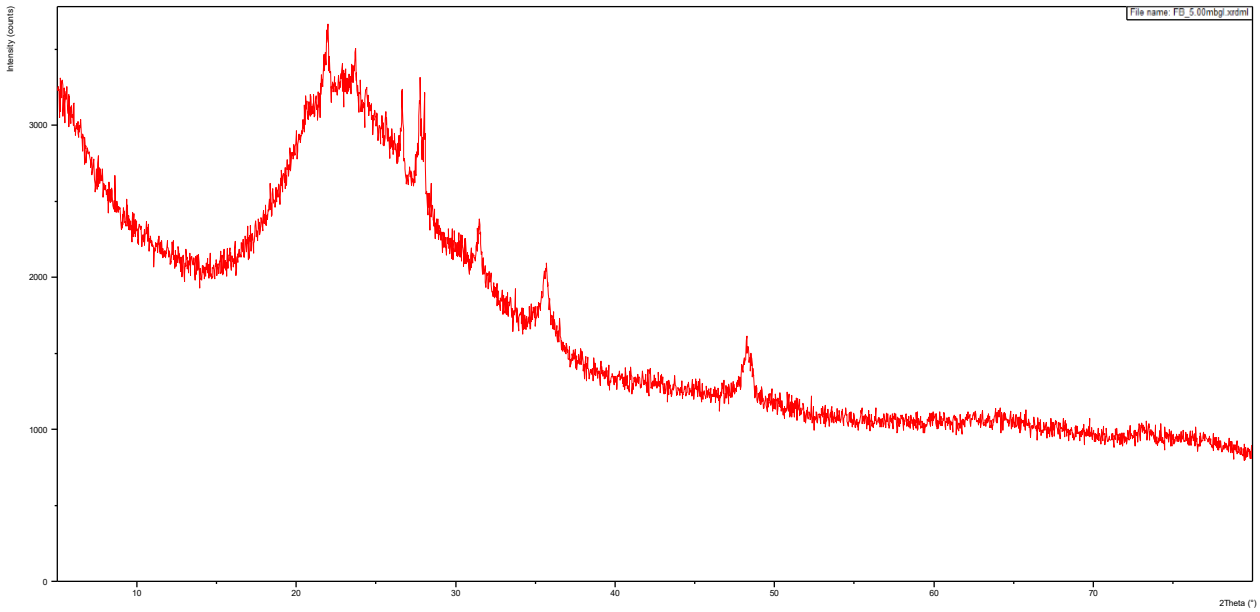

Figure 4.99. Ferrybank 5.00mbgl XRD Diffractogram.

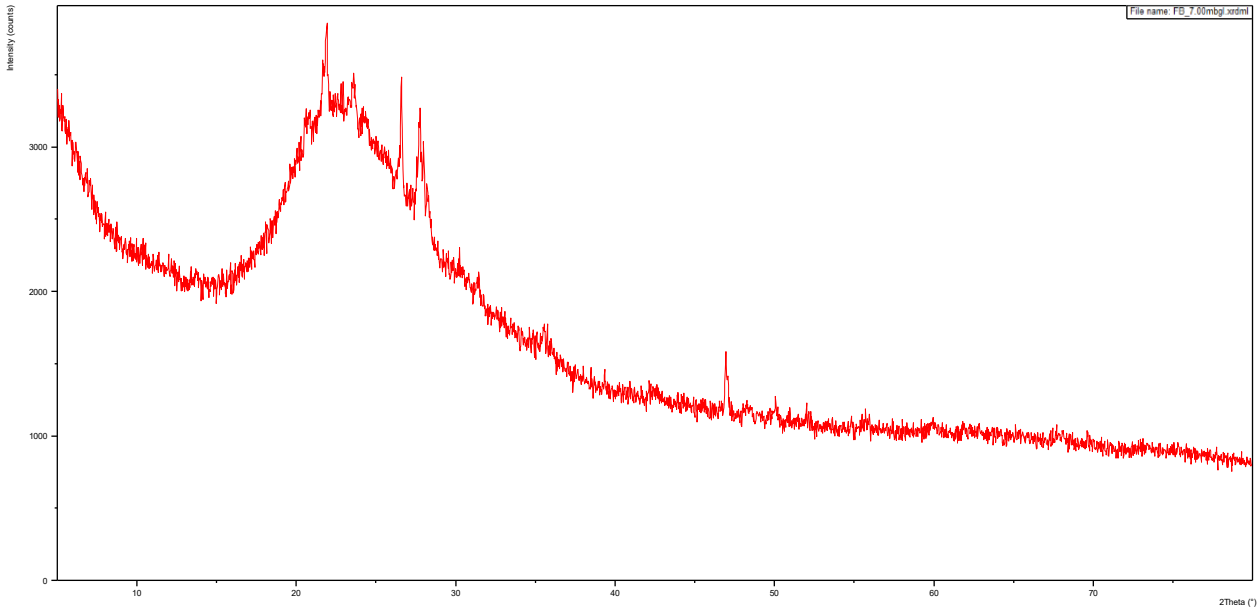

Figure 4.100. Ferrybank 7.00mbgl XRD Diffractogram.

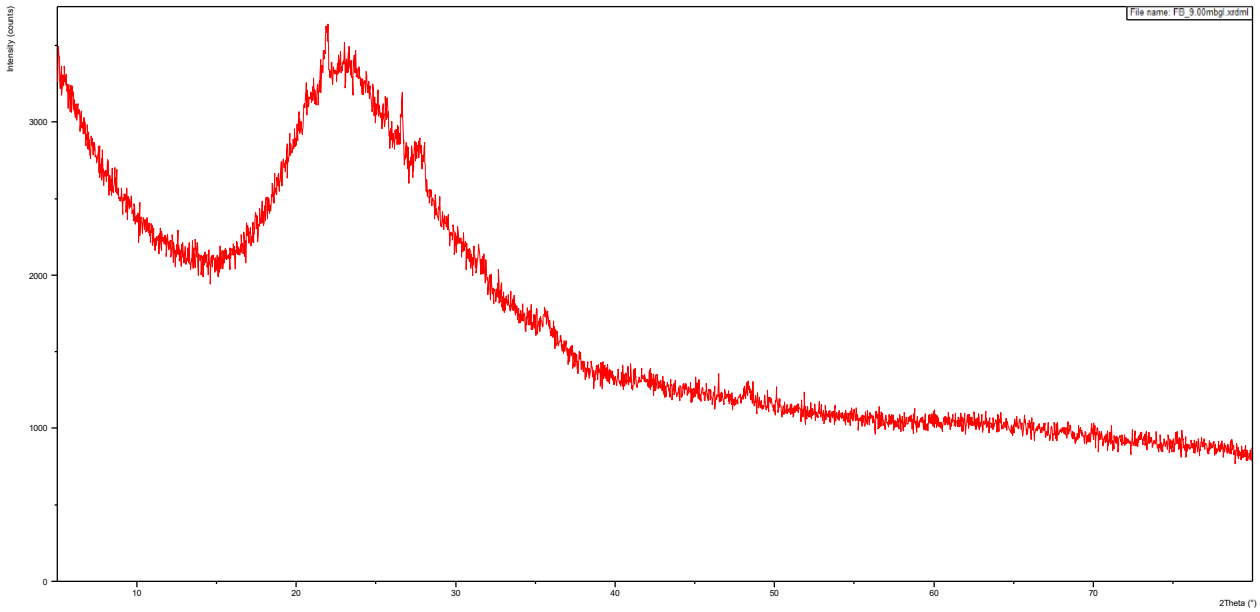

Figure 4.101. Ferrybank 9.00mbgl XRD Diffractogram.

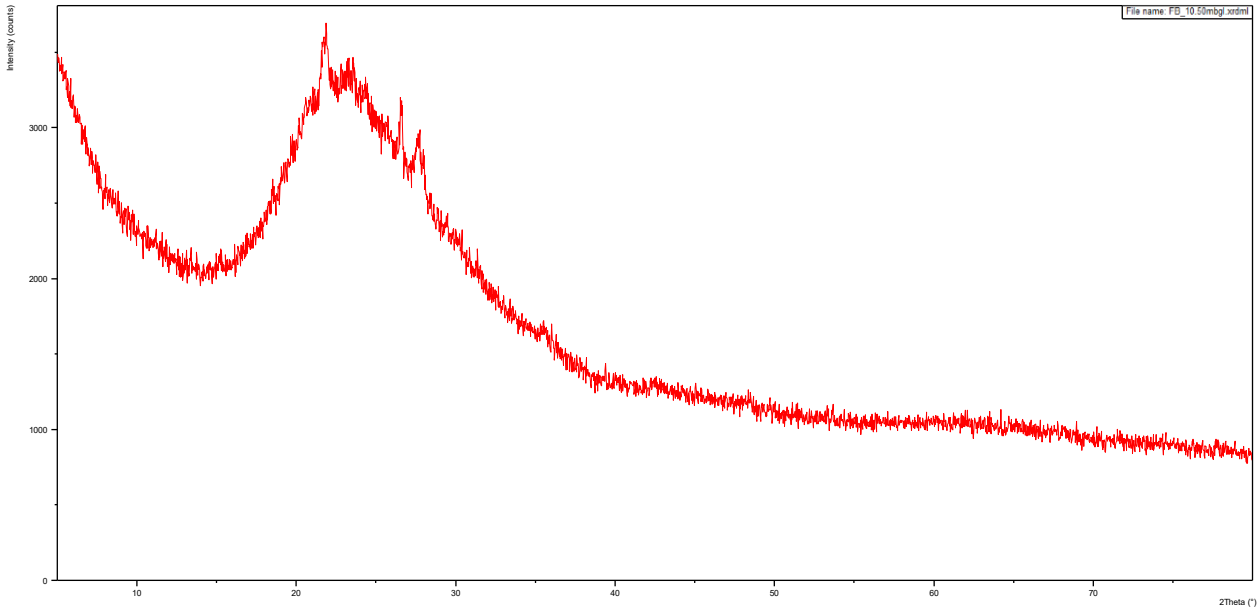

Figure 4.102. Ferrybank 10.50mbgl XRD Diffractogram.

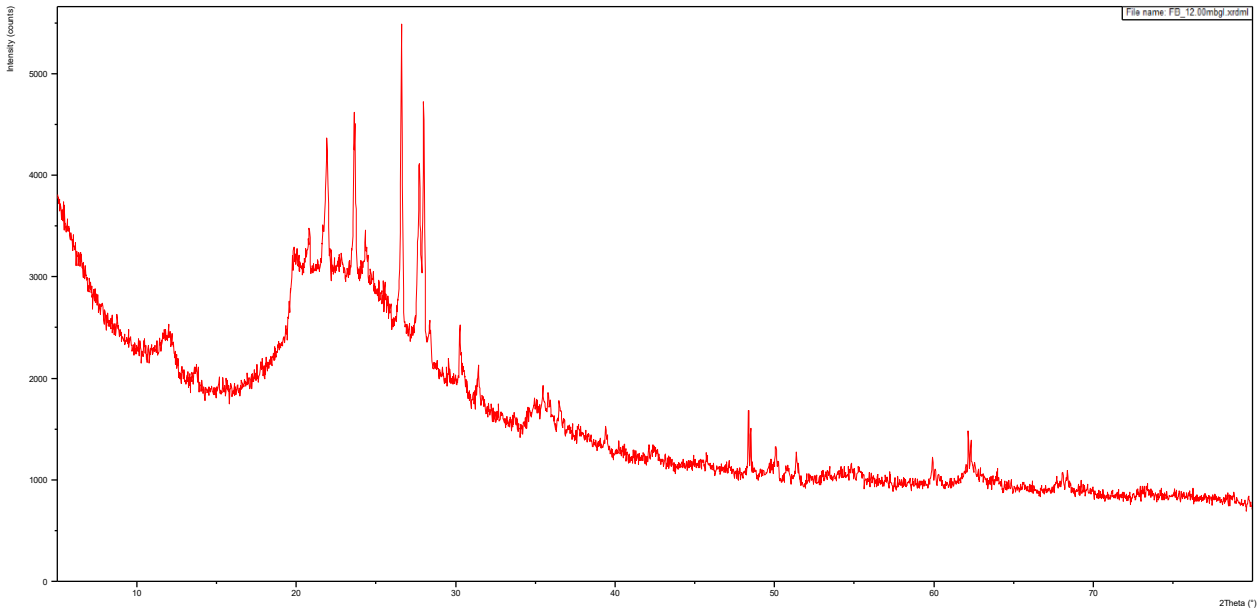

Figure 4.103. Ferrybank 12.00mbgl XRD Diffractogram.

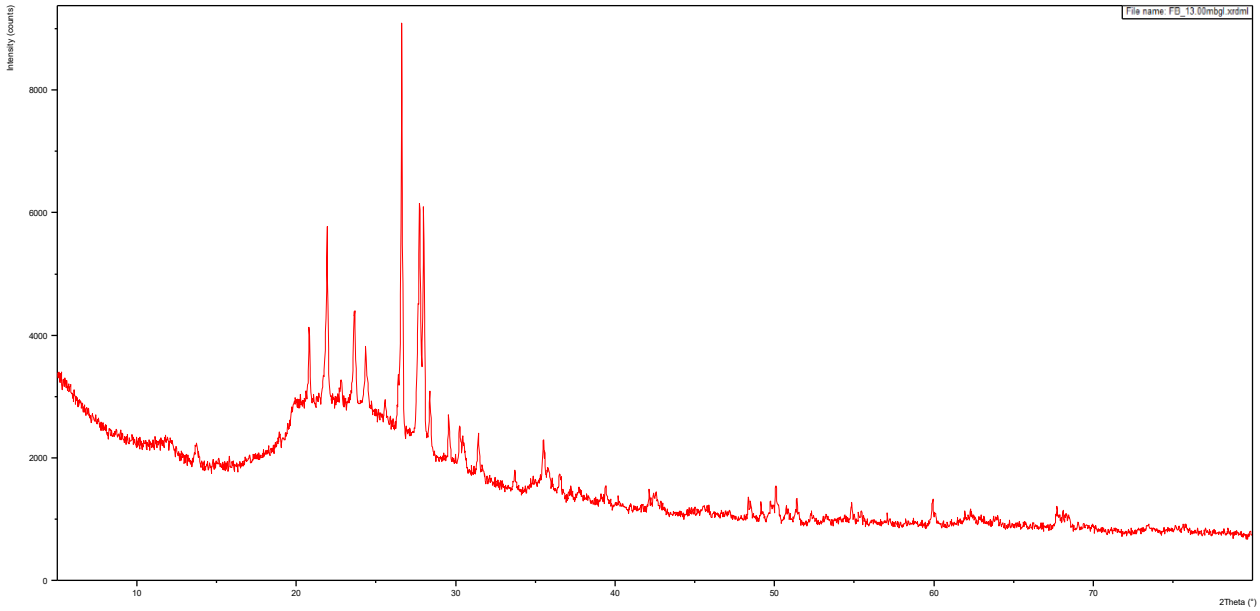

Figure 4.104. Ferrybank 13.00mbgl XRD Diffractogram.

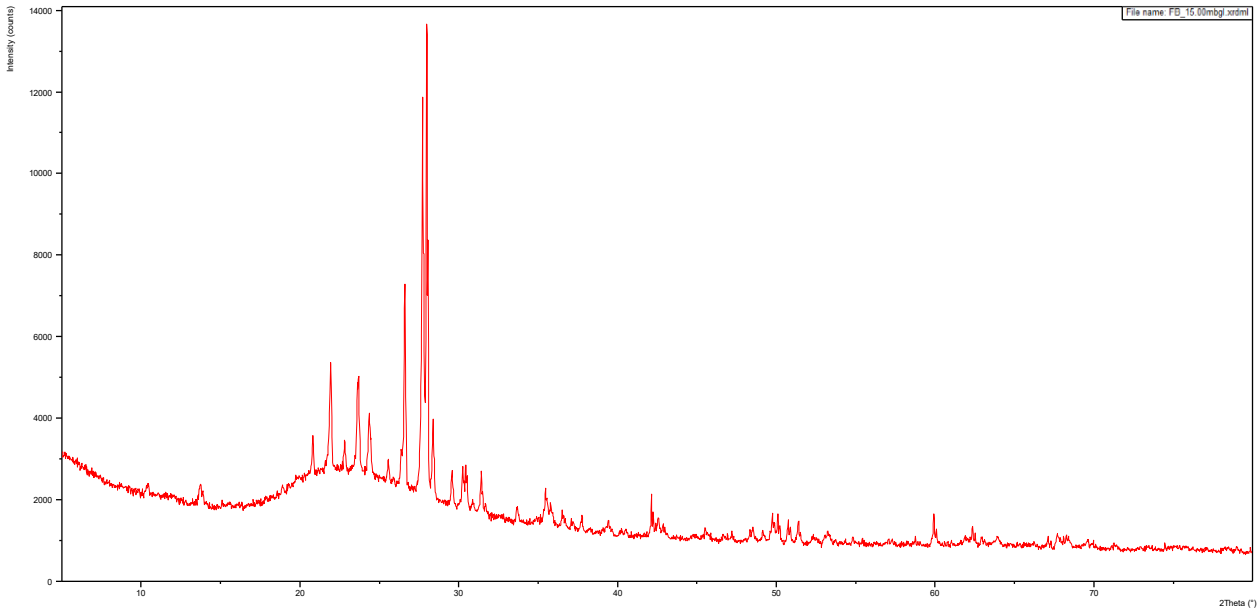

Figure 4.105. Ferrybank 15.00mbgl XRD Diffractogram.

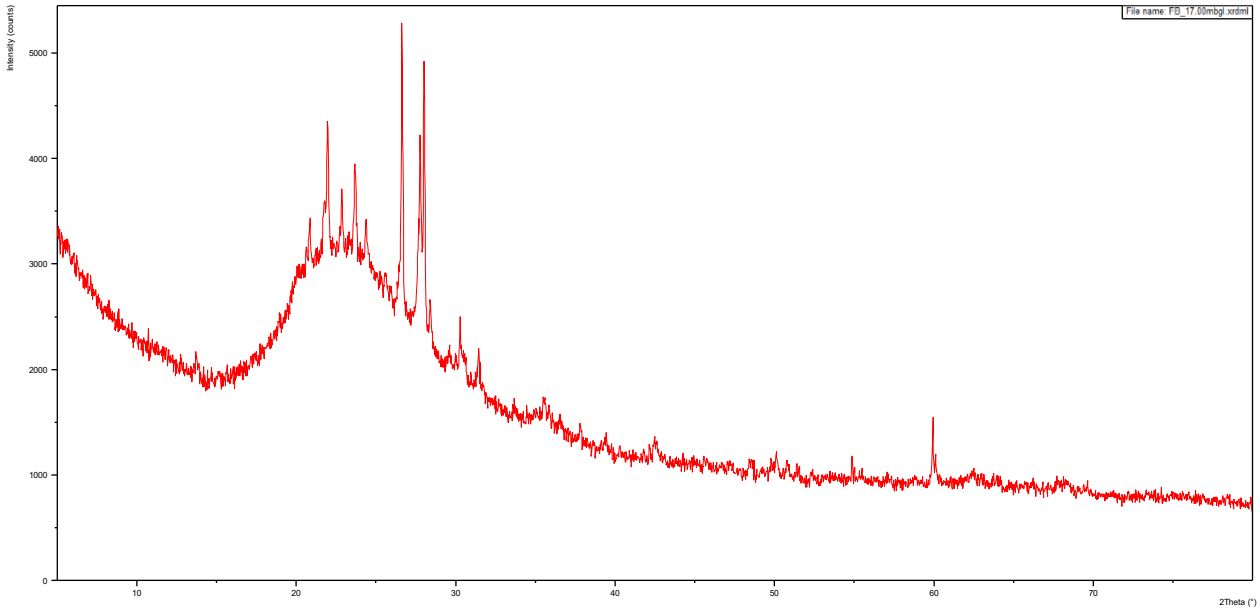

Figure 4.106. Ferrybank 17.00mbgl XRD Diffractogram.

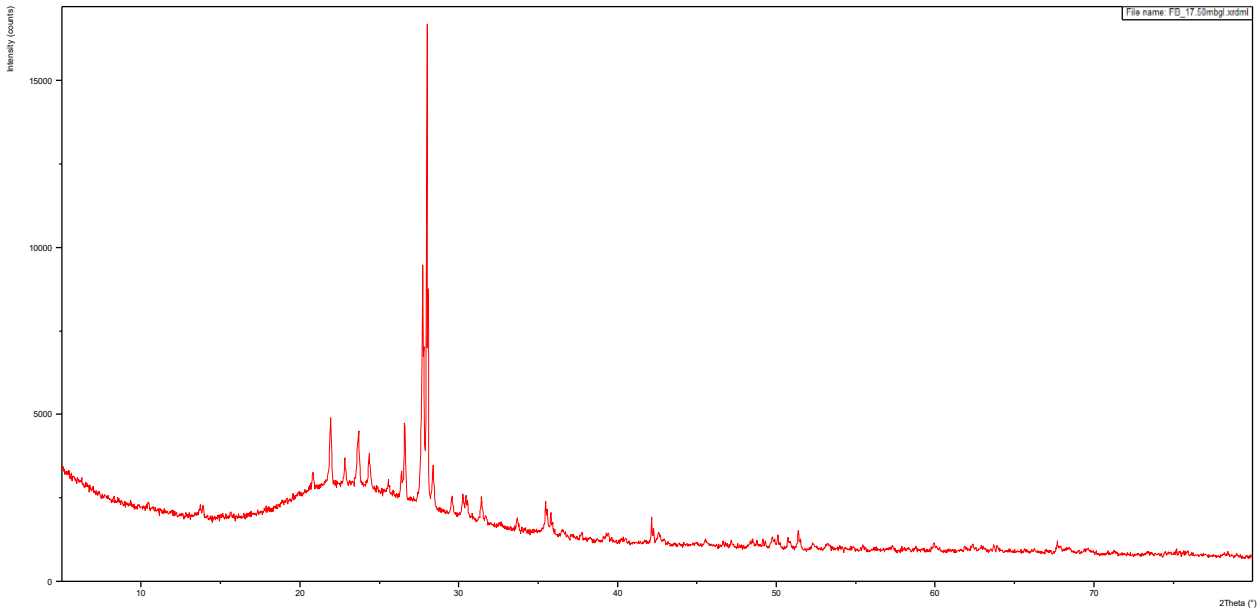

Figure 4.107. Ferrybank 17.50mbgl XRD Diffractogram.

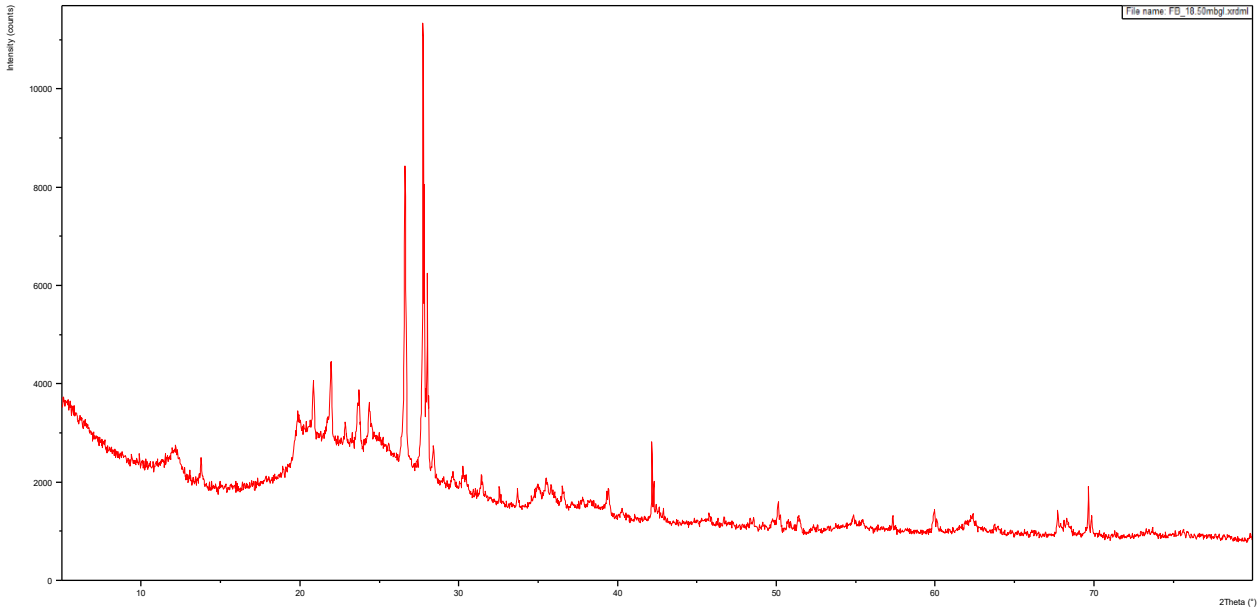

Figure 4.108. Ferrybank 18.50mbgl XRD Diffractogram.

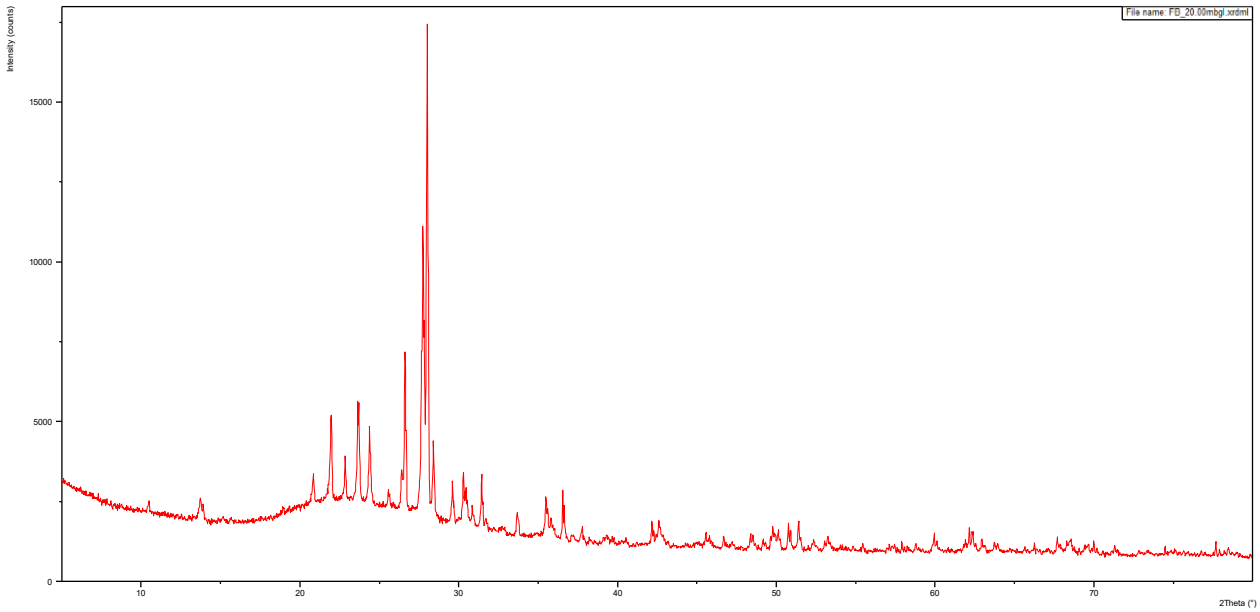

Figure 4.109. Ferrybank 20.00mbgl XRD Diffractogram.

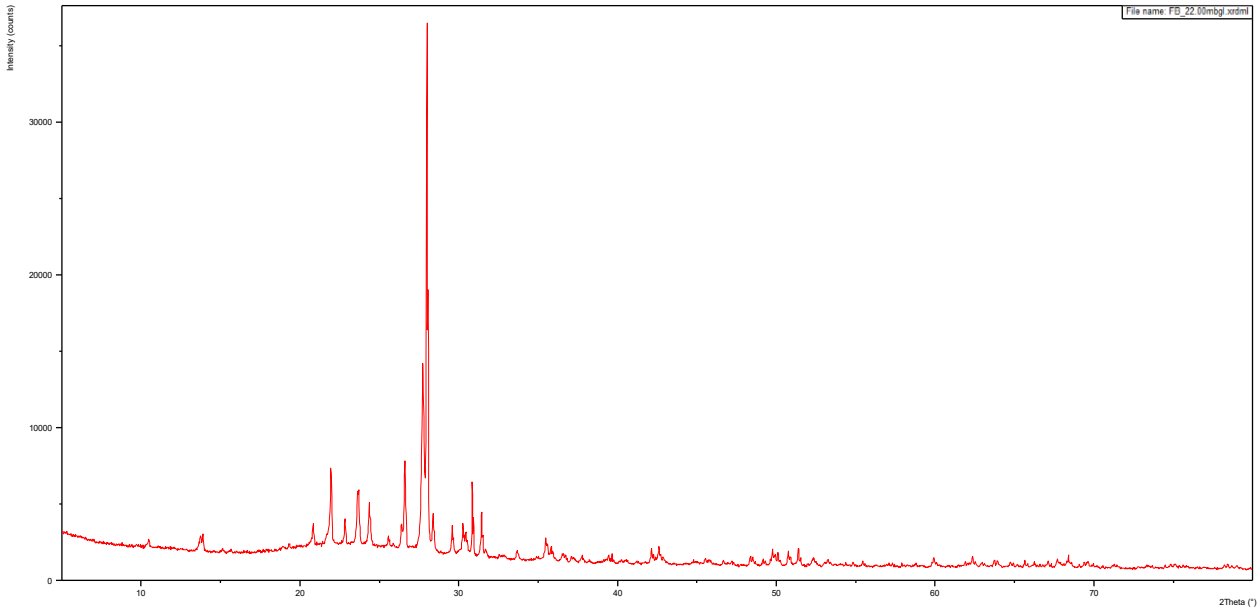

Figure 4.110. Ferrybank 22.00mbgl XRD Diffractogram.

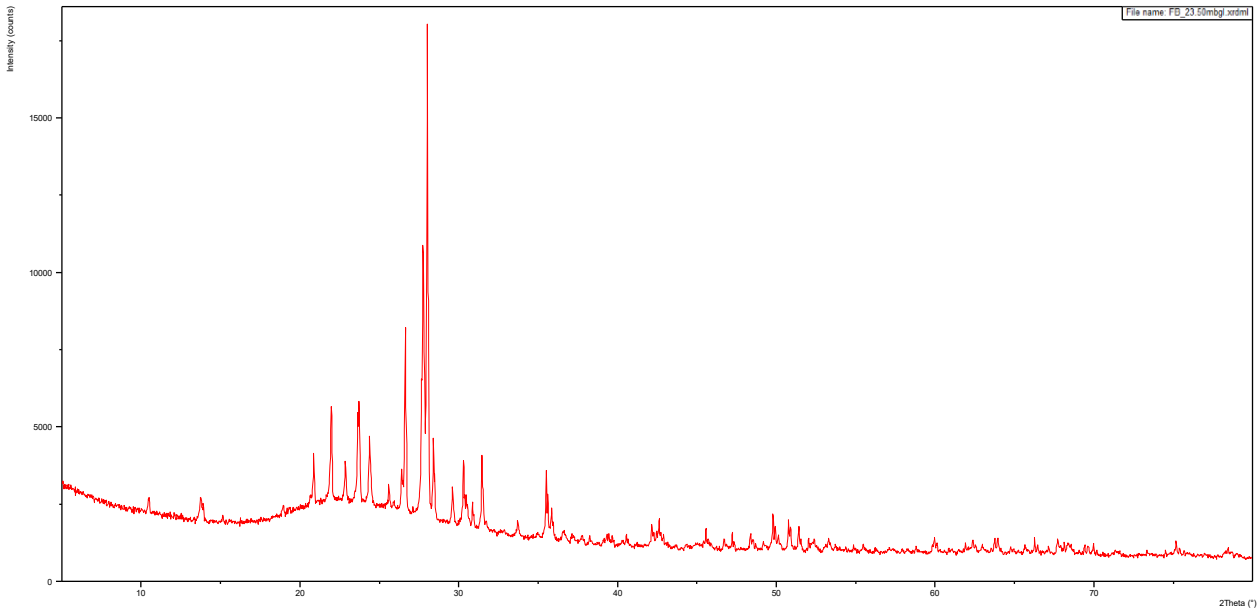

Figure 4.111. Ferrybank 23.50mbgl XRD Diffractogram.

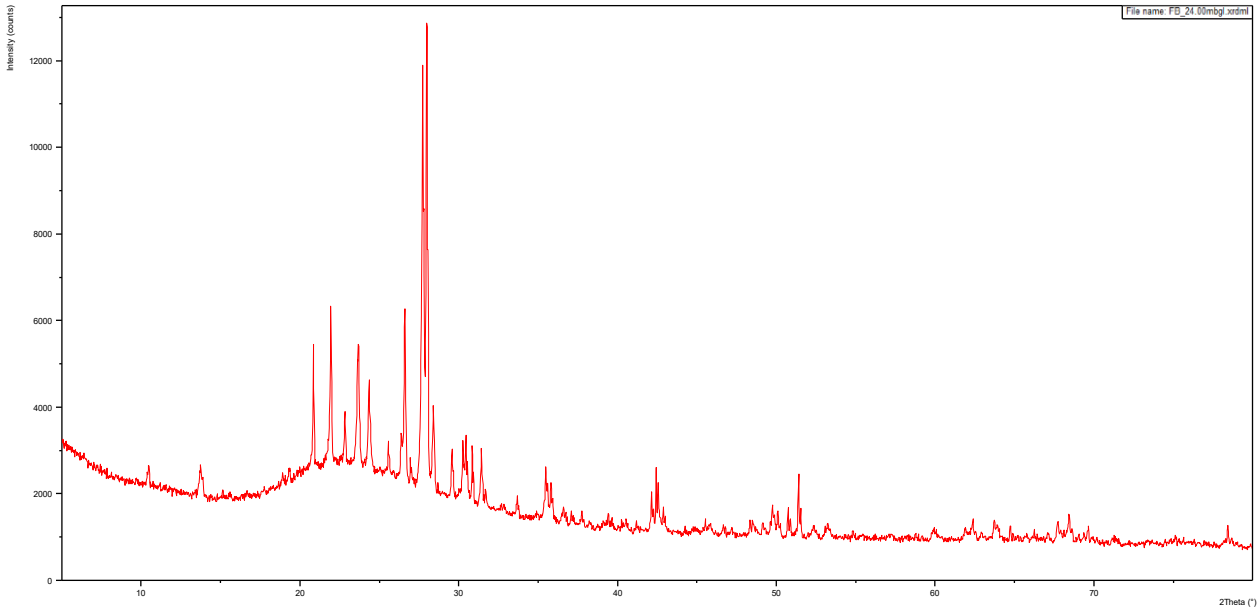

Figure 4.112. Ferrybank 24.00mbgl XRD Diffractogram.

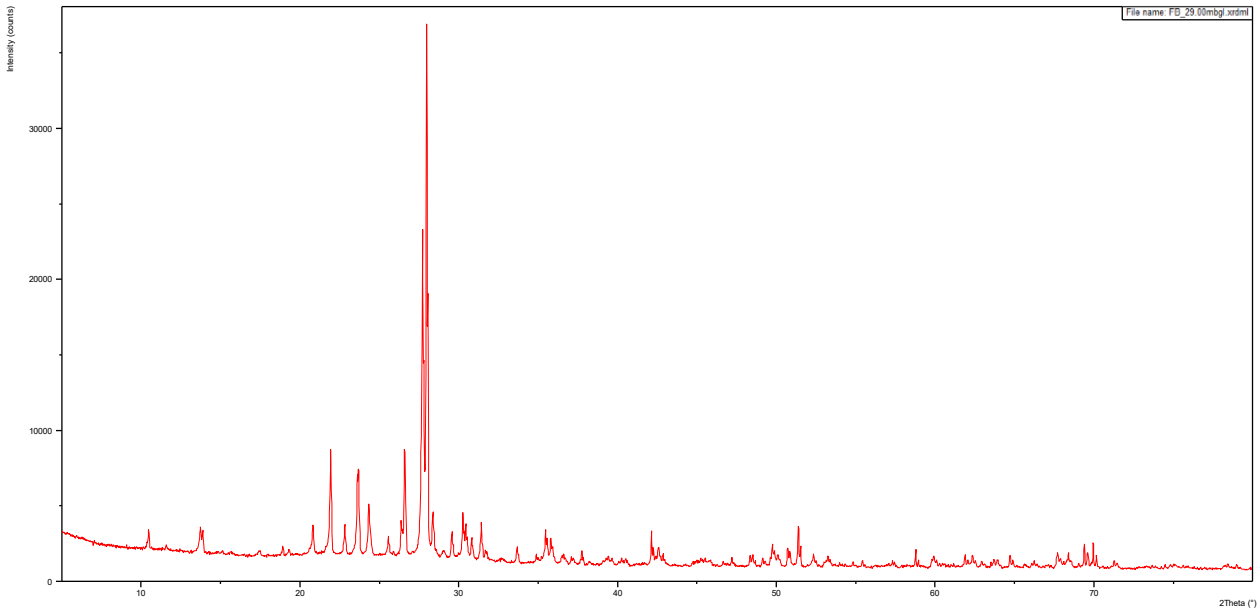

Figure 4.113. Ferrybank 29.00mbgl XRD Diffractogram.

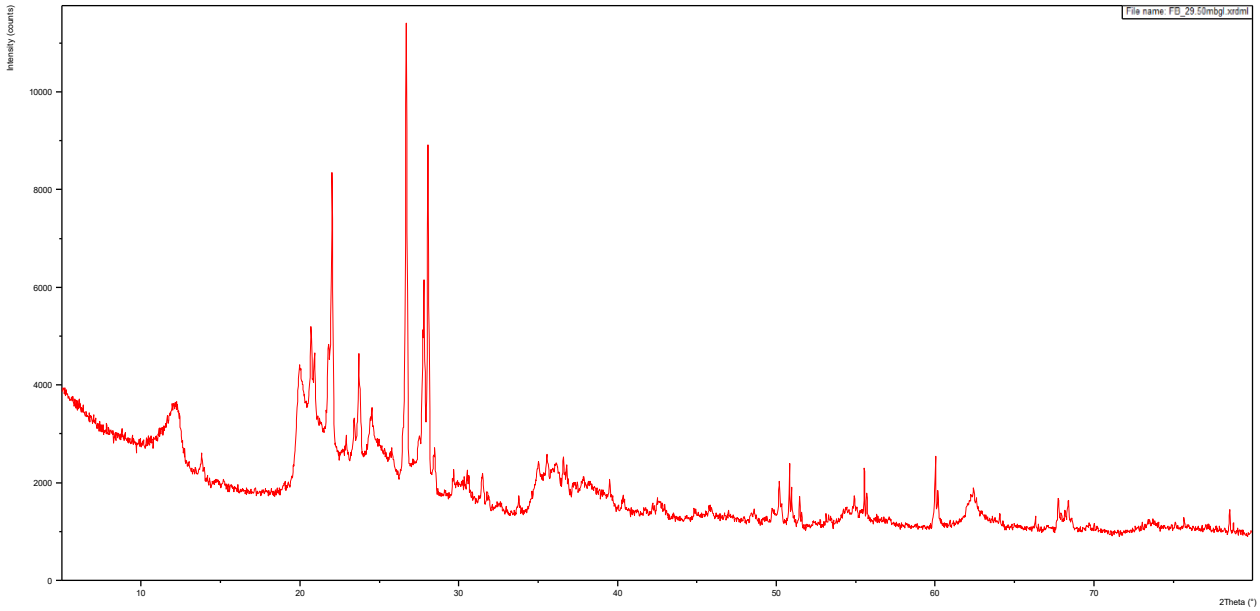

Figure 4.114. Ferrybank 29.50mbgl XRD Diffractogram.

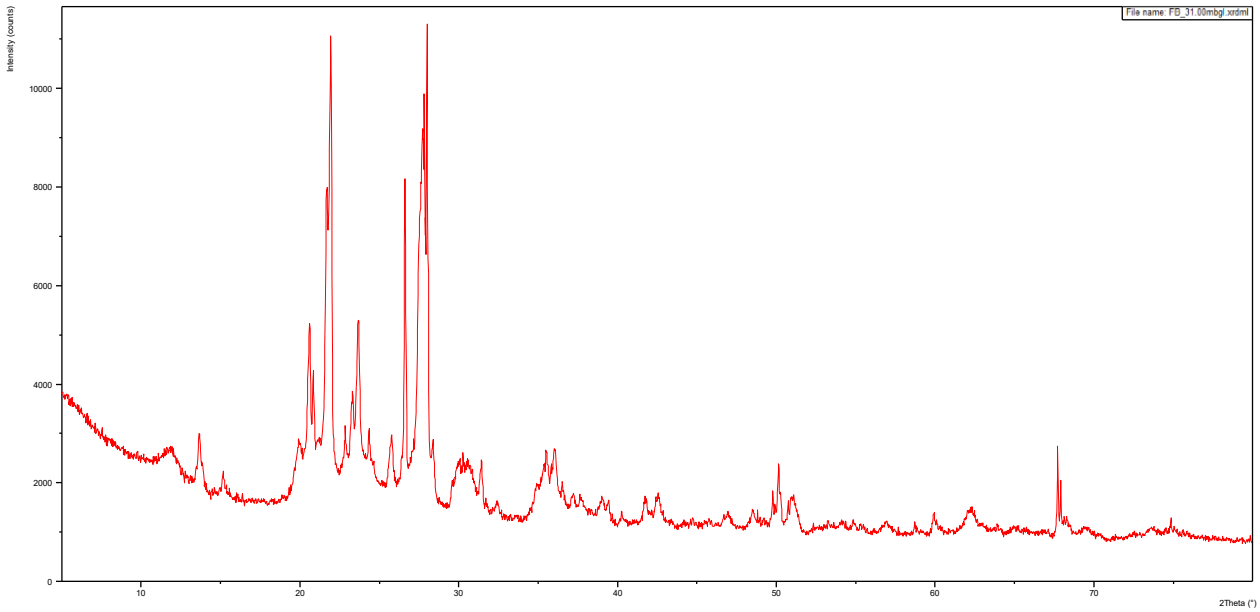

Figure 4.115. Ferrybank 31.00mbgl XRD Diffractogram.

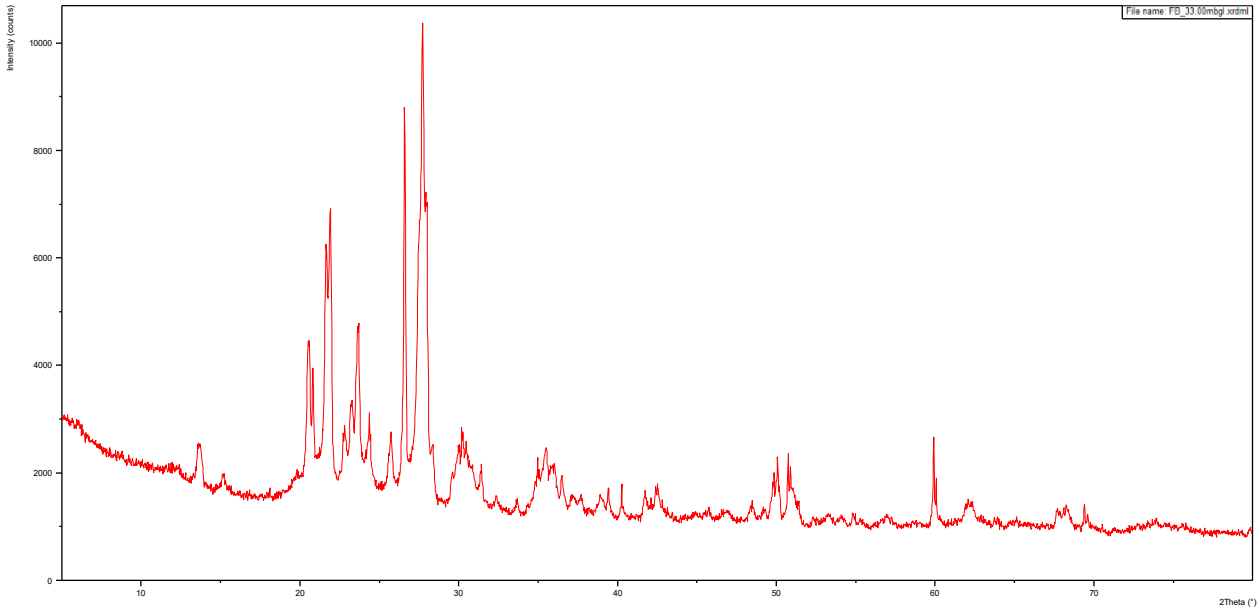

Figure 4.116. Ferrybank 33.00mbgl XRD Diffractogram.

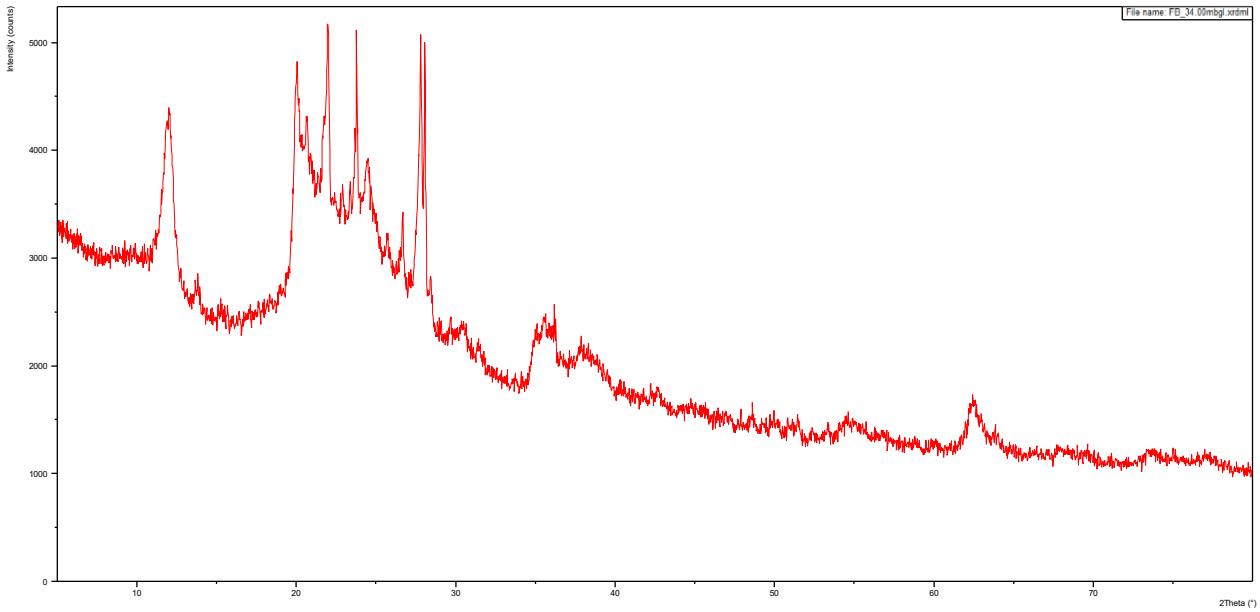

Figure 4.117. Ferrybank 34.00mbgl XRD Diffractogram.

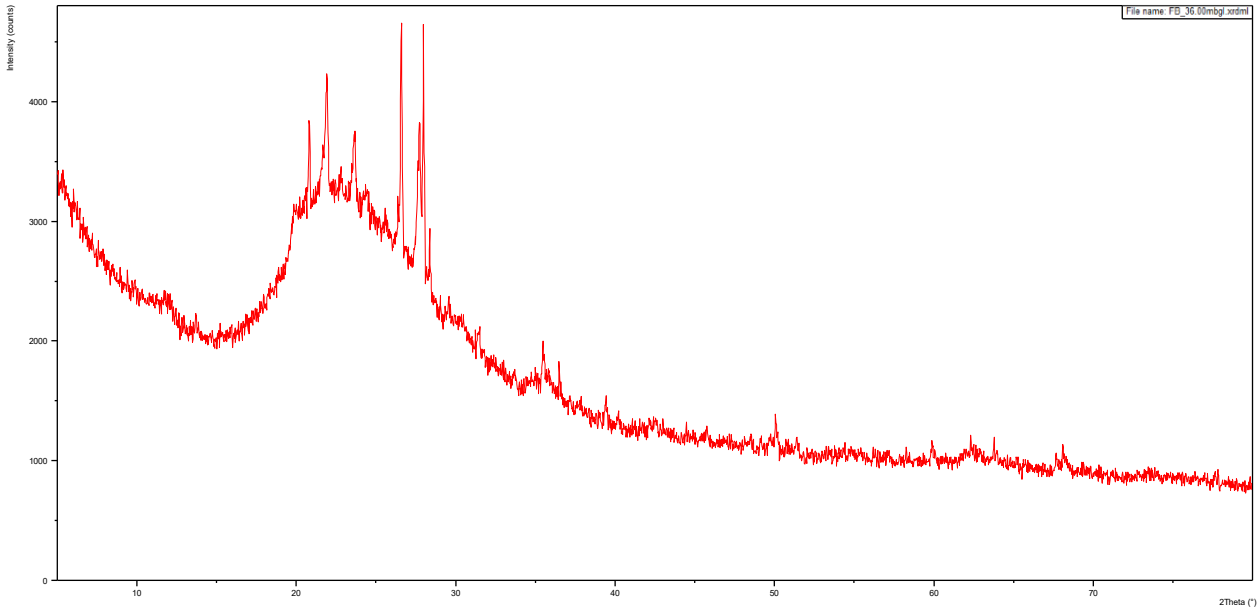

Figure 4.118. Ferrybank 36.00mbgl XRD Diffractogram.

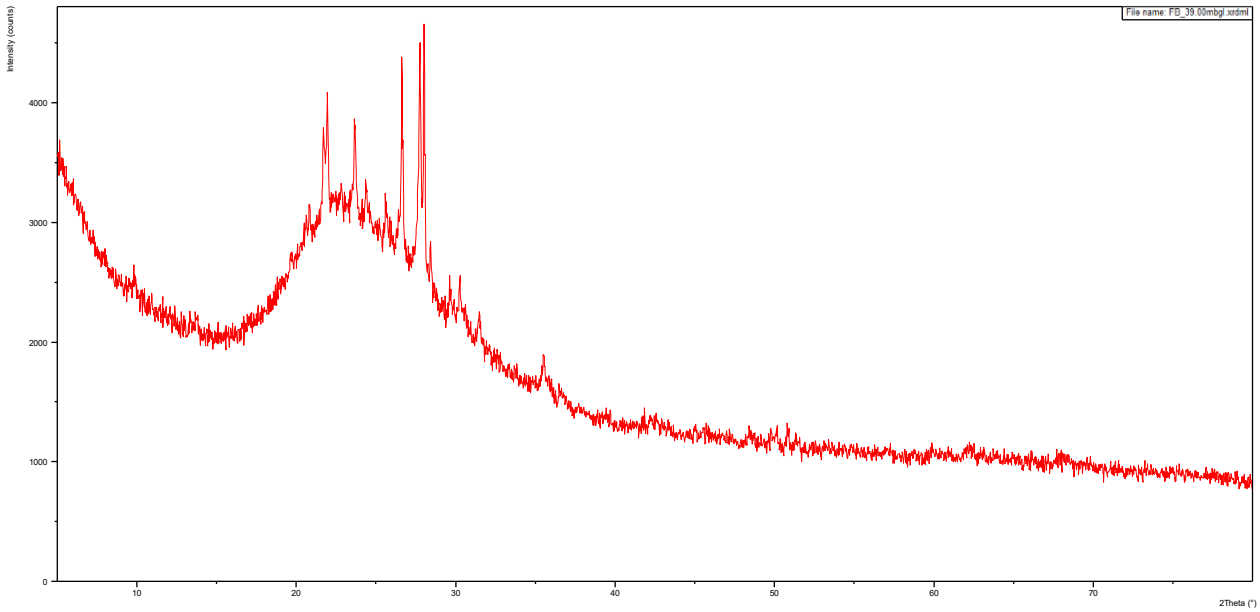

Figure 4.119. Ferrybank 39.00mbgl XRD Diffractogram.

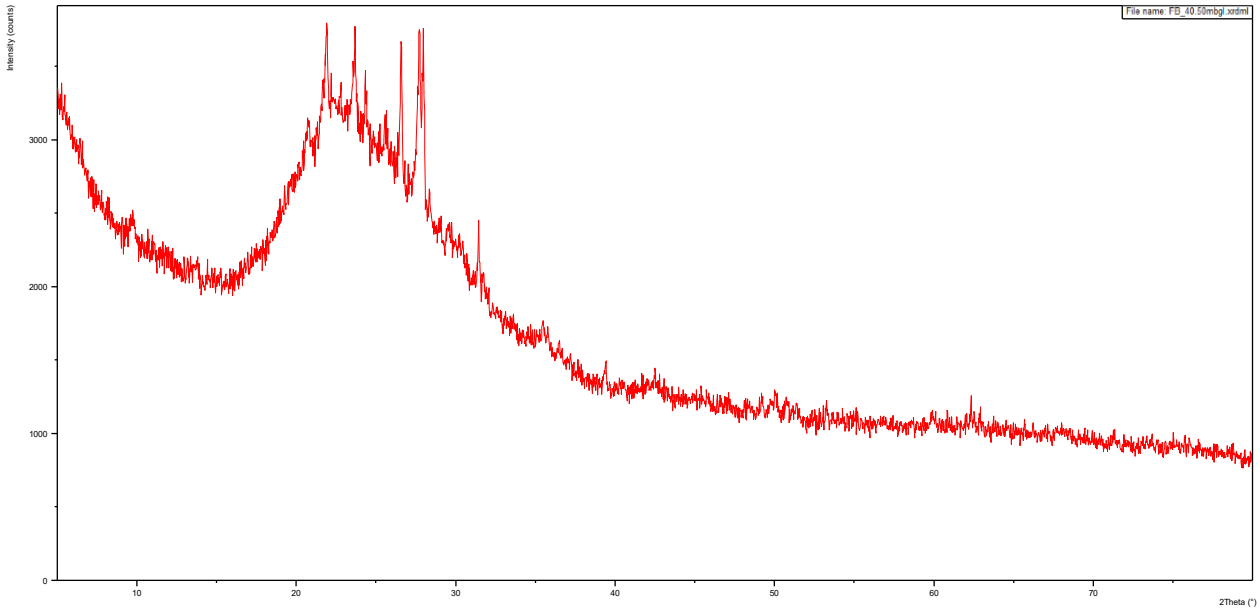

Figure 4.120. Ferrybank 40.50mbgl XRD Diffractogram.

Appendix 4. Stratigraphic Logs.

- Legend.

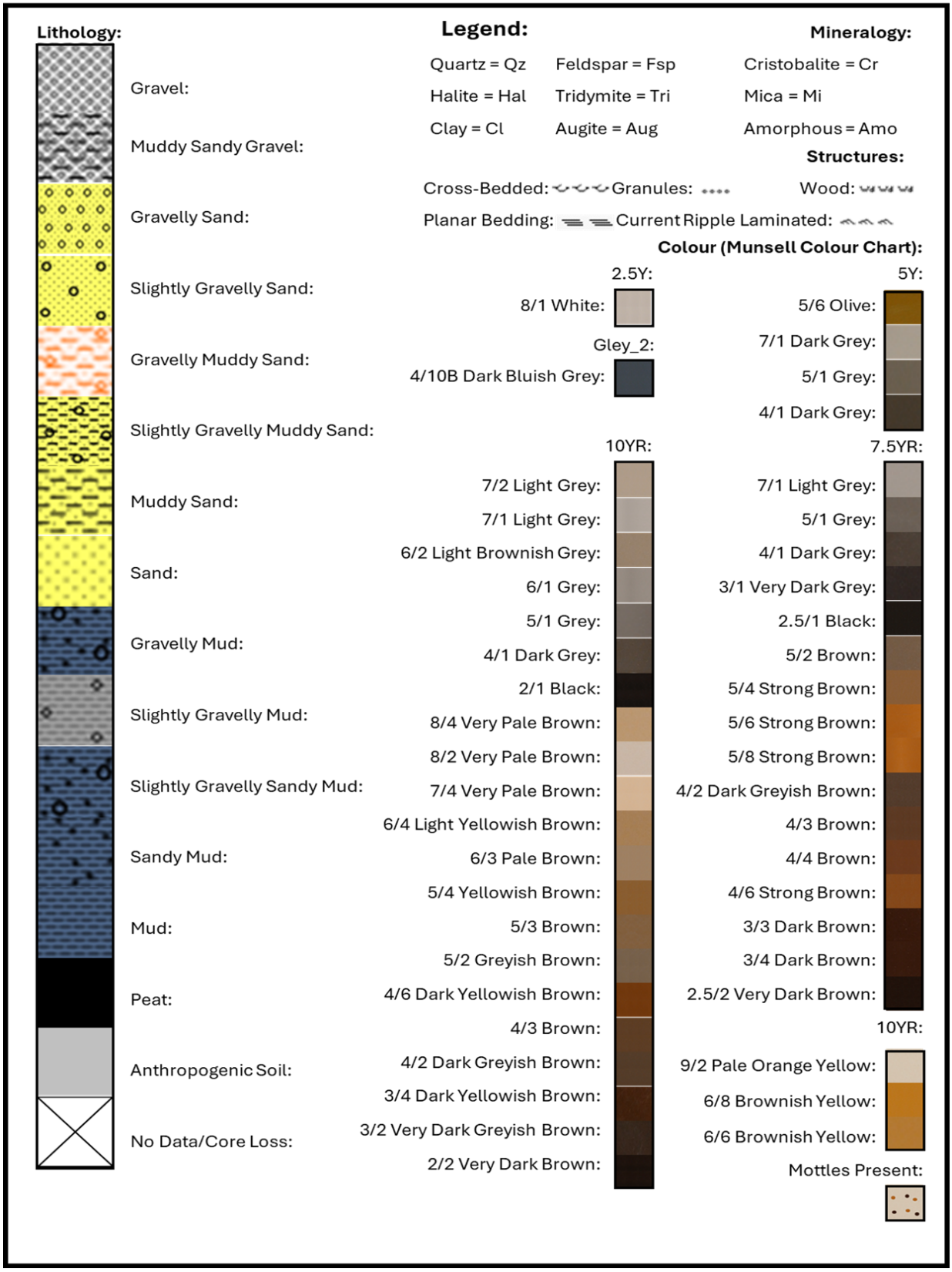

Figure 4.121. Lithologic Log Legend.

- 20-1006.

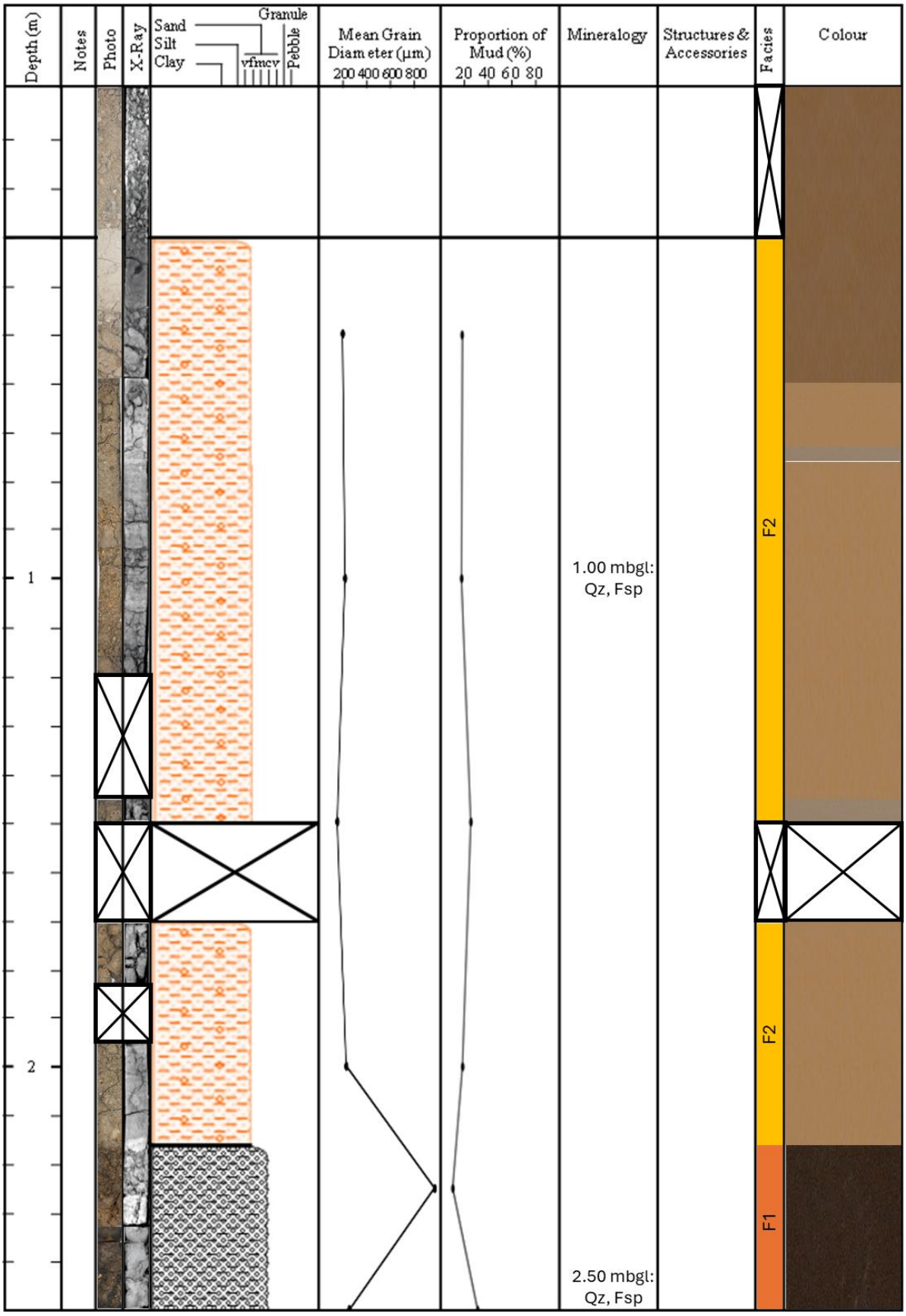

Figure 4.122. 20-1006 Core Log: 0.00-2.50 mbgl.

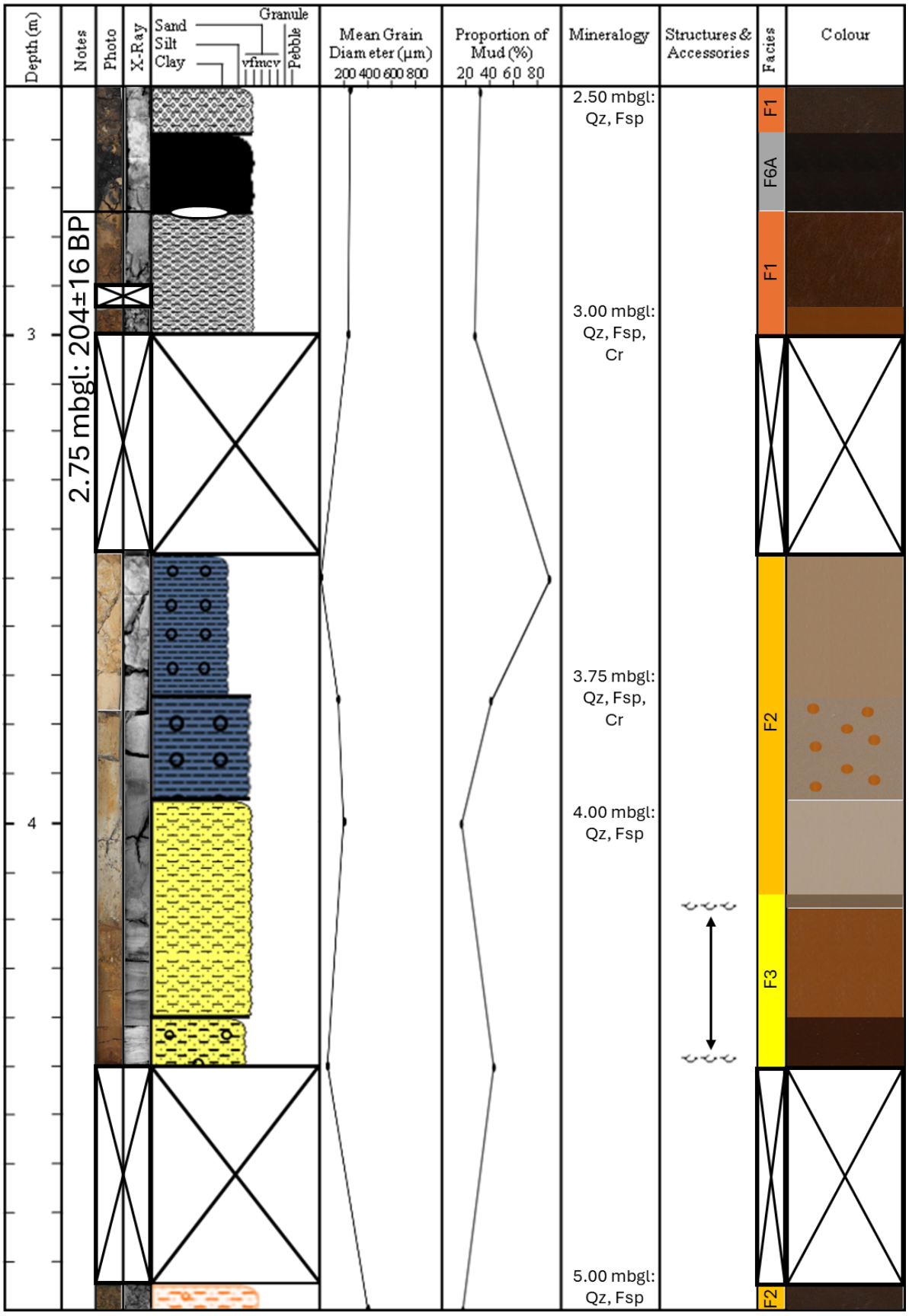

Figure 4.123. 20-1006 Core Log: 2.50-5.00 mbgl.

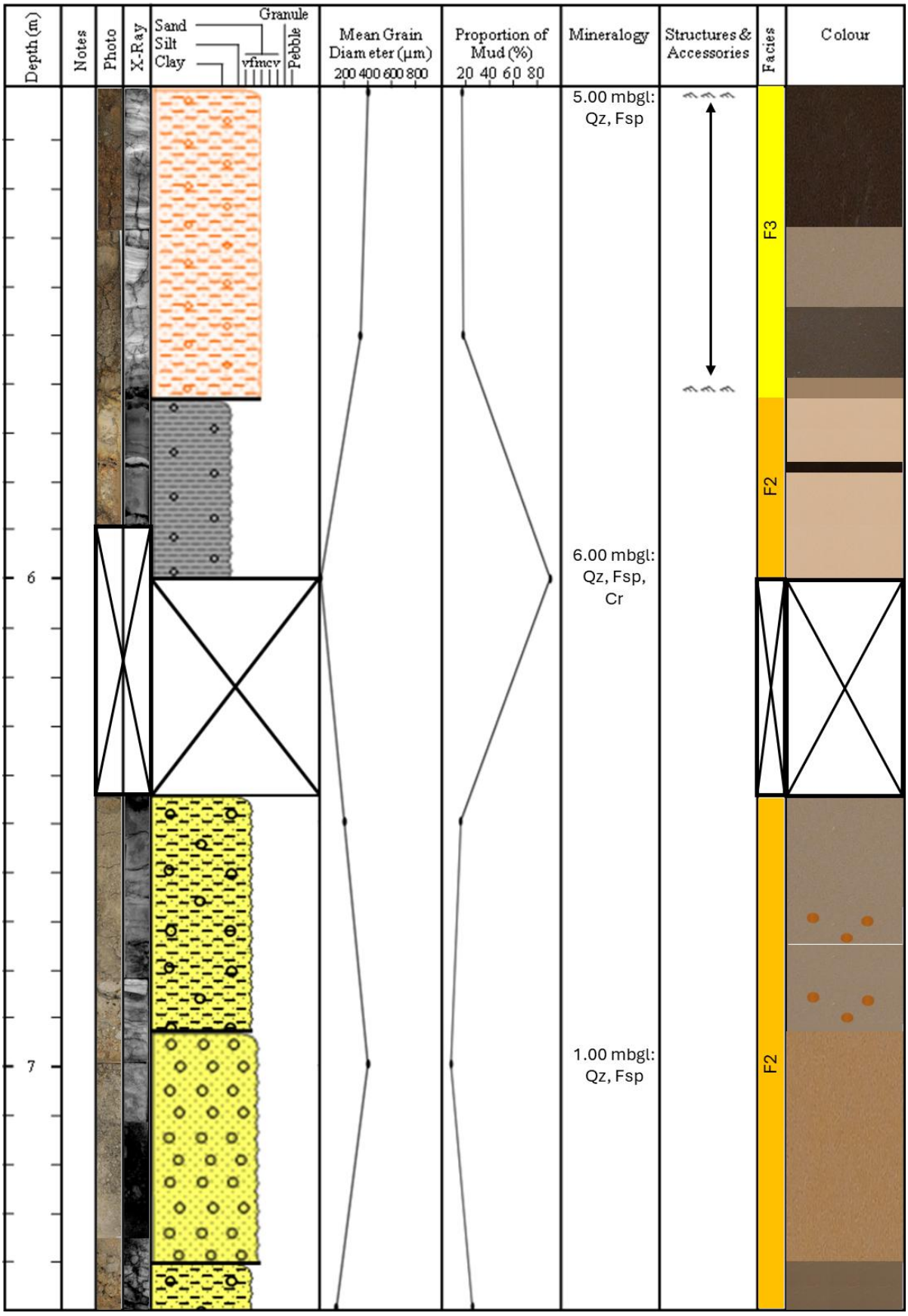

Figure 4.124. 20-1006 Core Log: 5.00-7.50 mbgl.

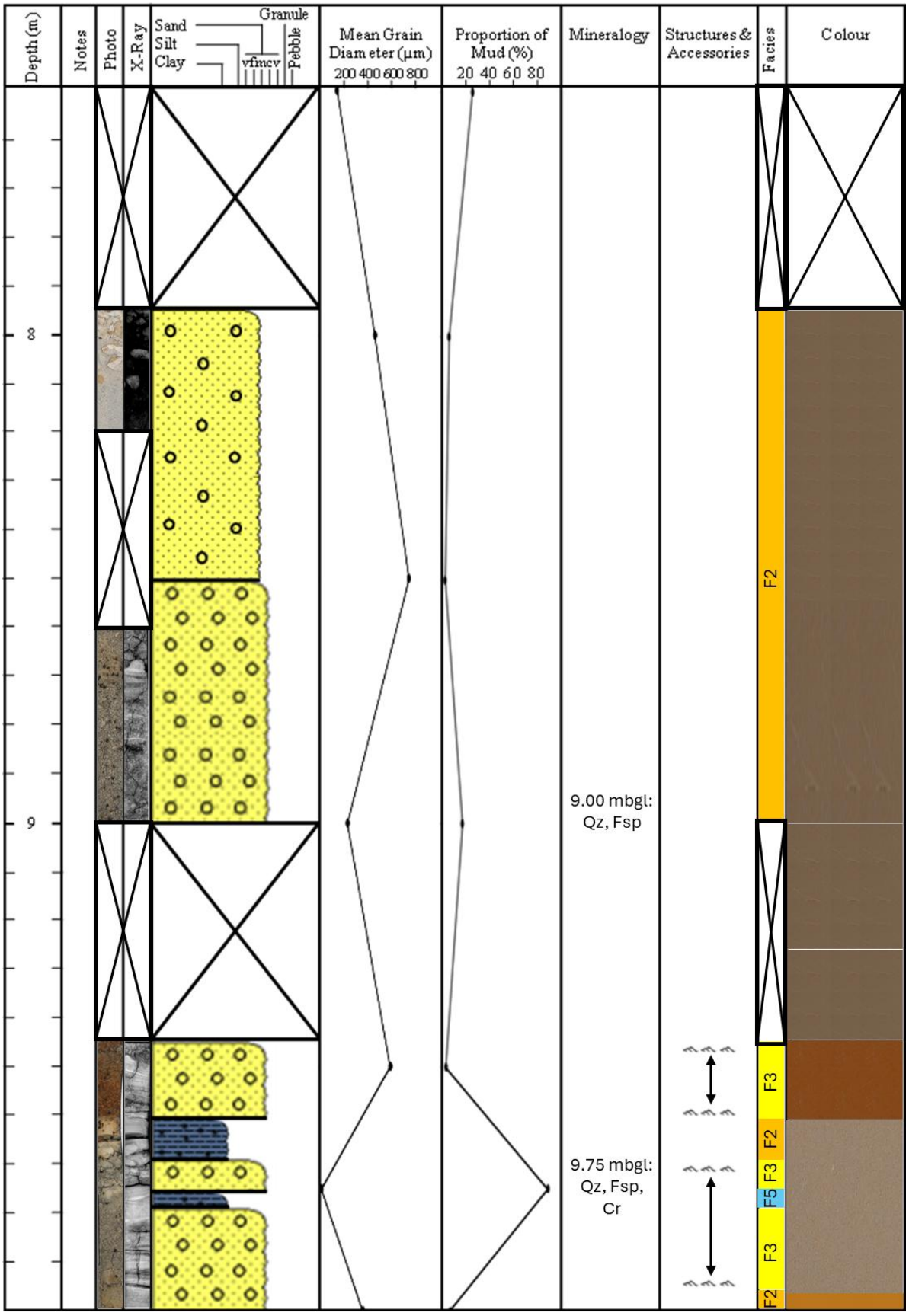

Figure 4.125. 20-1006 Core Log: 7.50-10.00 mbgl.

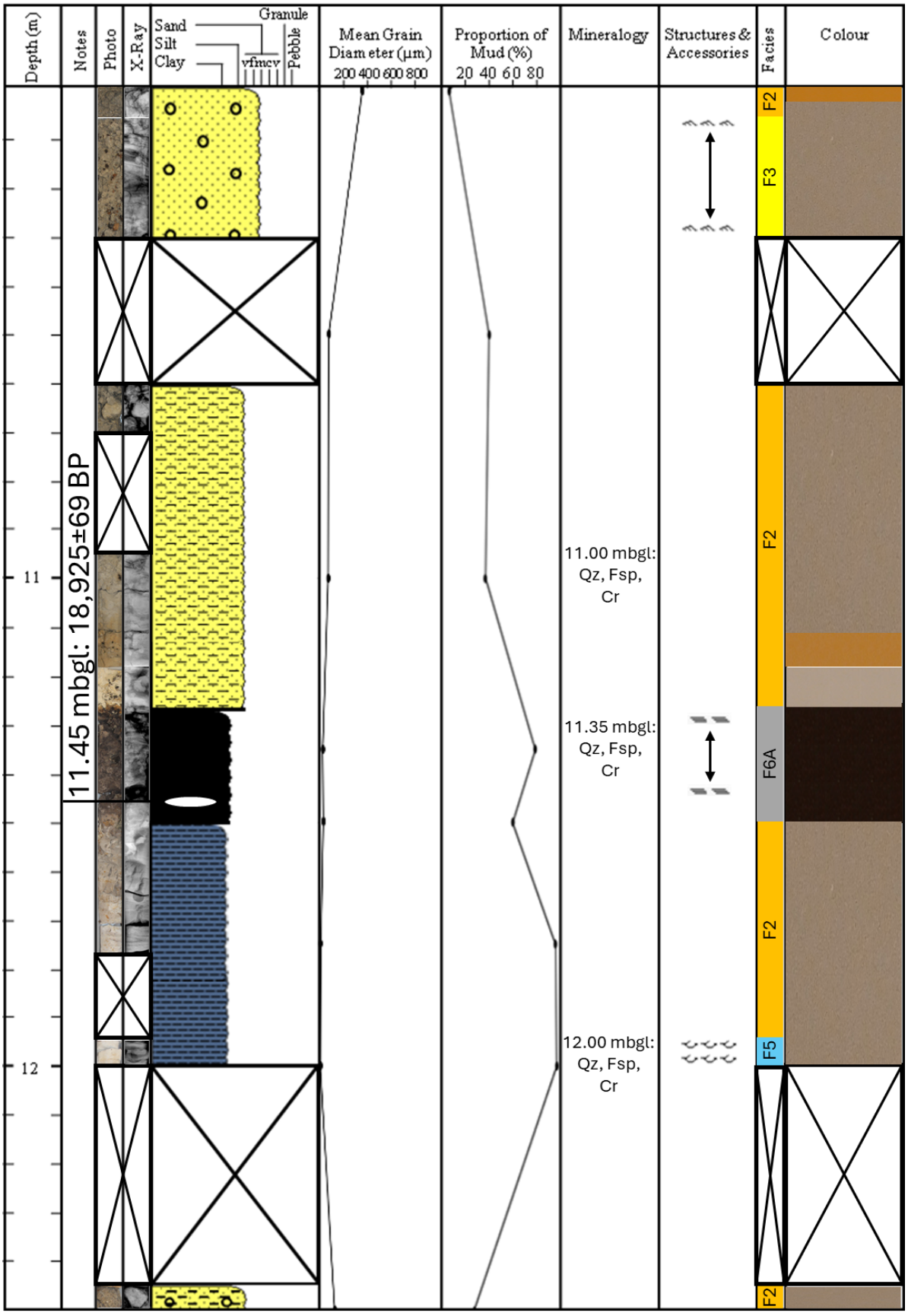

Figure 4.126. 20-1006 Core Log: 10.00-12.50 mbgl.

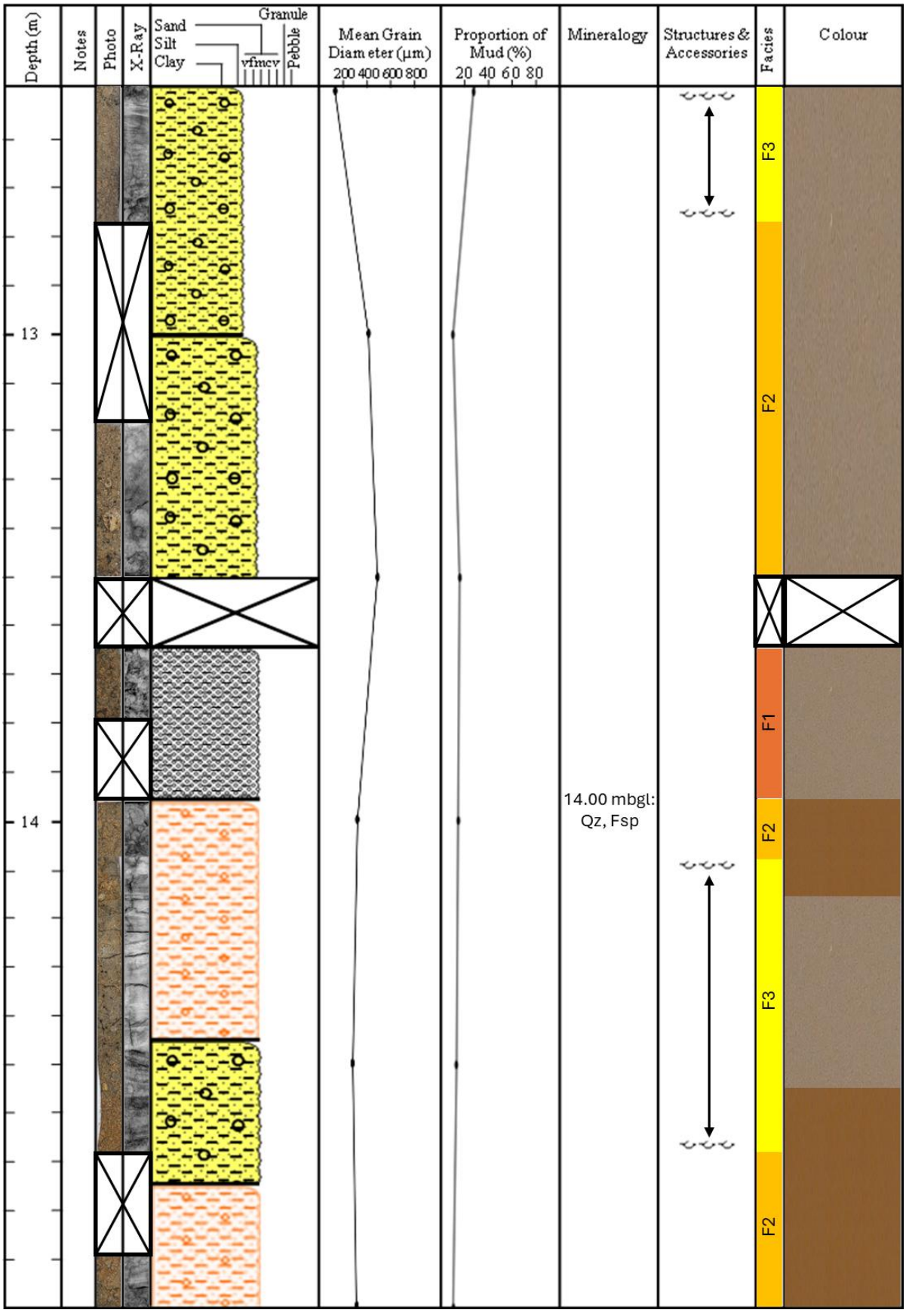

Figure 4.127. 20-1006 Core Log: 12.50-15.00 mbgl.

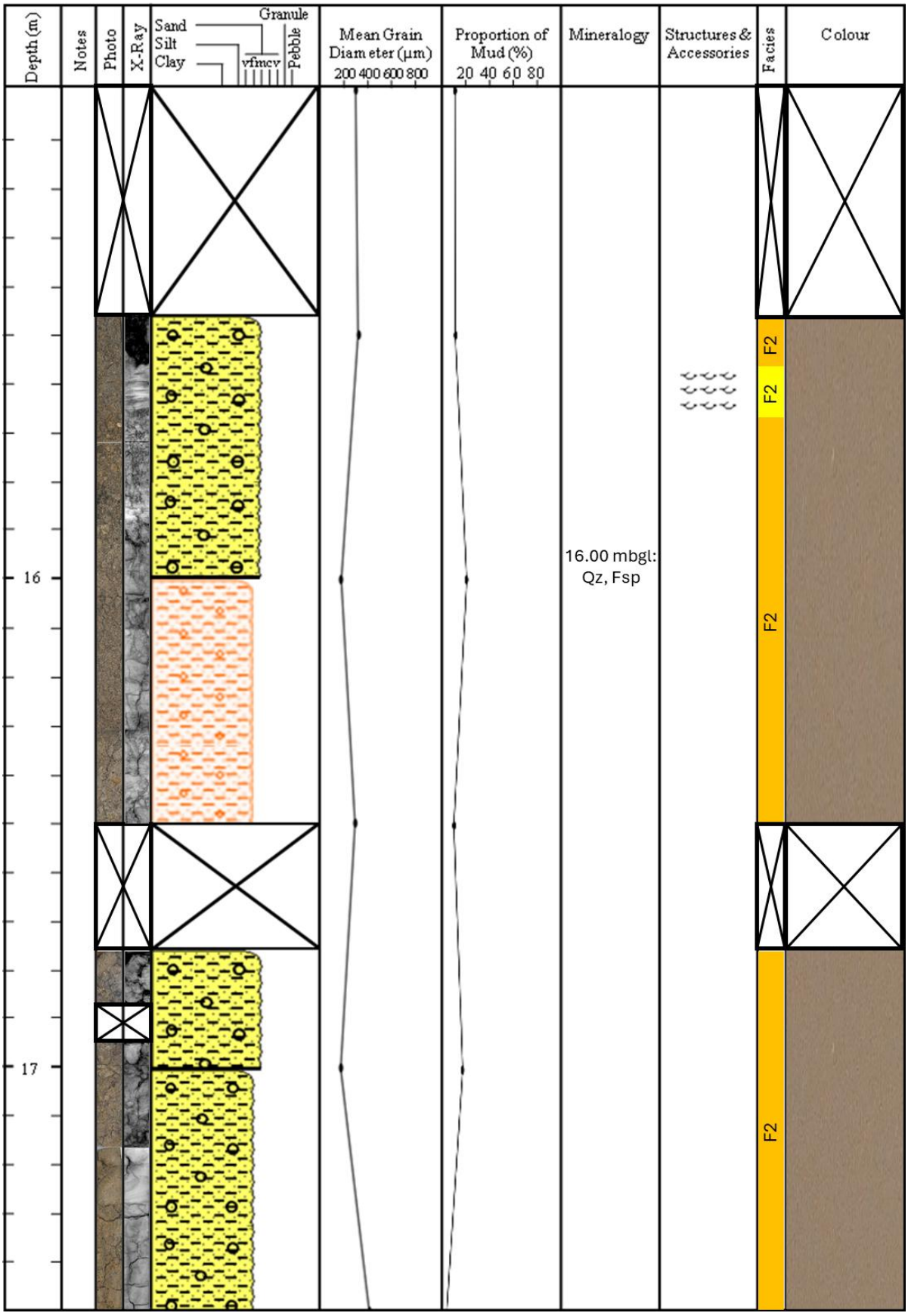

Figure 4.128. 20-1006 Core Log: 15.00-17.50 mbgl.

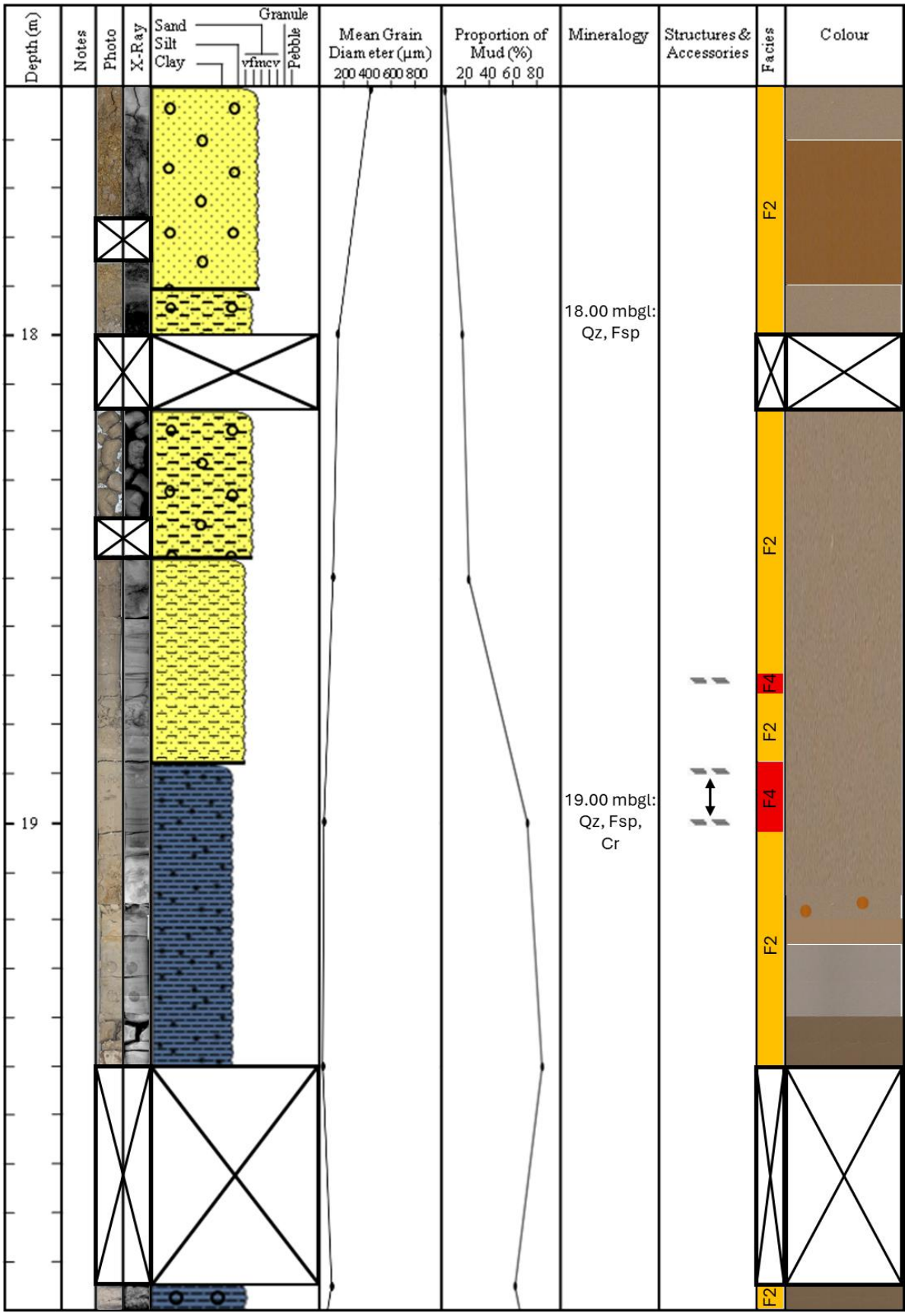

Figure 4.129. 20-1006 Core Log: 17.50-20.00 mbgl.

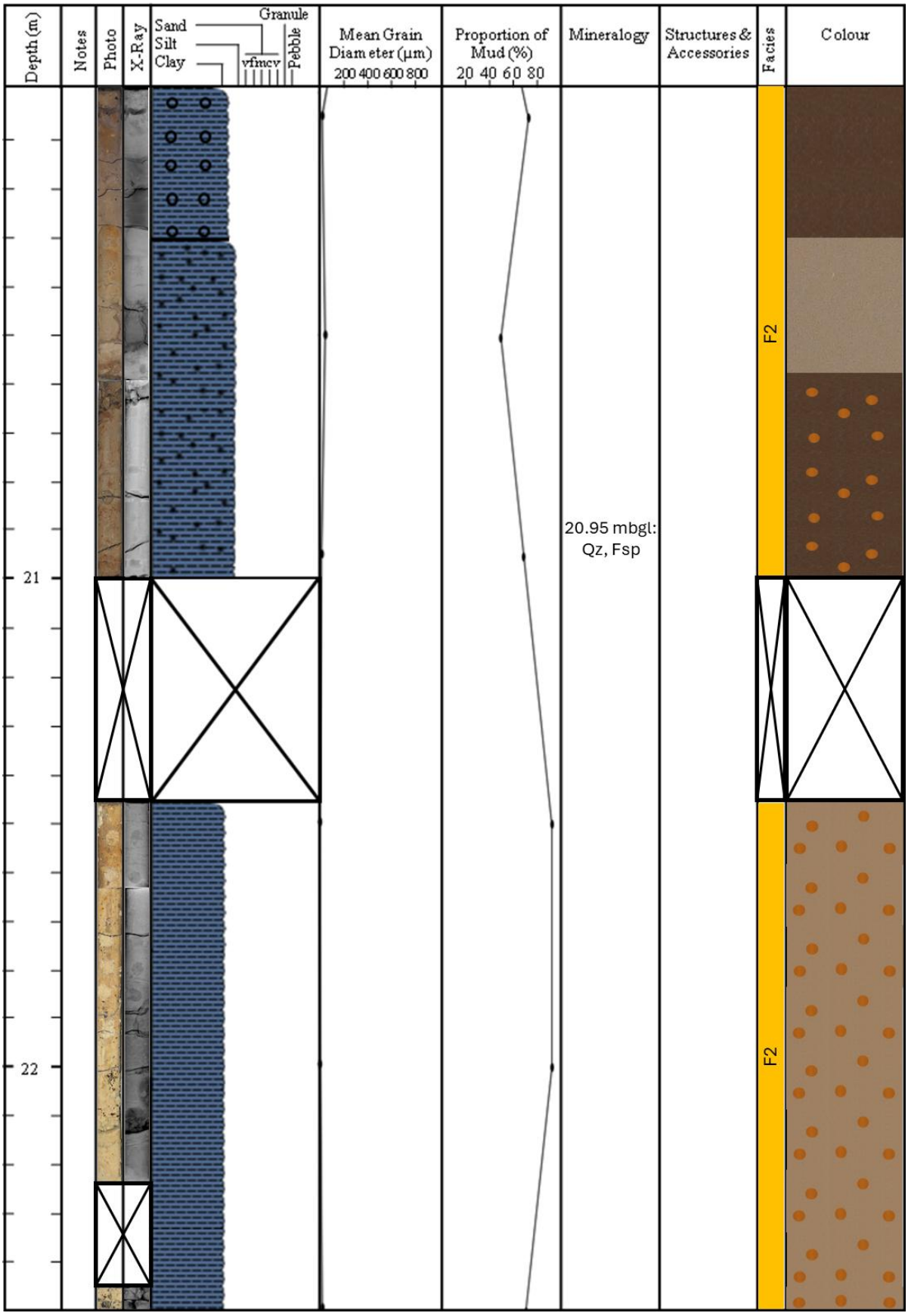

Figure 4.130. 20-1006 Core Log: 20.00-22.50 mbgl.

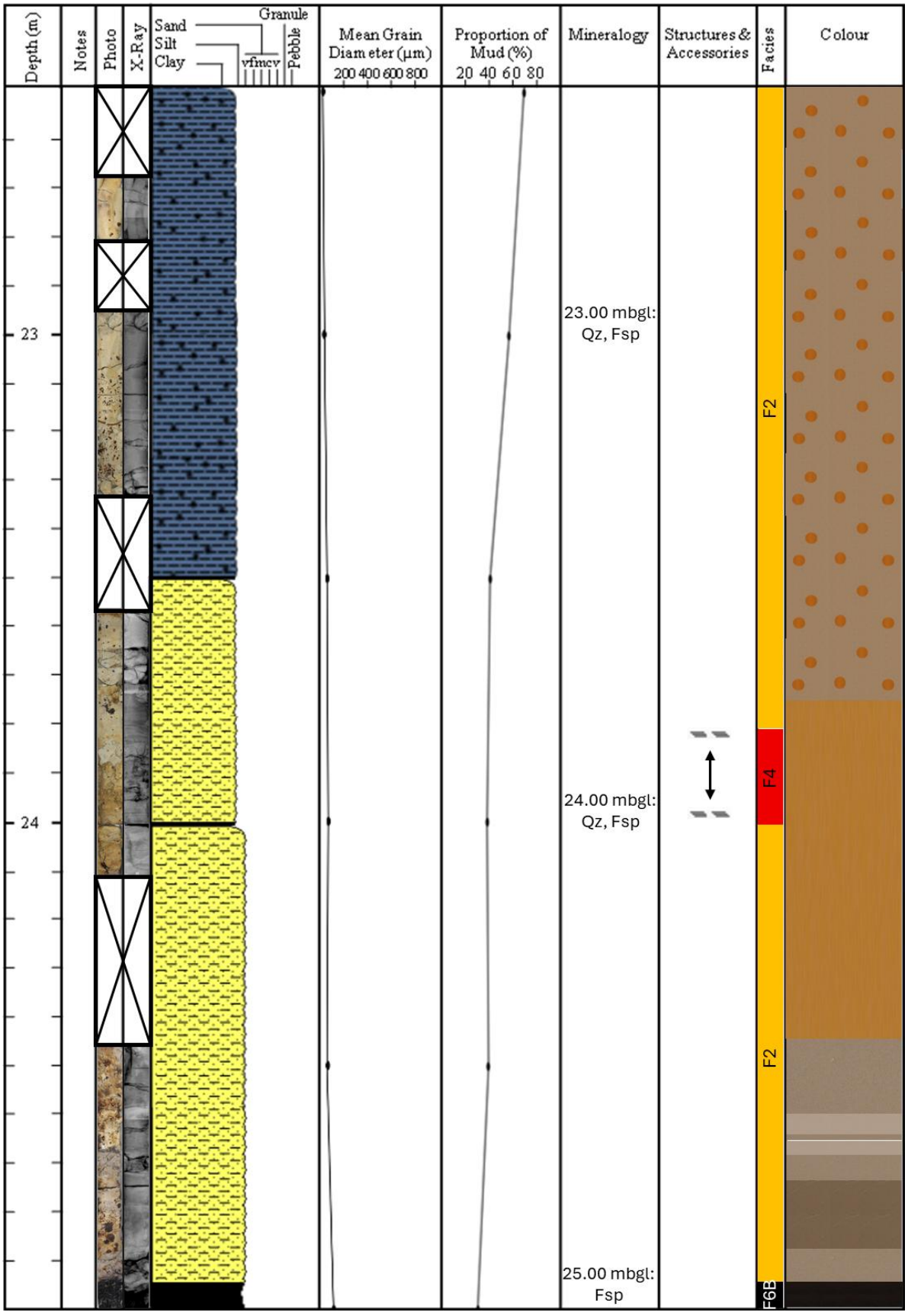

Figure 4.131. 20-1006 Core Log: 22.50-25.00 mbgl.

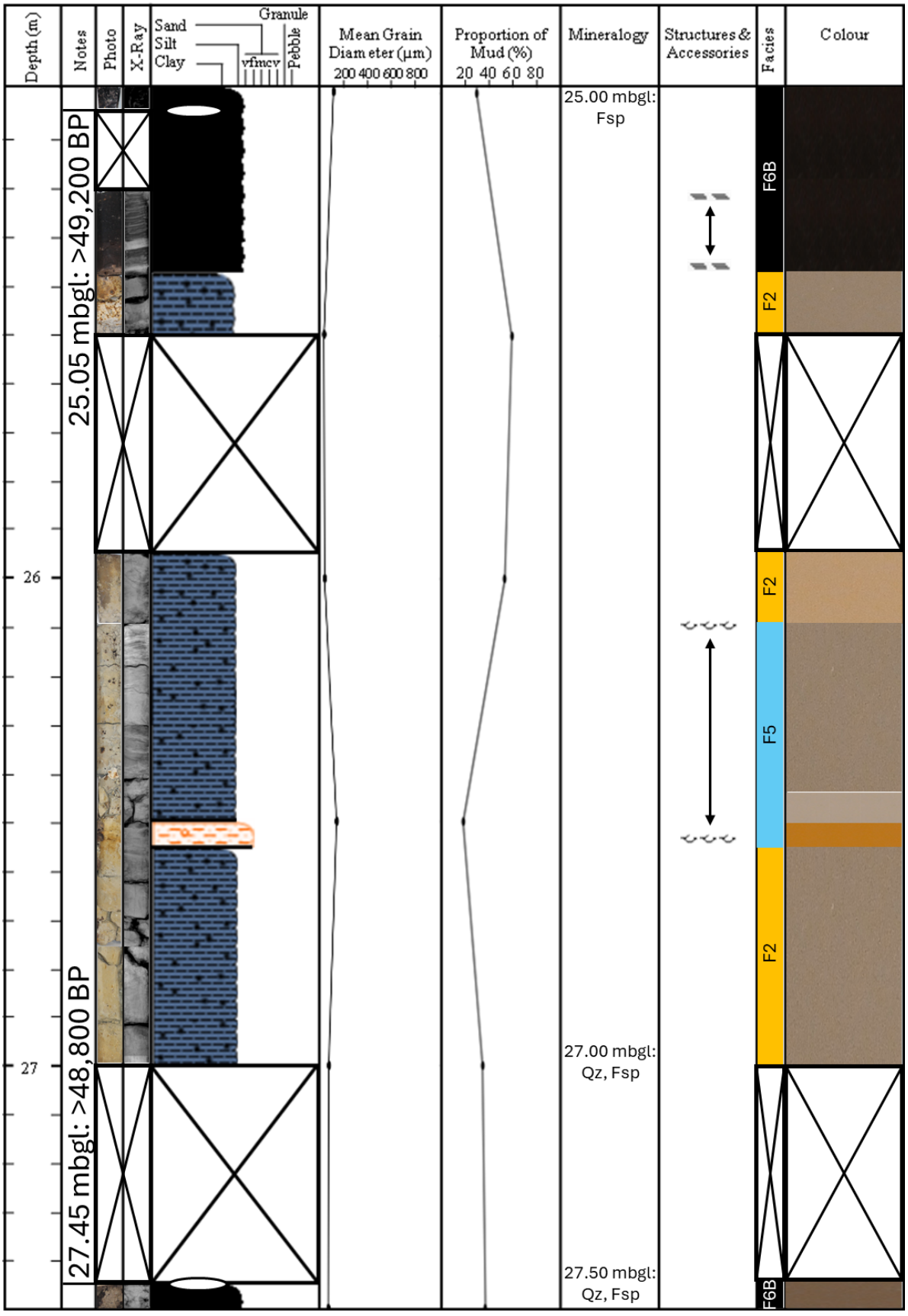

Figure 4.132. 20-1006 Core Log: 25.00-27.50 mbgl.

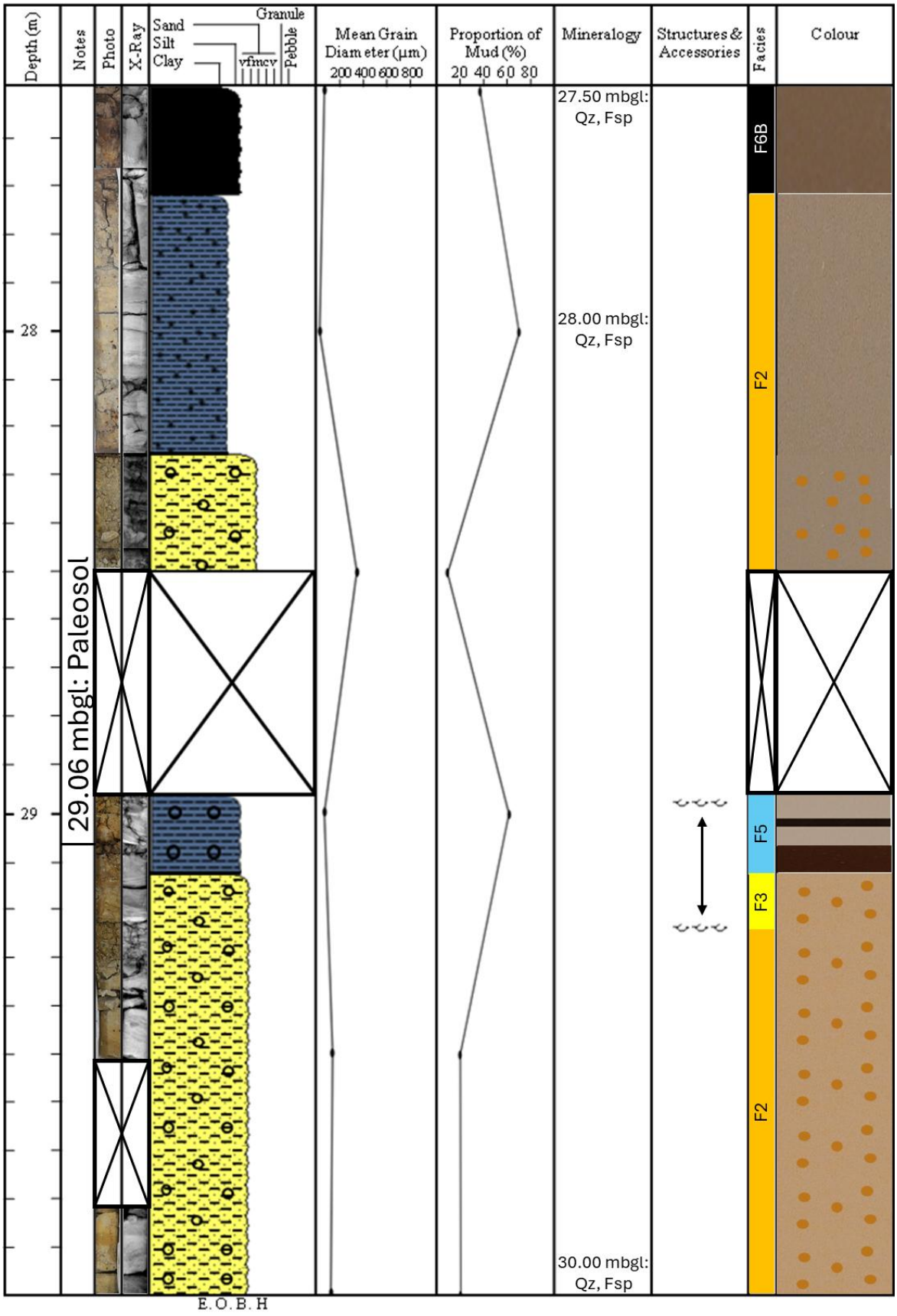

Figure 4.133. 20-1006 Core Log: 27.50-30.00 mbgl.

- 21-0437.

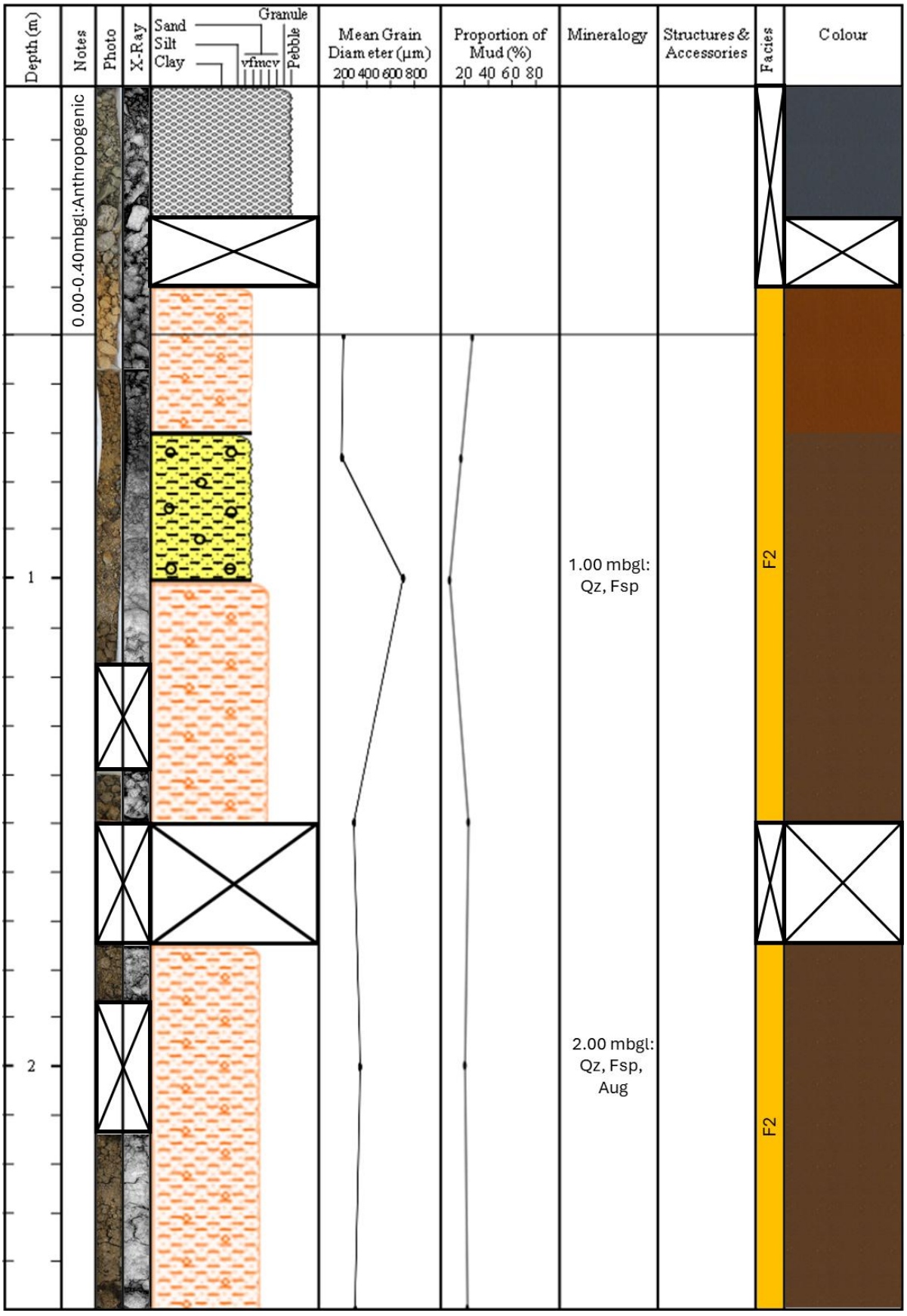

Figure 4.134. 21-0437 Core Log: 0.00-2.50 mbgl.

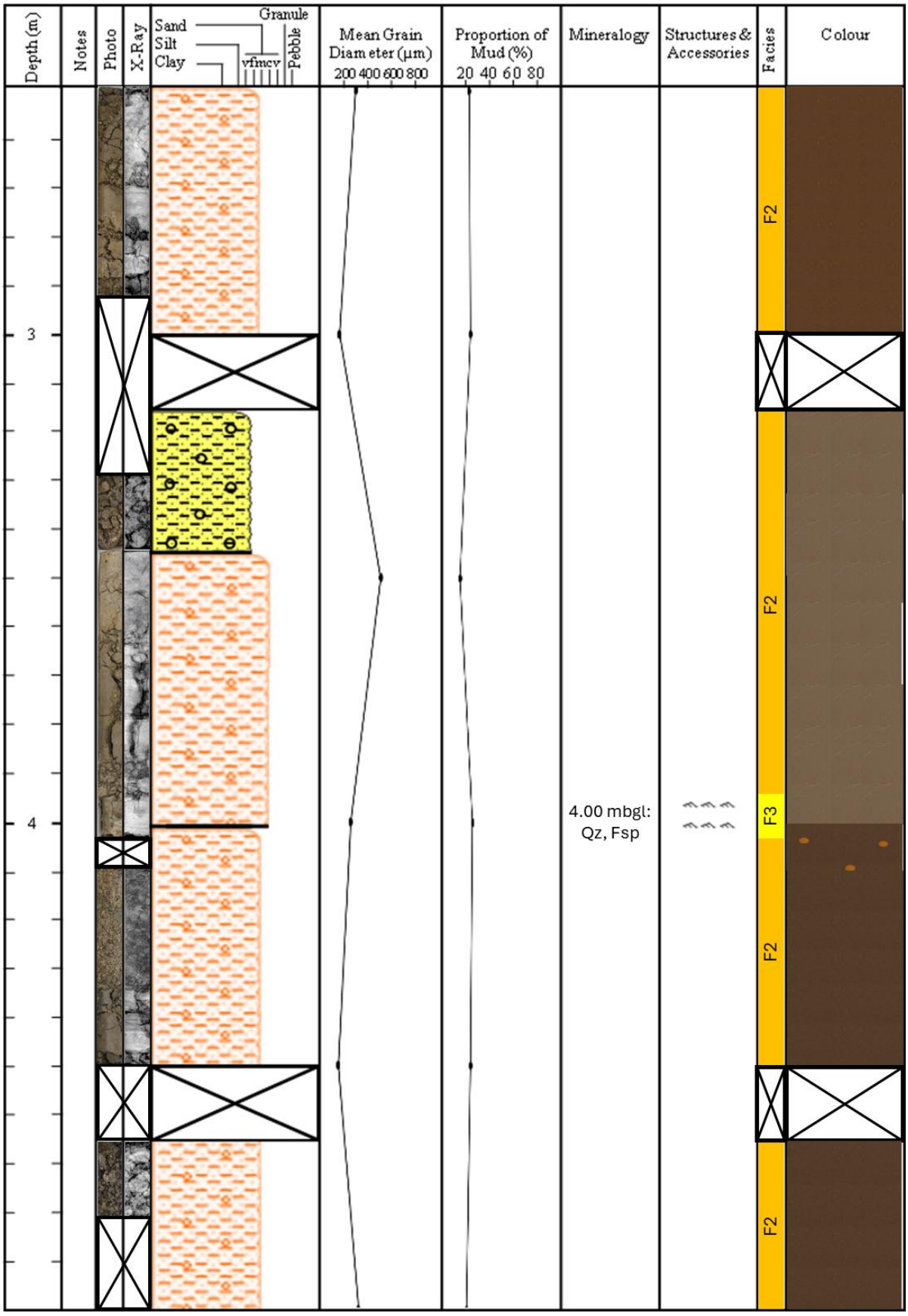

Figure 4.135. 21-0437 Core Log: 2.50-5.00 mbgl.

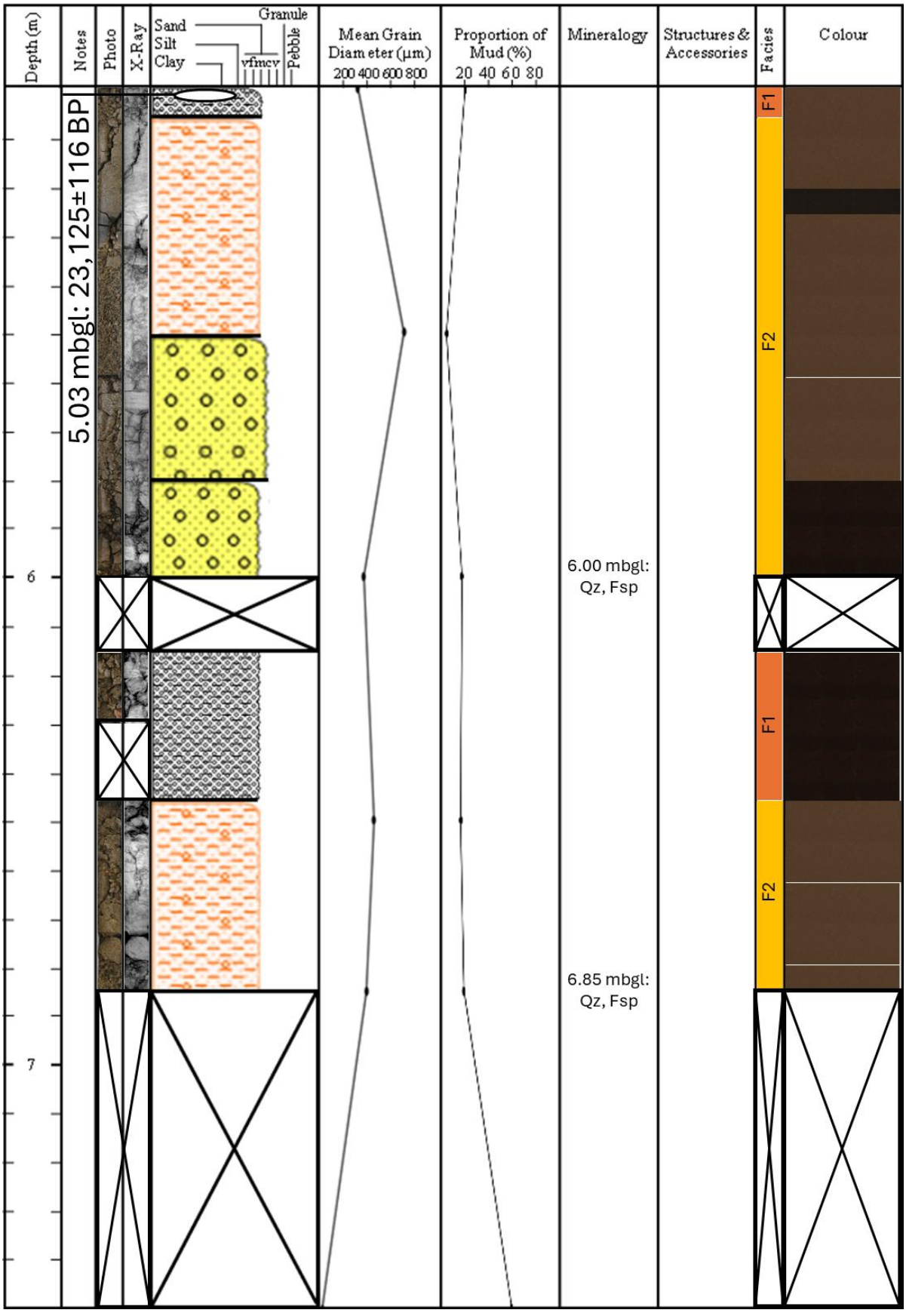

Figure 4.136. 21-0437 Core Log: 5.00-7.50 mbgl.

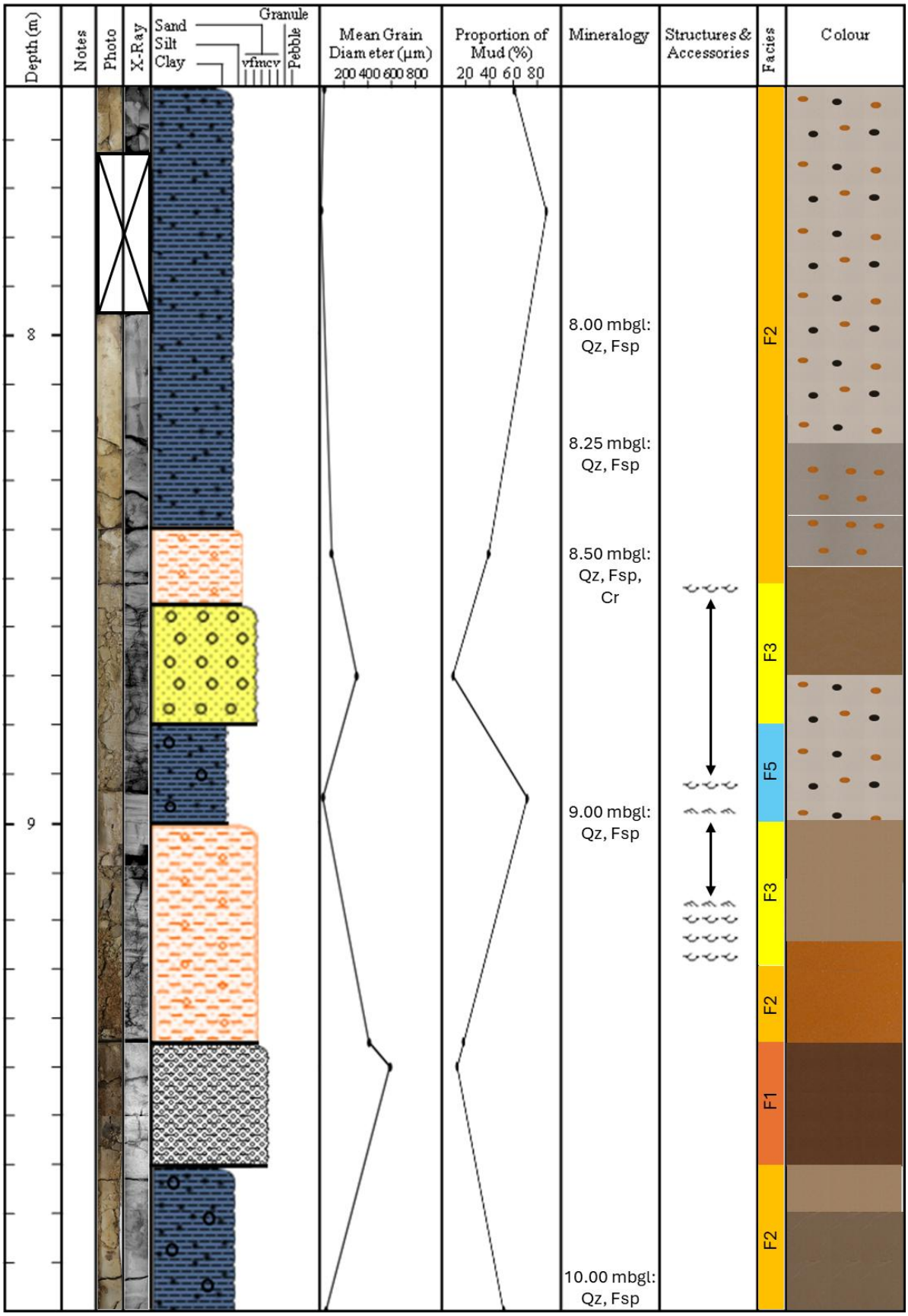

Figure 4.137. 21-0437 Core Log: 7.50-10.00 mbgl.

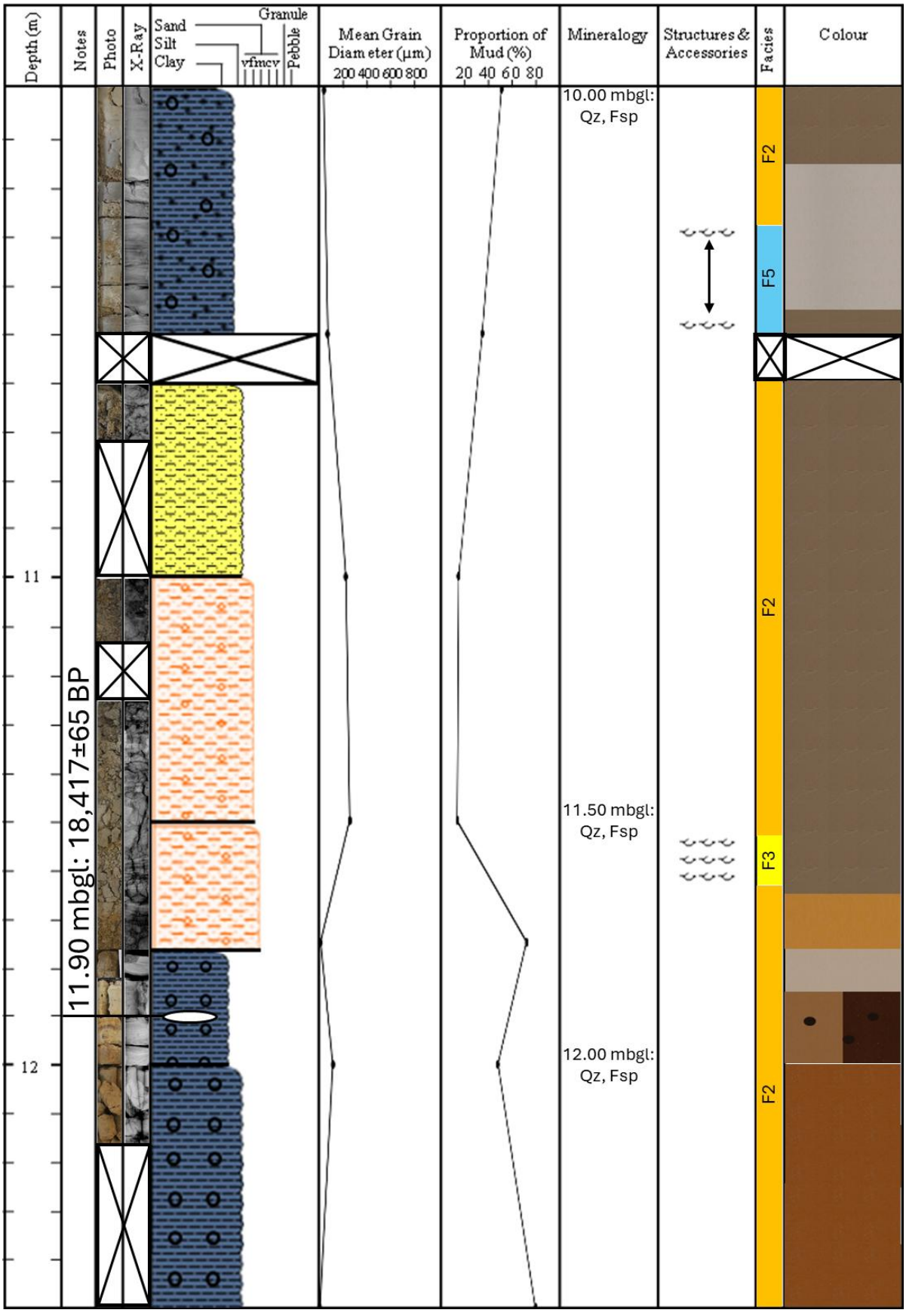

Figure 4.138. 21-0437 Core Log: 10.00-12.50 mbgl.

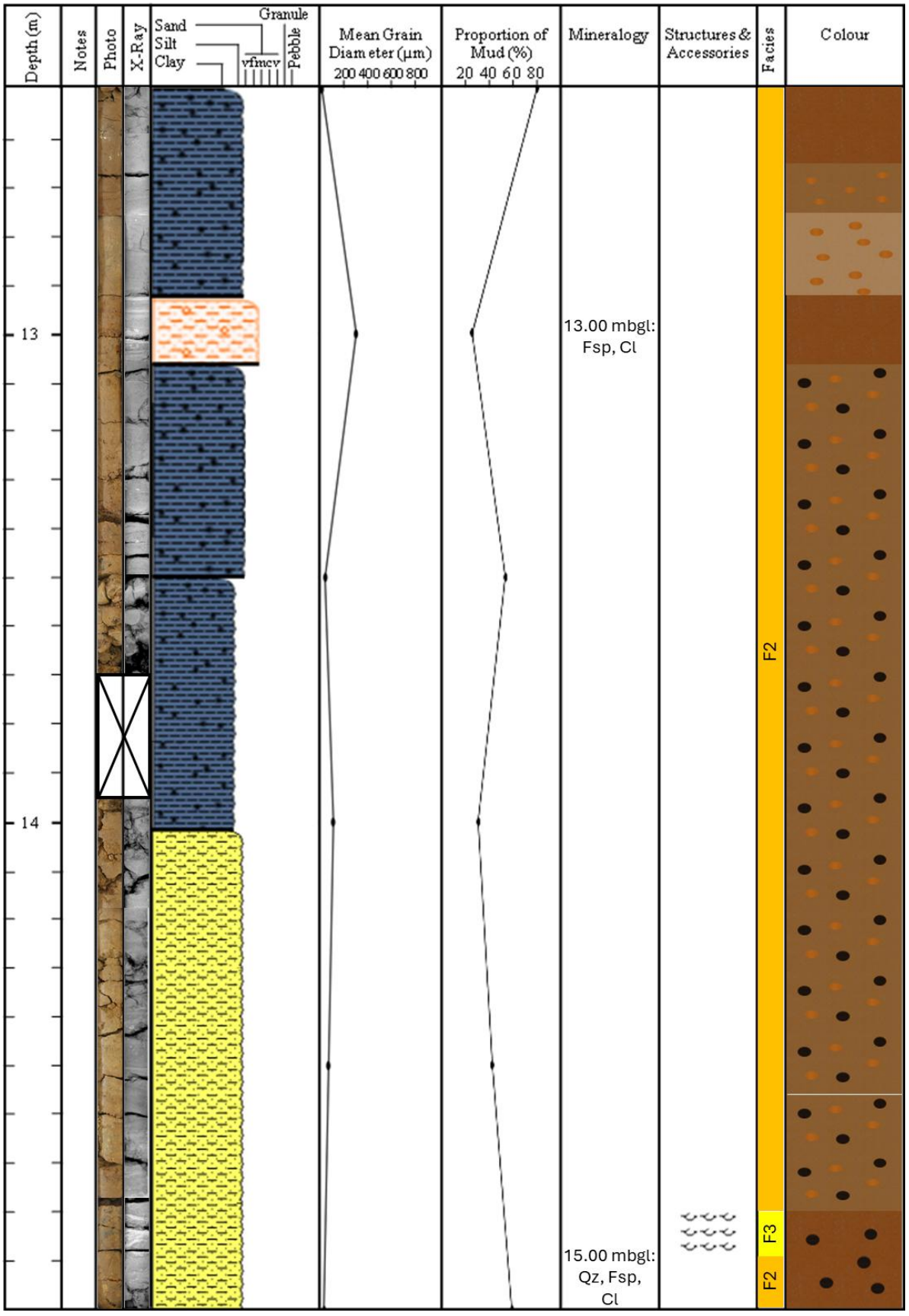

Figure 4.139. 21-0437 Core Log: 12.50-15.00 mbgl.

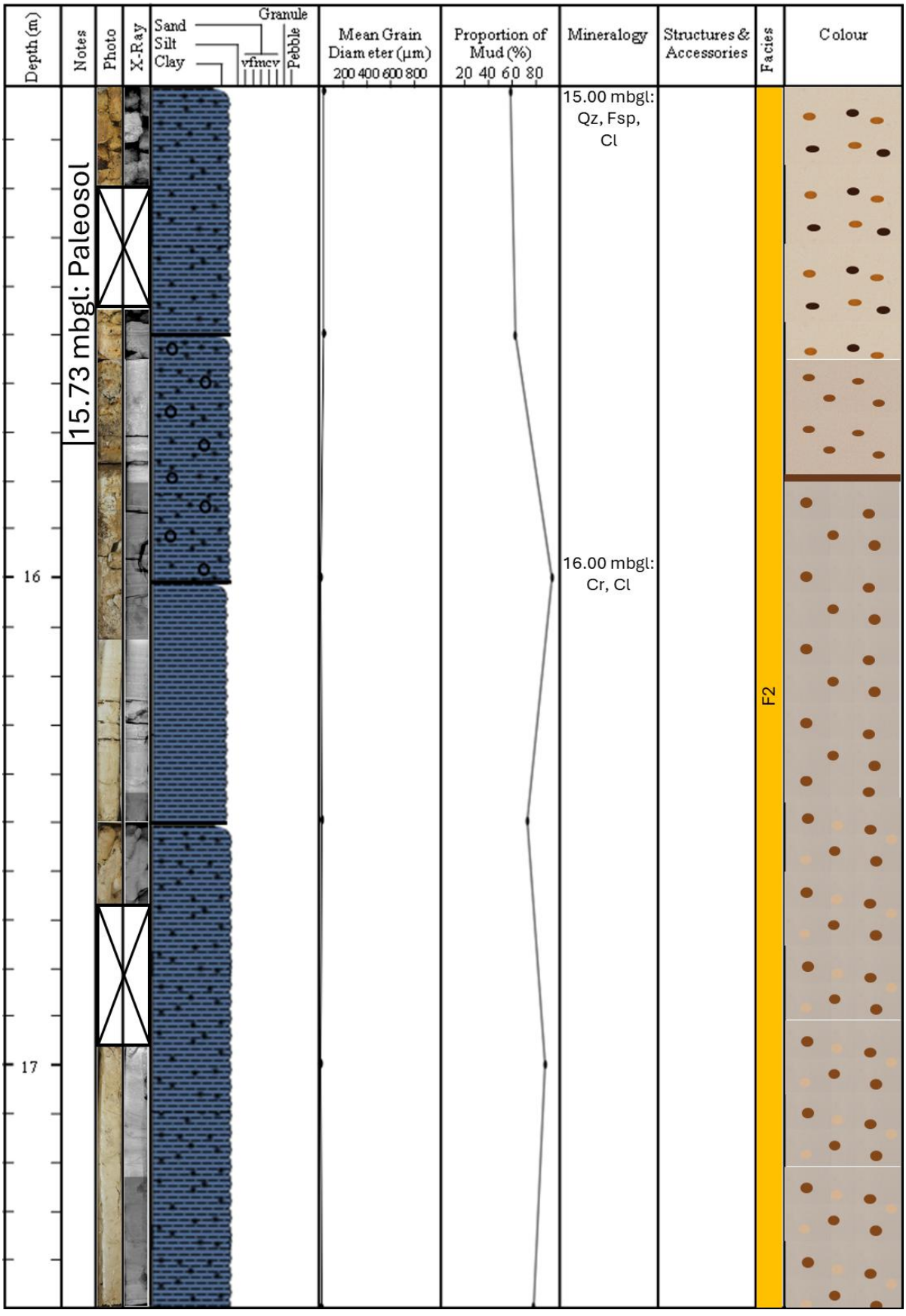

Figure 4.140. 21-0437 Core Log: 15.00-17.50 mbgl.

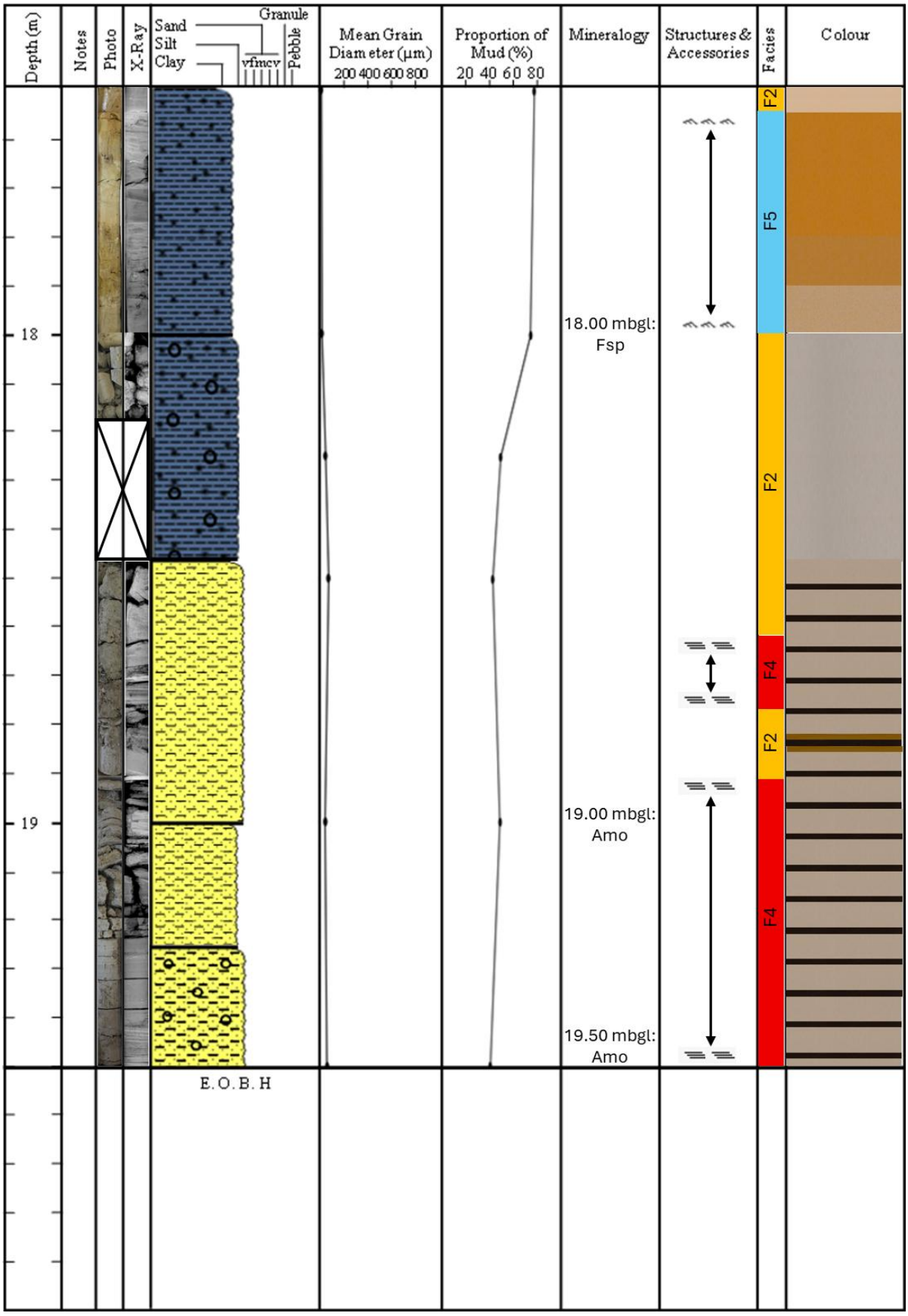

Figure 4.141. 21-0437 Core Log: 17.50-19.50 mbgl.

- Ferrybank.

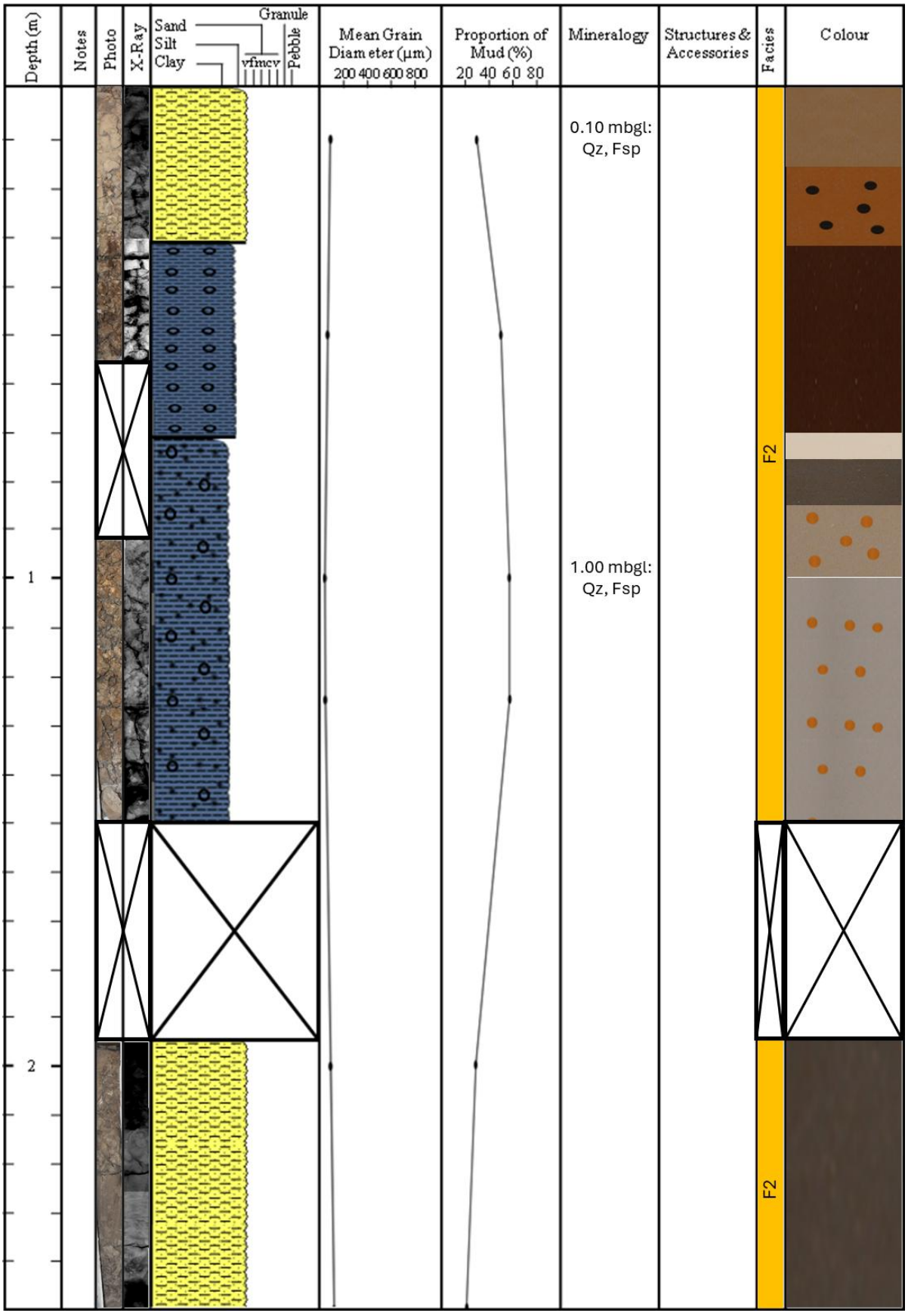

Figure 4.142. Ferrybank Core Log: 0.00-2.50 mbgl.

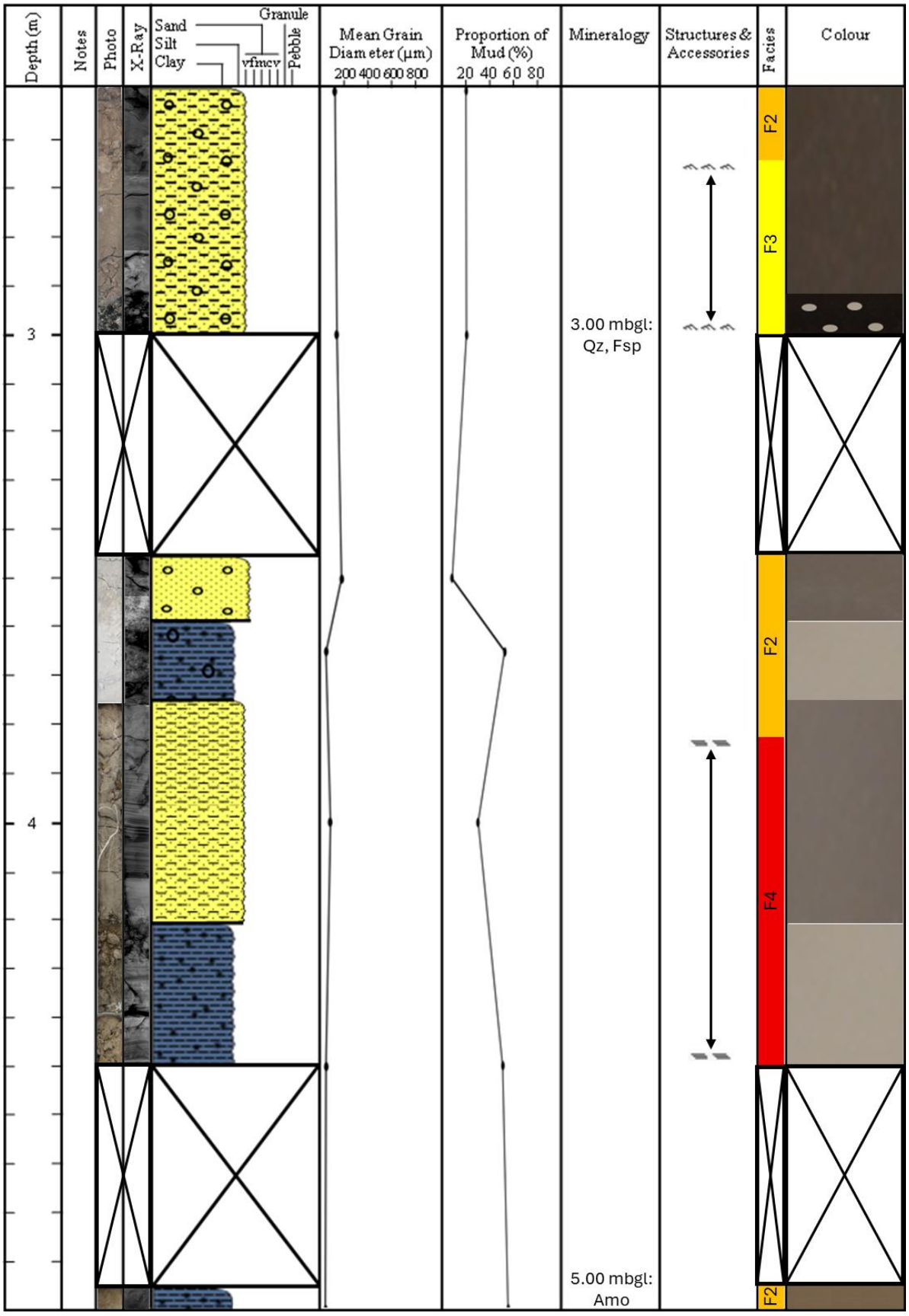

Figure 4.143. Ferrybank Core Log: 2.50-5.00 mbgl.

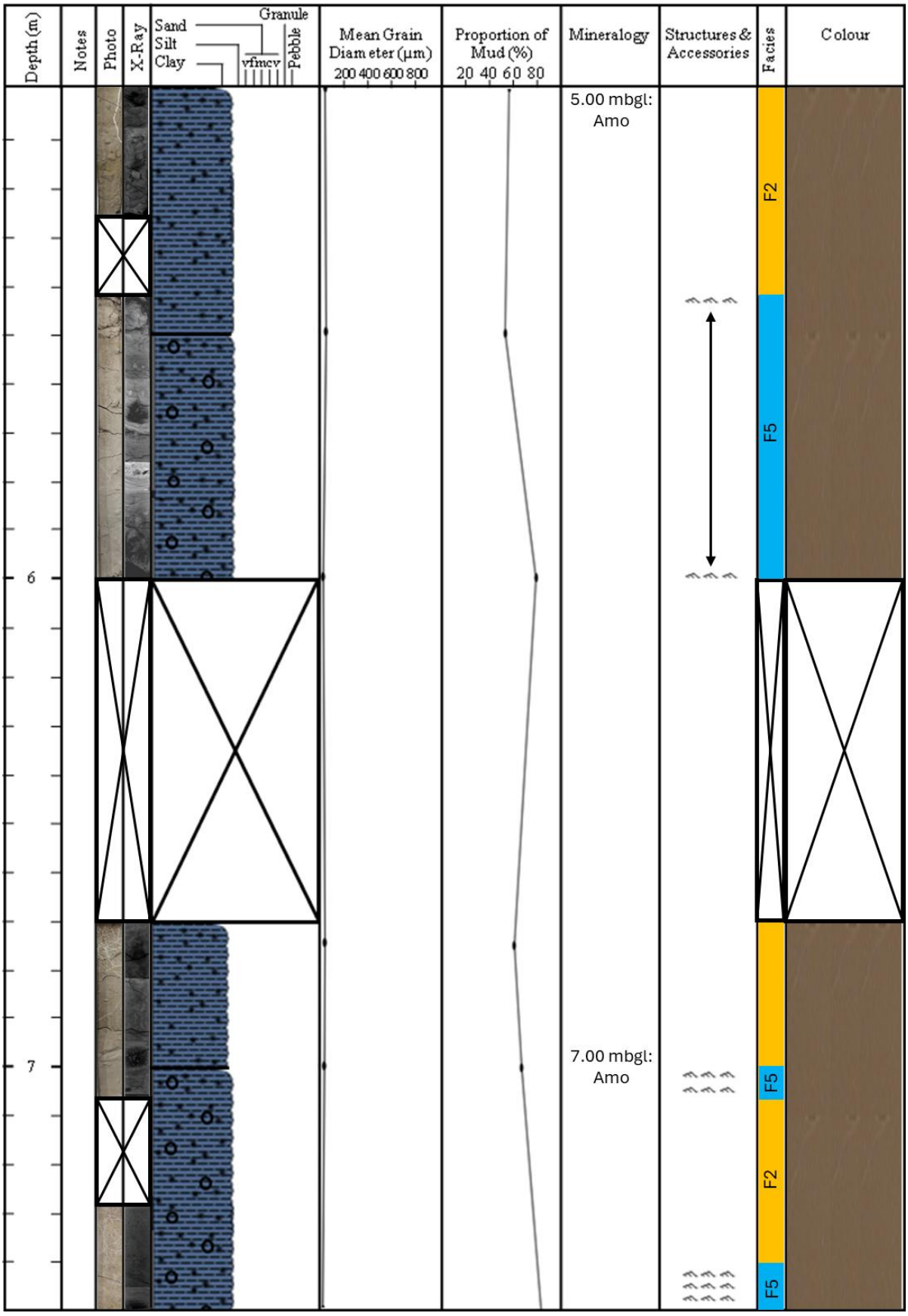

Figure 4.144. Ferrybank Core Log: 5.00-7.50 mbgl.

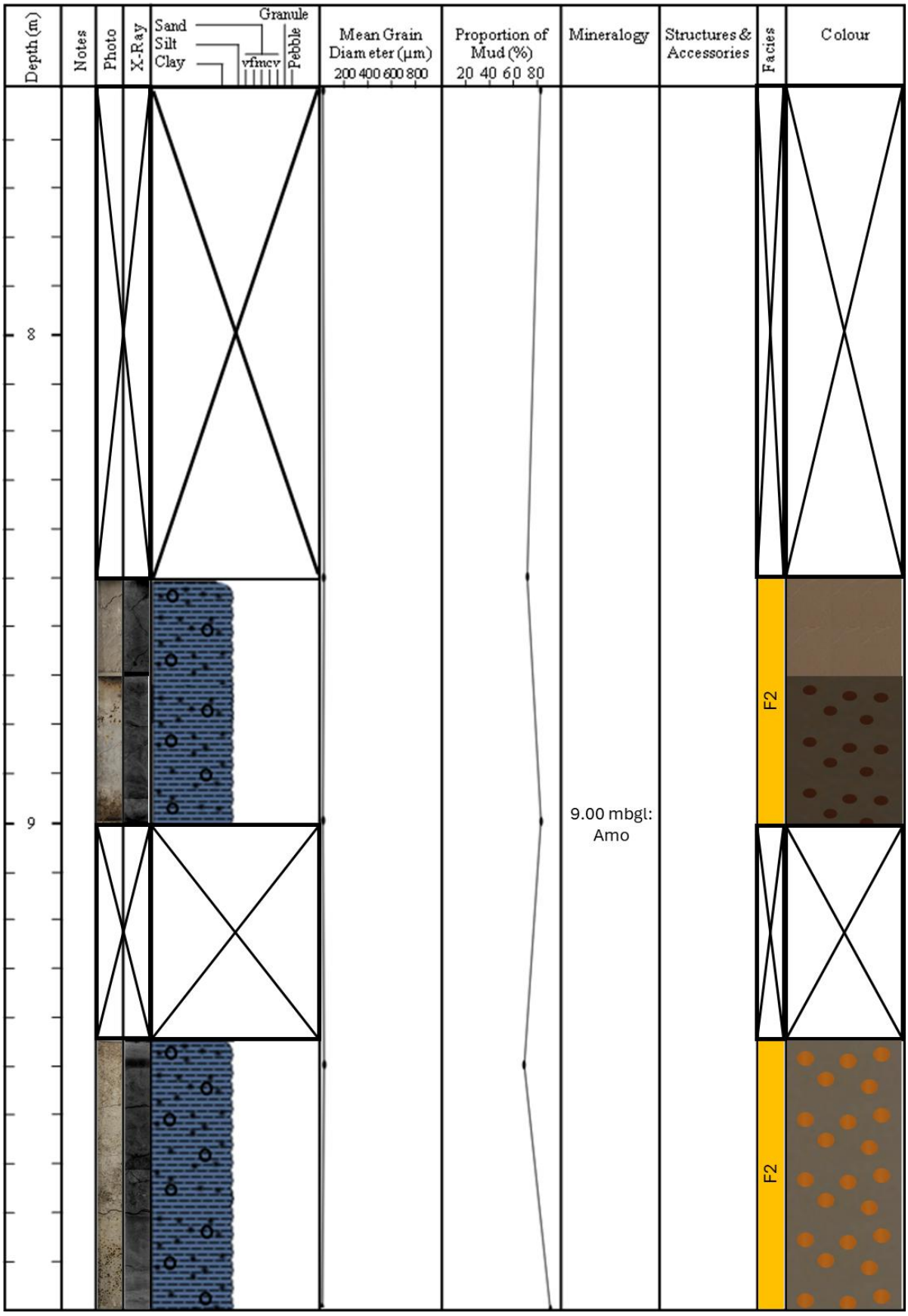

Figure 4.145. Ferrybank Core Log: 7.50-10.00 mbgl.

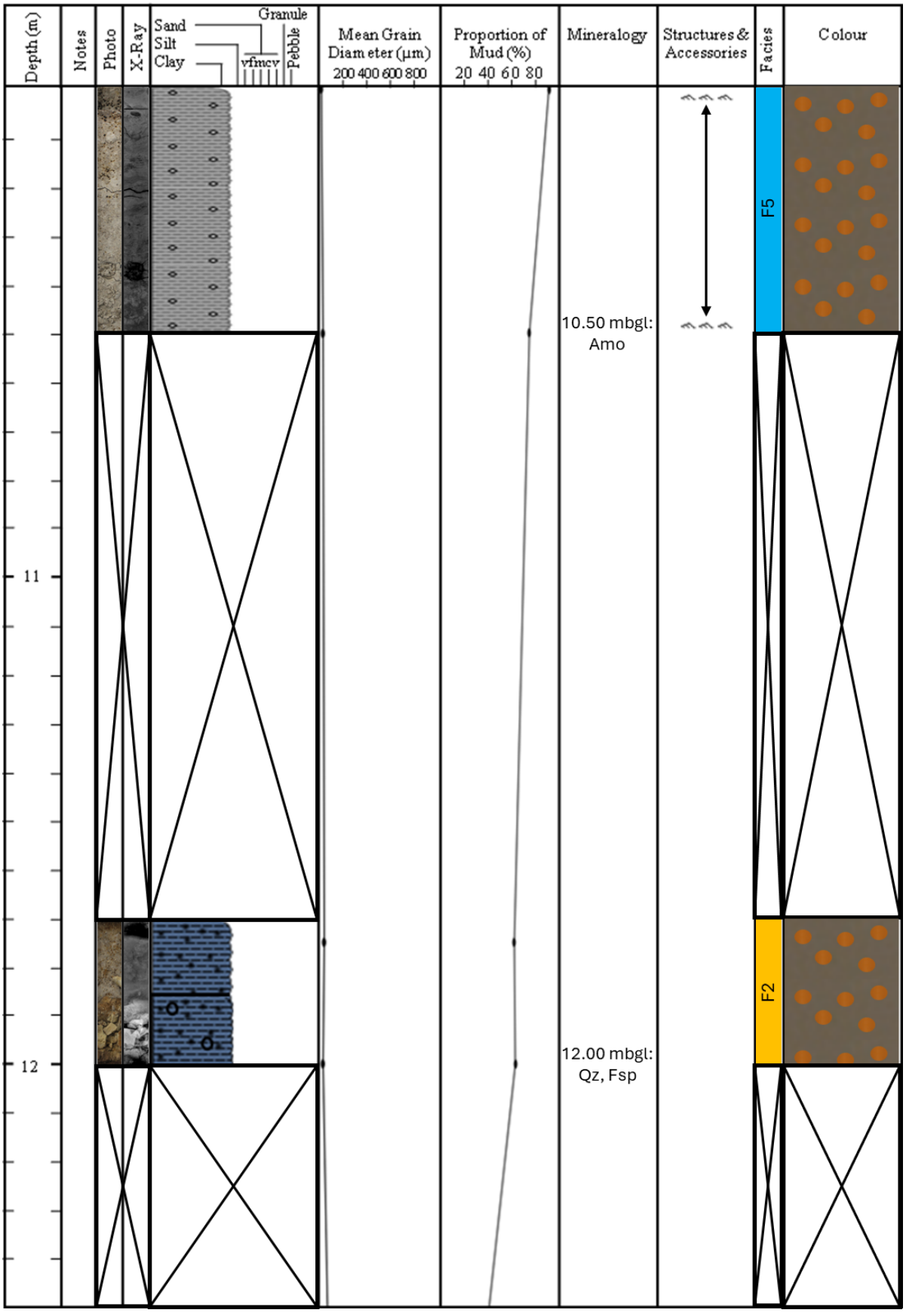

Figure 4.146. Ferrybank Core Log: 10.00-12.50 mbgl.

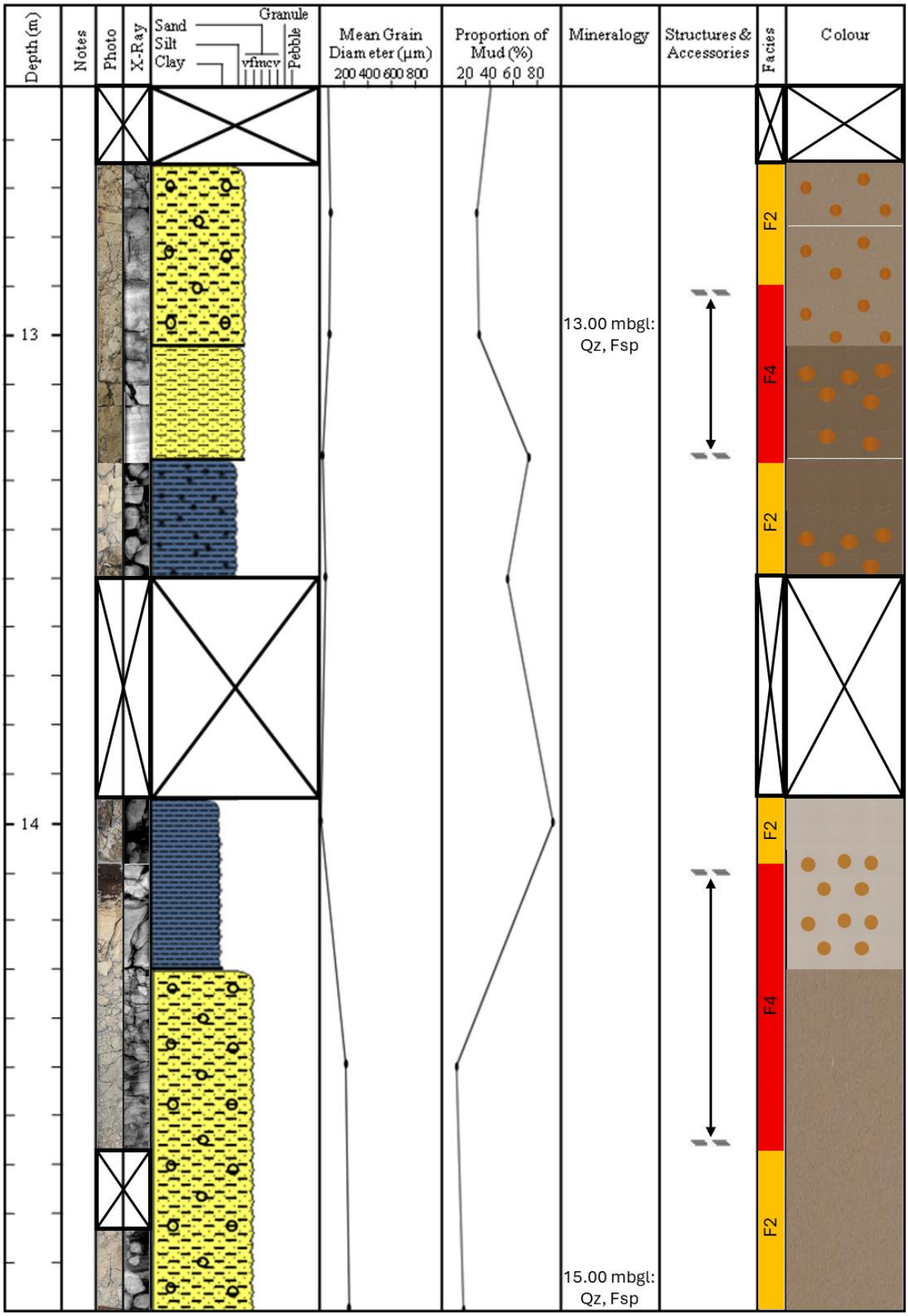

Figure 4.147. Ferrybank Core Log: 12.50-15.00 mbgl.

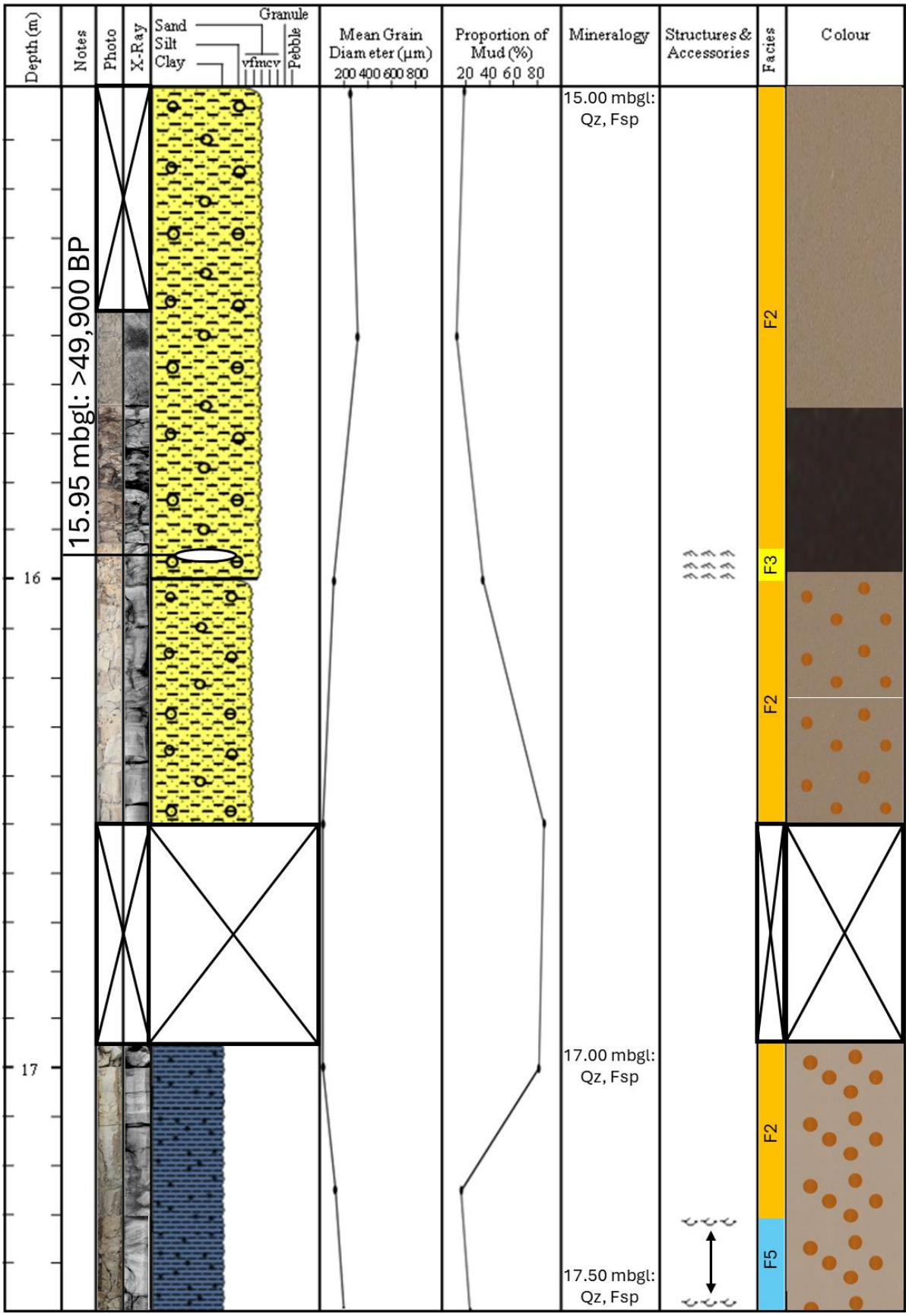

Figure 4.148. Ferrybank Core Log: 15.00-17.50 mbgl.

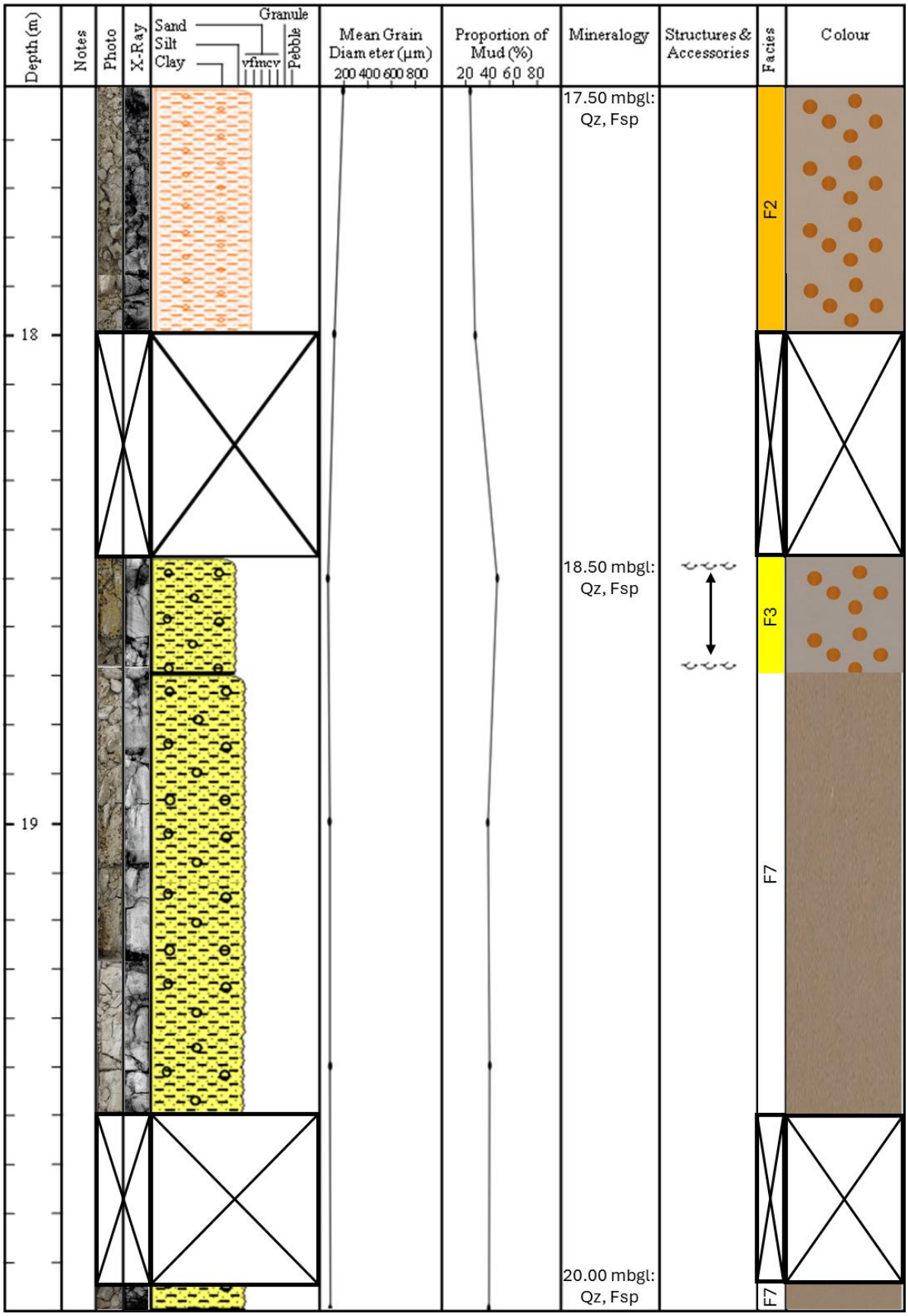

Figure 4.149. Ferrybank Core Log: 17.50-20.00 mbgl.

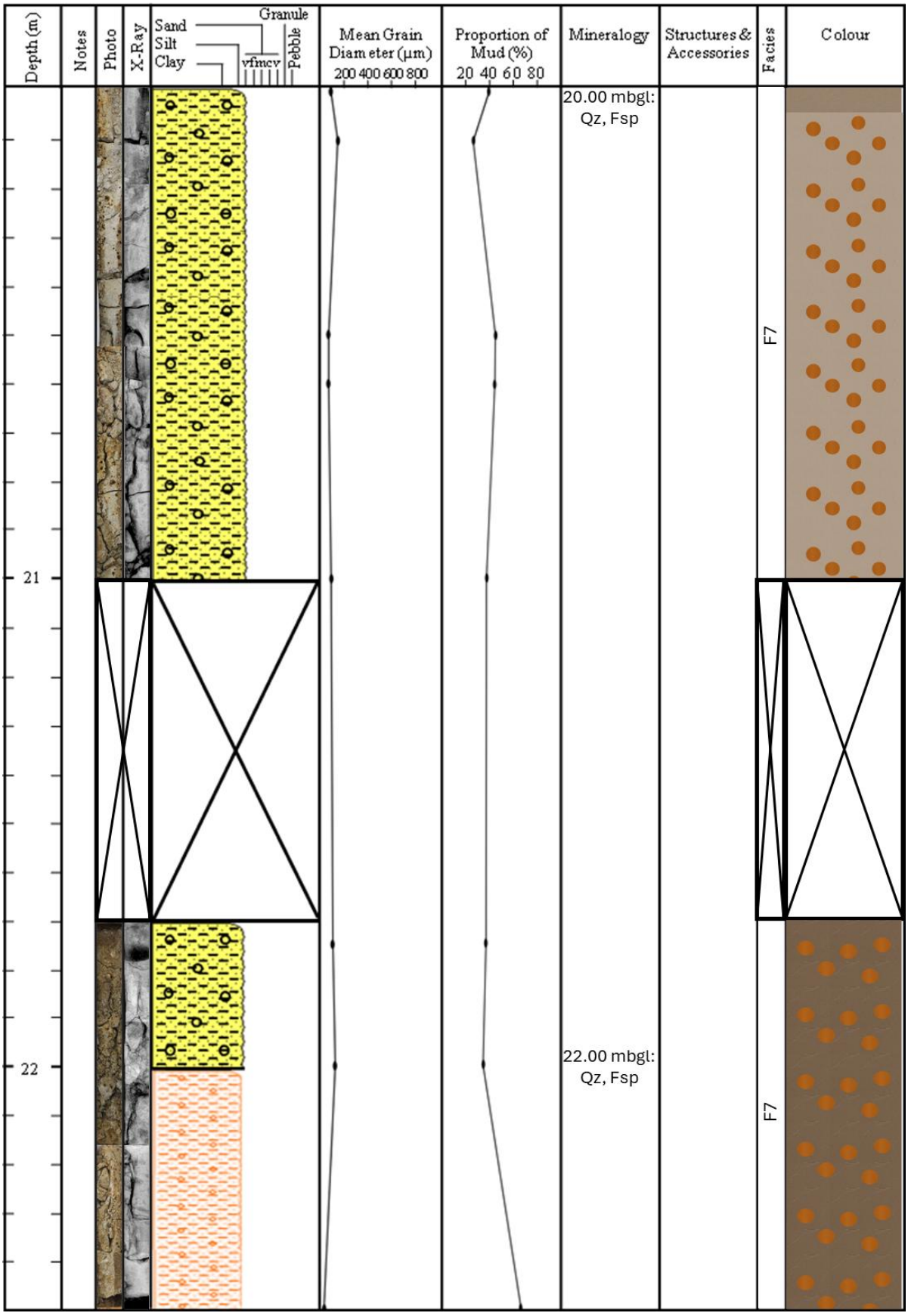

Figure 4.150. Ferrybank Core Log: 20.00-22.50 mbgl.

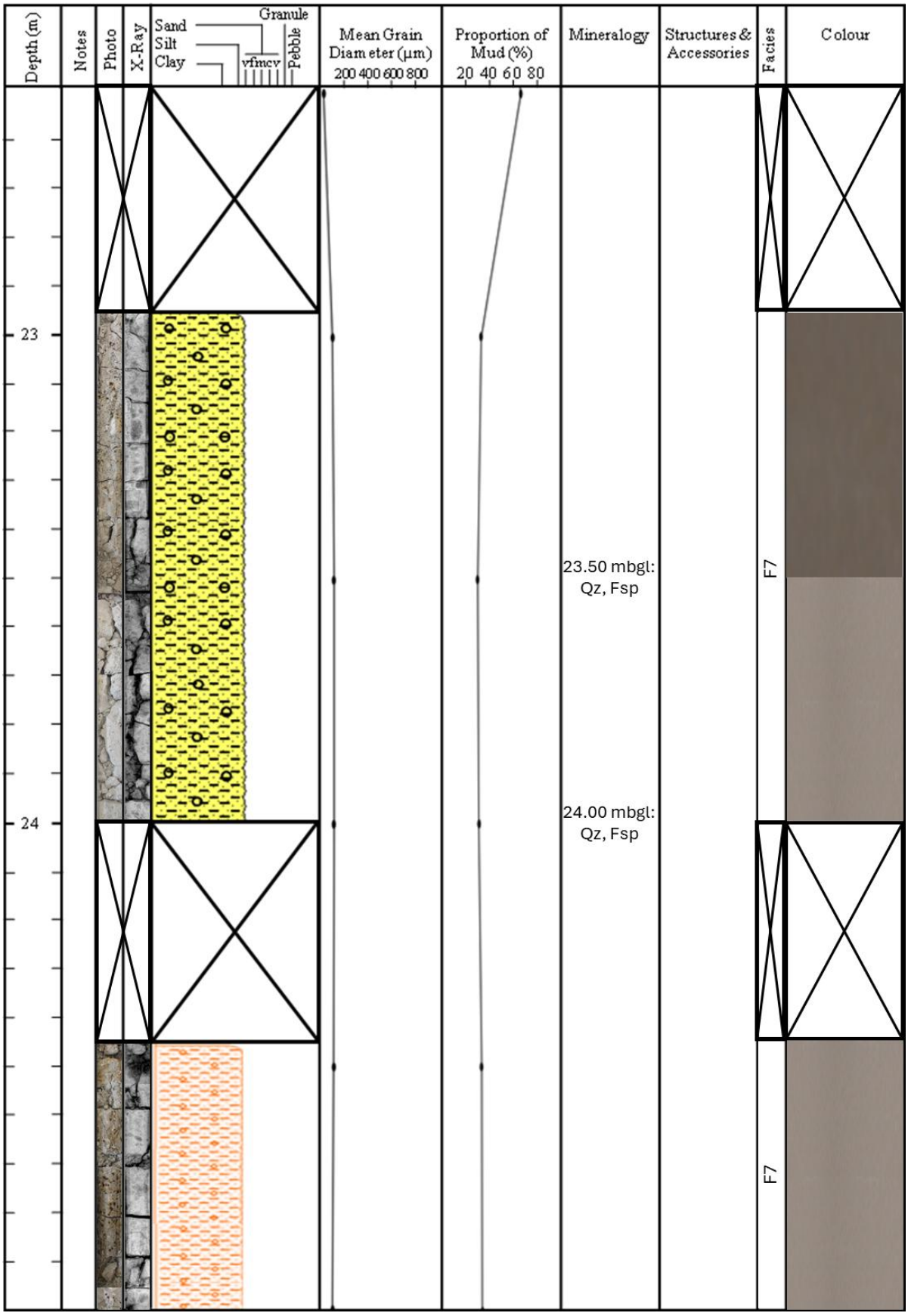

Figure 4.151. Ferrybank Core Log: 22.50-25.00 mbgl.

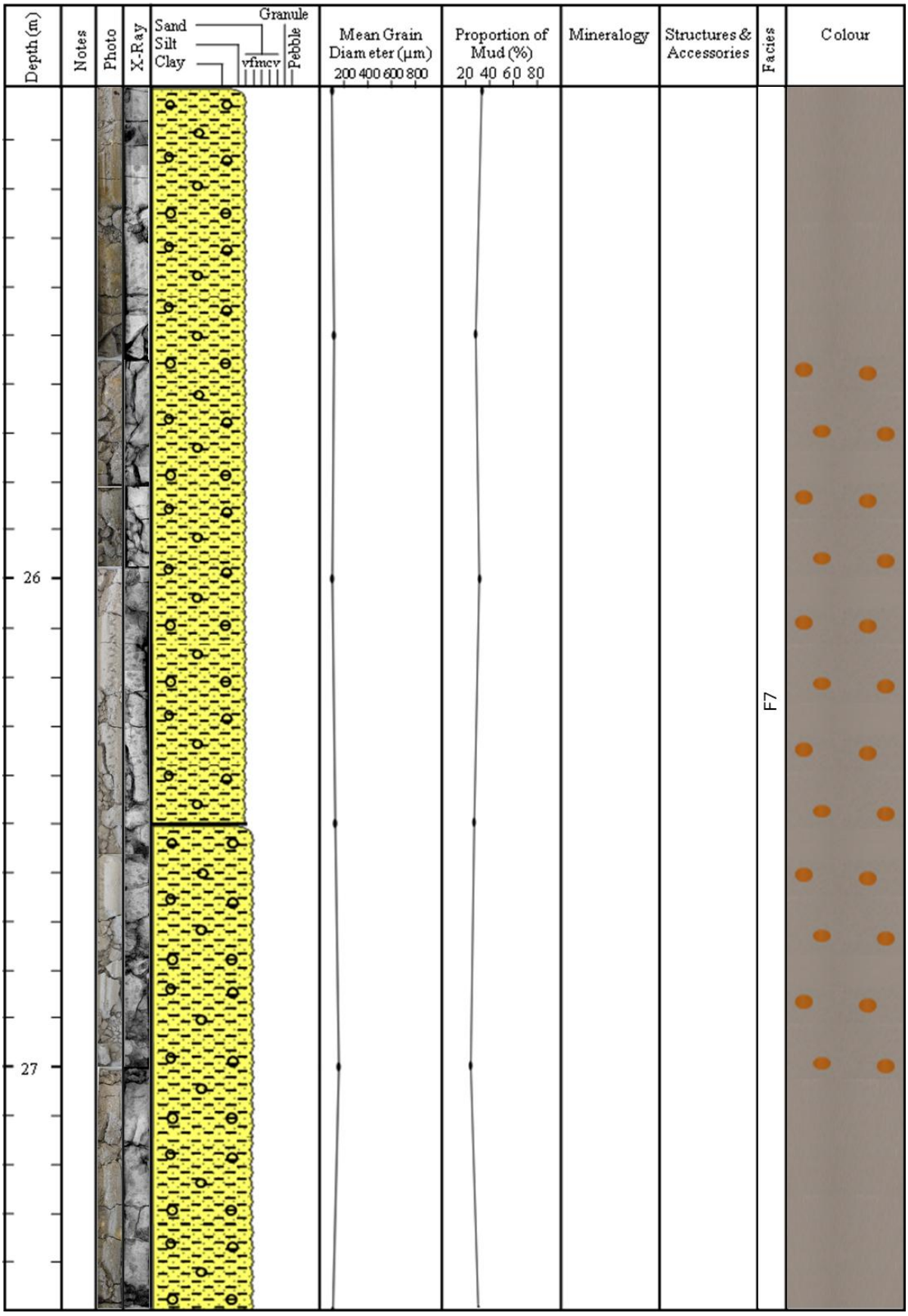

Figure 4.152. Ferrybank Core Log: 25.00-27.50 mbgl.

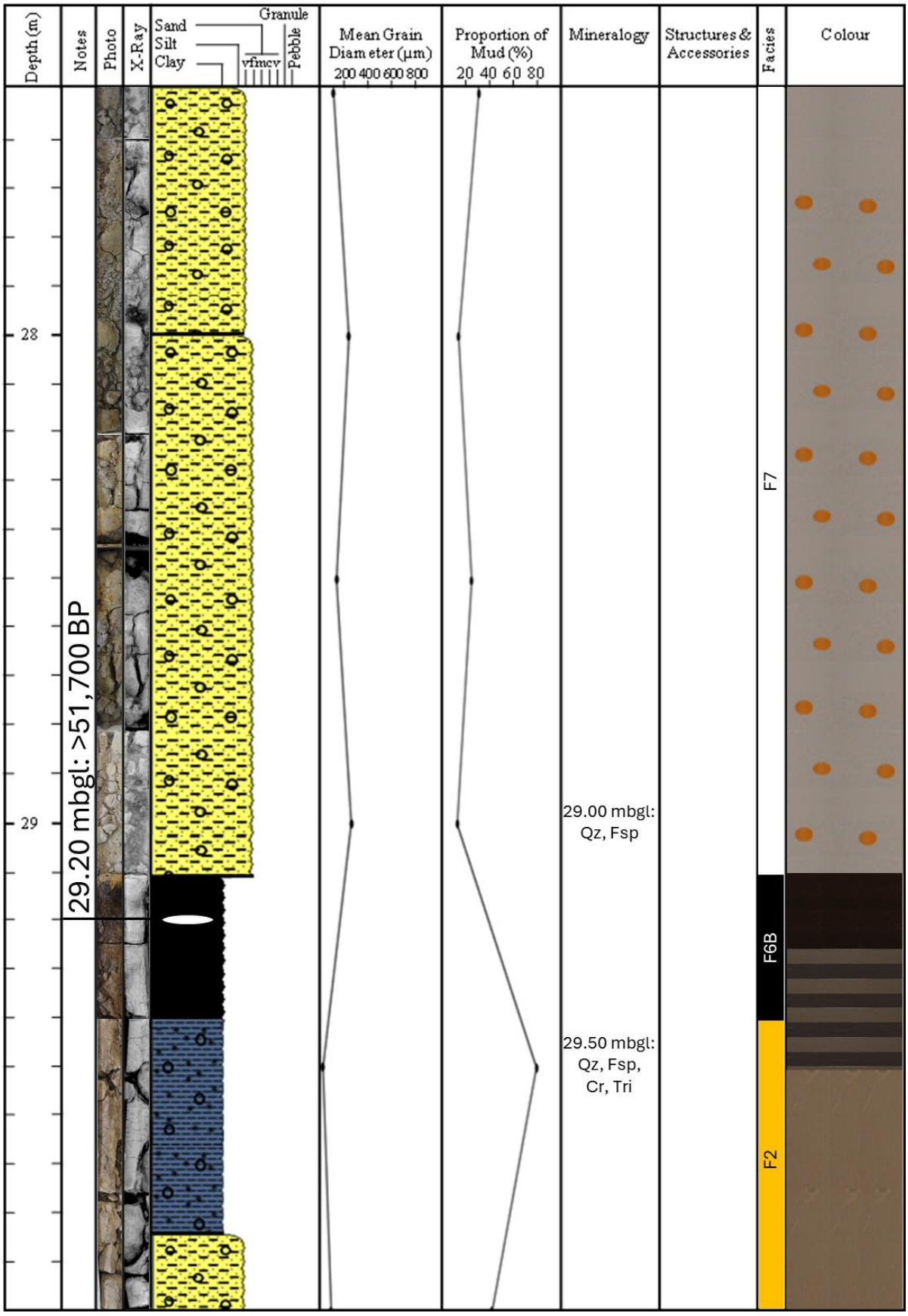

Figure 4.153. Ferrybank Core Log: 27.50-30.00 mbgl.

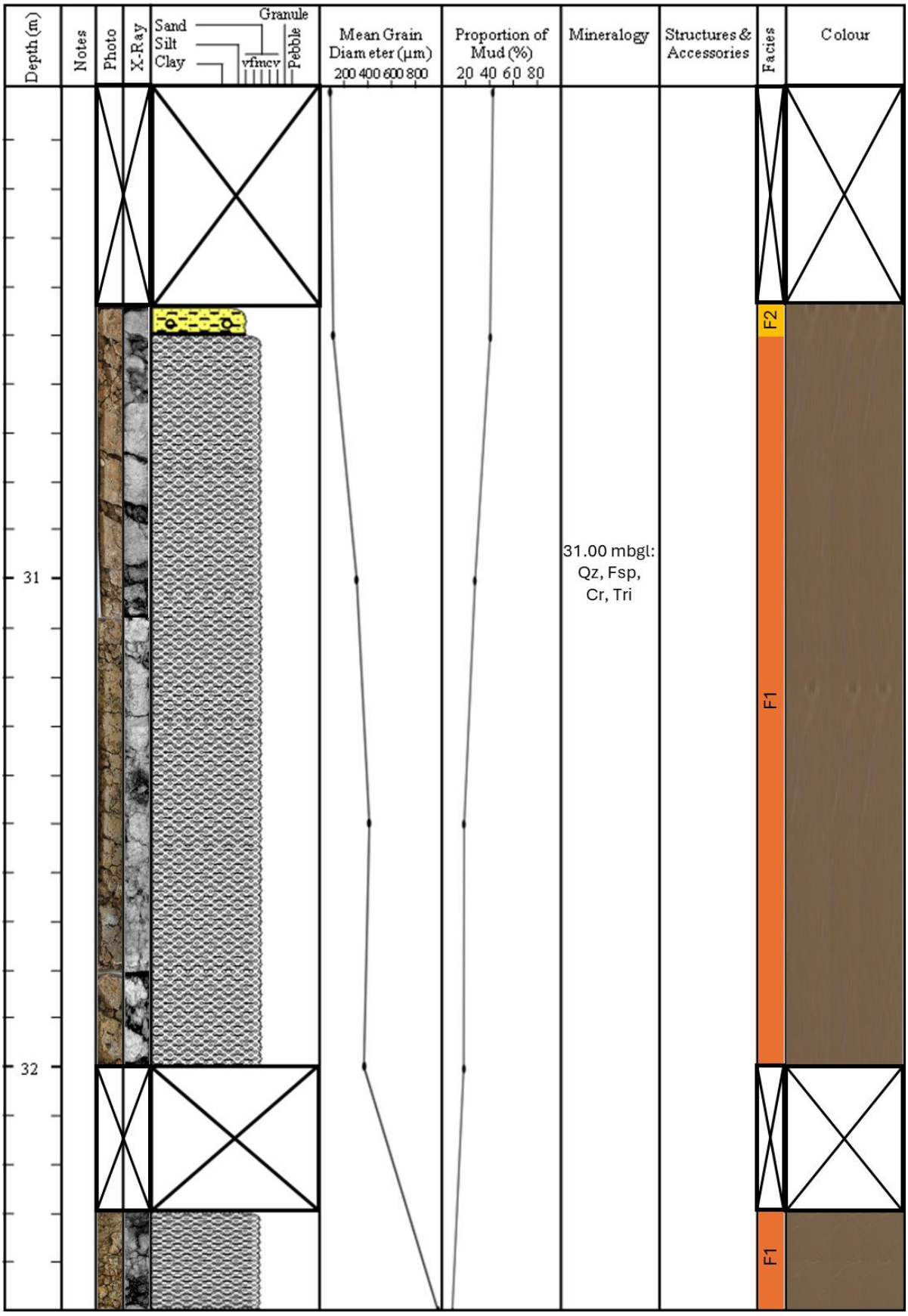

Figure 4.154. Ferrybank Core Log: 30.00-32.50 mbgl.

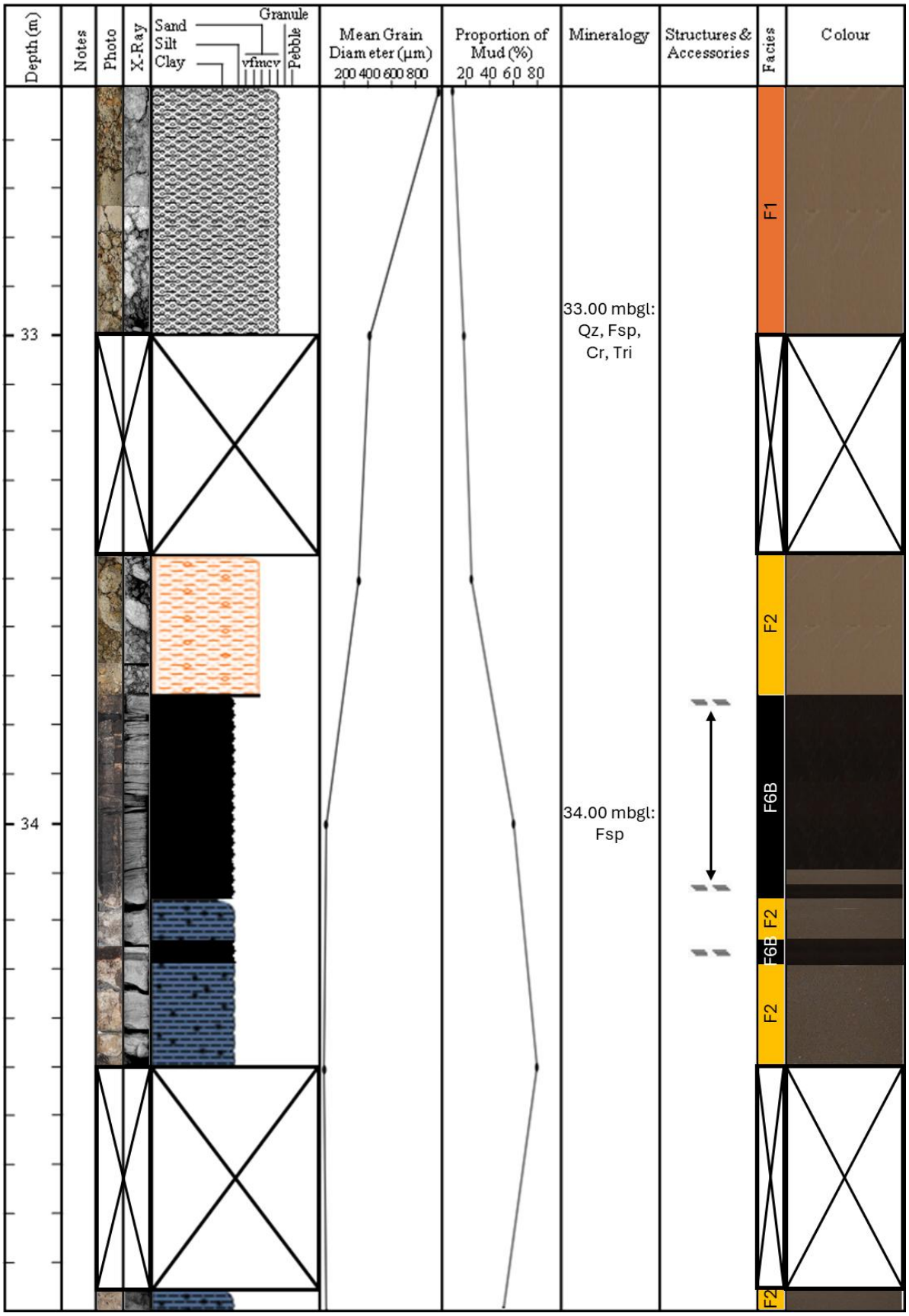

Figure 4.155. Ferrybank Core Log: 32.50-35.00 mbgl.

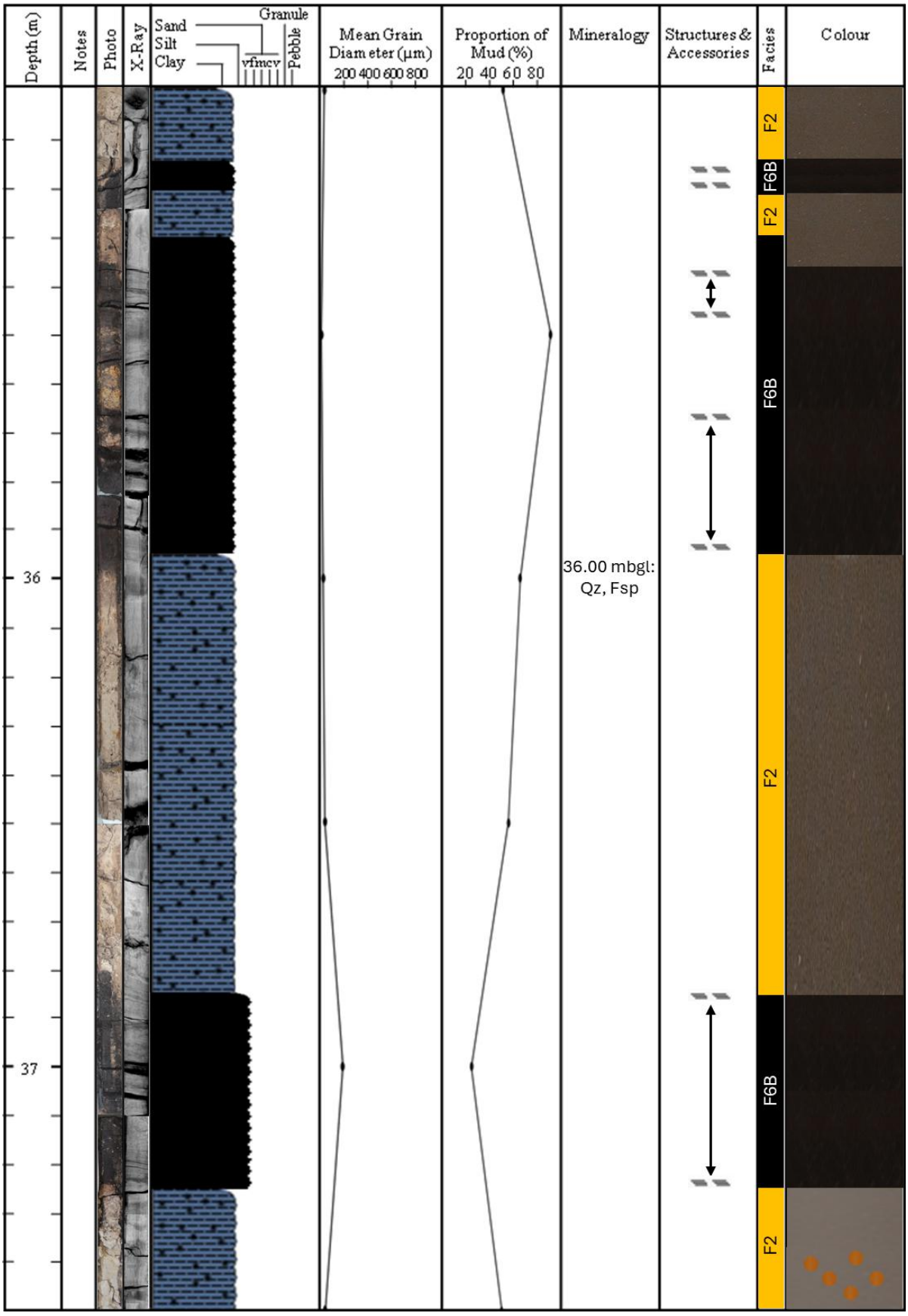

Figure 4.156. Ferrybank Core Log: 35.00-37.50 mbgl.

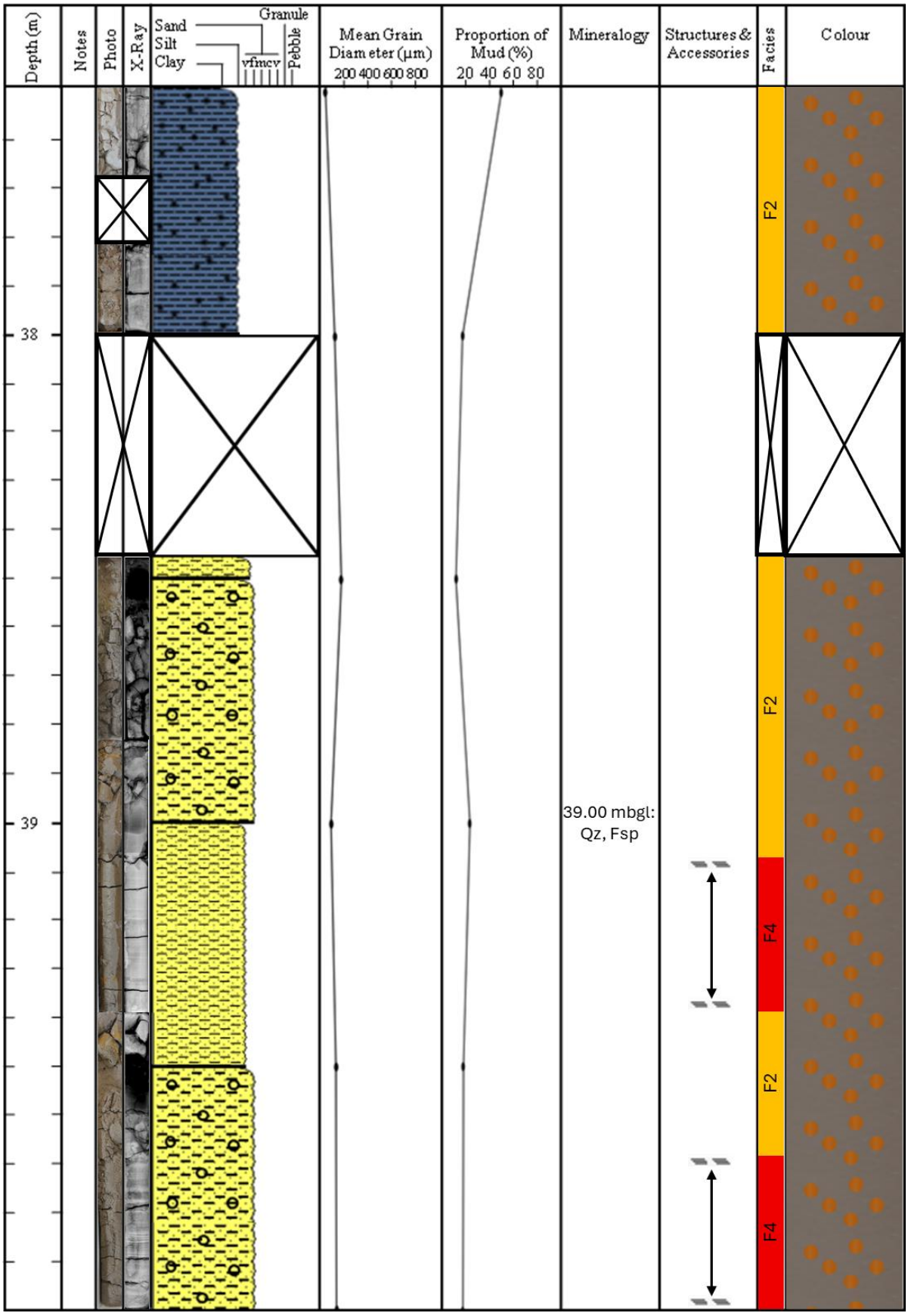

Figure 4.157. Ferrybank Core Log: 37.50-40.00 mbgl.

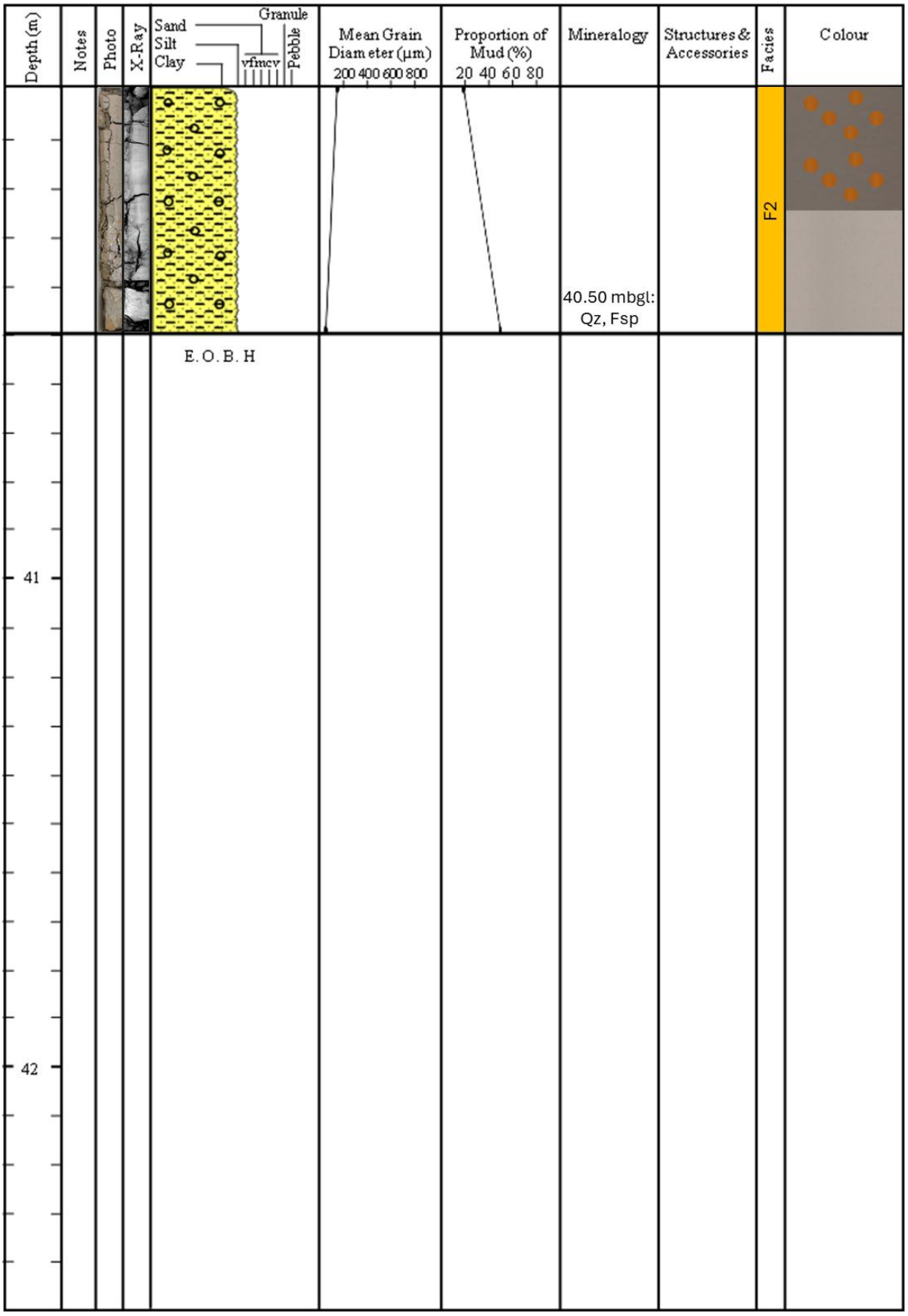

Figure 4.158. Ferrybank Core Log: 40.00-40.50 mbgl.